PROBING SPECTRAL PROPERTIES OF HADRONS IN HOT AND DENSE HADRONIC MATTER

By

SABYASACHI GHOSH

Variable Energy Cyclotron Centre, Kolkata

A thesis submitted to

The Board of Studies in Physical Sciences

For the Degree of

DOCTOR OF PHILOSOPHY

of

HOMI BHABHA NATIONAL INSTITUTE

August, 2012

Homi Bhabha National Institute

Recommendation of the Viva Voce Board

As members of the Viva Voce Board, we certify that we have read the dissertation prepared by **Sabyasachi Ghosh** entitled **Probing Spectral Properties of hadrons in hot and dense hadronic matter** and recommend that it may be accepted as fulfilling the dissertation requirement for the degree of Doctor of Philosophy.

....**Date:**

Chairman- Prof. A. K. Chaudhuri

....**Date:**

Convener- Prof. S. Sarkar

....**Date:**

Member 1- Prof. J. Alam

....**Date:**

Member 2- Prof. M. G. Mustafa

Finally approval and acceptance of this dissertation is contingent upon the candidate's submission of the final copies of the dissertation to HBNI.

I hereby certify that I have read this dissertation prepared under my direction and recommend that it may be accepted as fulfilling the dissertation requirement.

Date:

Place:

STATEMENT BY AUTHOR

This dissertation has been submitted in partial fulfillment of requirements for an advanced degree at Homi Bhabha National Institute (HBNI) and is deposited in the Library to be made available to borrowers under rules of the HBNI.

Brief quotation from this dissertation are allowable without special permission, provided that accurate acknowledgement of source is made. Requests for permission for extended quotation from or reproduction of this manuscript in whole or in part may be granted by the Competent Authority of HBNI when in his or her judgement the proposed use of the material is in the interests of scholarship. In all other instances, however, permission must be obtained from the author.

Sabyasachi Ghosh

DECLARATION

I, hereby declare that the investigation presented in the thesis has been carried out by me. The work is original and has not been submitted earlier as a whole or in part for a degree/diploma at this or any other Institution/University.

Sabyasachi Ghosh

ACKNOWLEDGEMENT

First, I would like to thank my advisor, Dr. Sourav Sarkar (VECC, Kolkata), for his sustained patience, constant encouragement, valuable guidance and support very inception till completion of my PhD period. The main mathematical tools of my research program is thermal field theory. Whatever I learn about it is completely because of his personal teaching. His guidance helped me also during the writing any articles in my PhD period.

I wish to express my gratitude to Dr. Samir Mallik (SINP, Kolkata) and Dr. Jan-e Alam (VECC, Kolkata) for their constant suggestions and help throughout the past five years. I look forward to our continued collaboration.

Sincere acknowledgement is expressed to other senior collaborators Dr. Ashis Kumar Chaudhuri, Dr. Bedangadas Mohanty and some of my friends Santosh Kumar Das, Payal Mohanty, Victor Roy for their active collaboration in some of the research activities.

I would like to give some special thanks to my year mates Haridas Pai, Santosh Kumar Das, Payal Mohanty and Victor Roy as well as to my Seniors Jajati da, Suprio da, Prasun da and at last to all my juniors.

My special thanks go to Avishek Mishra and Trambak Bhattacharya for their careful reading my thesis and giving very useful suggestions to enrich it.

Words of acknowledgement remain incomplete if I do not express my sincere and deep sense indebtedness to my family members. So I express my deep sense of gratitude to my parent, wife, sisters, elder brothers, my late grandfather and all other members of my family for their constant love and encouragement throughout the study. Lastly my sincere thanks to Mrs. Aparna Mazumder who has been caring me with motherly love specially when I first joined VECC, far away from my own family.

Synopsis

According to the cosmological big bang model the universe has undergone several phase transitions (GUT, Electroweak, quark to hadron etc) at different stages of its evolution. The quark-hadron transition occurred in the universe when it was a few microsecond old and is the only transition which can be accessed in the laboratory. In this phase transition, the chiral condensate is one of the order parameter measuring the breaking of chiral symmetry and its study is important to understand the origin of the mass of hadrons. Numerical simulation of QCD thermodynamics on the lattice predict that at high temperature and/or baryon density, this condensate should vanish and chiral symmetry should be restored. It is expected that the resulting changes in the vacuum structure of QCD will affect the correlation functions of vector and axial-vector currents of QCD. They may change in the medium leading to an identical profile at the phase boundary signaling restoration of chiral symmetry. The correlator of vector current of QCD is directly accessible in heavy-ion collisions since it couples to photons and dileptons both of which undergo negligible final-state interaction. In low invariant mass, this is proportional to the spectral function of the low lying vector mesons. The change of the spectral properties of vector mesons in hot and dense medium is consequently reflected in the electromagnetic spectra, specially in the invariant mass spectra of lepton pairs.

We have investigated in-medium spectral properties of ρ and ω mesons by calculating their one-loop self-energy at finite temperature and density. All the branch cuts and the associated discontinuities of the self-energy functions have been discussed in details. The framework of real time thermal field theory that we use, enables us to evaluate the imaginary part of the self-energy from the branch cuts for real and positive values of energy and momentum without having to resort to analytic continuation as in the imaginary time approach. In addition to the unitary cut, present already in the vacuum amplitude, the thermal amplitude generates a new, so-called Landau cut. An extensive set of spin one-half and three-half 4-star resonances in the baryonic loops are taken with the full relativistic baryon propagator in the loop diagrams. The novelty of this full relativistic approach is that the baryons and anti-baryons naturally appear on an equal footing and the additional singularities which are not considered in the Lindhard function approach are automatically included. For the spin 3/2 resonances, an extra term, contributing only in off-mass shell, is added to the Lagrangian because a symmetry is associated with a point transformation under which the free Lagrangian for the Rarita-Schwinger field remains invariant up to a change in the value of its free parameter. Along with the baryon loops, we have included relevant meson loops to get a full modified spectral function of ρ and ω. An almost flattened spectral density of ρ followed by ω are found at very high temperature and density.

The integrated yield after space-time evolution using relativistic hydrodynamics with quark gluon plasma in the initial state leads to a very good agreement with the experimental data from In-In collisions obtained by the NA60 collaboration. The variation of the inverse slope of the transverse mass (M_T) distribution can be used as an efficient tool to predict the presence of two different phases of the matter during the evolution of the system. The sensitivities of the effective temperature obtained from the slopes of the M_T spectra to the medium effects are studied.

With the help of the same frame work we have studied two other hadrons - nucleon (N) and D meson. Using full relativistic baryon propagator as internal line, our nucleon spectral function differs from the one in non-relativistic approximation, used in some earlier calculations. By taking D meson as a probe of the strongly-interacting matter, we have studied its spectral as well as transport properties with the help of covariant formalism of heavy meson chiral perturbation theory. Owing to the Landau cut contribution, the spectral modification of D mesons may result in a downward shift of the pole leading to opening of sub-threshold channels of J/ψ decay providing nontrivial contribution to its suppression in heavy ion collisions.

List Of Publications

Refereed Journals:

1. **Observing many body effects on lepton pair production from low mass enhancement and flow at RHIC and LHC energies.**
   Sabyasachi Ghosh, Sourav Sarkar, Jan-e Alam (VECC, India).
   Eur. Phys. J. C **71** (2011) 1760.
   e-print : arXiv:1009.1260v2 [nucl-th].

2. **ρ self energy at finite temperature and density in the real-time formalism**
   Sabyasachi Ghosh, Sourav Sarkar (VECC, India).
   Nucl. Phys. A **870** (2011) 94
   e-print : arXiv:1109.2773v1 [nucl-th].

3. **Dragging D mesons by hot hadrons.**
   Sabyasachi Ghosh, Santosh K Das, Sourav Sarkar, Jan-e Alam (VECC, India).
   Phys. Rev. D **84** (2011) 011503 (R).
   e-print : arXiv:1104.0163v3 [nucl-th].

4. **Baryonic loop in the rho-meson self-energy.**
   Sabyasachi Ghosh, Sourav Sarkar, (VECC, India) , S. Mallik (SINP, India).
   Phys. Rev. C **83** (2011) 018201.

5. **Relativistic spectral function of nucleon in hot nuclear matter.**
   Sabyasachi Ghosh, Sourav Sarkar, (VECC, India) , S. Mallik (SINP, India).
   Phys.Rev.C **82** (2010) 045202.
   e-print : arXiv:1004.2162v2 [hep-ph].

6. **Analytic structure of ρ meson propagator at finite temperature.**
   Sabyasachi Ghosh, Sourav Sarkar, (VECC, India) , S. Mallik (SINP, India).
   Eur. Phys. J. C **70** (2010) 251.
   e-print : arXiv:0911.3504v4 [hep-ph].

7. **Drag coefficient of B mesons in hot hadronic matter.**
   Santosh K das, Sabyasachi Ghosh, Sourav Sarkar, Jan-e Alam (VECC, India).
   Phys.Rev.D **85** (2012) 074017.
   e-print : arXiv:1109.3359v3 [hep-ph].

8. **Elliptic flow of thermal dileptons as a probe of QCD matter.**
   Payal Mohanty, Victor Roy, Sabyasachi Ghosh, Santosh K. Das,
   Bedangadas Mohanty, Sourav Sarkar, Jane Alam, Asis K. Chaudhuri (VECC, India).
   Phys. Rev. C **85** (2012) 031903 (R).
   e-print : arXiv:1111.2159v2 [nucl-th].

9. **Effect of spectral modification of ρ on shear viscosity of a pion gas.**
   Sukanya Mitra, Sabyasachi Ghosh, Sourav Sarkar (VECC, India).
   Phys. Rev. C **85** (2012) 064917
   e-print : arXiv:1204.2388v1 [nucl-th].

Arxiv Submission:

1. **Analysis of ω self-energy at finite temperature and density in the real-time formalism**
   Sabyasachi Ghosh, Sourav Sarkar (VECC, India).
   e-print : arXiv:1207.2251v1 [nucl-th]

Conference Proceedings in Journals:

1. **The ρ meson in hot hadron matter and low mass dilepton spectra.**
   Sabyasachi Ghosh, Sourav Sarkar, Jan-e Alam (VECC, India).
   Nucl. Phys. A **862** (2011) 294.
   e-print : arXiv:1101.5946v1 [nucl-th].

2. **In-medium vector mesons and low mass lepton pairs from heavy ion collisions.**
   Sourav Sarkar, Sabyasachi Ghosh (VECC, India)
   Journal of Physics: Conference Series 374 (2012) 012010.
   e-print : arXiv:1204.0893v1 [nucl-th].

Conference Proceedings:

1. **Propagation of rho meson in hot hadronic matter.**
   Sabyasachi Ghosh, Sourav Sarkar, (VECC, India) , S. Mallik (SINP, India).
   Proceedings of DAE Symp. on Nucl. Phys. (India) **55** (2010) 632.

2. **Spectral properties of nucleon in hot nuclear matter.**
   Sabyasachi Ghosh, Sourav Sarkar, (VECC, India) , S. Mallik (SINP, India).
   Proceedings of DAE Symp. on Nucl. Phys. (India) **55** (2010) 634.

3. **In-medium ρ mesons, dilepton spectra and flow in heavy ion collisions**
   Sabyasachi Ghosh, Sourav Sarkar, Jan-e Alam (VECC, India).
   Proceedings of DAE Symp. on Nucl. Phys. (India) **55** (2010) 592.

4. **Dragging D by hot hadrons.**
   Sabyasachi Ghosh, Santosh K Das, Sourav Sarkar, Jan-e Alam (VECC, India).
   Proceedings of DAE Symp. on Nucl. Phys. (India) **56** (2011) 974.

5. **Baryonic loops in the ρ self energy at finite temperature and density**

   Sabyasachi Ghosh, Sourav Sarkar (VECC, India).

   Proceedings of DAE Symp. on Nucl. Phys. (India) **56** (2011) 990.

6. **Spectral properties of charmed mesons at finite temperature.**

   Sabyasachi Ghosh, Sukanya Mitra, Sourav Sarkar (VECC, India).

   Proceedings of DAE Symp. on Nucl. Phys. (India) **56** (2011) 918.

7. **Transport coefficients of B mesons in hot hadronic matter.**

   Santosh K Das, Sabyasachi Ghosh, Sourav Sarkar, Jan-e Alam (VECC, India).

   Proceedings of DAE Symp. on Nucl. Phys. (India) **56** (2011) 944.

8. **Probing Elliptic Flow of QCD Matter by Lepton Pairs**

   Payal Mohanty, Victor Roy, Sabyasachi Ghosh, Santosh K Das, Bedangadas Mohanty, Sourav Sarkar, Jan-e Alam, Asis K Chaudhuri (VECC, India).

   Proceedings of DAE Symp. on Nucl. Phys. (India) **56** (2011) 910.

Notation and Conventions

In the thesis, I have used the natural units, $\hbar = c = k_B = 1$. The matric tensor used is $g^{\mu\nu} = \text{diag}(1, -1, -1, -1)$. Most of the notation is introduced during the discussion and the frequently used notations are enlisted below:

$\theta(x_0)$	step function, $\theta(x_0) = 1$ when $x_0 > 0$ $= 0$ when $x_0 < 0$
$\mathcal{T}$	time order product
$\epsilon(q_0)$	Sign function, $\epsilon(q_0) = +1$ when $q_0 > 0$ $= -1$ when $q_0 < 0$
β	$\beta = 1/T$, where T is temperature
Δ	Scalar propagator or scalar part of any propagator
S	Spin $\frac{1}{2}$ propagator
$D^{\mu\nu}$	Spin 1 propagator
$G^{\mu\nu}$	Four dimensionally transverse part of Spin 1 propagator
$\Pi, \Pi^{\mu\nu}$	Self-energy of Spin 0 and 1 particle respectively
Σ	Self-energy of Spin $\frac{1}{2}$ particle
μ	chemical potential
$n_\pm$	Particle and anti-particle distribution function
M	invariant mass
m_π	mass of pion
m_N	mass of nucleon
m_B	mass of baryon
$\epsilon_{\mu\nu\lambda\sigma}$	Levi civita symbol representing totally antisymmetric tensor, with $\epsilon^{0123} = 1$
J^P	spin (J) parity (P) quantum no.
T_i	initial temperature
T_c	transition temperature
T_{ch}	chemical freeze out temperature
T_F	kinetic freeze out temperature
$W^{\mu\nu}$	electromagnetic current correlation function
$s,\ t,\ u$	Madelstam Variables, where $s = (p_1 + p_2)^2,\ t = (p_1 - p_3)^2,\ u = (p_1 - p_4)^2$

Contents

List of Figures

List of Tables

Chapter 1

Introduction

In the journey of understanding the origin of matter, the main objective of our research is to look for the basic constituents of matter and know their basic interactions. Probing the matter at Fermi scale (10^{-15} m) we have seen a drastically condensed structure - nucleus, which may be considered to possess the total mass of the matter. As per contemporary wisdom, the nucleus can be divided into nucleons which are further made up of quarks. Similar to atomic system, the mass of the nucleus is also very easily reproduced by adding the rest mass of individual nucleons and the extra masses of the components provide the binding energy of the nucleus. In 1960's it was discovered that the nucleon (with mass $\sim$ 940 MeV) is built of three valence quarks of up (u) and down (d). Mysteriously the bare masses of u and d quarks are only about 5-10 MeV and our traditional mass counting philosophy fails to understand the nucleon mass in terms of masses of quark constituents. This 98 % of nucleon mass is believed to generate form spontaneously breaking of chiral symmetry of the strong interaction. To be familiar with the mysterious world of quarks and gluons inside the nucleon (or hadron), let us begin with the QCD Lagrangian, describing the strong interaction of quarks and gluons in Standard Model (SM).

$$\mathcal{L}_{\rm QCD} = \sum_f \overline{\psi}_f (i\gamma^\mu D_\mu - m_f)\psi_f - \frac{1}{4} G^a_{\mu\nu} G^{\mu\nu}_a \tag{1.1}$$

where ψ_f denotes a quark field of flavor f and mass m_f, $D_\mu = \partial_\mu - ig_s n^a A^a_\mu/2$ is the covariant derivative and $G^a_{\mu\nu} = \partial_\mu A^a_\nu - \partial_\nu A^a_\mu + g_s f^{abc} A^b_\mu A^c_\nu$ is the gluon field strength tensor. The structure constants of $\mathrm{SU(3)_{color}}$ are denoted by f^{abc} where the group indices a, b, c take values from 1 to 8. The three and four gluon couplings endow QCD with special properties which is very different from Quantum Electro Dynamics (QED) - the

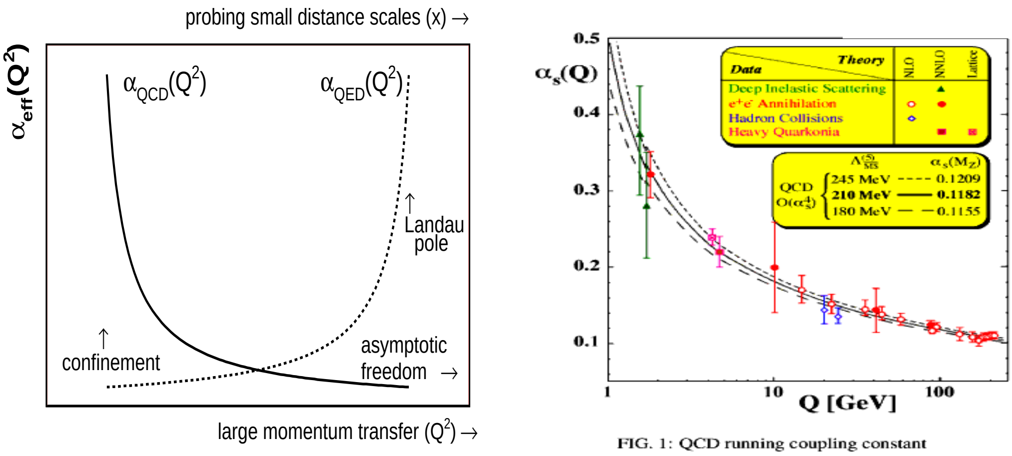

Figure 1.1: Left : Variation of QED and QCD coupling with momentum transfer (Q) show an almost opposite trend [6]. Right : Running QCD coupling $\alpha_s(Q)$ from various measurements compared to theory [7].

theory of electromagnetic interaction. In QED the intermediate gauge particle, photon does not have electric charge so it does not interact with itself. Renormalization of QED loop diagrams render the electromagnetic coupling constant ($\alpha_e = e^2/4\pi$) dependent on the momentum transfer Q and $\alpha_e(Q^2)$ increases with the increasing of Q. In QCD the intermediate gauge particle, gluons unlike photons carry color charge and are self interacting. Due to self interacting loop diagrams of gluons, QCD renormalization imposes almost an opposite trend (see Fig. 1.1) in momentum dependence of strong coupling constant ($\alpha_s = g_s^2/4\pi$). This shows at short distances, or large Q, $\alpha_s(Q^2)$ decreases logarithmically which means that the quarks and gluons appear to be weakly coupled at very short distances, a behavior referred to as *asymptotic freedom* [1, 2]. QCD renormalization introduces a scale $\Lambda_{\rm QCD}$ known as the QCD scale parameter which has a value $\sim$ 200 MeV. For $Q^2 >> \Lambda_{\rm QCD}$ the value of α_s is small and standard perturbation theory works with a high level of accuracy as tested in deep inelastic scattering and many other high energy processes. For $Q^2 \sim \Lambda_{\rm QCD}^2$ on the other hand, the coupling is large and color degrees of freedom get confined within hadrons like p, n, π, ρ etc. which are the relevant degrees of freedom in this domain. Along with confinement, chiral symmetry is spontaneously broken; both these phenomena are responsible for the origin of hadronic masses and bindings. So this nonperturbative domain of QCD is a very crucial region where quark confinement [3, 4, 5] and the mass generation occur, posing formidable challenges for their theoretical understanding [8]. An ab-initio study of these nonperturbative features of QCD is only possible through numerical simulations on a space-time lattice, a field which has seen substantial progress in recent times. An alternative way to investigate the dynamics of strong interaction in the hadronic world is to construct effective theories based on the symmetry structure of the underlying theory and chiral symmetry plays a major role here.

1.1 Chiral Symmetry breaking in Hadronic spectrum

To discuss the chiral symmetry associated with QCD, let us rewrite Eq. (1.1) in the limit of massless quarks [1] as

$$\mathcal{L}_{\rm QCD} = i \sum_{f=u,d} \overline{\psi}_f^R \gamma^\mu D_\mu \psi_f^R + i \sum_f \overline{\psi}_f^L \gamma^\mu D_\mu \psi_f^L - \frac{1}{4} G^a_{\mu\nu} G_a^{\mu\nu} \tag{1.2}$$

where $\psi_f^{L,R} = \frac{1}{2}(1 \mp \gamma_5)\psi_f$ are respectively left and right chirality components of quark field ψ_f. In this limit of vanishing quark masses, QCD Lagrangian (1.2) remains invariant under independent transformations of left and right handed quark fields

$$\psi_f^{L,R} \to U_{L,R} \psi_f^{L,R} \quad , \qquad U_{L,R} = e^{i\alpha^a_{L,R}\tau^a/2} \tag{1.3}$$

where $\alpha^a_{L,R}(a = 1, 2, 3)$ are three real angles and τ_a are the Pauli matrices. Since the unitary matrices $U_{L,R}$ belong to the groups $\mathrm{SU}(2)_{L,R}$ respectively, of which the three Pauli matrices τ_a are the generators. $\mathcal{L}_{\rm QCD}$ (1.2) is invariant under global $\mathrm{SU}(2)_L \times \mathrm{SU}(2)_R$ symmetry leading to the conserved Noether currents $J^{\mu a}_{L,R} = \overline{\psi}_f^{L,R} \gamma^\mu \frac{\tau^a}{2} \psi_f^{L,R}$. This implies that chirality or handedness is preserved and the associated symmetry of the strong interaction in this limit is known as chiral symmetry. However, in reality the mass terms

$$\sum_f (\overline{\psi}_f^L m_f \psi_f^R + \overline{\psi}_f^R m_f \psi_f^L) \tag{1.4}$$

of the QCD Lagrangian (1.1) mixes the chiralities and breaks this symmetry explicitly. Because of small masses, the chiral symmetry for two flavor (u and d) is still supposed to be a good symmetry of strong interaction.

[1] With respect to other quarks (s, c, b and t), this limit may be well justified for u and d quarks because of their small masses

The observable particles i.e. hadrons are eigenstates of parity and so it is useful to work with the vector and axial-vector Noether currents

$$J^{\mu a}_{V,A} = \overline{\psi}_f \gamma^\mu \left\{ \begin{array}{c} \mathbf{1} \\ \gamma^5 \end{array} \right\} \frac{\tau^a}{2} \psi_f \tag{1.5}$$

which are related to the left and right handed currents by

$$J^{\mu a}_{V,A} = J^{\mu a}_R \pm J^{\mu a}_L. \tag{1.6}$$

The triplet of charges $Q^a_{V,A} = \int d^3x J^{0a}_{V,A}(x)$ are the corresponding (quantum) generators of $\mathrm{SU}(2)_R \times \mathrm{SU}(2)_L$ which commute with the Hamiltonian of QCD

$$[Q^a_{V,A}, H] = 0. \tag{1.7}$$

The states that from irreducible representation (basis) of the $\mathrm{SU}(2)_V$ group can be connected by

$$Q_V|A\rangle = |B\rangle \tag{1.8}$$

From Eq. (1.8) and (1.7) it follows immediately that

$$\begin{aligned} E_A &= \langle A|H|A\rangle \\ &= \langle A|Q^\dagger_V H Q_V|A\rangle \quad (\text{since } H = Q^\dagger_V Q_V H = Q^\dagger_V H Q) \\ &= \langle B|H|B\rangle \quad = E_B \end{aligned} \tag{1.9}$$

Thus the symmetry of Hamiltonian H is manifest in the degeneracies of the energy eigenstates corresponding to the irreducible representations of the symmetry group. However implicit in the statement of (1.8) and hence (1.9) is invariance of the ground state under symmetry transformation. Since $|A\rangle$ and $|B\rangle$ must be related to the ground state $|0\rangle$ through some appropriate creation operators ϕ_A and ϕ_B

$$\begin{gathered} |A\rangle = \phi_A|0\rangle \ , \qquad |B\rangle = \phi_B|0\rangle \\ \text{and} \ \ Q_V \phi_A Q^\dagger_V = \phi_B \end{gathered} \tag{1.10}$$

Eq. (1.8) follows only if [9]

$$Q_V|0\rangle = 0 \tag{1.11}$$

It was shown by Vafa and Witten [10] that the vector charges annihilate the vacuum $Q^a_V|0\rangle = 0$. Isospin symmetry i.e. $\mathrm{SU}(2)_V$ is consequently realized in the usual Wigner-Weyl mode which is reflected in the spectrum through the almost degenerate doublet of

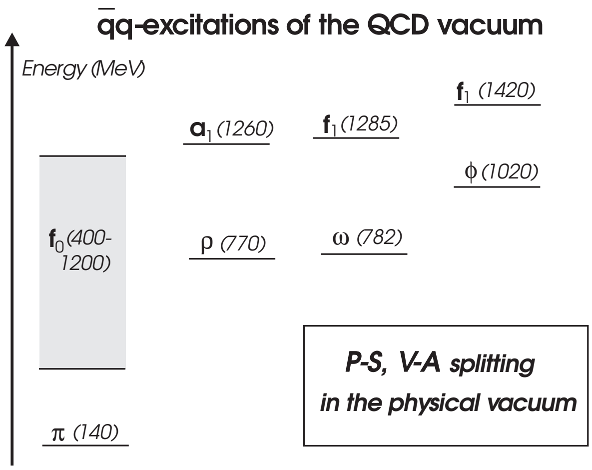

Figure 1.2: Hadronic spectra in vacuum do not show any mass degeneracy of chiral partners. π, ρ with spin-parity quantum no. $J^P = 0^-,\ 1^-$ are well separated from their Chiral partners f_0, a_1 ($J^P = 0^+,\ 1^+$) respectively. Figure is taken from [37]

the proton and neutron, the triplet of the ρ^+, ρ^0, ρ^- etc. In addition to the vector charges, if the axial charges also annihilate the vacuum i.e. $Q_A^a|0\rangle = 0$, parity doublets should exist in the spectrum. If chiral symmetry were realized in the conventional (Wigner-Weyl) fashion one would expect there also to exist nearly degenerate but opposite parity states (say $|P\rangle$) generated by the action of the time-independent axial charges $Q_A^a = \int d^3x J_A^{0a}(x)$ on these states [11]. Indeed since

$$\begin{aligned} H|P\rangle &= E_P|P\rangle\ , \\ \text{Hence } H(Q_A|P\rangle) &= Q_A(H|P\rangle) \quad \text{(using Eq. 1.7)} \\ &= E_P(Q_A|P\rangle) \end{aligned} \tag{1.12}$$

we see that $Q_A|P\rangle$ must also be an eigenstate of the Hamiltonian (H) with the same eigenvalue as $|P\rangle$, which would seem to require the existence of parity doublets. This however does not appear to be realized in nature. For example, the ρ meson with $J^P = 1^-$ is separated by about 500 MeV in mass from its chiral partner the a_1 with $J^P = 1^+$ (see Fig. 1.2). So are the masses of the nucleon and its chiral partner, the $N^*(1535)$. One can resolve this apparent paradox by postulating that parity-doubling is avoided because the axial symmetry is spontaneously broken. Then according to a theorem due to Goldstone, when a continuous symmetry is broken in this fashion a massless boson having the quantum numbers of the broken generator must also be generated - in this case a pseudoscalar - and when the axial charge acts on a single particle eigenstate $|P\rangle$ one does not get a new single particle eigenstate of opposite parity in return [12]. Rather one generates one or more of these massless pseudoscalar bosons (denoted by a)

$$Q_A|P\rangle = |Pa\rangle + ... \tag{1.13}$$

and the interactions of such "Goldstone bosons" with each other and with other particles are found to vanish as the four-momentum goes to zero [13]. In QCD then, according to Goldstone's argument, one would expect three massless pseudoscalar states to exist there - one for each spontaneously broken SU(2) axial generator, which would be the Goldstone bosons of QCD. Examination of the particle data tables reveals, however, that no such massless 0^- particles exist. There exists three $(2^2 - 1)$ 0^- particles - π^+, π^0 and π^- (for 2-flavor QCD) which are much lighter than their hadronic siblings. However, these states are certainly not massless and this causes us to ask what has gone wrong with what appears to be rigorous reasoning. The answer is found in the feature that our discussion thus far has neglected the piece of the QCD Lagrangian which is associated with quark mass. The actual masses of these Nambu Goldstone Bosons (NGBs) are obtained in chiral perturbation theory through an expansion in the (small) actual masses of the quarks.

Hence the summary of this section is that the appearance of pions as massless (approximately) NGBs and non appearance of parity doublets in degenerate states are two crucial outcome of spontaneous chiral symmetry breaking.

1.2 Chiral condensate

It is a general result that for any operator P, if

$$\langle 0|[Q, P]|0\rangle \neq 0 \tag{1.14}$$

then this expectation value is an order parameter of the symmetry generated by Q. Introducing $P^b = \overline{\psi}\gamma^5\tau^b\psi$ we get

$$[Q_A^a, P^b] = -\delta^{ab}\overline{\psi}\psi \tag{1.15}$$

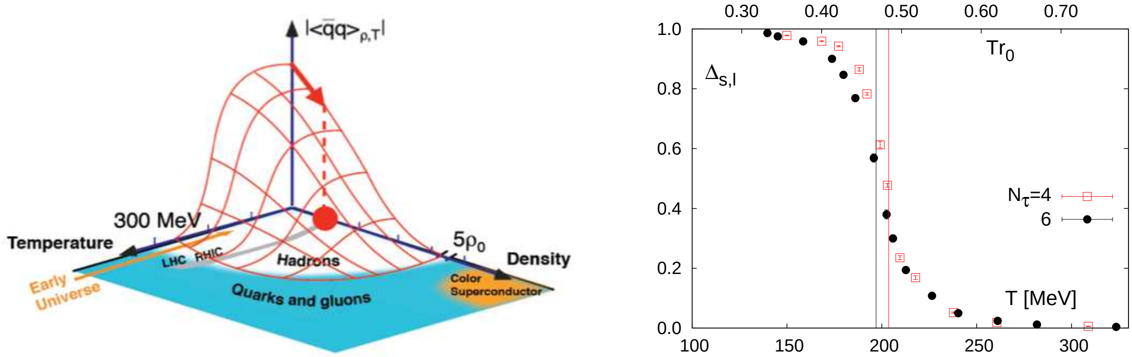

Figure 1.3: Left : Variation of the quark condensate $\langle 0|\overline{\psi}\psi|0\rangle$ in T-ρ plane [18]. Right : LQCD results of the chiral condensate as a function of temperature, taken from [19].

and so

$$Q_A^a|0\rangle \neq 0$$
$$\Rightarrow \langle 0|\overline{\psi}\psi|0\rangle \neq 0. \tag{1.16}$$

The chiral condensate, as it is called, is the order parameter and its non-zero value indicates the spontaneous breaking of chiral symmetry. Its value can be obtained from the Gell-Mann-Oakes-Renner relation [14]

$$m_\pi^2 F_\pi^2 = -(m_u + m_d)\langle 0|\overline{\psi}\psi|0\rangle + O(m_{u,d}^2) \tag{1.17}$$

which relates the pion mass and decay constant to the symmetry breaking parameters, $\langle 0|\overline{\psi}\psi|0\rangle$ (spontaneous) and $m_{u,d}$ (explicit). For $F_\pi = 93$ MeV obtained from $\pi^+ \to \mu^+\nu_\mu$ decay, one gets $\langle 0|\overline{\psi}\psi|0\rangle \simeq -(250\text{MeV})^3$ indicating that the strength of spontaneous symmetry breaking is quite large. Such vacuum expectation values of other scalar operators e.g. $\langle 0|G_{\mu\nu}G^{\mu\nu}|0\rangle$ etc. serve to parameterize the QCD vacuum and their values cannot be estimated perturbatively. In the relativistic collisions of heavy ions the vacuum structure of QCD is expected to undergo a strong modification which in turn will be manifested through the temperature and/or density dependence of the condensates [15]. A first estimate can be obtained by means of a virial expansion, approximating the hot and dense medium produced in such collisions by a non-interacting gas of pions and nucleons [16, 17]. The thermal average of the chiral condensate in the chiral limit ($m_\pi = 0$) can be expressed as

$$\langle\overline{\psi}\psi\rangle_\beta = \langle 0|\overline{\psi}\psi|0\rangle(1 - \frac{T^2}{8F_\pi^2} - \frac{\rho}{3\rho_0}) \tag{1.18}$$

where ρ_0 is the nuclear saturation density. The value of the chiral condensate thus decreases with temperature T and baryon density ρ which has been pictorially shown in Fig (1.3). Here one sees that at high enough temperature T and/or density ρ, the quark condensate $\langle\overline{\psi}\psi\rangle_\beta$ drops to zero [20, 21]. At normal nuclear densities ($\rho = \rho_0$) and $T = 0$ (i.e. the center of a heavy nucleus) the condensate has dropped by almost 35%. This corresponds to partial restoration of chiral symmetry. Gerber and Leutwyler [22] have evaluated this quantity up to and including terms of $O(T^6)$ using effective field theory to find that the value of the condensate at $T \sim 160$ MeV is about half its vacuum value. Lattice simulations of QCD thermodynamics show a substantial change in the energy and entropy density within a narrow temperature range around $T_c = 170$ MeV. This is accompanied by a rapid decrease followed by vanishing of the value of the chiral condensate indicating that chiral symmetry is restored in the Wigner-Weyl mode [23]. The order of the transition and the value of T_c however, depends on the number of flavors as well as the value of the current quark mass.

Now the question is that how can we measure this in-medium change of chiral condensate $\langle\overline{\psi}\psi\rangle_\beta$? Experimentally, this chiral order parameter can not be measured directly. Despite the fact that the condensate is not an experimental observable, it is hardly conceivable that such a strong modification of the QCD vacuum should not have spectacular consequences on hadronic properties, namely on the hadronic spectral functions. In next section we will focus on the hadronic spectral function in vacuum and in medium.

1.3 Hadronic spectral function

In vacuum all hadrons except proton (almost a stable particle) live for a very short time interval, quantified by mean life time (τ) and they decay to other hadrons or leptons. These daughter particles may decay further and successive processes will continue still they disintegrate to some stable particles (proton, electron, neutrino etc.). To describe this unstable nature of hadrons let us start from the basic quantum mechanical description of decay phenomena. The exponential decay law can be beautifully constructed by considering a non-stationary wave function [24] of parent hadron (H). For a certain mean life time $\tau = \frac{1}{\Gamma_d}$ (Γ_d is called decay width of H) and energy $\omega \simeq m_H$ (m_H is mass

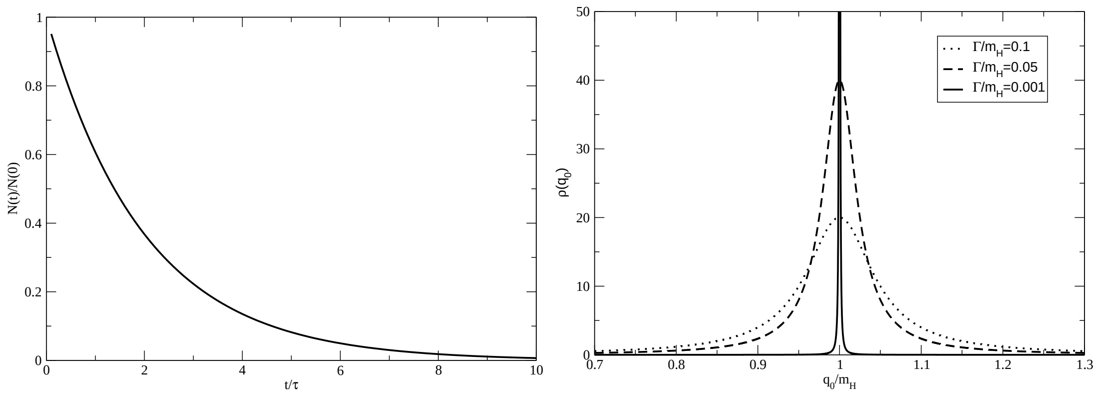

Figure 1.4: Probability in time (left) and energy (right) for unstable particle
.

of H), the wave function of the H is

$$\psi(t) = \psi(0)e^{-i\omega t}e^{-\frac{\Gamma_d t}{2}} \tag{1.19}$$

Hence the decay probability of unstable particle will be

$$\frac{N(t)}{N(0)} = \frac{|\psi(t)|^2}{|\psi(0)|^2} = e^{-\Gamma_d t} \tag{1.20}$$

which represents the famous exponential decay law. Taking Fourier transformation of the wave function from time variable (t) to energy variable (q_0), the probability exhibits a Breit-Wigner distribution as a function of q_0

$$\begin{aligned} \frac{|\widetilde{\psi}(q_0)|^2}{|\widetilde{\psi}(\omega)|^2} &= \frac{\Gamma_d^2/4}{(q_0-\omega)^2+\Gamma_d^2/4} \\ &= \frac{\Gamma_d}{2}\varrho(q_0) \end{aligned} \tag{1.21}$$

where

$$\varrho(q_0) = -\mathrm{Im}\frac{1}{q_0-\omega+i\Gamma_d/2} \tag{1.22}$$

Left panel of Fig. (1.4) shows the exponential decay probability with time (t) where x-axis is normalized by mean life time (τ). The right panel of the figure shows the Breit-Wigner type probability distribution as a function of energy. From this figure we see as we decrease Γ_d or increase τ, the function becomes narrower and in the zero width limit, it becomes a delta function

$$\lim_{\Gamma_d\to 0}\varrho(q_0) = \pi\delta(q_0-\omega) \tag{1.23}$$

In QFT the spectral function appears as a consequence of the Kallen-Lehman representation of the two point function of local fields. The Feynman propagator $-i\Delta(q^2)$ is defined as the time ordered product of two point functions of fields

$$\begin{aligned}\text{i.e. } \Delta(q^2) &= i\int d^4x e^{iq\cdot x}\langle 0|\mathcal{T}\phi(x)\phi(0)|0\rangle \\ &= i\int d^4x e^{iq\cdot x}\{\theta(x_0)\langle 0|\phi(x)\phi(0)|0\rangle + \theta(-x_0)\langle 0|\phi(0)\phi(x)|0\rangle\} \quad (1.24)\end{aligned}$$

To dissect the two point function $\langle 0|\mathcal{T}\phi(x)\phi(0)|\rangle$, we will insert the identity operator, in the form of a sum over a complete set of states, between $\phi(x)$ and $\phi(0)$.

$$\begin{aligned}\Delta(q^2) = i\int d^4x e^{iq\cdot x}\sum_n\int \frac{d^3p}{(2\pi)^3}\frac{1}{2\omega_p(n)}\{\theta(x_0)\langle 0|\phi(x)|n_p\rangle\langle n_p|\phi(0)|0\rangle \\ + \theta(-x_0)\langle 0|\phi(0)|n_p\rangle\langle n_p|\phi(x)|0\rangle\} \quad (1.25)\end{aligned}$$

where the identity operator is

$$\mathbf{1} = \sum_n\int \frac{d^3p}{(2\pi)^3}\frac{1}{2\omega_p(n)}|n_p\rangle\langle n_p| \quad (1.26)$$

The sum runs over all states with arbitrary number of particles with an integration over all the particle momenta in each of the multi-particle states. These states are eigenstates of the energy-momentum operator $\hat{p^\mu}$,

$$\hat{p^\mu}|n_p\rangle = |n_p\rangle p_n^\mu \quad (1.27)$$

Using the relation $\phi(x) = e^{ip\cdot x}\phi(0)e^{-ip\cdot x}$ and Eq. (1.27) in Eq. (1.25), we have

$$\Delta(q^2) = i\int d^4x\sum_n\{\theta(x_0)e^{i(q-p_n)\cdot x}|\langle 0|\phi(0)|n_p\rangle|^2 + \theta(-x_0)e^{i(q+p_n)\cdot x}|\langle 0|\phi(0)|n_p\rangle|^2\} \quad (1.28)$$

which after some simplification gives

$$\Delta(q^2) = \int_0^\infty \frac{dq'^2}{2\pi}\varrho(q'^2)\frac{-1}{q^2 - q'^2 + i\eta} \quad (1.29)$$

for which

$$\varrho(q^2) = 2\mathrm{Im}\Delta(q^2) \quad (1.30)$$

where $\varrho(q'^2)$ is a positive spectral function,

$$\varrho(q'^2) = \sum_n(2\pi)\delta(q'^2 - m_n^2)|\langle 0|\phi(0)|n_p\rangle|^2 \quad (1.31)$$

This general representation of interacting propagator is known as the Kallen-Lehmann representation. In free field theory the spectral function is just a delta function whereas in interacting field theory, the spectral function contain all possible intermediate quantum fluctuation in between two points. These are quantified by the self-energy $\Pi_{\rm vac}$ in terms of which the interacting propagator (Δ)is obtained by solving the Dyson's equation,

$$\Delta = \Delta_0 - \Delta_0 \Pi_{\rm vac} \Delta, \quad \Delta_0 = \frac{-1}{q^2 - m_H^2 + i\eta} \tag{1.32}$$

which gives

$$\Delta = 2{\rm Im} \frac{-1}{q^2 - m_H^2 - \Pi_{\rm vac}} \tag{1.33}$$

Hence

$$\varrho(q) = 2{\rm Im} \frac{-1}{q^2 - m_H^2 + i\{-{\rm Im}\Pi_{\rm vac}(q)\}} \tag{1.34}$$

Comparing with the quantum mechanical expression (1.22), we see that the quantity ${\rm Im}\Pi_{\rm vac}(q)$ (Imaginary part of vacuum self-energy) is related to the decay width and is given by

$${\rm Im}\Pi_{\rm vac}(q = m_H) = m_H \Gamma_d \tag{1.35}$$

Now in presence of medium the unstable hadrons H may collide with other thermalized particles and its collision rate ($\Gamma_{col} = \rho\sigma v$, where ρ is density of the medium, σ is the cross section of H with other thermalized particles and v is the velocity of H.) adds to the decay rate Γ_d so as to attenuate the probability amplitude more rapidly. Thus the exponential attenuation factor become $e^{-(\Gamma_d + \Gamma_{col})t/2}$. Simultaneously the spectral profile will be wider in medium compare to vacuum. In QFT at finite temperature these two contributions appear automatically. The expression of self-energy at finite temperature can be written as

$$\Pi = \Pi_{\rm vac} + \Pi_{\rm med} \tag{1.36}$$

which will be elaborately discussed in Ch. 3. The total self-energy depends on the medium parameter (temperature, density) along with the momentum. Through an explicit calculation of QFT at finite temperature, one can get a modified spectral profile of hadrons in thermal bath.

1.4 Probing the in-medium spectral properties of hadrons via heavy ion collision

Our aim is to characterize strongly interacting matter by investigating the spectral function of a hadron when it propagates through hot and dense matter. Colliding heavy ions at ultra-relativistic energies, $E_{lab} >> m_N$, is the only way to produce and study bulk properties of the strongly interacting matter which last existed naturally almost 14 billion years ago, a few microseconds after the Big Bang. Several large-scale experiment at ultra-relativistic bombarding energies have been conducted over the past twenty years to study this form of matter. Matter at large density but moderate temperatures (SIS,BEVALAC) or matter at both large density and temperature (AGS) can be generated in these experiments. From SPS (at CERN) to RHIC (at BNL) to LHC (at CERN) the center of mass energy per nucleon has increased from $\sqrt{s} = 17.3$ GeV to $\sqrt{s} = 200$ GeV to $\sqrt{s} = 5.5$ TeV producing matter with high temperature and low baryon density. Therefore, a large region of the QCD phase diagram can be investigated through the variation of the colliding energy. In collisions of two nuclei at ultra-relativistic energies, a large amount of energy is deposited in a small region of space in a short duration of time. In this region, the energy density is therefore very large (of the order of few GeV/fm^3). This energy density, an order of magnitude greater than the energy density of nuclear matter in equilibrium, may favor the formation of a new form of matter such as Quark-Gluon Plasma. This kind of quark-hadron phase transition has been essentially confirmed by numerical QCD lattice calculation at finite temperature. There are some interesting phenomena which have received special importance in the QGP. Some of them are discussed below.

(1) Jet quenching : When two protons collide at high energies, pairs of their constituent quarks or gluons may collide with each other and scatter back to back, quickly breaking up again into jets or spray of particles such as pions and kaons. If the jets propagate through a medium formed after the nuclear collision due to multiple scattering, they suffer further interaction with the medium and loss their energy. This parton energy loss is referred to as jet quenching [25, 26] and provides fundamental information on the thermodynamical and transport properties of the traversed medium. Results from nucleus-nucleus collisions at the RHIC [27, 28] have shown evidence for the quenching

effect through the suppression of inclusive high p_T hadron production.

(2) J/ψ suppression : Suppression of J/ψ production in high energy heavy ion collisions relative to p-p collisions is considered as a signature of QGP. This was pointed out almost 30 years ago by Matsui and Satz [29]. In the hot QGP environment, the quark and gluon move freely and due to Debye screening of color charges the string tension vanishes. Hence the interaction between the $c\overline{c}$ quarks will be too weak to dissociate in medium. Again the probability of forming a c quark ($\sim e^{-m_c/T}$)is less than that of lighter quark ($q = u, d, s$) ($\sim e^{-m_q/T}$). For charm and anti-charm quarks traveling through the plasma, the abundance of u, d, s quarks and anti-quarks results in a high possibility that the c and $\overline{c}$ can hadronize by combining with the light quarks and anti-quarks forming open charm particles, which will result in the suppression of J/ψ in QGP.

(3) Elliptic flow : In non-central heavy-ion collisions, the initial spatial anisotropy of the almond shape overlap region of the colliding nuclei is transformed into an anisotropy in momentum space through interactions between the particles. As the system expands, anisotropy is reduced and the system becomes more spherical, thus the driving force quenches itself. The azimuthal momentum anisotropy [30] of particle emission from non-central heavy-ion collisions can be quantified as the coefficients of the Fourier expansion

$$\frac{dN}{p_T dp_T d\phi dy} = \frac{dN}{2\pi p_T dp_T dy}[1 + 2\sum_{n=1}^{\infty} v_n \cos\{n(\phi - \psi)\}] \tag{1.37}$$

where ϕ is the azimuthal angle of the particle and ψ is the angle subtended by the reaction plane containing the beam axis and impact parameter with x-direction. The second coefficient of the expansion, v_2 , is usually referred to as elliptic flow.

Typical heavy-ion collision is believed to evolve as follows. Two Lorentz-contracted nuclei approach each other at close to the speed of light until primordial nucleon-nucleon collisions occur. After subsequent re-interactions for $\tau_0 = 0.5 - 1$fm/c the Quark-Gluon Plasma (QGP) is supposedly created. Driven by the pressure gradient the QGP expands and cools (for a duration of $\tau_{\rm QGP} \sim 3 - 5$fm/c). The hadronization then follows with further expansion in the hadronic phase until the chemical freeze-out point when inelastic interactions cease and particle abundances get frozen. Further expansion/cooling proceeds until kinetic freeze-out when elastic interactions stop and particle transverse momentum spectra gets fixed. The total fireball lifetime is approximately $10 - 15$fm/c depending on the beam energy. Hence the modified hadrons come to the detector (after traversing a long path compared to the dimension of the hot matter) carrying only the information of freeze out surface. They loose in-medium information of the matter in early stages (*i.e.* before freeze out). Instead of hadronic probes, electromagnetic probes (dileptons and photons) are considered to be superior in order to extract the in-medium information from the interior of the matter. Their interaction rate in the strongly interacting matter is small enough for them to escape the interior of the matter unaffected.

In the nineties, enhancement of dilepton production in heavy ion collisions at low invariant mass as compared to conventional hadronic cocktails (see Fig. 1.5) was first observed. The pioneering experiments on dilepton, which exhibited such kind of enhancement, started in the late 1980's at the Lawrence Berkeley Laboratory with DLS (Dilepton Spectrometer) [31, 32, 33] and at the CERN SPS with the CERES [34] and HELIOS [35] detector system in the energy ranges of $\sqrt{s}$ = 2-3 GeV and 17 GeV, respectively. A number of authors have analyzed the dilepton spectra from heavy ion collisions; the treatments differing both in the construction of the ρ spectral function as well as the space time evolution scenario employed. This includes the nature of phase transition, the equation of state as well as numerical values of the parameters like the initial temperature, the thermalisation time, the phase transition temperature as well as the chemical and kinetic freeze-out temperatures. We do not attempt to review or summarize the considerable amount of work which has been done on this topic except to mention the most recent few. The NA60 experiment at the CERN SPS measured dimuon pairs in In-In collisions in which an excess was observed over the contribution from hadronic decays at freeze-out in the mass region below the ρ peak [36]. This was attributed to the broadening of the ρ in hot and dense medium [37, 38], in contrast to the earlier data from the CERES collaboration [39] which is unable to differentiate between the broadening and the pole shift of the ρ spectral function [40]. The NA60 data for the entire (measured) invariant mass range is reproduced by taking into account dilepton productions from Drell-Yan processes, $q\bar{q}$ annihilation, thermally broadened in-medium ρ, decays of ρ at the freeze-out surface and primordial ρ produced from the initial hard scattering [41]. The dilepton yield evaluated with the in-medium spectral functions of ρ and ω mesons deduced from empirical forward scattering amplitudes [42]

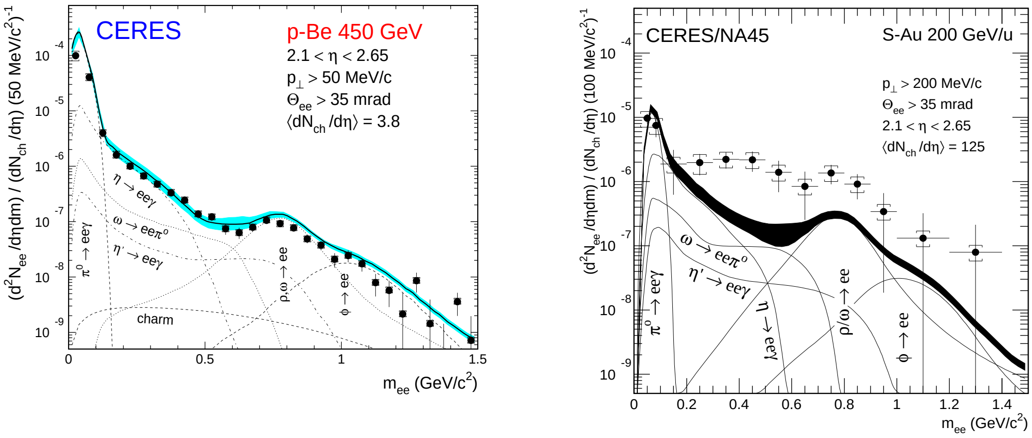

Figure 1.5: Dilepton spectra from heavy-ion collisions as measured by the CERES/NA45 collaboration. Data of P-Be collisions (Left) can be reproduced by the hadronic cocktail contributions as extrapolated from hadron multiplicities in p+p data but this cocktail fitting fail to reproduce the data of S+Au collisions (Right). The plot is taken from [39].

does not reproduce the data well at the low invariant mass ($M < 0.5$ GeV) region. The PHENIX experiment reported a substantial excess of electron pairs in the same region of invariant mass [43]. The data has been investigated by several groups e.g. [44, 45, 46]. The yield in all these cases have remained insufficient to explain the PHENIX data [47]. Thus the issue of low mass lepton pair yield still remains an unsettled issue.

We have done an explicit thermal field theoretical calculation of in-medium spectral functions of light vector mesons (ρ and ω). By coupling their spin averaged spectral strength with dilepton channels and convoluting that static rate by hydrodynamical space time evolution with appropriate initial conditions, we have carried out a detailed investigation of the low mass dilepton yield in heavy ion collisions.

1.5 Organization of the thesis

The thesis is organized as follows. In Chapter 2, we have derived propagator at finite temperature in the formalism of thermal field theory (QFT at finite temperature). We have used the real time formalism of thermal field theory. Starting from spin 0 and spin $\frac{1}{2}$ propagator we have written down a general form of propagator in vacuum as well as in medium. In the last section of this chapter we have provided the Dyson-Schwinger form of spectral function for propagator of spin 0, $\frac{1}{2}$ and 1. Chapter 3 is devoted to a general evaluation of one-loop self-energy at finite temperature in real time thermal field theory. At the end of this general calculation we have discussed each special cases where we can notice the differences in the phase space part. Associated branch cuts in the one loop self-energy and their diagrammatic interpretation are discussed. In the chapters 4 and 5 we have discussed one-loop self-energy of two light vector mesons (spin 1) - ρ and ω. We have provided a unified description of the various sources modifying their propagation in a meson and baryon gas at finite temperature and density. In the baryonic loops, we have considered an exhaustive set of spin one-half and three-half 4-star resonances. These modified spectral function of ρ and ω leads to a large enhancement (mostly due to ρ modification) of dilepton production below the bare peak of the rho. This has been shown in Chapter 6. The integrated dilepton yield after space-time evolution using relativistic hydrodynamics with quark gluon plasma in the initial state leads to very good agreement with the experimental data from In-In collisions obtained by the NA60 collaboration. Effective temperatures are extracted from the inverse slope of the transverse mass distributions for various invariant mass windows of dileptons and they may be used to characterize the partonic phase. In next two chapters (Ch 7 and 8) we have studied the in-medium properties of two more hadrons - nucleon (spin $\frac{1}{2}$) and D meson (spin 0). In Chapter 8 we have also studied the transport properties of D as well as B mesons. Chapter 9 contains the thesis summary and related discussions.

Chapter 2

Propagators in real-time thermal field theory

In the macroscopic classical world, the idea of propagation of a particle from one point to another is very simple as the Hamiltonian of the particle predictively determine its certain trajectory, which can be compared with our experience of daily life. But when we go to the microscopic quantum world, it becomes very hard to visualize the picture of propagation because the particle, owing to Heisenberg's uncertainty principle, does not follow any certain trajectory. Only a probabilistic description can be proposed for this particle[1]. Now if this particle is propagating with very high velocity then along with the probabilistic features one has to incorporate the idea of special theory of relativity where the mass of the propagating particle can be more than the mass of the particle at rest. The quantum mechanical evolution operator, e^{-iHt} gives the probability of a state after time t, where H is the Hamiltonian operator of the particle which gives an energy eigenvalue E after operating on the state in momentum space. In non-relativistic and relativistic cases, the energy eigenvalues of the free particle propagating with momentum $\vec{q}$ are $E = \frac{\vec{q}^2}{2m}$ and $E = \sqrt{\vec{q}^2 + m^2}$ respectively. The probability amplitudes for a free particle propagating from $x(= t_x, \vec{x})$ to $y(= t_y, \vec{y})$ for the two cases are given by [49]

$$\begin{aligned} G(t_x, t_y, \vec{x}, \vec{y}) &= \langle y| e^{-iH(t_y - t_x)} |x\rangle \\ &\sim e^{\frac{im(\vec{y}-\vec{x})^2}{2(t_y - t_x)}} \qquad \text{for } E = \frac{\vec{q}^2}{2m} \\ &\sim e^{im(\vec{y}-\vec{x})^2 - (t_y - t_x)^2} \qquad \text{for } E = \sqrt{\vec{q}^2 + m^2} \end{aligned} \tag{2.1}$$

[1]In fact, our classical trajectory in the macroscopic world may be considered as a net result of all possible probabilistic paths in microscopic domain by using the unitarity of quantum mechanics [48].

The above relations show for $(\vec{y}-\vec{x}) > (t_y - t_x)$ i.e. in the space-like region, the probability amplitude is non-zero which means that probabilities of a particle at two points can be communicated by a signal with speed faster than the speed of light. In other word causality is violated in this description. Interestingly, the causality violation can not be cured even using the relativistic energy momentum relation. This may suggest us to proceed from one particle description to many particle relativistic quantum mechanical description (i.e. quantum field theory). Quantum Field Theory (QFT) solves this causality problem in a miraculous way. The commutation of fields at two points is an appropriate quantity to check whether the measurements at two points outside the light cone are affected by each other or not. This commutator can be expressed as

$$\langle 0|[\phi(x),\phi(y)]|0\rangle = -i\Delta^+(x-y) - \{-i\Delta^-(x-y)\} \tag{2.2}$$

where

$$\begin{aligned} -i\Delta^+(x-y) &= \langle 0|\phi(x)\phi(y)|0\rangle = \int \frac{d^3q}{(2\pi)^3 2\omega} e^{-iq(x-y)} \\ -i\Delta^-(x-y) &= \langle 0|\phi(y)\phi(x)|0\rangle = \int \frac{d^3q}{(2\pi)^3 2\omega} e^{iq(x-y)} \end{aligned} \tag{2.3}$$

are positive and negative energy solutions of Klein-Gordon equation (for scalar field, ϕ) with delta current source. These two quantities $\Delta^+(x-y)$ and $\Delta^-(x-y)$ in space-like region are individually non-zero ($\Delta^{\pm}(x-y)|_{t_y-t_x\to 0} \sim e^{m|\vec{y}-\vec{x}|}$) but in Eq. (2.2) they cancel each other. So the causality is preserved in QFT and the new theoretical outcome is the negative energy solution or antiparticle. This negative energy propagation is basic to restore causality because it absorbs the positive energy propagation in space-like region. In this way we get a mathematical expression of causal propagation of a relativistic particle in the microscopic world.

2.1 Free vacuum propagator

In QFT, the intrinsic spin of the particle is included in the field operator. The expressions of field operators as well as their corresponding Euler-Lagrange equations are different for particles with different spin and therefore their corresponding propagation amplitudes are also different. We will start this section with the derivation of vacuum propagator for only spin 0 (scalar) particle and spin 1/2 (fermion) particle. At the end of the section we will write down the propagator for particles with spin 0, 1/2, 1, 3/2 in a general spectral representation.

2.1.1 Scalar propagator

Let us familiarize ourselves with three kinds of forms of propagator- (1) Retarded propagator, (2) Advanced propagator and (3) Feynman propagator which are generally used in QFT. Only for scalar particle we will derive these forms as for other particles only numerator part, containing the spin sum states, has to be changed.

The propagator are defined in terms of commutation relation of field operators at two points with different time ordering. These three kinds of propagator can mathematically be expressed as [49, 50]

$$-i\Delta_R(x-y) = \theta(t_x - t_y)[\langle 0|\phi(x)\phi(y)|0\rangle - \langle 0|\phi(y)\phi(x)|0\rangle] \tag{2.4}$$

$$-i\Delta_A(x-y) = \theta(t_y - t_x)[\langle 0|\phi(x)\phi(y)|0\rangle - \langle 0|\phi(y)\phi(x)|0\rangle] \tag{2.5}$$

and

$$\begin{aligned} -i\Delta_F(x-y) &= \langle 0|\mathcal{T}[\phi(x)\phi(y)]|0\rangle \\ &= \theta(t_x - t_y)\langle 0|\phi(x)\phi(y)|0\rangle + \theta(t_y - t_x)\langle 0|\phi(y)\phi(x)|0\rangle \end{aligned} \tag{2.6}$$

All of them satisfy the Klein-Gordon Equation with (four-dimensional) point source,

$$(\Box_x^2 + m^2)\Delta(x-y) = \delta^4(x-y) \tag{2.7}$$

where Δ is a general expression for all the three propagators. Using the spatial Fourier's relations

$$\begin{aligned} \Delta(t_x - t_y, \vec{x} - \vec{y}) &= \int \frac{d^3\vec{q}}{(2\pi)^3} e^{i\vec{q}\cdot(\vec{x}-\vec{y})} \Delta(t_x - t_y, \vec{q}) \\ \delta^3(\vec{x} - \vec{y}) &= \int \frac{d^3\vec{q}}{(2\pi)^3} e^{i\vec{q}\cdot(\vec{x}-\vec{y})} \end{aligned} \tag{2.8}$$

in Eq. (2.7), we get

$$\begin{aligned} (\frac{\partial^2}{\partial t_x^2} - (i\vec{q})^2 + m^2)\Delta(t_x - t_y, \vec{q}) &= \delta(t_x - t_y) \\ \Rightarrow (\frac{\partial^2}{\partial t_x^2} + \omega^2)\Delta(t_x - t_y, \vec{q}) &= \delta(t_x - t_y) \end{aligned} \tag{2.9}$$

with $\omega = \sqrt{\vec{q}^2 + m^2}$. Here t_y will be treated as a spectator point. The solution of the equation

$$(\frac{\partial^2}{\partial t_x^2} + \omega^2)\Delta(t_x, t_y) = 0 \ , \qquad t_x \neq t_y \tag{2.10}$$

is

$$\begin{aligned} \Delta(t_x, t_y) &= A(t_y)e^{-i\omega t} + B(t_y)e^{i\omega t} \ , \qquad t_x > t_y \\ &= C(t_y)e^{-i\omega t} + D(t_y)e^{i\omega t} \ , \qquad t_x < t_y \end{aligned} \tag{2.11}$$

Feynman propagator Δ_F :

According to Feynman boundary conditions, the positive and negative frequencies should propagate for $t_x > t_y$ and $t_x < t_y$ respectively. Using the conditions in (2.11), we get

$$B(t_y) = C(t_y) = 0 \tag{2.12}$$

Another two boundary conditions [51] are

$$\begin{aligned} &A(t_y)e^{-i\omega t} = D(t_y)e^{i\omega t} \qquad \text{(as } \Delta(t_x, t_y) \text{ should be continuous at } t_x = t_y\text{)} \\ &A(t_y)(-i\omega)e^{-i\omega t} + D(t_y)(+i\omega)e^{i\omega t} = 1 \\ &\qquad \text{(as the discontinuity of } \frac{\partial}{\partial t_x}\Delta(t_x, t_y) \text{ at } t_x = t_y \text{ should be unity)} \end{aligned} \tag{2.13}$$

The solution satisfying the above boundary conditions is

$$\begin{aligned} \Delta_F(t_x, t_y) &= \frac{i}{2\omega}e^{-i\omega(t_x - t_y)} \ , \qquad t_x > t_y \\ &= \frac{i}{2\omega}e^{i\omega(t_x - t_y)} \ , \qquad t_x < t_y \end{aligned} \tag{2.14}$$

which can be combined (putting $t_y = 0$ and $t_x = t$) as

$$\Delta_F(t, \vec{q}) = \frac{i}{2\omega}[\theta(t)e^{-i\omega t} + \theta(-t)e^{i\omega t}] \tag{2.15}$$

Using the integral representation of the Heaviside step function,

$$\theta(t) = \pm i \lim_{\eta \to 0} \int_{-\infty}^{\infty} \frac{dq_0'}{2\pi} \frac{e^{\mp i q_0' t}}{q_0' \pm i\eta} \ , \tag{2.16}$$

Eq. (2.15) can be evaluated as

$$\begin{aligned} \Delta_F(t, \vec{q}) &= \frac{i}{2\omega}[i \int \frac{dq_0'}{2\pi} \frac{e^{-i(q_0'+\omega)t}}{q_0' + i\eta} + i \int \frac{dq_0'}{2\pi} \frac{e^{-i(q_0'+\omega)(-t)}}{q_0' + i\eta}] \\ &= \int \frac{dq_0}{2\pi} e^{-i(q_0)t}(-\frac{1}{2\omega})[\frac{1}{q_0 - \omega + i\eta} - \frac{1}{q_0 + \omega - i\eta}] \\ &\quad \text{(using } q_0' = q_0 - \omega, \ - q_0 - \omega \text{ for first and second part of the integrand respectively)} \\ &= \int \frac{dq_0}{2\pi} e^{-i(q_0)t} \Delta_F(q^2) \end{aligned} \tag{2.17}$$

where

$$\Delta_F(q^2) = \frac{-1}{q^2 - m^2 + i\eta} \tag{2.18}$$

This is standard form of Feynman propagator in momentum space.

<u>Retarded propagator Δ_R</u> :

As neither positive nor negative energy should propagate for $t_x < t_y$ in retarded propagation, our second part of Eq. (2.11) will vanish

$$\text{i.e. } C(t_y) = D(t_y) = 0 \tag{2.19}$$

Similar to previous case, the others two constants, which are left, have to be fixed by the boundary conditions of continuity of amplitude and discontinuity of first derivative [51],

$$\begin{aligned} A(t_y)e^{-i\omega t_y} + B(t_y)e^{i\omega t_y} &= 0 \qquad\qquad \text{and} \\ A(t_y)(-i\omega)e^{-i\omega t_y} + B(t_y)(+i\omega)e^{i\omega t_y} &= 1 \end{aligned} \tag{2.20}$$

Determining the coefficients coming from the above relations and putting in Eq. (2.11) we have

$$\begin{aligned} \Delta_R(t_x, t_y) &= \frac{i}{2\omega}[e^{-i\omega(t_x - t_y)} - e^{i\omega(t_x - t_y)} \ , \qquad t_x > t_y \\ &= 0 \ , \qquad\qquad t_x < t_y \end{aligned} \tag{2.21}$$

i.e. (for $t_y = 0$ and $t_x = t$)

$$\Delta_R(t, \vec{q}) = \frac{i}{2\omega}\theta(t)[e^{-i\omega t} + e^{i\omega t}] \tag{2.22}$$

Taking the temporal Fourier's transformation of (2.22) by using the step function (2.16), we get retarded propagator in momentum space

$$\Delta_R(q^2) = \frac{-1}{q^2 - m^2 + i\epsilon(q_0)\eta} \tag{2.23}$$

<u>Advanced propagator Δ_A</u> :

Considering the propagation for $t_y > t_x$ (i.e. $A(t_y) = B(t_y) = 0$) and following the same procedure we can achieve the expression of advanced propagator in momentum space.

$$\Delta_A(q^2) = \frac{-1}{q^2 - m^2 - i\epsilon(q_0)\eta} \tag{2.24}$$

2.1.2 Fermion propagator

Fermion propagation is different from the boson propagation due to different quantization relations as well as the different equation of motions. Free Fermion field ψ is governed by the Dirac's equation

$$(i\partial\!\!\!/ - m)\psi = 0 \tag{2.25}$$

In the interaction picture there will be a current source on the right hand side of Eq. (2.25). The Green function is defined by the equation,

$$(i\partial\!\!\!/ - m)_{ab} S_F(x-y) = \delta^4(x-y) I_{ab}; \qquad a,\ b \text{ are Dirac indices} \tag{2.26}$$

where

$$\begin{aligned} -iS_F(x-y) &= \langle 0|\mathcal{T}\{\psi_a(x)\overline{\psi}_b(y)\}|0\rangle \\ &= \theta(t_x - t_y)\langle 0|\psi_a(x)\overline{\psi}_b(y)|0\rangle - \theta(t_y - t_x)\langle 0|\overline{\psi}_b(y)\psi_a(x)|0\rangle \end{aligned} \tag{2.27}$$

Straight forward spinor algebra of fermion field give us

$$\begin{aligned} \langle 0|\psi_a(x)\overline{\psi}_b(y)|0\rangle &= \int \frac{d^3q}{(2\pi)^3 2\omega} \sum_s u_a^s(q)\overline{u}_b^s(q) e^{-iq(x-y)} \\ &= (i\partial\!\!\!/ + m)_{ab} \int \frac{d^3q}{(2\pi)^3 2\omega} e^{-iq(x-y)} \qquad \text{as } \sum_s u_a^s(q)\overline{u}_b^s = (q\!\!\!/ + m)_{ab} \end{aligned} \tag{2.28}$$

$$\begin{aligned} \langle 0|\overline{\psi}_b(y)\psi_a(x)|0\rangle &= \int \frac{d^3q}{(2\pi)^3 2\omega} \sum_s v_a^s(q)\overline{v}_b^s(q) e^{iq(x-y)} \\ &= -(i\partial\!\!\!/ + m)_{ab} \int \frac{d^3q}{(2\pi)^3 2\omega} e^{iq(x-y)} \qquad \text{as } \sum_s v_a^s(q)\overline{v}_b^s = (q\!\!\!/ - m)_{ab} \end{aligned} \tag{2.29}$$

So we can express the fermion propagator in terms of scalar propagator as

$$S_F(x-y) = (i\partial\!\!\!/ + m)\Delta_F(x-y) \tag{2.30}$$

From Eq. (2.17) we can write

$$\begin{aligned} \Delta_F(x-y) &= \int \frac{d^3\vec{q}}{(2\pi)^3} e^{i\vec{q}\cdot(\vec{x}-\vec{y})} \Delta_F(t_x - t_y, \vec{q}) \\ &= \int \frac{d^4\vec{q}}{(2\pi)^4} e^{-iq(x-y)} \Delta_F(q^2) \end{aligned} \tag{2.31}$$

and putting it in Eq.(2.30) we will get

$$S_F(x-y) = \int \frac{d^4\vec{q}}{(2\pi)^4} e^{-iq(x-y)} S_F(q) \tag{2.32}$$

where

$$S_F(q) = (\not{q} + m)\Delta_F(q) \tag{2.33}$$

<u>**General representation of vacuum propagator**</u> **:**

Getting motivation from the Eq. (2.18) and (2.33), we can write a general representation of the propagator[2] of a particle with any spin as

$$P(q) = \zeta(q)\Delta_F(q) \tag{2.34}$$

where ζ is the sum of spin states of the particle and its expression for different spin particles are given below

$$\begin{aligned} \zeta(q) &= 1\ , && S=0 \\ &= (\not{q}+m)\ , && S=\frac{1}{2} \\ &= (-g^{\mu\nu} + \frac{q^\mu q^\nu}{m^2})\ , && S=1 \\ &= (\not{q}+m)(\{-g_{\mu\nu} + \frac{2}{3m^2}q_\mu q_\nu + \frac{1}{3}\gamma_\mu\gamma_\nu + \frac{1}{3m}(\gamma_\mu q_\nu - \gamma_\nu q_\mu)\})\ , && S=\frac{3}{2} \end{aligned} \tag{2.35}$$

In spectral representation they can be expressed as

$$P(q) = \int \frac{dq_0'}{2\pi} \frac{\varrho(q_0', \vec{q})}{q_0' - q_0 - i\eta\epsilon(q_0)} \tag{2.36}$$

where

$$\varrho(q_0', \vec{q}) = 2\pi\epsilon(q_0')\zeta(q_0', \vec{q})\delta({q_0'}^2 - \omega^2) \tag{2.37}$$

represent the general form of free spectral function.

2.2 Free propagator at finite temperature

Let us proceed to quantum field theory at finite temperature after briefly recapitulating quantum statistical mechanics. According to quantum mechanical ensemble theory, the

[2]The propagator defined in Feynman rule is exactly equal to $-iP(q)$.

expectation value of any physical quantity A, which is dynamically represented by an operator $\hat{A}$, is given by

$$\langle A \rangle = \frac{1}{N} \sum_{k}^{N} \langle \psi_k^* | \hat{A} | \psi_k \rangle \tag{2.38}$$

where $|\psi_k(t)\rangle$ denotes the physical state in which the kth system of the ensemble happens to be at time t and $k = 1, 2, ..N$ for an ensemble of N identical systems.

In this theory, density matrix (ρ_{mn}) is the most important quantity which involves a double averaging process - once due to probabilistic aspect of the quantum mechanical states and again due to statistical aspect of the ensemble. The statistical average is clearly seen in (2.38). The information of quantum average can be understood if we expand the $|\psi_k(t)\rangle$ as

$$|\psi_k(t)\rangle = \sum_n a_n^k(t) |\phi_n\rangle \tag{2.39}$$

where $a_n^k(t)$ is coefficient giving the probability amplitude for kth system to be in the various orthonormal states $|\phi_n\rangle$. So Eq. (2.38) is now given by

$$\begin{aligned} \langle A \rangle &= \frac{1}{N} \sum_{k}^{N} [\sum_{m,n} a_n^{k*} a_m^k A_{nm}] \\ &= Tr(\hat{\rho}\hat{A}) \end{aligned} \tag{2.40}$$

where

$$\begin{aligned} A_{nm} &= \langle \phi_n | \hat{A} | \phi_m \rangle \\ \text{and } \rho_{mn} &= \frac{1}{N} \sum_{k=1}^{N} \sum_{m,n} a_m^k a_n^{k*} \end{aligned} \tag{2.41}$$

Depending upon the ensemble, the form of density matrix ($\hat{\rho}$) will be different. For example, in the canonical ensemble it has the form

$$\hat{\rho} = \frac{e^{-\beta \hat{H}}}{Z} \ , \quad Z = \mathrm{Tr} e^{-\beta \hat{H}}. \tag{2.42}$$

It is interesting to note that the quantum mechanical time evolution operator $e^{-i\hat{H}t}$ becomes the density operator by the replacement $t = -i\beta$. This analogy provides us with a way to incorporate the ensemble average by evolving the time parameter in complex plane instead of real axis only. This is the basis of the Thermal Field Theory (TFT) [52, 53, 54, 55, 56].

Region of analyticity : Instead of vacuum expectation value if we take thermal expectation value of the two point function of field operators, then the vacuum propagator will be transformed to thermal propagator. For scalar particle it is defined as[3]

$$\langle\phi(\tau_x,\vec{x})\phi(\tau_y,\vec{y})\rangle_\beta = \frac{1}{Z}\sum_m e^{-\beta E_m}\langle m|\phi(\tau_x,\vec{x})\phi(\tau_y,\vec{y})|m\rangle \tag{2.43}$$

which can be simplified as

$$\begin{aligned}\langle\phi(\tau_x,\vec{x})\phi(\tau_y,\vec{y})\rangle_\beta &= \frac{1}{Z}\sum_{m,n} e^{-\beta E_m}\langle m|\phi(\tau_x)|n\rangle\langle n|\phi(\tau_y)|m\rangle\ , \qquad \sum_n |n\rangle\langle n| = \hat{1}\\ &= \frac{1}{Z}\sum_{m,n} e^{-\beta E_m}\langle m|e^{i\hat{H}\tau_x}\phi(0)e^{-i\hat{H}\tau_x}|n\rangle\langle n|e^{i\hat{H}\tau_y}\phi(0)e^{-i\hat{H}\tau_y}|m\rangle\\ &= \frac{1}{Z}\sum_{m,n} e^{-iE_n(\tau_x-\tau_y)}e^{iE_m(\tau_x-\tau_y+i\beta)}\langle m|\phi(0)|n\rangle\langle n|\phi(0)|m\rangle \qquad (2.44)\end{aligned}$$

Note that the factor

$$\begin{aligned}e^{iE_m(\tau_x-\tau_y+i\beta)} &= e^{iE_m[Re(\tau_x-\tau_y)+i\{Im(\tau_x-\tau_y)+\beta\}]}\\ &= e^{iE_m Re(\tau_x-\tau_y)}e^{-E_m[Im(\tau_x-\tau_y)+\beta]} \qquad (2.45)\end{aligned}$$

has a non oscillatory part in complex τ-plane which must be exponentially damped in order that the correlation function is well behaved for $E_m \to \infty$. This is possible only when

$$\begin{aligned}&\mathrm{Im}(\tau_x-\tau_y)+\beta \geq 0\\ &\Rightarrow \mathrm{Im}(\tau_x-\tau_y) \geq -\beta \qquad (2.46)\end{aligned}$$

Similarly the factor

$$e^{-iE_n(\tau_x-\tau_y)} = e^{-iE_n Re(\tau_x-\tau_y)}e^{E_n Im(\tau_x-\tau_y)} \tag{2.47}$$

will be a damped only when

$$\mathrm{Im}(\tau_x-\tau_y) \leq 0 \tag{2.48}$$

Combining Eq. (2.48) and Eq. (2.46) we get the region of analyticity in τ-plane as

$$-\beta \leq \mathrm{Im}(\tau_x-\tau_y) \leq 0 \tag{2.49}$$

In real time formalism of thermal field theory, the contour is chosen so as to include the real axis.

[3]For representing complex time in TFT, we have replaced 't' by 'τ'. $\langle\ \rangle_\beta$ represents thermal average.

<u>KMS relation</u> :

The thermal propagator for a scalar field is given by

$$\begin{aligned}\Delta_F^\beta(x-y) &= \langle \mathcal{T}_c \phi(x)\phi(y)\rangle_\beta \\ &= \theta_c(\tau_x-\tau_y)\Delta_+^\beta(x-y)+\theta_c(\tau_y-\tau_x)\Delta_-^\beta(x-y)\end{aligned} \tag{2.50}$$

where $\mathcal{T}_c$ and θ_c denote respectively time ordering and step function with respect to the contour. The expressions of positive and negative energy propagation in medium having temperature $T=\frac{1}{\beta}$ are respectively given by

$$\begin{aligned}\Delta_+^\beta(x-y) = \langle\phi(x)\phi(y)\rangle_\beta = \frac{1}{Z}\sum_m \langle m|e^{-\beta H}\phi(x)\phi(y)|m\rangle \\ \Delta_-^\beta(x-y) = \langle\phi(y)\phi(x)\rangle_\beta = \frac{1}{Z}\sum_m \langle m|e^{-\beta H}\phi(y)\phi(x)|m\rangle\end{aligned} \tag{2.51}$$

These two quantities are linked by a relation, called Kubo Martin Schwinger(KMS) relation [57, 58, 52]

$$\Delta_+^\beta(\tau_x-\tau_y,\vec{x}-\vec{y}) = \Delta_-^\beta(\tau_x-\tau_y+i\beta,\vec{x}-\vec{y}) \tag{2.52}$$

2.2.1 Scalar propagator at finite temperature

The equation of motion of scalar propagator is given by

$$(\partial_c^2+m^2)\Delta_F^\beta(x-y) = \delta_c(\tau_x-\tau_y)\delta^3(\vec{x}-\vec{y}) \tag{2.53}$$

Proceeding with same strategy as for vacuum [recalling the Eq. (2.8) and Eq. (2.9)], we get the temporal part of differential equation as

$$(\frac{\partial^2}{\partial\tau_x^2}+\omega^2)\Delta_F^\beta(\tau_x-\tau_y,\vec{q}) = \delta_c(\tau_x-\tau_y) \tag{2.54}$$

and for $\tau_x \neq \tau_y$, we get same solution as Eq. (2.11) for vacuum case.

Using the KMS boundary condition (2.52) for scalar particle, we get relations among the coefficients of A, B, C and D as

$$\begin{aligned}A(\tau_y)e^{-\beta\omega} &= C(\tau_y) \\ B(\tau_y)e^{\beta\omega} &= D(\tau_y)\end{aligned} \tag{2.55}$$

The continuity and discontinuity boundary conditions at the spectator point give the values of rest of the unknowns,

$$\begin{aligned} A(\tau_y) &= \frac{i}{2\omega} e^{i\omega\tau_y}(1+n) \\ B(\tau_y) &= \frac{i}{2\omega} e^{-i\omega\tau_y} n \end{aligned} \tag{2.56}$$

with $n = \frac{1}{e^{\beta\omega}-1}$.

Using these, the positive and negative energy solutions of propagation amplitude in thermal bath can be expressed as

$$\begin{aligned} \Delta_+^\beta(\tau_x, \tau_y) &= \frac{i}{2\omega}[e^{-i\omega(\tau_x-\tau_y)}(1+n) + e^{i\omega(\tau_x-\tau_y)} n] \\ \Delta_-^\beta(\tau_x, \tau_y) &= \frac{i}{2\omega}[e^{-i\omega(\tau_x-\tau_y)} n + e^{i\omega(\tau_x-\tau_y)}(1+n)] \end{aligned} \tag{2.57}$$

So the scalar propagator at finite temperature is given by

$$\Delta_F^\beta(\tau_x, \tau_y, \vec{q}) = \frac{i}{2\omega}[e^{-i\omega(\tau_x-\tau_y)}(\theta_c(\tau_x - \tau_y) + n) + e^{i\omega(\tau_x-\tau_y)}(\theta_c(\tau_y - \tau_x) + n)] \tag{2.58}$$

2.2.2 Fermion propagator at finite temperature

We now derive fermion propagator at finite temperature and density. In this case the equation of motion is

$$(i\partial\!\!\!/_c - m) S_F^\beta(x-y) = \delta_c(\tau_x - \tau_y)\delta^3(\vec{x} - \vec{y}) \;\; \text{(omitting Dirac indices)} \tag{2.59}$$

Similar to the vacuum case, we can link the thermal fermion propagator with the scalar one by

$$S_F^\beta(x-y) = (i\partial\!\!\!/_c + m)\Delta_F^\beta(x-y) \tag{2.60}$$

and get the same equation as for scalar propagator i.e. Eq. (2.53). So guided by Eq. (2.58) we guess a most general solution as

$$\Delta_F^\beta(\tau_x, \tau_y) = \frac{i}{2\omega}[e^{-i\omega(\tau_x-\tau_y)}(\theta_c(\tau_x - \tau_y) - E) + e^{i\omega(\tau_x-\tau_y)}(\theta_c(\tau_y - \tau_x) - F)] \tag{2.61}$$

where E and F are two unknown coefficients being the functions of energy ω (the conjugate variable of τ). Using (2.61) in (2.60), we get

$$S_F^\beta(\tau_x, \tau_y) = (i\gamma^0\partial_0 + i\vec{\gamma}\cdot\vec{\bigtriangledown} + m)\int \frac{d^3\vec{q}}{(2\pi)^3}\frac{e^{i\vec{q}\cdot(\vec{x}-\vec{y})}}{2\omega}[e^{-i\omega(\tau_x-\tau_y)}(\theta_c(\tau_x - \tau_y) - E)$$

$$
\begin{aligned}
&\qquad\qquad + e^{i\omega(\tau_x-\tau_y)}(\theta_c(\tau_y-\tau_x)-F)] \\
&= \int \frac{d^3\vec{q}}{(2\pi)^3}\frac{e^{i\vec{q}\cdot(\vec{x}-\vec{y})}}{2\omega}[(\gamma^0\omega-\vec{\gamma}\cdot\vec{q}+m)e^{-i\omega(\tau_x-\tau_y)}(\theta_c(\tau_x-\tau_y)-E) \\
&\qquad\qquad + (-\gamma^0\omega-\vec{\gamma}\cdot\vec{q}+m)e^{i\omega(\tau_x-\tau_y)}(\theta_c(\tau_y-\tau_x)-F)] \\
&= \int \frac{d^3\vec{q}}{(2\pi)^3}e^{i\vec{q}\cdot(\vec{x}-\vec{y})}S_F^\beta(\tau_x,\tau_y,\vec{q})
\end{aligned}
\tag{2.62}
$$

where

$$
S_F^\beta(\tau_x,\tau_y,\vec{q}) = S_+^\beta(\tau_x,\tau_y,\vec{q})\theta_c(\tau_x-\tau_y) - S_-^\beta(\tau_x,\tau_y,\vec{q})\theta_c(\tau_y-\tau_x) \tag{2.63}
$$

with

$$
\begin{aligned}
S_+^\beta(\tau_x,\tau_y,\vec{q}) &= \frac{1}{2\omega}[(\gamma^0\omega-\vec{\gamma}\cdot\vec{q}+m)e^{-i\omega(\tau_x-\tau_y)}(1-E)+(-\gamma^0\omega-\vec{\gamma}\cdot\vec{q}+m)e^{i\omega(\tau_x-\tau_y)}(-F)] \\
S_-^\beta(\tau_x,\tau_y,\vec{q}) &= -\frac{1}{2\omega}[(\gamma^0\omega-\vec{\gamma}\cdot\vec{q}+m)e^{-i\omega(\tau_x-\tau_y)}(-E)+(-\gamma^0\omega-\vec{\gamma}\cdot\vec{q}+m)e^{i\omega(\tau_x-\tau_y)}(1-F)]
\end{aligned}
\tag{2.64}
$$

The KMS relation (2.52) for bosonic field identifies the coefficients E and F as Bose-Einstein distribution functions. So we proceed in similar way to identify Fermi-Dirac distribution function from the KMS relation for fermionic fields, which is given by

$$
S_+(\tau_x-\tau_y,\vec{x}-\vec{y}) = e^{-\beta\mu}S_-(\tau_x-\tau_y+i\beta,\vec{x}-\vec{y}) \tag{2.65}
$$

Applying this boundary condition in Eq. (2.63) and equating the coefficients of each oscillatory function ($e^{\pm i\omega(\tau_x-\tau_y)}$), we get $E=n_+$ and $F=n_-$, where $n_\pm = \frac{1}{e^{\beta(\omega\mp\mu)}+1}$ are the fermion and anti-fermion distribution function. So Eq. (2.63) now becomes

$$
\begin{aligned}
S_F^\beta(\tau_x,\tau_y,\vec{q}) = \frac{1}{2\omega}&[(\gamma^0\omega-\vec{\gamma}\cdot\vec{q}+m)e^{-i\omega(\tau_x-\tau_y)}(\theta_c(\tau_x-\tau_y)-n_+) \\
&+(-\gamma^0\omega-\vec{\gamma}\cdot\vec{q}+m)e^{i\omega(\tau_x-\tau_y)}(\theta_c(\tau_y-\tau_x)-n_-)]
\end{aligned}
\tag{2.66}
$$

So far we got Eq. (2.58) and Eq. (2.66) as the three-momentum dependent thermal propagator of Bosons and Fermions respectively in τ-plane which may be expressed in spectral representation as

$$
\Delta(\tau_x,\tau_y,\vec{q}) = i\int_{-\infty}^{\infty}\frac{dq_0'}{2\pi}\rho(q_0',\vec{q})e^{-iq_0'(\tau_x-\tau_y)}[\theta_c(\tau_x-\tau_y)+\{n\epsilon(q_0')-\theta(-q_0')\}] \tag{2.67}
$$

$$
S(\tau_x,\tau_y,\vec{q}) = i\int_{-\infty}^{\infty}\frac{dq_0'}{2\pi}\sigma(q_0',\vec{q})e^{-iq_0'(\tau_x-\tau_y)}[\theta_c(\tau_x-\tau_y)-\{(n_+\theta(q_0')+n_-\theta(-q_0'))\epsilon(q_0')+\theta(-q_0')\}] \tag{2.68}
$$

where

$$\rho(q_0', \vec{q}) = 2\pi\epsilon(q_0')\delta(q_0'^2 - \omega^2) \qquad \text{and} \tag{2.69}$$

$$\sigma(q_0', \vec{q}) = 2\pi\epsilon(q_0')(\gamma^0 q_0' + \vec{\gamma}\cdot\vec{q} + m)\delta(q_0'^2 - \omega^2) \tag{2.70}$$

are the bosonic and fermionic spectral function for free theory (i.e. no interaction is considered). We have already defined a general form of the free spectral function as $\varrho(q_0', \vec{q})$ in Eq. (2.37). The $\rho(q_0', \vec{q})$ and $\sigma(q_0', \vec{q})$ may be considered as particular cases of the $\varrho(q_0', \vec{q})$. So we can write the two expressions (2.67) and (2.68) in a single expression as

$$P(\tau_x, \tau_y, \vec{q}) = i\int_{-\infty}^{\infty} \frac{dq_0'}{2\pi}\varrho(q_0', \vec{q})e^{-iq_0'(\tau_x - \tau_y)}[\theta_c(\tau_x - \tau_y) + \epsilon_q f(q_0')] \tag{2.71}$$

where $\epsilon_q f(q_0') = \epsilon_q N_q \epsilon(q_0') - \theta(-q_0')$. In special cases,

$$\begin{aligned} \epsilon_q = +1, \quad N_q = n[\theta(q_0') + \theta(-q_0')] = n \quad \text{for boson} \\ \text{and} \;\; \epsilon_q = -1, \quad N_q = n_+\theta(q_0') + n_-\theta(-q_0') \quad \text{for fermion} \end{aligned} \tag{2.72}$$

with BE distribution n and FD distributions $n_\pm$. One can check that we can regain the Eq. (2.15)[4]by putting $N_q = 0$ (for T=0) as well as the free scalar spectral function in Eq. (2.71).

2.2.3 Free thermal propagator in general form

Here we are interested in the expression of Feynman propagator at finite temperature in four momentum space. So far we have established the relations for the spatial Fourier transforms of propagators keeping the time coordinate in the complex time plane. Of the variety of possible contours in the complex time plane [59], two are specially interesting, namely the closed one [60] and the symmetrical one [61].

We have chosen the latter contour (Fig.2.1) which begins from $-T$ (say) on the real axis and ends at $-T - i\beta$, nowhere moving upwards [62]. Our choice is that of Fig. (2.1), which for $T \to \infty$, reduces to two parallel lines, the real line and the one shifted by $-i\beta/2$, to be denoted by subscripts 1 and 2 respectively [63, 61]. Now along

[4]More generalized form of Eq. (2.15) will be

$$P(\tau_x, \tau_y, \vec{q}) = i\int_{-\infty}^{\infty} \frac{dq_0'}{2\pi}\varrho(q_0', \vec{q})e^{-iq_0'(\tau_x - \tau_y)}[\theta(\tau_x - \tau_y) - \theta(-q_0')] \tag{2.73}$$

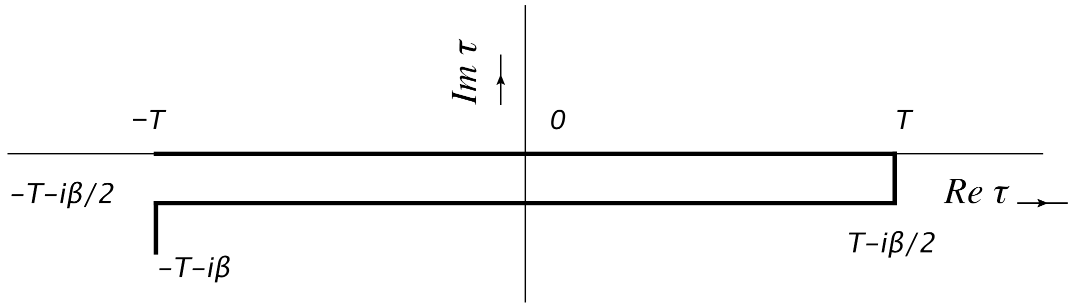

Figure 2.1: Contour in time plane for real time formalism

.

ab	11	12	21	22
τ_x, τ_y	$\tau_x = t$ $\tau_y = t' = 0$	$\tau_x = t$ $\tau_y = -t' - i\beta/2 = -i\beta/2$	$\tau_x = t - i\beta/2$ $\tau_y = -t' = 0$	$\tau_x = -t - i\beta/2$ $\tau_y = -t' - i\beta/2 = -i\beta/2$
$\theta(\tau_x - \tau_y)$	$= \theta(t)$	=0 $(\tau_x < \tau_y)$	=1 $(\tau_x > \tau_y)$	$= \theta(-t)$

Table 2.1: Table showing the four possible sets of two points in complex time plane and their corresponding values of step function $\theta(\tau_x - \tau_y)$.

the contour there are four possible ways of choosing the two points in complex time plane. So after temporal Fourier transform of $P(\tau_x, \tau_y, \vec{q})$ we get four components of thermal propagator in four momentum space,

$$
\begin{aligned}
P_{xy}(q_0, \vec{q}) &= i\int_{-\infty}^{\infty} dt_x e^{iq_0(t_x - t_y)} P(\tau_x - \tau_y, \vec{q}) \qquad x, y = 1, 2 \\
&= \int_{-\infty}^{\infty} \frac{dq_0'}{2\pi} \varrho(q_0', \vec{q}) \Lambda_{xy} \qquad \text{[using Eq. (2.71)]} \qquad (2.74)
\end{aligned}
$$

where

$$
\Lambda_{xy} = i\int_{-\infty}^{\infty} dt_x e^{i(q_0)(t_x - t_y) - i(q_0')(\tau_x - \tau_y)} [\theta_c(\tau_x - \tau_y) + \epsilon_q f(q_0')] \qquad (2.75)
$$

From Fig. (2.1), we see that the contour extends from $-\infty$ to $+\infty$ in first line but in second line it follows completely opposite direction along real axis of τ-plane. So we have to put an extra negative sign in real part of τ at any point of second line (for example,

$\tau_b = -t' - i\beta/2$ for 12-component as shown in Table.2.1). Now the time corresponding any point on the second line is always greater than that of the first line, so θ function for 12 and 21 components results is a definite numerical value (i.e. one or zero). In case of 11 and 22 components, θ function is written in a functional form as two points in both cases are located on the same line. Detailed evaluation (we will take $t_x = t$ and $t_y = 0$) of the four components are as follows.

$\underline{P_{11}}$:

$$\begin{aligned}
\Lambda_{11} &= i\int_{-\infty}^{\infty} dt e^{i(q_0-q_0')t}[\theta(t) + \epsilon_q f(q_0')] \\
&= \frac{1}{2\pi}\int_{-\infty}^{\infty} d\nu \int_{-\infty}^{\infty} dt \frac{e^{i(q_0-q_0'+\nu)t}}{\nu - i\eta} + i\epsilon_q \int_{-\infty}^{\infty} dt e^{i(q_0-q_0')t} f(q_0') \\
&= \int_{-\infty}^{\infty} d\nu \frac{\delta(q_0 - q_0' + \nu)}{\nu - i\eta} + 2\pi i\epsilon_q \delta(q_0 - q_0') f(q_0') \\
&\qquad \text{as } \theta(t) = \frac{-i}{2\pi}\int_{-\infty}^{\infty} d\nu \frac{e^{i\nu t}}{\nu - i\eta} \text{ and } \int_{-\infty}^{\infty} dt e^{i\nu t} = 2\pi\delta(\nu) \\
&= \frac{1}{q_0' - q_0 - i\eta} + 2i\pi\epsilon_q \delta(q_0' - q_0) f(q_0) \qquad (2.76)
\end{aligned}$$

$$\begin{aligned}
2i\pi\epsilon_q\delta(q_0' - q_0)f(q_0) &= i\pi\delta(q_0' - q_0)[2\epsilon_q N_q \epsilon(q_0) - 2\theta(-q_0')] \\
&= i\pi\delta(q_0' - q_0)[2\epsilon_q N_q \epsilon(q_0) + \{\theta(q_0') - \theta(-q_0') - 1\}] \quad \text{as } \theta(-q_0') = 1 - \theta(q_0') \\
&= i\pi\delta(q_0' - q_0)[2\epsilon_q N_q \epsilon(q_0) + \{\epsilon(q_0') - 1\}] \quad \text{as } \epsilon(q_0') = \theta(q_0') - \theta(q_0') \quad (2.77)
\end{aligned}$$

Using Eq. (2.77) in Eq. (2.76) and rearranging, it follows

$$\begin{aligned}
\Lambda_{11} &= \frac{1}{q_0' - q_0 - i\eta} + i\pi\delta(q_0' - q_0)[2\epsilon_q N_q \epsilon(q_0) + \{\epsilon(q_0') - 1\}] \\
&= \mathcal{P}[\frac{1}{q_0' - q_0}] + i\pi\delta(q_0' - q_0) + i\pi\delta(q_0' - q_0)[2\epsilon_q N_q \epsilon(q_0) + \{\epsilon(q_0') - 1\}] \\
&= \frac{1}{q_0' - q_0 + i\eta\epsilon(q_0')} + \epsilon_q 2\pi i\delta(q_0' - q_0) N_q \epsilon(q_0) \qquad (2.78)
\end{aligned}$$

Using this Λ_{11} in Eq. (2.74) we can get P_{11} with two different parts which are separately evaluated below.

$$\begin{aligned}
&\int_{-\infty}^{\infty} \frac{dq_0'}{2\pi} \varrho(q_0', \vec{q})[\frac{1}{q_0' - q_0 - i\eta\epsilon(q_0)}] \\
&\quad = \int_{-\infty}^{\infty} \frac{dq_0'}{2\pi} \frac{2\pi\epsilon(q_0')\zeta}{2\omega}[\delta(q_0' - \omega) + \delta(q_0' + \omega)][\frac{1}{q_0' - q_0 - i\eta\epsilon(q_0')}] \\
&\qquad \text{(using free spectral function from Eq.2.37)}
\end{aligned}$$

$$= \frac{\zeta}{2\omega}[\frac{1}{\omega - q_0 - i\eta} - \frac{1}{-\omega - q_0 + i\eta}]$$
$$= \zeta\Delta_F(q^2) \qquad \text{where } \Delta_F(q^2) = \frac{-1}{q^2 - m^2 + i\eta} \tag{2.79}$$

and

$$\int_{-\infty}^{\infty} \frac{dq_0'}{2\pi}\varrho(q_0', \vec{q})[\epsilon_q 2\pi i\delta(q_0' - q_0)N_q\epsilon(q_0)]$$
$$= \int_{-\infty}^{\infty} \frac{dq_0'}{2\pi}\frac{2\pi\epsilon(q_0')\zeta}{2\omega}[\delta(q_0' - \omega) + \delta(q_0' + \omega)][\epsilon_q 2\pi i\delta(q_0' - q_0)N_q\epsilon(q_0)]$$
$$= \frac{\zeta\epsilon_q 2\pi i N_q}{2\omega}[\delta(q_0 - \omega) + \delta(q_0 + \omega)]$$
$$= \zeta\epsilon_q 2\pi i N_q\delta(q^2 - m^2) \tag{2.80}$$

So

$$P_{11} = \zeta[\Delta(q^2) + \epsilon_q 2\pi N_q i\delta(q^2 - m^2)] \tag{2.81}$$

$\underline{P_{12}:}$

$$\begin{aligned} \Lambda_{12} &= i\int_{-\infty}^{\infty} dt e^{i(q_0 - q_0')t}e^{q_0'\beta/2}[0 + \epsilon_q f(q_0')] \\ &= 2i\pi\epsilon_q e^{q_0'\beta/2}\delta(q_0' - q_0)f(q_0') \end{aligned} \tag{2.82}$$

Using Eq. (2.82) in Eq. (2.74) and then putting the general expression of free spectral function, we get

$$\begin{aligned} P_{12} &= \int_{-\infty}^{\infty} \frac{dq_0'}{2\pi}\varrho(q_0', \vec{q})[2i\pi\epsilon_q e^{q_0'\beta/2}\delta(q_0' - q_0)f(q_0')] \\ &= \int_{-\infty}^{\infty} \frac{dq_0'}{2\pi}[\frac{\zeta 2\pi\epsilon(q_0')}{2\omega}\{\delta(q_0' - \omega) + \delta(q_0' + \omega)\}] \\ &\qquad [2i\pi\epsilon_q e^{q_0'\beta/2}\delta(q_0' - q_0)\{N_q(q_0')\epsilon(q_0') - \epsilon_q\theta(-q_0')\}] \\ &= \frac{\zeta 2i\pi\epsilon_q e^{q_0\beta/2}}{2\omega}[\{\delta(q_0 - \omega) + \delta(q_0 + \omega)\}][\{N_q(q_0) - \epsilon_q\theta(-q_0)\epsilon(q_0)\}] \\ &= \frac{\zeta 2i\pi\epsilon_q}{2\omega}[\{n_+ e^{\beta\omega/2}\delta(q_0 - \omega) + \{n_- - \epsilon_q\epsilon(-\omega)\}e^{-\beta\omega/2}\delta(q_0 + \omega)\}] \\ &\qquad \text{as } \theta(\pm q_0)\delta(q_0 \mp \omega) = \delta(q_0 \mp \omega), \quad \theta(\mp q_0)\delta(q_0 \mp \omega) = 0 \\ &= \frac{\zeta 2i\pi\epsilon_q}{2\omega}[\sqrt{n_+(1 + \epsilon_q n_+)}\delta(q_0 - \omega) + \epsilon_q\sqrt{n_-(1 + \epsilon_q n_-)}\delta(q_0 + \omega)] \\ &\qquad [\text{ as } n_+ e^{\beta\omega/2} = \frac{e^{\frac{\beta}{2}(\omega - \mu)}}{e^{\beta(\omega - \mu)} - \epsilon_q}e^{\beta\mu/2} = \sqrt{n_+(1 + \epsilon_q n_+)}e^{\beta\mu/2} \\ &\qquad \text{and } (\epsilon_q + n_-)e^{-\beta\omega/2} = \frac{\epsilon_q e^{\beta(\omega + \mu)}}{e^{\beta(\omega + \mu)} - \epsilon_q}e^{-\beta\omega/2} = \epsilon_q\sqrt{n_-(1 + \epsilon_q n_-)}e^{\beta\mu/2}\ ] \end{aligned}$$

$$= \quad 2\pi i\epsilon_q N_{2q} e^{\beta\mu/2}\delta(q^2-m^2)\ , \quad N_{2q} = \sqrt{n_+(1+\epsilon_q n_+)}\ \theta(q_0) + \epsilon_q\sqrt{n_-(1+\epsilon_q n_-)}\ \theta(-q_0) \tag{2.83}$$

$\underline{P_{21}}$ **:**

In this case as $\theta(\tau_x - \tau_y) = 1$, so

$$\begin{aligned} \Lambda_{12} &= i\int_{-\infty}^{\infty} dt e^{i(q_0-q_0')t} e^{-q_0'\beta/2}[1+\epsilon_q f(q_0')] \\ &= 2i\pi e^{-q_0'\beta/2}\delta(q_0'-q_0)[1+\epsilon_q f(q_0')] \end{aligned} \tag{2.84}$$

and putting it in Eq. (2.74), we get

$$\begin{aligned} P_{21} &= \int_{-\infty}^{\infty}\frac{dq_0'}{2\pi}\varrho(q_0',\vec{q})[2i\pi e^{-q_0'\beta/2}\delta(q_0'-q_0)\{1+\epsilon_q f(q_0')\}] \\ &= \int_{-\infty}^{\infty}\frac{dq_0'}{2\pi}[\frac{\zeta 2\pi\epsilon(q_0')}{2\omega}\{\delta(q_0'-\omega)+\delta(q_0'+\omega)\}] \\ &\qquad [2i\pi e^{-q_0'\beta/2}\delta(q_0'-q_0)\{1+\epsilon_q N_q(q_0')\epsilon(q_0') - \theta(-q_0')\}] \\ &= \frac{\zeta 2i\pi e^{q_0\beta/2}}{2\omega}[\{\delta(q_0-\omega)+\delta(q_0+\omega)\}][\{\epsilon_q N_q(q_0)+\theta(q_0)\epsilon(q_0)\}] \\ &= \frac{\zeta 2i\pi\epsilon_q}{2\omega}[\{\epsilon_q n_+ + \epsilon(\omega)\}e^{-\beta\omega/2}\delta(q_0-\omega) + n_- e^{\beta\omega/2}\delta(q_0+\omega)] \\ &= \frac{\zeta 2i\pi}{2\omega}[\sqrt{n_+(1+\epsilon_q n_+)}\delta(q_0-\omega) + \epsilon_q\sqrt{n_-(1+\epsilon_q n_-)}\delta(q_0+\omega)] \\ &\qquad [\text{ as } (\epsilon_q n_+ + 1)e^{\beta\omega/2} = \frac{e^{\beta(\omega-\mu)}}{e^{\beta(\omega-\mu)}-\epsilon_q}e^{-\beta\omega/2} = \sqrt{n_+(1+\epsilon_q n_+)}e^{-\beta\mu/2} \\ &\qquad \text{and } \epsilon_q n_- e^{\beta\omega/2} = \frac{\epsilon_q e^{\frac{\beta}{2}(\omega+\mu)}}{e^{\beta(\omega+\mu)}-\epsilon_q}e^{-\beta\mu/2} = \epsilon_q\sqrt{n_-(1+\epsilon_q n_-)}e^{-\beta\mu/2}\ ] \\ &= \zeta 2\pi i N_{2q} e^{-\beta\mu/2}\delta(q^2-m^2) \end{aligned} \tag{2.85}$$

$\underline{P_{22}}$ **:**

$$\begin{aligned} \Lambda_{22} &= i\int_{-\infty}^{\infty} dt e^{i(q_0-q_0')t}[\theta(-t)+\epsilon_q f(q_0')] \\ &= \frac{-1}{2\pi}\int_{-\infty}^{\infty} d\nu\int_{-\infty}^{\infty} dt\frac{e^{i(q_0-q_0'+\nu)t}}{\nu+i\eta} + i\epsilon_q\int_{-\infty}^{\infty} dt e^{i(q_0-q_0')t}f(q_0') \\ &= -\int_{-\infty}^{\infty} d\nu\frac{\delta(q_0-q_0'+\nu)}{\nu+i\eta} + 2\pi\epsilon_q\delta(q_0'-q_0)f(q_0') \\ &\qquad \text{as } \theta(-t) = \frac{i}{2\pi}\int_{-\infty}^{\infty} d\nu\frac{e^{-i\nu(-t)}}{\nu+i\eta} \text{ and } \int_{\infty}^{\infty} dt e^{i\nu t} = 2\pi\delta(\nu) \\ &= \frac{-1}{q_0'-q_0+i\eta} + 2i\pi\epsilon_q\delta(q_0'-q_0)f(q_0) \end{aligned} \tag{2.86}$$

Rearranging it like 11-component we have

$$
\begin{aligned}
P_{22} &= \int_{-\infty}^{\infty} \frac{dq_0'}{2\pi}\varrho(q_0',\vec{q})[\frac{-1}{q_0'-q_0+i\eta\epsilon(q_0)} + \epsilon_q 2\pi i\delta(q_0'-q_0)N_q\epsilon(q_0)] \\
&= \int_{-\infty}^{\infty} \frac{dq_0'}{2\pi}\frac{2\pi\epsilon(q_0')\zeta}{2\omega}[\delta(q_0'-\omega)+\delta(q_0'+\omega)] \\
&\qquad\qquad [\frac{-1}{q_0'-q_0+i\eta\epsilon(q_0')} + \epsilon_q 2\pi i\delta(q_0'-q_0)N_q\epsilon(q_0)] \\
&= \frac{\zeta}{2\omega}[\{\frac{-1}{\omega-q_0+i\eta} - \frac{-1}{-\omega-q_0-i\eta}\} + 2\pi\epsilon_q N_q\{\delta(q_0-\omega)+\delta(q_0+\omega)\}] \\
&= \zeta[\frac{1}{q_0^2-\omega^2-i\eta} + 2\pi\epsilon_q N_q\delta(q_0^2-\omega^2)] \qquad (2.87)
\end{aligned}
$$

So the $P_{xy}(q_0,\vec{q})$ in 2×2 matrix form can be expressed as

$$
\begin{aligned}
P_{xy} &= \int_{-\infty}^{\infty}\frac{dq_0'}{2\pi}\varrho(q_0',\vec{q})\begin{pmatrix} \frac{1}{(q_0'-q_0)-i\eta} + \epsilon_q 2\pi i\delta(q_0'-q_0)f(q_0') & \epsilon_q 2\pi i e^{\beta q_0'/2}\delta(q_0'-q_0)f(q_0') \\ 2\pi i e^{-\beta q_0'/2}\delta(q_0'-q_0)[1+\epsilon_q f(q_0')] & \frac{-1}{(q_0'-q_0)+i\eta} + \epsilon_q 2\pi i\delta(q_0'-q_0)f(q_0') \end{pmatrix} \\
&= \zeta\begin{pmatrix} \frac{-1}{(q^2-m^2)+i\eta} + \epsilon_q 2\pi i\delta(q^2-m^2)N_q & \epsilon_q 2\pi i e^{\beta\mu/2}\delta(q^2-m^2)N_{2q} \\ 2\pi i e^{-\beta\mu/2}\delta(k^2-m^2)N_{2q} & \frac{1}{(q^2-m^2)+i\eta} + \epsilon_q 2\pi i\delta(q^2-m^2)N_q \end{pmatrix}
\end{aligned}
$$
(2.88)

The matrix in the first line of Eq. (2.88) gives the spectral representation of the thermal propagator and it may be used to express dressed or interacting prpagator by putting the interaction details in ϱ whereas second matrix represents the form of free thermal propagator after putting free spectral function. The matrix Λ_{xy} as well as P_{xy} can now be diagonalized by U_{xy},

$$
\begin{aligned}
U_{xy} &= \begin{pmatrix} N_{2q}/\sqrt{N_q} & \epsilon_q\sqrt{N_q}e^{\beta\mu/2} \\ \sqrt{N_q}e^{-\beta\mu/2} & N_{2q}/\sqrt{N_q} \end{pmatrix} \\
\text{i.e. } U_{xy} &= \begin{pmatrix} N_{2q}/\sqrt{N_q} & -\sqrt{N_q}e^{\beta\mu/2} \\ \sqrt{N_q}e^{-\beta\mu/2} & N_{2q}/\sqrt{N_q} \end{pmatrix} \quad \text{for fermion} \\
&= \begin{pmatrix} \sqrt{n(1+n)} & \sqrt{n} \\ \sqrt{n} & \sqrt{n(1+n)} \end{pmatrix} \quad \text{for boson} \qquad (2.89)
\end{aligned}
$$

The diagonalization procedure is as follows.

$$
\begin{aligned}
P_{xy} &= \begin{pmatrix} P_{11} & P_{12} \\ P_{21} & P_{22} \end{pmatrix} \\
&= U_{xx'}\overline{P}_{x'y'}U_{y'y} = U\begin{pmatrix} \overline{P} & 0 \\ 0 & -\overline{P}^* \end{pmatrix}U \qquad (2.90)
\end{aligned}
$$

where

$$\overline{P} = \int_{-\infty}^{\infty} \frac{dq_0'}{2\pi} \frac{\varrho(q_0', \vec{q})}{q_0 - q_0' - i\eta\epsilon(q_0)}$$
$$= \zeta \frac{-1}{q^2 - m^2 + i\eta} \tag{2.91}$$

So the diagonal elements of the free thermal propagator is exactly the same as vacuum Feynman propagator. We can relate this to any component of P_{ab}. The relation with 11-component is

$$P_{11} = \frac{N_{2q}^2}{N_q}\overline{P} - \epsilon_q N_q \overline{P}^* \tag{2.92}$$

In spectral representation this relation can be expressed as

$$P_{11} = \int_{\infty}^{\infty} \frac{dq_0}{2\pi} \varrho(q_0', \vec{q})[\frac{1}{(q_0 - q_0') - i\eta} + \epsilon_q 2\pi i \delta(q_0 - q_0') f(q_0')]$$
$$= \int_{\infty}^{\infty} \frac{dq_0}{2\pi} \varrho(q_0', \vec{q})[\mathcal{P}(\frac{1}{(q_0 - q_0')}) + i\pi\{1 + 2\epsilon_q f(q_0)\}\delta(q_0 - q_0')]$$
$$\text{So,} \quad \mathrm{Im}P_{11} = \frac{\varrho(q_0, \vec{q})}{2}\{1 + 2\epsilon_q f(q_0)\} \tag{2.93}$$

From Eq. (2.91) and (2.93), we can get a relation among the $\varrho(q_0, \vec{q})$, $\overline{P}$ and P_{11},

$$\varrho(q_0, \vec{q}) = 2\epsilon(q_0)\mathrm{Im}\overline{P} = \frac{1}{1 + 2\epsilon_q f(q_0)} 2\ \mathrm{Im}P_{11}$$
$$\mathrm{Re}\overline{P} = \mathrm{Re}P_{11} \tag{2.94}$$

The factor containing the thermal distribution function multiplied with P_{11} can be converted to hyperbolic function. Considering $|q_0| = \omega$ i.e. $n_\pm = \frac{1}{e^{\beta(|q_0| \mp \mu)} - \epsilon_q}$,

$$\frac{1}{1 + 2\epsilon_q f(q_0)} = \frac{1}{1 + 2\epsilon_q\{n_+\theta(q_0) + n_-\theta(-q_0)\}\epsilon(q_0) - 2\theta(-q_0)}$$
$$= \frac{1}{1 + 2\epsilon_q n_+} = \frac{e^{\frac{\beta}{2}(|q_0| - \mu)} - \epsilon_q e^{-\frac{\beta}{2}(|q_0| - \mu)}}{e^{\frac{\beta}{2}(|q_0| - \mu)} + \epsilon_q e^{-\frac{\beta}{2}(-|q_0| - \mu)}} \quad \text{for } q_0 > 0$$
$$= \frac{1}{-1 + 2\epsilon_q n_-} = \frac{e^{\frac{\beta}{2}(-|q_0| - \mu)} - \epsilon_q e^{-\frac{\beta}{2}(-|q_0| - \mu)}}{e^{\frac{\beta}{2}(-|q_0| - \mu)} + \epsilon_q e^{-\frac{\beta}{2}(|q_0| - \mu)}} \quad \text{for } q_0 < 0$$
$$\tag{2.95}$$

Hence for any value of q_0, we can write this factor as

$$\frac{1}{1 + 2\epsilon_q f(q_0)} = \frac{e^{\frac{\beta}{2}(q_0 - \mu)} - \epsilon_q e^{-\frac{\beta}{2}(q_0 - \mu)}}{e^{\frac{\beta}{2}(q_0 - \mu)} + \epsilon_q e^{-\frac{\beta}{2}(-q_0 - \mu)}}$$
$$= \coth\{\frac{\beta}{2}(q_0 - \mu)\} \qquad \text{for fermion, i.e. } \epsilon_q = -1$$
$$= \tanh\{\frac{\beta}{2}(q_0)\} \qquad \text{for boson, i.e. } \epsilon_q = +1,\ \mu = 0 \tag{2.96}$$

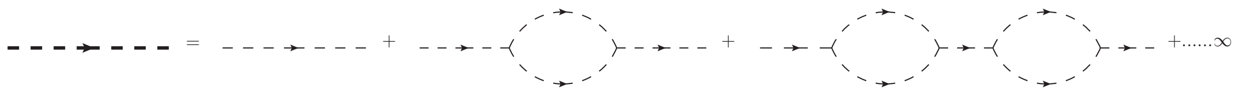

Figure 2.2: The diagramatic representation of Dyson's equation. Thin and bold dashed lines stand for free and interacting propagators respectively.

So Eq. (2.94) is now given by

$$\varrho(q_0,\vec{q}) = 2\epsilon(q_0)\mathrm{Im}\overline{P} = 2\,\coth\{\frac{\beta}{2}(q_0-\mu)\}\mathrm{Im}P_{11} \;\; \text{for fermion}$$
$$= 2\,\tanh\{\frac{\beta}{2}(q_0)\}\mathrm{Im}P_{11} \;\; \text{for boson} \tag{2.97}$$

2.3 Interacting thermal propagator

2.3.1 Scalar propagator

So far we have discussed about the structure of free (vacuum or thermal) propagator. The exact propagators ($-i\Delta(q)$) is obtained perturbatively by summing loop diagrams as shown in Fig. (2.2). This is actually a geometric progression with free propagator ($-i\Delta_0(q)$) as the first term and the self-energy ($-i\Pi(q)$) as the common ratio.

$$\begin{aligned}
-i\Delta(q) &= -i\Delta_0(q) + \{-i\Delta_0(q)\}\{-i\Pi(q)\}\{-i\Delta_0(q)\} \\
&\quad + \{-i\Delta_0(q)\}\{-i\Pi(q)\}\{-i\Delta_0(q)\}\{-i\Pi(q)\}\{-i\Delta_0(q)\} + ... \\
\Delta(q) &= \frac{\Delta_0(q)}{1-\{-\Delta_0(q)\Pi(q)\}} \\
&= \frac{-1}{q^2-m^2-\Pi(q)} \qquad \text{as} \;\; \Delta_0^{-1} = -(q^2-m^2)
\end{aligned} \tag{2.98}$$

The above equation can be expressed as

$$\Delta(q) = \Delta_0(q) - \Delta_0(q)\Pi(q)\Delta(q) \tag{2.99}$$

which is a general self-consistent equation for the interacting propagator of any spin and is known as Dyson's equation. The real part of vacuum self-energy (a divergent quantity) is absorbed by the mass renormalization technique. Therefore Eq. (2.98) can be written as

$$\Delta(q) = \frac{-1}{q^2-m^2-i\mathrm{Im}\Pi(q)} \tag{2.100}$$

The imaginary part of self-energy [$\mathrm{Im}\Pi(q)$] is nonvanishing in certain regions of q-axis, where $\Pi(q)$ has a discontinuity. Due to presence of this nonzero $\mathrm{Im}\Pi(q)$, the spectral function $\varrho(q)$ will exhibit a Breit-Wigner type structure.

$$\begin{aligned}\varrho(q) &= 2\epsilon(q_0)\mathrm{Im}\Delta(q)\\ &= \frac{2\epsilon(q_0)\mathrm{Im}\Pi(q)}{\{q^2-m^2\}^2+\{\mathrm{Im}\Pi(q)\}^2}\end{aligned} \tag{2.101}$$

In the limit of vanishing $\mathrm{Im}\Pi(q)$, the spectral function reduces to its form of δ-function for free propagator.

$$\begin{aligned}\varrho(q) &= \lim_{\{-\mathrm{Im}\Pi\}\to 0} 2\epsilon(q_0)\mathrm{Im}[\frac{-1}{q^2-m^2+i\{-\mathrm{Im}\Pi(q)\}}]\\ &= \lim_{\{-\mathrm{Im}\Pi\}\to 0} 2\epsilon(q_0)[\frac{\{-\mathrm{Im}\Pi(q)\}}{(q^2-m^2)^2+\{-\mathrm{Im}\Pi(q)\}^2}]\\ &= 2\epsilon(q_0)\pi\delta(q^2-m^2) \qquad [\text{since } \lim_{\eta\to 0}\frac{\eta/\pi}{(x^2+\eta^2}=\delta(x)\ ]\end{aligned} \tag{2.102}$$

In real time thermal field theory the Dyson's equation can be expressed in 2×2 matrix form as

$$\Delta^{ab}(q)=\Delta_0^{ab}(q)-\Delta_0^{ac}(q)\Pi^{cd}(q)\Delta^{db}(q) \tag{2.103}$$

As discussed in the Eq. (2.88) the free and the exact propagator has the same spectral representation. So the exact propagator can be diagonalised in the same way as the free thermal propagator. Multiplying left side by $(\Delta_0^{ea})^{-1}$ and right side by $(\Delta^{bf})^{-1}$ we get

$$\begin{aligned}\Pi^{ef} &= (\Delta^{ef})^{-1}-(\Delta_0^{ef})^{-1}\\ &= (U^{eg}\overline{\Delta}^{gh}U^{hf})^{-1}-(U^{eg}\overline{\Delta}_0^{gh}U^{hf})^{-1}\\ &= (U^{eg})^{-1}\overline{\Pi}^{gh}(U^{hf})^{-1}\end{aligned} \tag{2.104}$$

This leads to the Dyson's equation for diagonal matrices and is given by

$$\begin{aligned}&(U\overline{\Delta}U)^{ab}=(U\overline{\Delta}_0U)^{ab}-(\{U\overline{\Delta}_0U\}\{U^{-1}\overline{\Pi}U^{-1}\}\{U\overline{\Delta}U\})^{ab}\\ &\quad\overline{\Delta}^{ab}=\overline{\Delta}_0^{ab}-\{\overline{\Delta}_0\overline{\Pi}\ \overline{\Delta}\}^{ab}\\ &\text{where } \overline{\Delta}_0^{ab}=\begin{pmatrix}\overline{\Delta}_0 & 0\\ 0 & -\overline{\Delta}_0^*\end{pmatrix},\ \overline{\Pi}^{ab}=\begin{pmatrix}\overline{\Pi} & 0\\ 0 & -\overline{\Pi}^*\end{pmatrix},\ \overline{\Delta}^{ab}=\begin{pmatrix}\overline{\Delta} & 0\\ 0 & -\overline{\Delta}^*\end{pmatrix}\\ &\Rightarrow \overline{\Delta}=\overline{\Delta}_0-\overline{\Delta}_0\overline{\Pi}\ \overline{\Delta}\end{aligned} \tag{2.105}$$

Hence

$$\begin{aligned}\varrho(q) &= 2\epsilon(q_0)\mathrm{Im}\overline{\Delta}(q)\\ &= \frac{2\epsilon(q_0)\mathrm{Im}\overline{\Pi}(q)}{\{q^2-m^2-\mathrm{Re}\overline{\Pi}(q)\}^2+\{\mathrm{Im}\overline{\Pi}(q)\}^2}.\end{aligned} \tag{2.106}$$

The thermal self-energy will be manifested in the spectral properties in two different ways. One is mass shift (Δm) that can be measured by finding the root of equation

$$[q^2 - m^2 - \mathrm{Re}\Pi_{\mathrm{th}}(q)]_{q=m+\Delta m} = 0 \tag{2.107}$$

and another is decay width enhancement ($\Delta\Gamma = \frac{\mathrm{Im}\overline{\Pi}(m) - \mathrm{Im}\Pi_V(m)}{m}$).

2.3.2 Fermion propagator

The form of Dyson's equation for diagonal element of thermal propgator is the same as in vacuum. So we directly jump to the discussion for diagonal part. Now general form of Dyson's Eq. (2.105) for spin 1/2 propagator can be written as (by replacing $\Delta_0 \to S_0$, $\Delta \to S$ and $\Pi \to \Sigma$ in Eq. (2.105))

$$\begin{aligned} \overline{S}^{-1} &= \overline{S}_0^{-1} + \overline{\Sigma}\ , \qquad S^{-1} = -(\not{q} - m) \\ \overline{S} &= \frac{-1}{\not{Q} - M} \end{aligned} \tag{2.108}$$

where $Q^\mu = q^\mu - \overline{\Sigma}^\mu$ and $M = m - \overline{\Sigma}_I$ with

$$\begin{aligned} \overline{\Sigma} &= \overline{\Sigma}_{\gamma^0}\gamma^0 - \vec{\overline{\Sigma}}_{\vec{\gamma}} \cdot \vec{\gamma} + \overline{\Sigma}_I I \\ &= \overline{\Sigma}_\mu \gamma^\mu + \overline{\Sigma}_I I \end{aligned} \tag{2.109}$$

For $\vec{q} = 0$,

$$\overline{S} = \overline{S}_{\gamma^0}\gamma^0 + \overline{S}_I I \tag{2.110}$$

where

$$\begin{aligned} \overline{S}_{\gamma^0} = \frac{Q_0}{Q_0^2 - M^2} \ \ &\text{and}\ \ \overline{S}_I = \frac{M}{Q_0^2 - M^2} \\ \text{with} \quad Q_0 &= q_0 - \overline{\Sigma}_{\gamma^0} \end{aligned} \tag{2.111}$$

Here $\overline{\Sigma}_{\gamma^0}$ and $\overline{\Sigma}_I$ contain the information of medium inputs (temperature and chemical potential).

2.3.3 Vector propagator

For the spin 1 field we have to take care of the Lorentz indices (along with thermal indices) in the Dyson's equation [64, 53] and after diagonalization the equation becomes

$$\overline{G}_{\mu\nu}(q) = \overline{G}^{(0)}_{\mu\nu}(q) - \overline{G}^{(0)}_{\mu\lambda}(q)\overline{\Pi}^{\lambda\sigma}_{\mathrm{tot}}(q)\overline{G}_{\sigma\nu}(q)\ , \tag{2.112}$$

where

$$\overline{G}^{(0)}_{\mu\nu}(q) = \left(-g_{\mu\nu} + \frac{q_\mu q_\nu}{q^2}\right)\frac{-1}{q^2 - m_\rho^2 + i\epsilon}, \tag{2.113}$$

is the four-dimensionally transverse[5] part of the diagonal element of thermal propagator. In the medium, presence of four velocity u_μ, introduces an additional scalar variable $u\cdot q$ in addition to q^2, leading to two independent tensors $P_{\mu\nu}$ and $Q_{\mu\nu}$ in terms of which the propagator and self-energy can be written as

$$\begin{aligned} \overline{G}_{\mu\nu} &= P_{\mu\nu}\overline{G}_t + Q_{\mu\nu}\overline{G}_l \\ \overline{\Pi}_{\mu\nu} &= P_{\mu\nu}\overline{\Pi}_t + Q_{\mu\nu}\overline{\Pi}_l \end{aligned} \tag{2.115}$$

with

$$P_{\mu\nu} = -g_{\mu\nu} + \frac{q_\mu q_\nu}{q^2} - \frac{q^2}{\overline{q}^2}\tilde{u}_\mu\tilde{u}_\nu, \;\; \tilde{u}_\mu = u_\mu - (u\cdot q)q_\mu/q^2 \tag{2.116}$$

and

$$Q_{\mu\nu} = \frac{(q^2)^2}{\overline{q}^2}\tilde{u}_\mu\tilde{u}_\nu, \;\; \overline{q}^2 = (u\cdot q)^2 - q^2 \;. \tag{2.117}$$

satisfying the projection properties

$$P\cdot P = -P, \qquad Q\cdot Q = -q^2 Q, \qquad P\cdot Q = 0 \tag{2.118}$$

While both P and Q are four-dimensionally transverse, P is also 3-dimensionally transverse. In the literature one generally finds the factor q^2 instead of $(q^2)^2$ in the definition of $Q_{\mu\nu}$. However, at finite temperature dynamical singularity can appear at $q^2 = 0$. The additional factor of q^2 keeps the kinematic covariant regular at that point. Using (2.115) and (2.118), the Dyson equation (2.112) becomes

$$\begin{aligned} P_{\mu\nu}\overline{G}_t + Q_{\mu\nu}\overline{G}_l &= \{(P_{\mu\nu} + \frac{Q_{\mu\nu}}{q^2})\Delta_0\} - \{P_{\mu\nu}\Delta_0\overline{\Pi}_t\overline{G}_t + q^4 Q_{\mu\nu}\frac{\Delta_0}{q^2}\overline{\Pi}_l\overline{G}_l\} \\ P_{\mu\nu}[\overline{G}_t - \frac{1}{\Delta_0^{-1} + \overline{\Pi}_t}] &+ Q_{\mu\nu}[\overline{G}_l - \frac{1/q^2}{\Delta_0^{-1} + q^2\overline{\Pi}_l}] = 0 \end{aligned} \tag{2.119}$$

Now equating coefficients of independent projection operators to zero,we reach our aim,

$$\overline{G}_t(q) = \frac{-1}{q^2 - m_\rho^2 - \overline{\Pi}_t(q)}, \qquad \overline{G}_l(q) = \frac{1}{q^2}\frac{-1}{q^2 - m_\rho^2 - q^2\overline{\Pi}_l(q)} \tag{2.120}$$

[5]

$$\overline{D}^0_{\mu\nu} = \overline{G}^{(0)}_{\mu\nu} + \frac{q^\mu q^\nu}{m^2 q^2}, \;\; \text{where } \overline{D}^0_{\mu\nu} = \left(-g_{\mu\nu} + \frac{q_\mu q_\nu}{m^2}\right)\frac{-1}{q^2 - m_\rho^2 + i\epsilon} \tag{2.114}$$

We should note that $q^\mu\overline{G}^{(0)}_{\mu\nu} = 0$ but the term $\frac{q^\mu q^\nu}{m^2 q^2}$ is not orthogonal to q^μ.

where

$$\overline{\Pi}_t = -\frac{1}{2}(\overline{\Pi}^\mu_\mu + \frac{q^2}{\vec{q}^2}\overline{\Pi}_{00}), \qquad \overline{\Pi}_l = \frac{1}{\vec{q}^2}\overline{\Pi}_{00}, \quad \overline{\Pi}_{00} \equiv u^\mu u^\nu \overline{\Pi}_{\mu\nu} \ . \tag{2.121}$$

Finally we note a kinematic relation between the transverse and the longitudinal components of the propagator at $\vec{q} = 0$. As $\vec{q} \to 0$, the structures of P_{ij} and Q_{ij} depend on how this limit is taken. This is eliminated, if we take

$$\overline{G}_t(q_0, \vec{q} = 0) = q_0^2 \, \overline{G}_l(q_0, \vec{q} = 0) \tag{2.122}$$

Clearly a similar relation must also hold between $\overline{\Pi}_{t,l}$, which is already implied by Eq. (2.120).

Chapter 3

Self-energy in real-time thermal field theory

3.1 Vacuum Self-energy

The vacuum in quantum field theory is a stormy sea of virtual particles originating from quantum fluctuations [48]. So during the propagation of any particle it can't be free from disturbances created by these virtual particles. The self-energy, which has already been introduced in section(2.3) of chapter(2), is generally believed to provide a quantitative measurement of the fluctuations. In the simplest possible self-energy diagram [Fig (3.1) or (3.2)], the propagating particle may create a virtual pair which are again annihilated after a short time mandated by the uncertainty principle. The amputated loop part of the diagram is known as one-loop self-energy. In a perturbative treatment, the self-energy consists of a series of loop diagrams with subsequent terms containing higher loops [65]. Here we are interested to study the effect of one-loop self-energy diagram on the propagation amplitude. From the mathematical expression of interacting propgator (2.98) in the previous chapter, we have seen how one-loop self-energy modifies the free propagation amplitude. Now we will focus on the detail expression of one-loop self-energy.

For a general description of one-loop self-energy, we can classify it into four possible diagrams as shown in Figs. (3.1) and (3.2). Now for fermion self-energy, boson-fermion (BF) internal lines (Fig.3.2) are only allowed whereas for boson self-energy, boson-boson [Fig.3.1(A)] as well as fermion-fermion internal lines are possible. There are two possible diagrams for fermion-fermion internal lines for boson self-energy shown in Fig.3.1(B) and

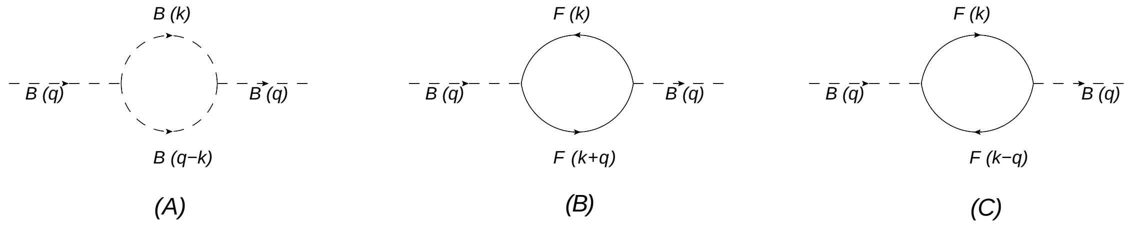

Figure 3.1: Diagram (A) shows the boson self-energy for boson-boson (BB) loop whereas others, (B) and (C) show the two possible diagrams for fermion-fermion loop. We have denoted the fermion internal line in negative direction of time as $\overline{F}$

.

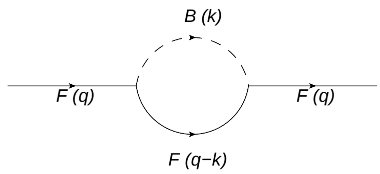

Figure 3.2: Fermion self-energy diagram for boson-fermion (BF) internal line

.

Fig	Fig.3.1 (A)	Fig.3.1 (B)	Fig.3.1 (C)	Fig.3.2
External line	B (Boson)	B	B	F (Fermion)
Internal lines	BB	$\overline{F}F$	$F\overline{F}$	BF
Momentum of lower internal line	$p = q - k$ i.e. $\epsilon_1 = +1$ $\epsilon_2 = -1$	$p = k + q$ i.e. $\epsilon_1 = +1$ $\epsilon_2 = +1$	$p = k - q$ i.e. $\epsilon_1 = -1$ $\epsilon_2 = +1$	$p = q - k$ i.e. $\epsilon_1 = +1$ $\epsilon_2 = -1$
Other sign functions $(\epsilon_F, \epsilon_k, \epsilon_p)$	$\epsilon_F = +1$ i.e. $\epsilon_k = +1$ $\epsilon_p = +1$	$\epsilon_F = -1$ i.e. $\epsilon_k = -1$ $\epsilon_p = -1$	$\epsilon_F = -1$ i.e. $\epsilon_k = -1$ $\epsilon_p = -1$	$\epsilon_F = +1$ i.e. $\epsilon_k = +1$ $\epsilon_p = -1$

Table 3.1: Table showing the values of different sign coefficients for four possible one-loop self-energy diagrams.

(C). Let us denote them by $\overline{F}F$ and $F\overline{F}$ respectively.

We can write the general expression of vacuum self-energy as

$$\begin{aligned} i\Pi_V(q^2) &= \epsilon_F \int \frac{d^4k}{(2\pi)^4} v_1(q,k,p)\{-iP(k^2,m_k)\}\{-iP(p^2,m_p)\}v_2(q,k,p) \\ \Pi_V(q^2) &= i\epsilon_F \int \frac{d^4k}{(2\pi)^4} L(k,q,p)\Delta(k^2,m_k)\Delta(p^2,m_p) \end{aligned} \tag{3.1}$$

where $L(k,q,p) = v_1(q,k,p)\zeta_k\zeta_p v_2(q,k,p)$ is the product of two vertex functions (v_1, v_2) and the numerator part of two internal lines (ζ_k, ζ_p). Recall that the general form of vacuum propagator, $P(k^2, m_k)$ is defined in Eq. (2.34) of the previous chapter. The extra negative sign for fermion-fermion ($\overline{F}F$ or $F\overline{F}$) internal lines will be taken care of by the sign coefficient ϵ_F. The general form of p is taken as $p = \epsilon_1 q_0 + \epsilon_2 k_0$ and the values of sign coefficients, ϵ_1, ϵ_2 for different loops are given in Table. (3.1).

Decomposing the internal lines into positive and negative frequency propagation as

$$\Delta(k^2,m_k) = \frac{-1}{k_0^2 - \omega_k^2 + i\eta} = \frac{-1}{2\omega_k}\left[\frac{1}{q_0 - (\omega_k - i\eta)} - \frac{1}{q_0 + (\omega_k - i\eta)}\right] \ , \tag{3.2}$$

Eq. (3.1) becomes

$$\Pi_V(q^2) = i\epsilon_F \int \frac{d^3k}{(2\pi)^3} \frac{1}{4\omega_k\omega_p} I_V \tag{3.3}$$

where

$$\begin{aligned} I_V &= \int \frac{dk_0 L(k_0)}{(2\pi)}\left[\left\{\frac{1}{k_0 - \omega_k + i\eta} - \frac{1}{k_0 + \omega_k - i\eta}\right\}\right. \\ &\qquad \left.\left\{\frac{1}{(\epsilon_1 q_0 + \epsilon_2 k_0) - \omega_p + i\eta} - \frac{1}{(\epsilon_1 q_0 + \epsilon_2 k_0) + \omega_p - i\eta}\right\}\right] \\ &= I_{V1} + I_{V2} + I_{V3} + I_{V4} \end{aligned} \tag{3.4}$$

with

$$\begin{aligned} I_{V1} &= \int \frac{dk_0 L(k_0)}{(2\pi)}\left\{\frac{1}{k_0 - \omega_k + i\eta}\,\frac{1}{(\epsilon_1 q_0 + \epsilon_2 k_0) - \omega_p + i\eta}\right\} \\ I_{V2} &= \int \frac{dk_0 L(k_0)}{(2\pi)}\left\{\frac{1}{k_0 - \omega_k + i\eta}\,\frac{(-1)}{(\epsilon_1 q_0 + \epsilon_2 k_0) + \omega_p - i\eta}\right\} \\ I_{V3} &= \int \frac{dk_0 L(k_0)}{(2\pi)}\left\{\frac{(1)}{k_0 + \omega_k - i\eta}\,\frac{1}{(\epsilon_1 q_0 + \epsilon_2 k_0) - \omega_p + i\eta}\right\} \\ I_{V4} &= \int \frac{dk_0 L(k_0)}{(2\pi)}\left\{\frac{1}{k_0 + \omega_k - i\eta}\,\frac{1}{(\epsilon_1 q_0 + \epsilon_2 k_0) + \omega_p - i\eta}\right\}. \end{aligned} \tag{3.5}$$

The four individual integrations can be done by residue theorem of complex variable.

	for $p = q - k$	for $p = q + k$
for I_{V1}	$\text{Poles}: \; k_0^{(1)} = \omega_k - i\eta$ $k_0^{(2)} = q_0 - \omega_p + i\eta$	$\text{Poles}: \; k_0^{(1)} = \omega_k - i\eta$ $k_0^{(2)} = -q_0 + \omega_p - i\eta$
	$I_{V1} = \frac{-iL_1}{q_0 - \omega_k - \omega_p + i\eta}$ $\text{Contour}: \; \text{Fig. 3.3(C)}$	$I_{V1} = 0$ $\text{Contour}: \; \text{Fig. 3.3(A)}$
for I_{V2}	$\text{Poles}: \; k_0^{(1)} = \omega_k - i\eta$ $k_0^{(2)} = q_0 + \omega_p - i\eta$	$\text{Poles}: \; k_0^{(1)} = \omega_k - i\eta$ $k_0^{(2)} = -q_0 - \omega_p + i\eta$
	$I_{V2} = 0$ $\text{Contour}: \; \text{Fig. 3.3(A)}$	$I_{V2} = \frac{(-1)iL_5}{-q_0 - \omega_k - \omega_p + i\eta}$ $\text{Contour}: \; \text{Fig. 3.3(C)}$
for I_{V3}	$\text{Poles}: \; k_0^{(1)} = -\omega_k + i\eta$ $k_0^{(2)} = q_0 - \omega_p + i\eta$	$\text{Poles}: \; k_0^{(1)} = -\omega_k + i\eta$ $k_0^{(2)} = -q_0 + \omega_p - i\eta$
	$I_{V3} = 0$ $\text{Contour}: \; \text{Fig. 3.3(B)}$	$I_{V3} = \frac{(-1)iL_2}{q_0 - \omega_k - \omega_p + i\eta}$ $\text{Contour}: \; \text{Fig. 3.3(C)}$
for I_{V4}	$\text{Poles}: \; k_0^{(1)} = -\omega_k + i\eta$ $k_0^{(2)} = q_0 + \omega_p - i\eta$	$\text{Poles}: \; k_0^{(1)} = -\omega_k + i\eta$ $k_0^{(2)} = -q_0 - \omega_p + i\eta$
	$I_{V4} = \frac{iL_4}{q_0 + \omega_k + \omega_p - i\eta}$ $\text{Contour}: \; \text{Fig. 3.3(C)}$	$I_{V4} = 0$ $\text{Contour}: \; \text{Fig. 3.3(B)}$

Table 3.2: Table showing the poles (denoted as $k_0^{(1)}$ and $k_0^{(2)}$) of integrands and results of individual integration (I_{Vi} with i=1,2,3,4) by putting their corresponding residues.

The poles of four integrands and their residues for two[1] possible internal momenta are given in Table. (3.2). The integrations will be done with the help of three possible contour as shown in Fig. (3.3). For the contour 3.3(A) and (B) the corresponding integrations will vanish because their poles are outside the contours (Cauchy's Theorem). For the contour 3.3(C), the integration will be nonvanishing. For example, residues of I_{V1} with $p = q - k$ is

$$\begin{aligned} \mathrm{Res}(I_{V1}) &= \lim_{k_0 \to k_0^{(2)}} (k_0 - k_0^{(2)}) \frac{L(k_0)}{(2\pi)} [\frac{1}{k_0 - k_0^{(1)}} \quad \frac{1}{k_0^{(2)} - k_0}] \\ &= \frac{-L(k_0)}{(2\pi)} [\frac{1}{q_0 - \omega_k - \omega_p + 2i\eta}]. \end{aligned} \tag{3.6}$$

Collecting those nonvanishing integrations for all possible self-energy graphs we can organize them as

$$\begin{aligned} I_V &= i[\frac{-L_1}{q_0 - \omega_k - \omega_p + i\eta} + \frac{L_4}{q_0 + \omega_k + \omega_p - i\eta}] \qquad , \text{for } p = q - k, k - q \\ &= i[\frac{-L_2}{q_0 - \omega_k - \omega_p + i\eta} + \frac{L_5}{q_0 + \omega_k + \omega_p - i\eta}] \qquad , \text{for } p = q + k \end{aligned} \tag{3.7}$$

where

$$\begin{aligned} &L_1 = L(k_0 = \omega_k) && L_4 = L(k_0 = q_0 + \omega_p) \\ &L_2 = L(k_0 = -\omega_k) && L_5 = L(k_0 = -q_0 - \omega_p) \\ &L_3 = L(k_0 = q_0 - \omega_p) && L_6 = L(k_0 = -q_0 + \omega_p). \end{aligned} \tag{3.8}$$

L_3 and L_6 will be appeared in our later calculations.

$$\begin{aligned} \Pi_V(q^2) &= -\epsilon_F \int \frac{d^3k}{(2\pi)^3} \frac{1}{4\omega_k\omega_p} [\frac{-L_1}{q_0 - \omega_k - \omega_p + i\eta} + \frac{L_4}{q_0 + \omega_k + \omega_p - i\eta}] \qquad , \text{for } p = q - k, k - q \\ &= -\epsilon_F \int \frac{d^3k}{(2\pi)^3} \frac{1}{4\omega_k\omega_p} [\frac{-L_2}{q_0 - \omega_k - \omega_p + i\eta} + \frac{L_5}{q_0 + \omega_k + \omega_p - i\eta}] \qquad , \text{for } p = q + k. \end{aligned} \tag{3.9}$$

The principal value of above expression give the real part of vacuum self-energy. This is a divergent quantity which after renormalization [66, 49, 67, 68] produces a finite value. The imaginary part of vacuum self-energy is directly related with the vacuum decay width. From Eq. (3.9), this part can be separated out to get

$$\mathrm{Im}\Pi_V(q^2) = -\pi\epsilon_F \int \frac{d^3k}{(2\pi)^3} \frac{1}{4\omega_k\omega_p} \{L_1\delta(q_0 - \omega_k - \omega_p) + L_2\delta(q_0 + \omega_k + \omega_p)\} \quad , \text{for } p = q - k, k - q$$

[1]As scalar part of propagator for $p = q - k$ and $p = k - q$ are exactly same so they will give same final results of integrations and that's why we have provided the information about the poles and residues for only $p = q - k$ case in the Table.

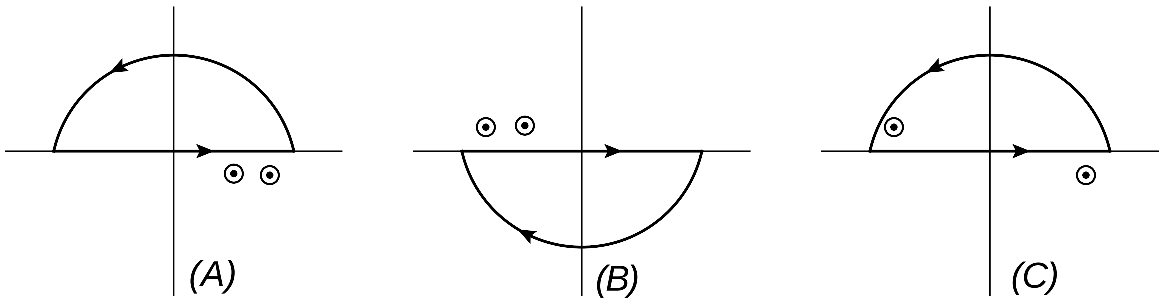

Figure 3.3:

$$= \quad -\pi\epsilon_F \int \frac{d^3k}{(2\pi)^3}\frac{1}{4\omega_k\omega_p}\{L_2\delta(q_0-\omega_k-\omega_p)+L_1\delta(q_0+\omega_k+\omega_p)\} \quad \text{, for } p=q+k. \tag{3.10}$$

3.2 Thermal Self-energy

Now we proceed to evaluate the one-loop self-energy at finite temperature. In real time thermal field theory we have seen that both thermal propagator and self-energy have 2×2 matrix structure and can be diagonalized. The diagonalization of thermal self-energy is slightly different from that of the thermal propagator, discussed previously in Eq. (2.104). In this case we have

$$\Pi_{ab} = (U^{-1}\begin{pmatrix}\overline{\Pi} & 0\\ 0 & -\overline{\Pi}^*\end{pmatrix}U^{-1})_{ab} \quad \text{where } U^{-1} = \begin{pmatrix} N_{2q}/\sqrt{N_q} & -\epsilon_q\sqrt{N_q}e^{\beta\mu/2}\\ -\sqrt{N_q}e^{-\beta\mu/2} & N_{2q}/\sqrt{N_q}\end{pmatrix}$$

$$\begin{aligned}\text{i.e. } U^{-1} &= \begin{pmatrix} N_{2q}/\sqrt{N_q} & \sqrt{N_q}e^{\beta\mu/2}\\ -\sqrt{N_q}e^{-\beta\mu/2} & N_{2q}/\sqrt{N_q}\end{pmatrix} \quad \text{for fermion}\\ &= \begin{pmatrix}\sqrt{n(1+n)} & -\sqrt{n}\\ -\sqrt{n} & \sqrt{n(1+n)}\end{pmatrix} \quad \text{for boson.}\end{aligned} \tag{3.11}$$

So $\Pi_{11} = \frac{N_{2q}^2}{N_q}\overline{\Pi} - \epsilon_q N_q\overline{\Pi}^*$ and in spectral representation,

$$\Pi_{11} = \int_{-\infty}^{\infty}\frac{dq_0}{2\pi}\Omega(q_0',\vec{q})[\frac{1}{(q_0-q_0')-i\eta}+\epsilon_q 2\pi i\delta(q_0-q_0')f(q_0')] \tag{3.12}$$

where $\Omega(q_0',\vec{q})$ is one-loop spectral density. Similar to thermal propagator, corresponding quantities for self-energy also follow the same relations (compare with Eq. 2.97)

$$\Omega(q_0',\vec{q}) = 2\epsilon(q_0)\mathrm{Im}\overline{\Pi}(q) = 2\coth(\beta\{(q_0-\mu_q)/2\})\mathrm{Im}\Pi^{11}(q) \quad \text{for fermion self}-\text{energy}$$

$$= 2\tanh(\beta q_0/2)\mathrm{Im}\Pi^{11}(q) \qquad\qquad \text{for boson self}-\text{energy}$$

$$\mathrm{Re}\overline{\Pi}_{\mu\nu}(q) = \mathrm{Re}\Pi^{11}_{\mu\nu}(q). \tag{3.13}$$

These spectral densities (Ω or ϱ) are closely related with retarded part of corresponding quantities.[2]

So we will now focus on the 11-component of the thermal self-energy matrix

$$\begin{aligned}\Pi^{11}(q) &= i\epsilon_F \int \frac{d^4k}{(2\pi)^4} v_1(q,k,p) P_{11}(k,m_k) P_{11}(p,m_p) v_2(q,k,p) \\ &= i\epsilon_F \int \frac{d^4k}{(2\pi)^4} L(k,q,p)\Delta_{11}(k,m_k)\Delta_{11}(p,m_p)\end{aligned} \tag{3.15}$$

where $L(k,q,p) = v_1(q,k,p)\zeta_k\zeta_p v_2(q,k,p)$ since the 11-component of thermal propagator has a form like

$$P_{11}(k,m_k) = \zeta_k \Delta_{11}(k,m_k) \qquad , \ \Delta_{11}(k,m_k) = \Delta(k) + \epsilon_k 2\pi i \delta(k^2 - m_k^2) N_k. \tag{3.16}$$

Each of the thermal internal lines has two parts containing the information of vacuum and medium separately. So $\Pi^{11}(q)$ also separates into vacuum and medium parts. The medium contribution has a part linear in the distribution function and a part quadratic in it. So we will decompose $\Pi^{11}(q)$ into three parts as

$$\Pi^{11}(q) = \Pi^{11}_V(q) + \Pi^{11}_n(q) + \Pi^{11}_{n^2}(q) \tag{3.17}$$

where $\Pi^{11}_V(q) = i\epsilon_F \int \frac{d^4k}{(2\pi)^4} L(k,q,p)\Delta(k)\Delta(p)$ is the vacuum part, and

$$\Pi^{11}_n(q) = i\epsilon_F \int \frac{d^4k}{(2\pi)^4} L(k,q,p)[\epsilon_k 2\pi i\delta(k^2 - m_k^2)N_k\Delta(p) + \epsilon_p 2\pi i\delta(p^2 - m_p^2)N_p\Delta(k)] \tag{3.18}$$

$$\Pi^{11}_{n^2}(q) = i\epsilon_F \int \frac{d^4k}{(2\pi)^4} L(k,q,p)[\{\epsilon_k 2\pi i\delta(k^2 - m_k^2)N_k\}\{\epsilon_p 2\pi i\delta(p^2 - m_p^2)N_p\}] \tag{3.19}$$

are the medium dependent part of self-energy, explicitly showing the linear and quadratic dependence on distribution function respectively.

[2]The retarded propgator, $P_R = \zeta\frac{-1}{(q^2-m^2)+i\eta_R\epsilon(q_0)}$ and diagonal element of thermal propagator, $\overline{P} = \zeta\frac{-1}{(q^2-m^2)+i\overline{\eta}}$ suggest the relations

$$\begin{aligned}\text{Re } P_R \text{ (or } \Pi_R) &= \mathrm{Re}\overline{P} \text{ (or } \overline{\Pi}) \\ \varrho \text{ (or } \Omega) = 2\mathrm{Im}P_R \text{ (or } \Pi_R) &= 2\epsilon(q_0)\mathrm{Im}\overline{P} \text{ (or } \overline{\Pi})\end{aligned} \tag{3.14}$$

Imaginary part of Self-energy take the place of η and so guided from the relation $\eta_R = \epsilon(q_0)\overline{\eta}$, we can intuitively proceed to above relation for imaginary part of self-energy.

$\underline{\Pi_n^{11}(q):}$

Considering the general form of $N_k = n_+^k\theta(k_0) + n_-^k\theta(-k_0)$, we can write

$$\begin{aligned} N_k\delta(k^2 - m_k^2) &= \frac{1}{2\omega_k}[n_+^k\theta(k_0) + n_-^k\theta(-k_0)][\delta(k_0-\omega_k) + \delta(k_0+\omega_k)] \\ &= \frac{1}{2\omega_k}[n_+^k\delta(k_0-\omega_k) + n_-^k\delta(k_0+\omega_k)]. \end{aligned} \tag{3.20}$$

Here we have used $\theta(k_0)\delta(k_0 \pm \omega_k) = \theta(\mp\omega_k)\delta(k_0 \pm \omega_k)$, where ω_k is always a positive quantity. Using Eq. (3.20) for momentum k as well as p in Eq. (3.18), we have

$$\Pi_n^{11}(q) = -\epsilon_F \int \frac{d^3k}{(2\pi)^3} I_n \tag{3.21}$$

where

$$\begin{aligned} I_n &= \int dk_0 L(k_0,k,q,p)[\frac{\epsilon_k}{2\omega_k}\{n_+^k\delta(k_0-\omega_k) + n_-^k\delta(k_0+\omega_k)\}\frac{-1}{p_0^2-\omega_p^2+i\eta} \\ &\quad + \frac{\epsilon_p}{2\omega_p}\{n_+^p\delta(p_0-\omega_p) + n_-^p\delta(p_0+\omega_p)\}\frac{-1}{k_0^2-\omega_k^2+i\eta}] \\ &= -\int dk_0 \frac{L(k_0)}{4\omega_k\omega_p}[\epsilon_k\{n_+^k\delta(k_0-\omega_k) + n_-^k\delta(k_0+\omega_k)\}\{\frac{1}{p_0-\omega_p+i\eta} - \frac{1}{p_0+\omega_p-i\eta}\} \\ &\quad + \epsilon_p\{n_+^p\delta(p_0-\omega_p) + n_-^p\delta(p_0+\omega_p)\}\{\frac{1}{k_0-\omega_k+i\eta} - \frac{1}{k_0+\omega_k-i\eta}\}] \\ &= -\frac{1}{4\omega_k\omega_p}\int dk_0 L(k_0)[\epsilon_k n_+^k\delta(k_0-\omega_k)\{\frac{1}{(\epsilon_1 q_0+\epsilon_2 k_0)-\omega_p+i\eta} - \frac{1}{(\epsilon_1 q_0+\epsilon_2 k_0)+\omega_p-i\eta}\} \\ &\quad + \epsilon_k n_-^k\delta(k_0+\omega_k)\{\frac{1}{(\epsilon_1 q_0+\epsilon_2 k_0)-\omega_p+i\eta} - \frac{1}{(\epsilon_1 q_0+\epsilon_2 k_0)+\omega_p-i\eta}\} \\ &\quad + \epsilon_p n_+^p\delta(\epsilon_1 q_0+\epsilon_2 k_0-\omega_p)\{\frac{1}{k_0-\omega_k+i\eta} - \frac{1}{k_0+\omega_k-i\eta}\} \\ &\quad + \epsilon_p n_-^p\delta(\epsilon_1 q_0+\epsilon_2 k_0+\omega_p)\{\frac{1}{k_0-\omega_k+i\eta} - \frac{1}{k_0+\omega_k-i\eta}\}] \\ &= -\frac{1}{4\omega_k\omega_p}[\{\frac{\epsilon_k n_+^k L_1}{(\epsilon_1 q_0+\epsilon_2\omega_k)-\omega_p+i\eta} - \frac{\epsilon_k n_+^k L_1}{(\epsilon_1 q_0+\epsilon_2\omega_k)+\omega_p-i\eta}\} \\ &\quad + \{\frac{\epsilon_k n_-^k L_2}{(\epsilon_1 q_0-\epsilon_2\omega_k)-\omega_p+i\eta} - \frac{\epsilon_k n_-^k L_2}{(\epsilon_1 q_0-\epsilon_2\omega_k)+\omega_p-i\eta}\} \\ &\quad + \{\frac{\epsilon_p n_+^p L_3}{\epsilon_2(-\epsilon_1 q_0+\omega_p)-\omega_k+i\eta} - \frac{\epsilon_p n_+^p L_3}{\epsilon_2(-\epsilon_1 q_0+\omega_p)+\omega_k-i\eta}\} \\ &\quad + \{\frac{\epsilon_p n_-^p L_4}{\epsilon_2(-\epsilon_1 q_0-\omega_p)-\omega_k+i\eta} - \frac{\epsilon_p n_-^p L_4}{\epsilon_2(-\epsilon_1 q_0-\omega_p)+\omega_k-i\eta}\}] \\ &= -\frac{1}{4\omega_k\omega_p}[\{\frac{\epsilon_k n_+^k L_1}{(\epsilon_1 q_0+\epsilon_2\omega_k)-\omega_p+i\eta} - \frac{\epsilon_2\epsilon_p n_+^p L_3}{(\epsilon_1 q_0+\epsilon_2\omega_k)-\omega_p-i\eta\epsilon_2}\} \\ &\quad + \{-\frac{\epsilon_k n_+^k L_1}{(\epsilon_1 q_0+\epsilon_2\omega_k)+\omega_p-i\eta} - \frac{\epsilon_2\epsilon_p n_-^p L_4}{(\epsilon_1 q_0+\epsilon_2\omega_k)+\omega_p-i\eta\epsilon_2}\} \end{aligned}$$

$$+\{\frac{\epsilon_k n^k_- L_2}{(\epsilon_1 q_0 - \epsilon_2\omega_k) - \omega_p + i\eta} + \frac{\epsilon_2\epsilon_p n^p_+ L_3}{(\epsilon_1 q_0 - \epsilon_2\omega_k) - \omega_p + i\eta\epsilon_2}\}$$
$$+\{-\frac{\epsilon_k n^k_- L_2}{(\epsilon_1 q_0 - \epsilon_2\omega_k) + \omega_p - i\eta} + \frac{\epsilon_2\epsilon_p n^p_- L_4}{(\epsilon_1 q_0 - \epsilon_2\omega_k) + \omega_p + i\eta\epsilon_2}\}]. \tag{3.22}$$

Here $L_3 = L\{k_0 = \epsilon_2(-\epsilon_1 q_0 + \omega_p)\}$ and $L_4 = L\{k_0 = \epsilon_2(-\epsilon_1 q_0 - \omega_p)\}$. Note that

$$\begin{aligned} L_3 &\to L_3, L_4 \to L_4 \qquad \text{for } p = q - k \\ L_3 &\to L_4, L_4 \to L_3 \qquad \text{for } p = k - q \\ L_3 &\to L_6, L_4 \to L_5 \qquad \text{for } p = k + q. \end{aligned} \tag{3.23}$$

Now using the complex identity $\frac{1}{x \pm i\eta} = \mathcal{P}(\frac{1}{x}) \mp i\pi\delta(x)$, we decompose $\Pi^{11}_n(q)$ into imaginary and real part as

$$\begin{aligned} \mathrm{Im}\Pi^{11}_n(q) &= -\epsilon_F \int \frac{d^3k}{(2\pi)^3} \mathrm{Im} I_n \\ &= -\epsilon_F \pi \int \frac{d^3k}{(2\pi)^3}\frac{1}{4\omega_k\omega_p}[(\epsilon_k n^k_+ L_1 + \epsilon_2^2\epsilon_p n^p_+ L_3)\delta(\epsilon_1 q_0 + \epsilon_2\omega_k - \omega_p) \\ &\quad + (\epsilon_k n^k_+ L_1 + \epsilon_2^2\epsilon_p n^p_- L_4)\delta(\epsilon_1 q_0 + \epsilon_2\omega_k + \omega_p) \\ &\quad +(\epsilon_k n^k_- L_2 + \epsilon_2^2\epsilon_p n^p_+ L_3)\delta(\epsilon_1 q_0 - \epsilon_2\omega_k - \omega_p) \\ &\quad + (\epsilon_k n^k_- L_2 + \epsilon_2^2\epsilon_p n^p_- L_4)\delta(\epsilon_1 q_0 - \epsilon_2\omega_k + \omega_p)] \\ &= -\epsilon_F \pi \int \frac{d^3k}{(2\pi)^3}\frac{1}{4\omega_k\omega_p}[L_1\{(\epsilon_k n^k_+ + \epsilon_p n^p_+)\delta(\epsilon_1 q_0 + \epsilon_2\omega_k - \omega_p) \\ &\quad + (\epsilon_k n^k_+ + \epsilon_p n^p_-)\delta(\epsilon_1 q_0 + \epsilon_2\omega_k + \omega_p)\} \\ &\quad +L_2\{(\epsilon_k n^k_- + \epsilon_p n^p_+)\delta(\epsilon_1 q_0 - \epsilon_2\omega_k - \omega_p) \\ &\quad + (\epsilon_k n^k_- + \epsilon_2^2\epsilon_p n^p_-)\delta(\epsilon_1 q_0 - \epsilon_2\omega_k + \omega_p)\}] \end{aligned} \tag{3.24}$$

and

$$\begin{aligned} \mathrm{Re}\Pi^{11}_n(q) &= -\epsilon_F \int \frac{d^3k}{(2\pi)^3} \mathrm{Re} I_n \\ &= \epsilon_F \int \frac{d^3k}{(2\pi)^3}\frac{1}{4\omega_k\omega_p}\mathcal{P}[\frac{\epsilon_k n^k_+ L_1 - \epsilon_2\epsilon_p n^p_+ L_3}{(\epsilon_1 q_0 + \epsilon_2\omega_k) - \omega_p} + \frac{-\epsilon_k n^k_+ L_1 - \epsilon_2\epsilon_p n^p_- L_4}{(\epsilon_1 q_0 + \epsilon_2\omega_k) + \omega_p} \\ &\quad +\frac{\epsilon_k n^k_- L_2 + \epsilon_2\epsilon_p n^p_+ L_3}{(\epsilon_1 q_0 - \epsilon_2\omega_k) - \omega_p} + \frac{-\epsilon_k n^k_- L_2 + \epsilon_2\epsilon_p n^p_- L_4}{(\epsilon_1 q_0 - \epsilon_2\omega_k) + \omega_p}]. \end{aligned} \tag{3.25}$$

The real part arises completely due to medium and vanishes at T=0. Due to the presence of distribution function, this part is free from any divergence Nonzero value of this real part may shift the pole.

$\underline{\Pi^{11}_{n^2}(q)\ :}$

$$\Pi^{11}_{n^2}(q) = -i2\pi\epsilon_F\epsilon_k\epsilon_p\int\frac{d^3k}{(2\pi)^3}I_{n^2} \tag{3.26}$$

where

$$\begin{aligned}
I_{n^2} &= \int dk_0 L(k_0)N_k\delta(k_0^2-\omega_k^2)N_p\delta(p_0^2-\omega_p^2)\\
&= \int\frac{dk_0 L(k_0)}{4\omega_k\omega_p}\{n_+^k\delta(k_0-\omega_k)+n_-^k\delta(k_0+\omega_k)\}\{n_+^p\delta(\epsilon_1 q_0+\epsilon_2 k_0-\omega_p)\\
&\qquad + n_-^p\delta(\epsilon_1 q_0+\epsilon_2 k_0+\omega_p)\}\\
&= \frac{1}{4\omega_k\omega_p}[L_1\{n_+^k n_+^p\delta(\epsilon_1 q_0+\epsilon_2\omega_k-\omega_p)+n_+^k n_-^p\delta(\epsilon_1 q_0+\epsilon_2\omega_k+\omega_p)\}\\
&\quad +L_2\{n_-^k n_+^p\delta(\epsilon_1 q_0-\epsilon_2\omega_k-\omega_p)+n_-^k n_-^p\delta(\epsilon_1 q_0-\epsilon_2\omega_k+\omega_p)\}].
\end{aligned} \tag{3.27}$$

Since this is a pure imaginary term, So

$$\begin{aligned}
\mathrm{Re}\Pi^{11}_{n^2}(q) &= 0\\
\mathrm{Im}\Pi^{11}_{n^2}(q) &= -2\pi\epsilon_F\epsilon_k\epsilon_p\int\frac{d^3k}{(2\pi)^3}I_{n^2}\\
&= -2\pi\epsilon_F\epsilon_k\epsilon_p\int\frac{d^3k}{(2\pi)^3}\frac{1}{4\omega_k\omega_p}[L_1\{n_+^k n_+^p\delta(\epsilon_1 q_0+\epsilon_2\omega_k-\omega_p)\\
&\quad +n_+^k n_-^p\delta(\epsilon_1 q_0+\epsilon_2\omega_k+\omega_p)\}+L_2\{n_-^k n_+^p\delta(\epsilon_1 q_0-\epsilon_2\omega_k-\omega_p)\\
&\qquad + n_-^k n_-^p\delta(\epsilon_1 q_0-\epsilon_2\omega_k+\omega_p)\}].
\end{aligned} \tag{3.28}$$

Collecting the imaginary part of self-energy from Eq. (3.28) and (3.24) we will get medium dependent part

$$\begin{aligned}
\mathrm{Im}\Pi^{11}_{\mathrm{med}} &= \mathrm{Im}\Pi^{11}_n+\mathrm{Im}\Pi^{11}_{n^2}\\
&= -\pi\epsilon_F\int\frac{d^3k}{(2\pi)^3}\frac{1}{4\omega_k\omega_p}[L_1\{(\epsilon_k n_+^k+\epsilon_p n_+^k+2\epsilon_k\epsilon_p n_+^k n_+^p)\delta(\epsilon_1 q_0+\epsilon_2\omega_k-\omega_p)\\
&\qquad + (\epsilon_k n_+^k+\epsilon_p n_-^p+2\epsilon_k\epsilon_p n_+^k n_-^p)\delta(\epsilon_1 q_0+\epsilon_2\omega_k+\omega_p)\}\\
&\quad +L_2\{(\epsilon_k n_-^k+\epsilon_p n_+^p+2\epsilon_k\epsilon_p n_-^k n_+^p)\delta(\epsilon_1 q_0-\epsilon_2\omega_k-\omega_p)\\
&\qquad + (\epsilon_k n_-^k+\epsilon_p n_-^p+2\epsilon_k\epsilon_p n_-^k n_-^p)\delta(\epsilon_1 q_0-\epsilon_2\omega_k+\omega_p)\}].
\end{aligned} \tag{3.29}$$

Now adding the vacuum part from Eq. (3.9) to above Eq. (3.29) we will get the 11-component total in-medium self-energy

$$\Pi^{11} = \Pi_V+\{\mathrm{Im}\Pi^{11}_n+\mathrm{Im}\Pi^{11}_{n^2}\}+\{\mathrm{Re}\Pi^{11}_n\}. \tag{3.30}$$

For the four possible cases, imaginary and real part of total self-energy are evaluated below. We have repeatedly made use of Eq. (3.10), (3.29), (3.25) to specialize to three cases with appropriate values of ϵ_1, ϵ_2 etc.

3.2.1 Boson self-energy for boson-boson (BB) loop

$$\begin{aligned}
\mathrm{Im}\Pi^{11} &= -\pi\int\frac{d^3k}{(2\pi)^3}\frac{1}{4\omega_k\omega_p}[L_1\{(1+n_+^k+n_+^p+2n_+^kn_+^p)\delta(q_0-\omega_k-\omega_p) \\
&\quad +(n_+^k+n_-^p+2n_+^kn_-^p)\delta(q_0-\omega_k+\omega_p)\}+L_2\{(n_-^k+n_+^p+2n_-^kn_+^p)\delta(q_0+\omega_k-\omega_p) \\
&\quad +(1+n_-^k+n_-^p+2n_-^kn_-^p)\delta(q_0+\omega_k+\omega_p)\}] \\
&= \coth(\frac{\beta(q_0-\mu_q)}{2})\epsilon(q_0)\mathrm{Im}\overline{\Pi} \quad \text{, using Eq.(3.13) for boson with nonvanishing } \mu_q \\
\text{where } \mathrm{Im}\overline{\Pi} &= -\epsilon(q_0)\pi\int\frac{d^3k}{(2\pi)^3}\frac{1}{4\omega_k\omega_p}[L_1\{(1+n_+^k+n_+^p)\delta(q_0-\omega_k-\omega_p) \\
&\quad +(-n_+^k+n_-^p)\delta(q_0-\omega_k+\omega_p)\}+L_2\{(n_-^k-n_+^p)\delta(q_0+\omega_k-\omega_p) \\
&\quad +(-1-n_-^k-n_-^p)\delta(q_0+\omega_k+\omega_p)\}].
\end{aligned} \tag{3.31}$$

In second step we have rearranged the distribution functions as (here $n_\pm^{k,p}=\frac{1}{e^{\beta(\omega_{k,p}\mp\mu)-1}}$)

$$\begin{aligned}
(1+n_+^k+n_+^p+2n_+^kn_+^p) &= \frac{(1+n_+^k)(1+n_+^p)+n_+^kn_+^p}{(1+n_+^k)(1+n_+^p)-n_+^kn_+^p}(1+n_+^k+n_+^p) \\
&= \coth(\frac{\beta\{(\omega_k+\omega_p)-(\mu_k+\mu_p)\}}{2})(1+n_+^k+n_+^p) \\
(n_+^k+n_-^p+2n_+^kn_-^p) &= \frac{(1+n_+^k)n_-^p+n_+^k(1+n_-^p)}{(1+n_+^k)n_-^p-n_+^k(1+n_-^p)}(-n_+^k+n_-^p) \\
&= \coth(\frac{\beta\{(\omega_k-\omega_p)-(\mu_k+\mu_p)\}}{2})(-n_+^k+n_-^p) \\
(n_-^k+n_+^p+2n_-^kn_+^p) &= \frac{n_-^k(1+n_+^p)+n_+^p(1+n_-^k)}{n_-^k(1+n_+^p)-n_+^p(1+n_-^k)}(n_-^k-n_+^p) \\
&= \coth(\frac{\beta\{(-\omega_k+\omega_p)-(\mu_k+\mu_p)\}}{2})(n_-^k+n_+^p) \\
(1+n_-^k+n_-^p+2n_-^kn_-^p) &= \frac{n_-^kn_-^p+(1+n_-^k)(1+n_-^p)}{n_-^kn_-^p-(1+n_-^k)(1+n_-^p)}(-1-n_-^k-n_-^p) \\
&= \coth(\frac{\beta\{(-\omega_k-\omega_p)-(\mu_k+\mu_p)\}}{2})(-1-n_-^k-n_-^p)
\end{aligned} \tag{3.32}$$

and each of the cothyperbolic functions are attached to the different δ-functions in such a systematic manner that we can convert them into a common function, $\coth(\frac{\beta(q_0-\mu_q)}{2})$, assuming $\mu_q=\mu_k+\mu_p$. For e.g. $\coth(\frac{\beta\{(\omega_k+\omega_p)-(\mu_k+\mu_p)\}}{2})\delta(q_0-\omega_k-\omega_p)=\coth(\frac{\beta(q_0-\mu_q)}{2})\delta(q_0-$

$\omega_k - \omega_p$). The general form of real part, Eq. (3.25) now produces the expression

$$\mathrm{Re}\overline{\Pi}(q) = \mathrm{Re}\Pi^{11}_n(q) = \int \frac{d^3k}{(2\pi)^3}\frac{1}{4\omega_k\omega_p}\mathcal{P}[\frac{n^k_+ L_1 + n^p_+ L_3}{q_0 - \omega_k - \omega_p} + \frac{-n^k_+ L_1 + n^p_- L_4}{q_0 - \omega_k + \omega_p} + \frac{n^k_- L_2 - n^p_+ L_3}{q_0 + \omega_k - \omega_p} + \frac{-n^k_- L_2 - n^p_- L_4}{q_0 + \omega_k + \omega_p}]. \tag{3.33}$$

In this case, external and internal, all lines contain bosons. In absence of conserved charges, $\mu_q = \mu_k = \mu_p = 0$ and therefore $n_\pm = n = \frac{1}{e^{\beta\omega}-1}$.

3.2.2 Fermion self-energy for boson-fermion (BF) loop

In this case only one of the boson internal lines is replaced by a fermion, so we will get expressions similar to as Eq. (3.31) and (3.33) in which the sign attached with n^p will be opposite i.e. $n^p \to -n^p$.

$$\begin{aligned}
\mathrm{Im}\overline{\Pi} &= -\epsilon(q_0)\pi \int \frac{d^3k}{(2\pi)^3}\frac{1}{4\omega_k\omega_p}[L_1\{(1 + n^k_+ - n^p_+)\delta(q_0 - \omega_k - \omega_p) \\
&\quad +(-n^k_+ - n^p_-)\delta(q_0 - \omega_k + \omega_p)\} + L_2\{(n^k_- + n^p_+)\delta(q_0 + \omega_k - \omega_p) \\
&\quad + (-1 - n^k_- + n^p_-)\delta(q_0 - \omega_k + \omega_p)\}] \\
\mathrm{Re}\overline{\Pi}(q) &= \int \frac{d^3k}{(2\pi)^3}\frac{1}{4\omega_k\omega_p}\mathcal{P}[\frac{n^k_+ L_1 - n^p_+ L_3}{q_0 - \omega_k - \omega_p} + \frac{-n^k_+ L_1 - n^p_- L_4}{q_0 - \omega_k + \omega_p} \\
&\quad + \frac{n^k_- L_2 + n^p_+ L_3}{q_0 + \omega_k - \omega_p} + \frac{-n^k_- L_2 + n^p_- L_4}{q_0 + \omega_k + \omega_p}].
\end{aligned} \tag{3.34}$$

The cancellation of the common hyperbolic function (here it is $\tanh\{\beta(q_0 - \mu_q)\}/2$) is still valid because for this case the distribution functions are rearranged as follows (here $n^k_\pm = \frac{1}{e^{\beta(\omega_k \mp \mu)}-1}$ and $n^p_\pm = \frac{1}{e^{\beta(\omega_p \mp \mu)}+1}$)

$$\begin{aligned}
(1 + n^k_+ - n^p_+ - 2n^k_+ n^p_+) &= \frac{(1+n^k_+)(1-n^p_+) - n^k_+ n^p_+}{(1+n^k_+)(1-n^p_+) + n^k_+ n^p_+}(1 + n^k_+ - n^p_+) \\
&= \tanh(\frac{\beta\{(\omega_k + \omega_p) - (\mu_k + \mu_p)\}}{2})(1 + n^k_+ - n^p_+) \\
(n^k_+ - n^p_- - 2n^k_+ n^p_-) &= \frac{-(1+n^k_+)n^p_- + n^k_+(1-n^p_-)}{-(1+n^k_+)n^p_- - n^k_+(1-n^p_-)}(-n^k_+ - n^p_-) \\
&= \tanh(\frac{\beta\{(\omega_k - \omega_p) - (\mu_k + \mu_p)\}}{2})(-n^k_+ - n^p_-) \\
(n^k_- - n^p_+ - 2n^k_- n^p_+) &= \frac{n^k_-(1-n^p_+) - n^p_+(1+n^k_-)}{n^k_-(1-n^p_+) + n^p_+(1+n^k_-)}(n^k_- + n^p_+) \\
&= \tanh(\frac{\beta\{(-\omega_k + \omega_p) - (\mu_k + \mu_p)\}}{2})(n^k_- + n^p_+) \\
(1 + n^k_- - n^p_- - 2n^k_- n^p_-) &= \frac{-n^k_- n^p_- + (1+n^k_-)(1-n^p_-)}{-n^k_- n^p_- - (1+n^k_-)(1-n^p_-)}(-1 - n^k_- + n^p_-)
\end{aligned}$$

$$= \tanh(\frac{\beta\{(-\omega_k - \omega_p) - (\mu_k + \mu_p)\}}{2})(-1 - n^k_- + n^p_-). \tag{3.35}$$

We have to assume $\mu_q = \mu_p$ to hold the relation $\mu_q = \mu_k + \mu_p$ as $\mu_k = 0$ (i.e. we should write in Eq. (3.34), $n^k_\pm = n^k = \frac{1}{e^{\beta\omega_k} - 1}$).

3.2.3 Boson self-energy for fermion-fermion loop

<u>$F\overline{F}$ **internal lines of** B **self-energy**</u> **:**

In this case momentum of lower internal line is $p = k - q$, so adding the corresponding vacuum expression of Eq. (3.10) to the medium part (3.29) with corresponding sign functions (see Table.3.1), we have

$$\begin{aligned}
\mathrm{Im}\Pi^{11} &= \pi\int\frac{d^3k}{(2\pi)^3}\frac{1}{4\omega_k\omega_p}[L_1\{(-n^k_+ - n^p_+ + 2n^k_+ n^p_+)\delta(-q_0 + \omega_k - \omega_p) \\
&\qquad + (-n^k_+ - n^p_- + 2n^k_+ n^p_-)\delta(-q_0 + \omega_k + \omega_p)\} \\
&\quad + L_2\{(-n^k_- - n^p_+ + 2n^k_- n^p_+)\delta(-q_0 - \omega_k - \omega_p) \\
&\qquad + (-n^k_- - n^p_- + 2n^k_- n^p_-)\delta(-q_0 - \omega_k + \omega_p)\}] \\
&\quad \pi\int\frac{d^3k}{(2\pi)^3}\frac{1}{4\omega_k\omega_p}\{L_1\delta(q_0 - \omega_k - \omega_p) + L_2\delta(q_0 + \omega_k + \omega_p)\} \\
&= \pi\int\frac{d^3k}{(2\pi)^3}\frac{1}{4\omega_k\omega_p}[L_1\{(-n^k_+ - n^p_+ + 2n^k_+ n^p_+)\delta(q_0 - \omega_k + \omega_p) \\
&\qquad + (1 - n^k_+ - n^p_- + 2n^k_+ n^p_-)\delta(q_0 - \omega_k - \omega_p)\} \\
&\quad + L_2\{(1 - n^k_- - n^p_+ + 2n^k_- n^p_+)\delta(q_0 + \omega_k + \omega_p) \\
&\qquad + (-n^k_- - n^p_- + 2n^k_- n^p_-)\delta(q_0 + \omega_k - \omega_p)\}] \\
&= \coth(\frac{\beta(q_0 - \mu_q)}{2})\epsilon(q_0)\mathrm{Im}\overline{\Pi} \\
\text{where } \mathrm{Im}\overline{\Pi} &= \epsilon(q_0)\pi\int\frac{d^3k}{(2\pi)^3}\frac{1}{4\omega_k\omega_p}[L_1\{(1 - n^k_+ - n^p_-)\delta(q_0 - \omega_k - \omega_p) \\
&\quad + (n^k_+ - n^p_+)\delta(q_0 - \omega_k + \omega_p)\} + L_2\{(-n^k_- + n^p_-)\delta(q_0 + \omega_k - \omega_p) \\
&\qquad + (-1 + n^k_- + n^p_+)\delta(q_0 + \omega_k + \omega_p)\}] \\
\text{and } \mathrm{Re}\overline{\Pi} &= -\int\frac{d^3k}{(2\pi)^3}\frac{1}{4\omega_k\omega_p}\mathcal{P}[\{\frac{-n^k_+ L_1 + n^p_+ L_4}{(-q_0 + \omega_k) - \omega_p} + \frac{n^k_+ L_1 + n^p_- L_3}{(-q_0 + \omega_k) + \omega_p} \\
&\quad + \frac{-n^k_- L_2 - n^p_+ L_4}{(-q_0 - \omega_k) - \omega_p} + \frac{n^k_- L_2 - n^p_- L_3}{(-q_0 - \omega_k) + \omega_p}] \\
&\qquad \text{(using the replacement } L_{3,4} \to L_{4,3} \text{ of(3.23).)} \\
&= -\int\frac{d^3k}{(2\pi)^3}\frac{1}{4\omega_k\omega_p}\mathcal{P}[\{\frac{n^k_+ L_1 - n^p_+ L_4}{q_0 - \omega_k + \omega_p} + \frac{-n^k_+ L_1 - n^p_- L_3}{q_0 - \omega_k - \omega_p}
\end{aligned}$$

$$+\frac{n_-^k L_2 + n_+^p L_4}{q_0+\omega_k+\omega_p} + \frac{-n_-^k L_2 + n_-^p L_3}{q_0+\omega_k-\omega_p}] \tag{3.36}$$

by using the relations

$$\begin{aligned}
(1-n_+^k-n_-^p+2n_+^k n_-^p) &= \frac{(1-n_+^k)(1-n_-^p)+n_+^k n_-^p}{(1-n_+^k)(1-n_-^p)-n_+^k n_-^p}(1-n_+^k-n_-^p) \\
&= \coth(\frac{\beta\{(\omega_k+\omega_p)-(\mu_k-\mu_p)\}}{2})(1-n_+^k-n_-^p) \\
(-n_+^k-n_+^p+2n_+^k n_+^p) &= \frac{-(1-n_+^k)n_-^p-n_+^k(1-n_-^p)}{-(1-n_+^k)n_-^p+n_+^k(1-n_-^p)}(n_+^k-n_+^p) \\
&= \coth(\frac{\beta\{(\omega_k-\omega_p)-(\mu_k-\mu_p)\}}{2})(n_+^k-n_+^p) \\
(-n_-^k-n_-^p+2n_-^k n_-^p) &= \frac{-n_-^k(1-n_-^p)-n_-^p(1-n_-^k)}{-n_-^k(1-n_-^p)+n_-^p(1-n_-^k)}(-n_-^k+n_-^p) \\
&= \coth(\frac{\beta\{(-\omega_k+\omega_p)-(\mu_k-\mu_p)\}}{2})(-n_-^k+n_-^p) \\
(1-n_-^k-n_+^p+2n_-^k n_+^p) &= \frac{n_-^k n_+^p+(1-n_-^k)(1-n_+^p)}{n_-^k n_+^p-(1-n_-^k)(1-n_+^p)}(-1+n_-^k+n_-^p) \\
&= \coth(\frac{\beta\{(-\omega_k-\omega_p)-(\mu_k-\mu_p)\}}{2})(-1+n_-^k+n_-^p).
\end{aligned} \tag{3.37}$$

Here we are assuming $\mu_k=\mu_p$ (since $\mu_q=0$) to maintain the cancellation of common hyperbolic functions, $\coth\{\frac{\beta(q_0-\mu_q)}{2}\}$ i.e. $\coth\{\frac{\beta q_0}{2}\}$.

$\overline{F}F$ internal lines of B self-energy :

$$\begin{aligned}
\mathrm{Im}\Pi^{11} &= \pi\int\frac{d^3k}{(2\pi)^3}\frac{1}{4\omega_k\omega_p}[L_1\{(-n_+^k-n_+^p+2n_+^k n_+^p)\delta(q_0+\omega_k-\omega_p) \\
&\qquad + (1-n_+^k-n_-^p+2n_+^k n_-^p)\delta(q_0+\omega_k+\omega_p)\} \\
&\quad +L_2\{(1-n_-^k-n_+^p+2n_-^k n_+^p)\delta(q_0-\omega_k-\omega_p) \\
&\qquad + (-n_-^k-n_-^p+2n_-^k n_-^p)\delta(q_0-\omega_k+\omega_p)\}] \\
&= \coth(\frac{\beta(q_0-\mu_q)}{2})\epsilon(q_0)\mathrm{Im}\overline{\Pi} \\
\text{where }\ \mathrm{Im}\overline{\Pi} &= \epsilon(q_0)\pi\int\frac{d^3k}{(2\pi)^3}\frac{1}{4\omega_k\omega_p}[L_2\{(-1+n_-^k+n_+^p)\delta(q_0-\omega_k-\omega_p) \\
&\quad +(-n_-^k+n_-^p)\delta(q_0-\omega_k+\omega_p)\} + L_1\{(n_+^k-n_+^p)\delta(q_0+\omega_k-\omega_p) \\
&\qquad + (1-n_+^k-n_-^p)\delta(q_0+\omega_k+\omega_p)\}] \\
\text{and }\ \mathrm{Re}\overline{\Pi} &= -\int\frac{d^3k}{(2\pi)^3}\frac{1}{4\omega_k\omega_p}\mathcal{P}[\{\frac{-n_+^k L_1+n_+^p L_6}{q_0+\omega_k-\omega_p}+\frac{n_+^k L_1+n_-^p L_5}{q_0+\omega_k+\omega_p} \\
&\quad +\frac{-n_-^k L_2-n_+^p L_6}{q_0-\omega_k-\omega_p}+\frac{n_-^k L_2-n_-^p L_5}{q_0-\omega_k+\omega_p}]
\end{aligned}$$

$$\text{(using the replacement } L_{3,4} \to L_{6,5} \text{ of(3.23).)} \quad (3.38)$$

So we can write the diagonal element of thermal self-energy in a general form as

$$\begin{aligned} \mathrm{Im}\overline{\Pi} &= -\epsilon(q_0)\epsilon_F\pi\int\frac{d^3k}{(2\pi)^3}\frac{1}{4\omega_k\omega_p}[C_1\delta(q_0-\omega_k-\omega_p)+C_2\delta(q_0-\omega_k+\omega_p) \\ &\qquad C_3\delta(q_0+\omega_k-\omega_p)+C_4\delta(q_0+\omega_k+\omega_p)] \end{aligned} \quad (3.39)$$

and

$$\begin{aligned} \mathrm{Re}\overline{\Pi} &= \epsilon_F\int\frac{d^3k}{(2\pi)^3}\frac{1}{4\omega_k\omega_p}\mathcal{P}[\frac{R_1}{q_0-\omega_k-\omega_p}+\frac{R_2}{q_0-\omega_k+\omega_p} \\ &\qquad +\frac{R_3}{q_0+\omega_k-\omega_p}+\frac{R_4}{q_0+\omega_k+\omega_p}]. \end{aligned} \quad (3.40)$$

where C_i's and R_i's (i=1,2,3,4) are given in Table.(3.3).

3.3 Branch cuts of self-energy

The regions, in which the four terms of imaginary part of self-energy are non-vanishing, give rise to cuts in the self-energy function. These regions are controlled by the respective δ-functions [52]. Thus, the first and the fourth terms are non-vanishing for $q^2 \geq (m_p + m_k)^2$, giving the unitary cut, while the second and the third are non-vanishing for $q^2 \leq (m_p - m_k)^2$, giving the so-called Landau cut.

We shall now obtain the cuts and the associated discontinuities of the self-energy function in the q_0 plane for fixed $|\vec{q}|$. Writing $d^3\vec{k} = 2\pi\sqrt{\omega_k^2 - m_k^2}\,\omega_k d\omega_k \sin\theta d\theta$, where θ is the angle betwen $\vec{q}$ and $\vec{k}$, we can readily integrate over $\cos\theta$ using the δ-functions. But we have to take into account the physical requirement, $|\cos\theta| \leq 1$, which, as we shall see presently, reduces the a priori range (m_k to ∞) of integration over ω_k.

First term of (3.39) :

The first term of (3.39), for which we have $(q_0 - \omega_k)^2 = \omega_p^2$, give

$$\begin{aligned} |\epsilon_1\vec{q}+\epsilon_2\vec{k}|^2+m_p^2 &= (q_0-\omega_k)^2 \qquad \text{as } \omega_p=\sqrt{|\epsilon_1\vec{q}+\epsilon_2\vec{k}|^2+m_p^2} \\ \Longrightarrow \cos\theta_0 &= \epsilon_1\epsilon_2\frac{S_k^2-2q_0\omega_k}{2|\vec{q}|\sqrt{\omega_k^2-m_k^2}}\,, \qquad S_k^2=q^2-m_p^2+m_k^2\,. \end{aligned} \quad (3.41)$$

Then the inequality $|\cos\theta_0| \leq 1$ becomes

$$q^2(\omega_k-\omega_{k+})(\omega_k-\omega_{k-}) \leq 0 \quad (3.42)$$

$\mathrm{Im}\overline{\Pi} = -\epsilon(q_0)\epsilon_F\pi\int\frac{d^3k}{(2\pi)^3}\frac{1}{4\omega_k\omega_p}[C_1\delta(q_0-\omega_k-\omega_p)+C_2\delta(q_0-\omega_k+\omega_p)$ $C_3\delta(q_0+\omega_k-\omega_p)+C_4\delta(q_0+\omega_k+\omega_p)]$				
	BB	BF	$F\overline{F}$	$\overline{F}F$
C_1	$L_1(1+n_+^k+n_+^p)$	$L_1(1+n_+^k-n_+^p)$	$L_1(1-n_+^k-n_-^p)$	$L_2(-1+n_-^k+n_+^p)$
C_2	$L_1(-n_+^k+n_-^p)$	$L_1(-n_+^k-n_-^p)$	$L_1(n_+^k-n_+^p)$	$L_2(-n_-^k+n_-^p)$
C_3	$L_2(n_-^k-n_+^p)$	$L_2(n_-^k+n_+^p)$	$L_2(-n_-^k+n_-^p)$	$L_1(n_+^k-n_+^p)$
C_4	$L_2(-1-n_-^k-n_-^p)$	$L_2(-1-n_-^k+n_-^p)$	$L_2(-1+n_-^k+n_+^p)$	$L_1(1-n_+^k-n_-^p)$
$\mathrm{Re}\overline{\Pi} = \epsilon_F\int\frac{d^3k}{(2\pi)^3}\frac{1}{4\omega_k\omega_p}\mathcal{P}[\frac{R_1}{q_0-\omega_k-\omega_p}+\frac{R_2}{q_0-\omega_k+\omega_p}$ $+\frac{R_3}{q_0+\omega_k-\omega_p}+\frac{R_4}{q_0+\omega_k+\omega_p}]$				
	BB	BF	$F\overline{F}$	$\overline{F}F$
R_1	$L_1n_+^k+L_3n_+^p$	$L_1n_+^k-L_3n_+^p$	$-L_1n_+^k-L_3n_-^p$	$-L_2n_-^k-L_6n_+^p$
R_2	$-L_1n_+^k+L_4n_-^p$	$-L_1n_+^k-L_4n_-^p$	$L_1n_+^k-L_4n_+^p$	$L_2n_-^k-L_5n_-^p$
R_3	$L_2n_-^k-L_3n_+^p$	$L_2n_-^k+L_3n_+^p$	$-L_2n_-^k+L_3n_-^p$	$-L_1n_+^k+L_6n_+^p$
R_4	$-L_2n_-^k-L_4n_-^p$	$-L_2n_-^k+L_4n_-^p$	$L_2n_-^k+L_4n_+^p$	$L_1n_+^k+L_5n_-^p$

Table 3.3: Table showing the detail expressions of C_i and R_i for four individual loops.

where $\omega_{k\pm}$ are the roots of the quadratic equation for ω_k,

$$\omega_{k\pm} = \frac{S_k^2}{2q^2}\{q_0 \pm |\vec{q}|\epsilon(S_k^2)W_k\}\,, \quad W_k(q^2) = \sqrt{1 - \frac{4q^2m_k^2}{S_k^4}}\,. \tag{3.43}$$

In the first term in (3.39), for which $q^2 \geq (m_p + m_k)^2$, as already stated, we have $S_k^2 > 0$ and $W_k < 1$, so that both ω_{k+} and ω_{k-} have the same sign like q_0. Then this term is non-zero only for positive q_0 with the integration variable ω_k restricted to $\omega_{k-} \leq \omega_k \leq \omega_{k+}$ and in terms of ω_k integration it become

$$\mathrm{Im}\,\overline{\Pi}_1(q_0, \vec{q}) = -\frac{1}{16\pi\vec{q}}\int_{\omega_{k-}}^{\omega_{k+}} d\omega_k C_1(\omega_p = q_0 - \omega_k, \cos\theta = \cos\theta_0), \qquad q_0 \geq \sqrt{(m_p + m_k)^2 + |\vec{q}|^2}\,. \tag{3.44}$$

Second term of (3.39) :

For the second term in (3.39), we split the region $q^2 \leq (m_p - m_k)^2$ into two segments, namely, $0 \leq q^2 \leq (m_p - m_k)^2$ and $-\vec{q}^{\,2} \leq q^2 \leq 0$ (as q_0^2 can't be negative) , denoting them as L_a and L_b respectively . The relevant region in q_0-axis for the two segments are determined below

For L_a,

$$\begin{aligned} -\vec{q}^{\,2} \leq (q_0^2 - \vec{q}^{\,2}) \leq 0 &\Longrightarrow 0 \leq q_0^2 \leq \vec{q}^{\,2} \\ &\Longrightarrow -\vec{q} \leq q_0 \leq \vec{q} \end{aligned} \tag{3.45}$$

and for L_b,

$$\begin{aligned} &0 \leq (q_0^2 - \vec{q}^{\,2}) \leq (m_p - m_k)^2 \\ &\Longrightarrow \vec{q}^{\,2} \leq q_0^2 \leq \vec{q}^{\,2} + (m_p - m_k)^2 \\ &\Longrightarrow q_0^2 - \{\vec{q}^{\,2} + (m_p - m_k)^2\} \leq 0 \qquad \text{and} \qquad q_0^2 - \vec{q}^{\,2} \geq 0 \\ &\Longrightarrow -\sqrt{\vec{q}^{\,2} + (m_p - m_k)^2} \leq q_0 \leq \sqrt{\vec{q}^{\,2} + (m_p - m_k)^2} \quad \text{and} \quad q_0 \geq \vec{q} \text{ or } q_0 \leq -\vec{q}. \end{aligned} \tag{3.46}$$

Now assuming $\omega_p \geq \omega_k$, $q_0 = \omega_k - \omega_p \leq 0$. So collecting from (3.45) and (3.46), relevant inequality for this term is given below

$$\begin{aligned} &-\sqrt{\vec{q}^{\,2} + (m_p - m_k)^2} \leq q_0 \leq -\vec{q} \qquad \text{(denoting as } L_{2b}) \\ &-\vec{q} \leq q_0 \leq 0 \qquad \text{(denoting as } L_{2a}). \end{aligned} \tag{3.47}$$

As the second term follow the same inequality (3.42) we get same roots $\omega_{k\pm}$ but unlike the previous term, ω_{k+} is negative for L_{2a} which can be immediately perceived by applying the conditions $S_k^2 < 0$ and $W_k > 1$ in Eq. (3.43). Now for $q^2 \leq 0$, inequality (3.42) gives $\omega_k \geq \omega_{k-} \geq \omega_{k+}$ i.e. $\omega_k \geq \omega_{k-}$ (other inequality $\omega_k \leq \omega_{k+} \leq \omega k-$ does not hold as ω_k can't be negative). So

$$\mathrm{Im}\,\overline{\Pi}_{2a}(q_0, \vec{q}) = -\frac{1}{16\pi\vec{q}}\int_{\omega_{k-}}^{\infty} d\omega_k C_2(\omega_p = -q_0 + \omega_k, \cos\theta = \cos\theta_0), \qquad -\vec{q} \leq q_0 \leq 0. \tag{3.48}$$

Now for L_{2b} $q^2 \geq 0$, $S_k^2 < 0$ and $W_k < 1$. So $\omega_{k\pm}$ both are positive and the integration become

$$\begin{aligned}\mathrm{Im}\,\overline{\Pi}_{2b}(q_0, \vec{q}) = -\frac{1}{16\pi\vec{q}}\int_{\omega_{k+}}^{\omega_{k-}} d\omega_k C_2(\omega_p = -q_0 + \omega_k, \cos\theta = \cos\theta_0)\\ -\sqrt{\vec{q}^{\,2} + (m_p - m_k)^2} \leq q_0 \leq -\vec{q}.\end{aligned} \tag{3.49}$$

<u>Third term of (3.39)</u> :

The third term has same q^2 region of the second term but $q_0 \geq 0$. So choosing from Eq. (3.45) and (3.46) relevant q_0-region is given below

$$\begin{aligned} &0 \leq q_0 \leq \vec{q} && \text{(denoting as } L_{3a}\text{)}\\ &\vec{q} \leq q_0 \leq \vec{q}\sqrt{\vec{q}^{\,2} + (m_p - m_k)^2} && \text{(denoting as } L_{3b}\text{).}\end{aligned} \tag{3.50}$$

The third term of (3.39) give different $\cos\theta_0$ which is evaluated as

$$\begin{aligned}(q_0 + \omega_k)^2 &= \omega_p^2\\ &= |\epsilon_1\vec{q} + \epsilon_2\vec{k}|^2 + m_p^2\\ \Longrightarrow \cos\theta_0 &= \epsilon_1\epsilon_2\frac{S_k^2 + 2q_0\omega_k}{2|\vec{q}|\sqrt{\omega_k^2 - m_k^2}}.\end{aligned} \tag{3.51}$$

The roots of inequality (3.42) will be

$$\widetilde{\omega}_{k\pm} = \frac{S_k^2}{2q^2}\{-q_0 \pm |\vec{q}|\epsilon(S_k^2)W_k\}. \tag{3.52}$$

Following same analysis for finding the $\widetilde{\omega}_k$ limits, the final expression of integration for this term is given by

$$\mathrm{Im}\,\overline{\Pi}_{3a}(q_0, \vec{q}) = -\frac{1}{16\pi\vec{q}}\int_{\widetilde{\omega}_{k-}}^{\infty} d\widetilde{\omega}_k C_3(\widetilde{\omega}_p = q_0 + \widetilde{\omega}_k, \cos\theta = \cos\theta_0)$$

$$
\begin{aligned}
& && 0 \le q_0 \le \vec{q} \\
\mathrm{Im}\,\overline{\Pi}_{3b}(q_0,\vec{q}) &= -\frac{1}{16\pi\vec{q}}\int_{\widetilde{\omega}_{k+}}^{\widetilde{\omega}_{k-}} d\widetilde{\omega}_k C_3(\widetilde{\omega}_p = q_0+\widetilde{\omega}_k, \cos\theta=\cos\theta_0) \\
& && \vec{q} \le q_0 \le \sqrt{\vec{q}^{\,2}+(m_p-m_k)^2}. \qquad (3.53)
\end{aligned}
$$

Forth term of (3.39) : The fourth term contributes entirely to negative values of q_0, $q_0 \le -\sqrt{\vec{q}^{\,2}+(m_p+m_k)^2}$ and following same roots $\widetilde{\omega}_{k\pm}$ as that of third term, this part of integration can be written as

$$
\mathrm{Im}\,\overline{\Pi}_4(q_0,\vec{q}) = -\frac{1}{16\pi\vec{q}}\int_{\widetilde{\omega}_{k-}}^{\widetilde{\omega}_{k+}} d\widetilde{\omega}_k C_4(\widetilde{\omega}_p = -q_0-\widetilde{\omega}_k, \cos\theta=\cos\theta_0), \qquad q_0 \le -\sqrt{(m_p+m_k)^2+|\vec{q}|^2}\,. \tag{3.54}
$$

The relevant limits and quantities of four different branch cut regions are organized in Table.(3.4). The detailed branch cut region in q_0-plane are shown in Fig. (3.4).

3.4 Physical significance one-loop self-energy

The distribution functions present in different terms of Eq. (3.39) may be understood in terms of decay and recombination (inverse decay) probabilities [69].

Before going to $T \neq 0$ let us discuss the imaginary part of oneloop self-energy in vacuum. It can be expressed as square of matrix element of decay , integrated over phase space. This is nothing but the optical theorem. Let us take a simple ϕ^3 theory and to comprehend the theorem, we prove the relation

$$
\frac{-\mathrm{Im}\Pi(q=m_q)}{m_q} = \Gamma_d(m_q) \tag{3.55}
$$

where

$$
\begin{aligned}
\Gamma_d(m_q) &= \frac{1}{2m_q}\int \frac{d^3k}{(2\pi)^3 2\omega_k}\frac{d^3p}{(2\pi)^3 2\omega_p}(2\pi)^4\delta(q-k-p)|\overline{M}|^2 \\
&= \frac{\vec{k}_{cm}}{8\pi m_q^2}|\overline{M}|^2 \qquad , \vec{k}_{cm} = \frac{\sqrt{(m_q^2-m_p^2-m_k^2)-4m_p^2m_k^2}}{2m_q}
\end{aligned} \tag{3.56}
$$

with square of spin averaged decay amplitude $|\overline{M}|^2 = \frac{1}{2s_q+1}\sum_{s_k,s_p}|M(\phi_q\to\phi_k,\phi_p)|^2$.
Now the Lagrangian of scalar ϕ^3 theory is given by

$$
\mathcal{L}_{int} = g\phi_q\phi_k\phi_p \tag{3.57}
$$

for which $M(\phi_q \to \phi_k, \phi_p)|^2 = g^2$ and so

$$\Gamma_d(m_q) = \frac{\sqrt{(m_q^2 - m_p^2 - m_k^2)^2 - 4m_p^2 m_k^2}}{16\pi m_q^3} g^2. \tag{3.58}$$

Now we turn to our self-energy calculation and using Eq. (3.44) at $q = m_q$ for T=0, we have

$$\begin{aligned}
\mathrm{Im}\Pi(q = m_q) &= -\frac{1}{16\pi\vec{q}} \int_{\omega_{k-}}^{\omega_{k+}} d\omega_k L(k_0 = \omega_k, \cos\theta = \cos\theta_0, q = m_q) \\
&= -\frac{1}{16\pi\vec{q}} g^2 [\omega_{k-}(q = m_q) - \omega_{k+}(q = m_q)] \qquad \text{as } L = v_1 \zeta_k \zeta_p v_2 = g^2 \\
&= -\frac{1}{16\pi\vec{q}} g^2 [\frac{S_k^2(q = m_q)}{2m_q^2} 2\vec{q} \sqrt{1 - \frac{4m_q^2 m_k^2}{S_k^4(q = m_q)}}] \\
\Longrightarrow \frac{-\mathrm{Im}\Pi(q = m_q)}{m_q} &= \frac{\sqrt{(m_q^2 - m_p^2 - m_k^2)^2 - 4m_p^2 m_k^2}}{16\pi m_q^3} g^2, \qquad (3.59)
\end{aligned}$$

using the relation $S_k^4(q = m_q) - 4m_q^2 m_k^2 = (m_q^2 - m_p^2 - m_k^2)^2 - 4m_p^2 m_k^2)$.

So the imaginary part of vacuum self-energy in the unitary cut region with positive invariant mass is related to vacuum decay width. Now the same term (3.44) for $T \neq 0$ can be interpreted as the vacuum width, convoluted with statistical weight factors. Here the statistical weight factor is $1 + n_+^k + n_+^p$ and it can be rearranged as $(1 + n_+^k)(1 + n_+^p) - n_+^k n_+^p$, indicating the decay process $\phi_q \to \phi_k \phi_p$ with bose enhanced probability $(1 + n_+^k)(1 + n_+^p)$ minus the inverse decay process $\phi_k \phi_p \to \phi_q$ with statistical probability $n_+^k n_+^p$. Similarly second and third terms represent in-medium forward and reverse scattering processes in Landau cut regions. For different loops, the diagrammatic interpretation of the four terms in (3.39) are assembled in Table.(2A). Here the ϕ_q, ϕ_k and ϕ_p represent general fields instead of scalar fields. From Table.(2A) one observes that the initial state of $\phi_{k,p}$ (or $\overline{\phi}_{k,p}$) field is attached with $n_+^{k,p}$ (or $n_-^{k,p}$) whereas their final state is attached with $(1 + \epsilon_{k,p} n_+^{k,p})$ (or $1 + \epsilon_{k,p} n_-^{k,p}$). So we see that due to presence of medium final state of boson experiences Bose enhancement whereas that of fermion faces Pauli suppression.

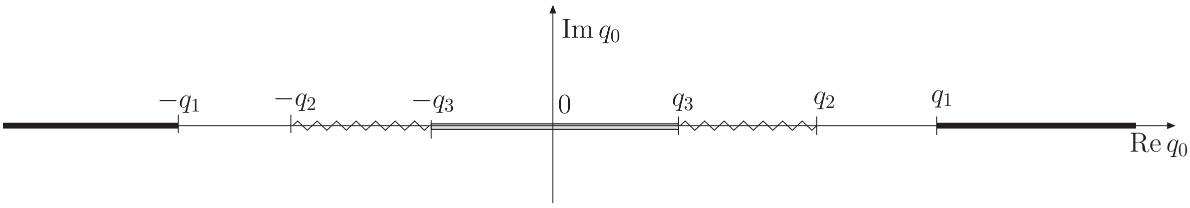

Figure 3.4: Branch cuts of self-energy function in q_0 plane for fixed $\vec{q}$. The quantities $q_{1,2,3}$ denote the end points of cuts discussed in the text : $q_1 = \sqrt{(m_p + m_k)^2 + |\vec{q}|^2}$, $q_2 = \sqrt{(m_p - m_k)^2 + |\vec{q}|^2}$ and $q_3 = |\vec{q}|$.

	$p=q-k$	$p=k-q$	$p=k+q$
1st term with $\delta(q_0-\omega_k-\omega_p)$	*Fig−1* 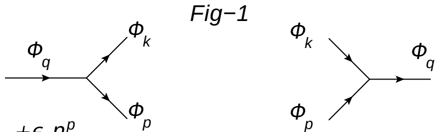 $1+\epsilon_k n^k_+ + \epsilon_p n^p_+ = (1+\epsilon_k n^k_+)(1+\epsilon_p n^p_+)$; $-\epsilon_k \epsilon_p n^k_+ n^p_+$	*Fig−1 with replacing* φ_p , $\bar{\varphi}_p$ *by* $\bar{\varphi}_p$, φ_p ; n^p_+, n^p_- *by* n^p_-, n^p_+	*Fig−4 with replacing* φ_k , $\bar{\varphi}_k$ *by* $\bar{\varphi}_k$, φ_k ; n^k_+, n^k_- *by* n^k_-, n^k_+
2nd term with $\delta(q_0-\omega_k+\omega_p)$	*Fig−2* 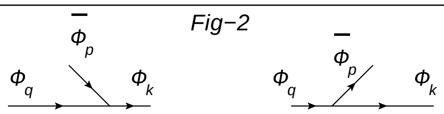 $-\epsilon_k n^k_+ + \epsilon_p n^p_- = (1+\epsilon_k n^k_+)\epsilon_p n^p_-$; $-\epsilon_k n^k_+(1+\epsilon_p n^p_-)$	*Fig−2 with same replacement*	*Fig−3 with same replacement*
3rd term with $\delta(q_0+\omega_k-\omega_p)$	*Fig−3* 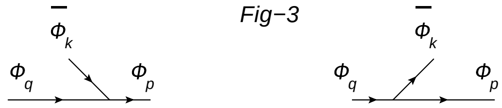 $\epsilon_k n^k_- - \epsilon_p n^p_+ = \epsilon_k n^k_-(1+\epsilon_p n^p_+)$; $-(1+\epsilon_k n^k_-)\epsilon_p n^p_+$	*Fig−3 with same replacement*	*Fig−2 with same replacement*
4th term with $\delta(q_0+\omega_k+\omega_p)$	*Fig−4* 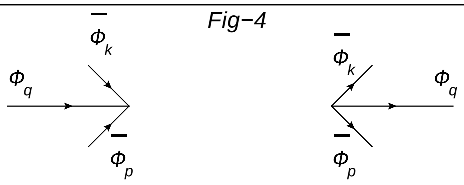 $-1-\epsilon_k n^k_- + \epsilon_p n^p_- = \epsilon_k n^k_- \epsilon_p n^p_-$; $-(1+\epsilon_k n^k_-)(1+\epsilon_p n^p_-)$	*Fig−4 with same replacement*	*Fig−1 with same replacement*

Table 2A : Table shows the diagramatic representation for individual terms of imaginary part of in−medium self−energy. In first column,the statistical weight factor for BB and BF loops are written in general way. In second and third column, we have mentioned about the replacement of fields and distribution functions.

	region in q_0	$\cos\theta_0$ and $q\cdot k$	Limits of ω_k
$\mathrm{Im}\,\overline{\Pi}_1$	$q_0 \geq \sqrt{\vec{q}^{\,2} + (m_k+m_p)^2}$	$\cos\theta_0 = \epsilon_1\epsilon_2\frac{S_k^2 - 2q_0\omega_k}{2\lvert\vec{q}\rvert\lvert\vec{k}\rvert}$ $q\cdot k = -\epsilon_1\epsilon_2\frac{S_k^2}{2}$	$\omega_{k-} = \frac{S_K^2}{2q^2}[q_0 - W_k]$ to $\omega_{k+} = \frac{S_k^2}{2q^2}[q_0 + W_k]$
$\mathrm{Im}\,\overline{\Pi}_{2b}$	$-\sqrt{\vec{q}^{\,2}(m_p-m_k)^2} \leq q_0 \leq -\lvert\vec{q}\rvert$	same as previous	$\omega_{k+} = \frac{S_k^2}{2q^2}[q_0 + W_k]$ to $\omega_{k-} = \frac{S_k^2}{2q^2}[q_0 - W_k]$
$\mathrm{Im}\,\overline{\Pi}_{2a}$	$-\lvert\vec{q}\rvert \leq q_0 \leq 0$	same as previous	to $\omega_{-} = \frac{S_k^2}{2q^2}[q_0 - W_k]$ to ∞
$\mathrm{Im}\,\overline{\Pi}_{3b}$	$\lvert\vec{q}\rvert \leq q_0 \leq \sqrt{\vec{q}^{\,2}(m_p-m_k)^2}$	$\cos\theta_0 = \epsilon_1\epsilon_2\frac{S_k^2 - 2q_0\widetilde{\omega}_k}{2\lvert\vec{q}\rvert\lvert\vec{k}\rvert}$ $q\cdot k = -\epsilon_1\epsilon_2\frac{S_k^2}{2}$	$\widetilde{\omega}_{+} = \frac{S_k^2}{2q^2}[-q_0 + W_k]$ to $\widetilde{\omega}_{-} = \frac{S_k^2}{2q^2}[-q_0 - W_k]$
$\mathrm{Im}\,\overline{\Pi}_{3a}$	$0 \leq q_0 \leq \lvert\vec{q}\rvert$	same as previous	$\widetilde{\omega}_{-} = \frac{S_k^2}{2q^2}[-q_0 - W_k]$ to ∞
$\mathrm{Im}\,\overline{\Pi}_4$	$q_0 \leq -\sqrt{\vec{q}^{\,2}(m_k+m_p)^2}$	same as previous	$\widetilde{\omega}_{-} = \frac{S_k^2}{2q^2}[-q_0 - W_k]$ to $\widetilde{\omega}_{+} = \frac{S_k^2}{2q^2}[-q_0 + W_k]$

Table 3.4: Table shows the different branch cuts and their corresponding variables which make the imaginary part of self-energy restrict to be nonzero on that cut region.

Chapter 4

Spectral properties of ρ meson in hot and dense matter

The in-medium propagation of vector mesons, particularly ρ, has been extensively studied [37, 70, 71]. The reason is, of course, that it controls the rates of dileptons and photons emitted from the hot and dense matter, created during the late stages heavy ion collisions. The NA60 experiment at the CERN SPS measured dimuon pairs in In-In collisions in which an excess was observed over the contribution from hadronic decays at freeze-out in the mass region below ρ peak [72]. This was attributed to the broadening of ρ in hot and dense medium [37]. More recently, the PHENIX experiment reported a substantial excess of electron pairs in the same region of invariant mass [43]. This has been investigated by several groups but the yield in all these cases have remained insufficient to explain the data. Thus the issue of low mass lepton pair yield in heavy ion collisions is far from closed and is one of the key issues to be addressed in the forthcoming Compressed Baryonic Matter(CBM) experiment to be performed at the FAIR facility in GSI [73].

The in-medium modification of ρ meson in presence of mesonic gas is generally believed to arise from two sources [37]. One is the change in its pion cloud, given essentially by the $\pi\pi$ self-energy loop [74]. The other is the collisions suffered by the vector meson with particles in the medium [75, 76, 77, 78, 79, 80].

In baryonic sector, most of the calculations were performed at zero temperature [81, 82, 83, 84, 85]. Finite temperature effects on the ρ spectral function in dense matter have been evaluated by Rapp et al [86] in terms of resonant interactions of the ρ with surrounding mesons and baryons in addition to modifying the pion cloud. Eletsky [80] and collaborators have also evaluated the spectral function of vector mesons at finite temperature and density in terms of forward scattering amplitudes constructed using experimental inputs assuming resonance dominance at low energies and a Regge-type approach at higher energies.

The sources modifying the free propagation of a particle find a unified description in terms of contributions from the branch cuts of the self energy function as shown by Weldon [69]. In addition to the unitary cut present already in vacuum, the thermal amplitude generates a new cut, the so called the Landau cut which provides the effect of collisions with the surrounding particles in the medium. Here we have used this formalism to obtain the ρ self-energy in mesonic [87] and baryonic matter [88, 89]

4.1 ρ self-energy in the medium

To study the ρ meson propagator, we do not start directly with the two-point function of the ρ meson field, but consider instead the related object, namely the two-point function of the vector current $V_\mu^i(x)$,

$$V_\mu^i(x) = \bar{q}(x)\gamma_\mu \frac{\tau^i}{2} q(x), \qquad q = \begin{pmatrix} u \\ d \end{pmatrix} \tag{4.1}$$

of the two-flavor QCD theory. Conceptually we then keep contact with the fundamental theory and deal with a conserved current. At the same time we can address directly the physical processes, such as dilepton production in heavy ion collisions which will be elaborately discussed in Ch. (6).

In the real time thermal field theory, the in medium two point function should have a same 2×2 matrix structure [64]. The thermal two point function is given by

$$T_{\mu\nu}^{ij,ab}(E,\vec{q}) = i \int d^3x d\tau \, e^{iq\cdot x} \langle T_c V_\mu^i(x) V_\nu^j(0) \rangle^{ab} \tag{4.2}$$

where $\langle \mathcal{O} \rangle$ denotes the ensemble average of an operator $\mathcal{O}$,

$$\langle \mathcal{O} \rangle = Tr(e^{-\beta H}\mathcal{O})/Tre^{-\beta H} \tag{4.3}$$

and Tr indicating trace over a complete set of states. The superscripts $a, b\,(=1,2)$ are thermal indices and T_c denotes time ordering with respect to a contour in the plane of the complex time variable [90]. The two point function of vector currents can be related

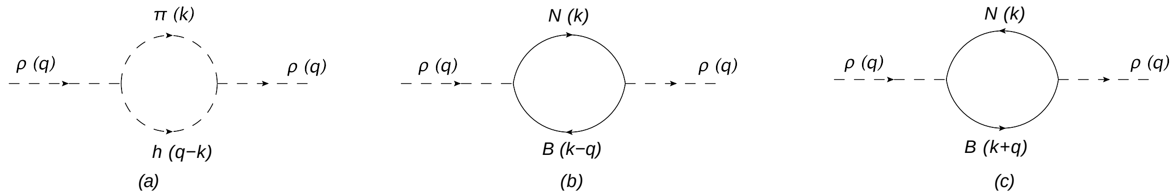

Figure 4.1: One-loop Feynman diagrams of in-medium ρ self-energy for mesonic loop (a) and for baryonic loops (b) and (c). Dashed lines are allotted for mesons (ρ, π, h) whereas the solid lines are fixed for baryons (N, B).

to the ρ meson propagator using the method of external fields [91] where one introduces a classical vector field $v^i_\mu(x)$ coupled to the vector current $V^i_\mu(x)$. The free propagator of the rho meson can be obtained by coupling the external field to the ρ meson field operator using the Lagrangian [92]

$$\mathcal{L}_{\rho v} = \frac{F_\rho}{m_\rho}\partial^\mu \vec{v}^\nu \cdot (\partial_\mu \vec{\rho}_\nu - \partial_\nu \vec{\rho}_\mu) \tag{4.4}$$

where $\mathrm{F}_\rho = 154$ MeV is obtained from the decay $\rho^0 \to e^+ \, e^-$.

The transverse ρ meson propagator $G^{ab}_{\mu\nu}$ is then obtained from the relation $T^{ab}_{\mu\nu} = K \; G^{ab}_{\mu\nu}$ where the factor $K = (F_\rho q^2/m_\rho)^2$ comes from the coupling of the current with the ρ field [87]. At finite temperature we have to deal with the diagonal element of the propagator matrix and recalling the equations (2.120), we can express its spin average form as

$$\overline{G} = \frac{1}{3}(2\;\overline{G}_t + q^2\overline{G}_l) \tag{4.5}$$

where

$$\overline{G}_t = \frac{-1}{q^2 - m^2_\rho - \overline{\Pi}_t} \quad , \quad \overline{G}_l = \frac{-1/q^2}{q^2 - m^2_\rho - q^2\overline{\Pi}_l}. \tag{4.6}$$

The free propagation of the ρ meson is modified by interactions in the medium which is populated by mesons and baryons. From Eq. (4.6) we see that the modification of ρ propagation is controlled by the in-medium one loop self-energy of ρ meson. Now due to presence of these thermal mesons and baryons in medium, we have to take in account all possible mesonic loops ($\overline{\Pi}^M_{t,l}$) and baryonic loops ($\overline{\Pi}^B_{t,l}$)

$$\text{i.e.} \;\; \overline{\Pi}_{t,l} = \sum_M \overline{\Pi}^M_{t,l} + \sum_B \overline{\Pi}^B_{t,l}. \tag{4.7}$$

The detailed evaluations of ρ self-energy for mesonic and baryonic loops are discussed below.

4.1.1 Mesonic loops

In meson loops, the general structure of one loop self-energy is shown in Fig. 5.1(a). One of the internal line is π and another is denoted as h which may be ω, h_1, a_1 as well as π itself. For the interaction vertices entering in the four different one loop graphs, we expand the relevant terms of the chiral Lagrangian and retain the lowest order terms to get [93, 94, 92]

$$\begin{aligned}\mathcal{L}_{int} &= \frac{F_\rho}{m_\rho}\partial^\mu\vec{v}^\nu\cdot(\partial_\mu\vec{\rho}_\nu-\partial_\nu\vec{\rho}_\mu)\\ &-\frac{2G_\rho}{m_\rho F_\pi^2}\partial_\mu\vec{\rho}_\nu\cdot\partial^\mu\vec{\pi}\times\partial^\nu\vec{\pi}\\ &+\frac{g_1}{F_\pi}\epsilon_{\mu\nu\lambda\sigma}(\partial^\nu\omega^\mu\vec{\rho}^\lambda-\omega^\mu\partial^\nu\vec{\rho}^\lambda)\cdot\partial^\sigma\vec{\pi}\\ &-\frac{g_2}{F_\pi}h_1^\mu(\partial_\mu\vec{\rho}_\nu-\partial_\nu\vec{\rho}_\mu)\cdot\partial^\nu\vec{\pi}\\ &+\frac{g_3}{F_\pi}(\partial_\mu\vec{\rho}_\nu-\partial_\nu\vec{\rho}_\mu)\cdot\vec{a}_1^\mu\times\partial^\nu\vec{\pi}.\end{aligned} \tag{4.8}$$

Here F_π is the pion decay constant, $F_\pi = 93$ MeV. The magnitude of other coupling constants may be determined from the observed decay rates of the particles [95]. Thus the decay rate $\Gamma(\rho^0\to e^+e^-) = 6.9$ KeV gives $F_\rho = 154$ MeV. The decay rate $\Gamma(\rho\to 2\pi) = 153$ MeV gives $G_\rho = 69$ MeV. Similarly the decay rates $\Gamma(\omega\to 3\pi) = 7.6$ MeV, $\Gamma(h_1\to\rho\pi)\simeq 360$ MeV and $\Gamma(a_1\to\rho\pi)\simeq 400$ MeV give respectively $g_1 = 0.87$, $g_2 = 1.0$ and $g_3 = 1.1$.

In chapter(3) we have already obtained the expression of thermal boson self-energy for boson-boson internal lines. Recapitulating the expression (3.31) and (3.33), here we combine them in a single expression,

$$\begin{aligned}\overline{\Pi}^{\mu\nu}_M(q) &= \int\frac{d^3k}{(2\pi)^3}\frac{1}{4\omega_k\omega_p}\Big[\frac{(1+n_+^k)L_1^{\mu\nu}+n_+^pL_3^{\mu\nu}}{q_0-\omega_k-\omega_p+i\eta\epsilon(q_0)}+\frac{-n_+^kL_1^{\mu\nu}+n_-^pL_4^{\mu\nu}}{q_0-\omega_k+\omega_p+i\eta\epsilon(q_0)}\\ &+\frac{n_-^kL_2^{\mu\nu}-n_+^pL_3^{\mu\nu}}{q_0+\omega_k-\omega_p+i\eta\epsilon(q_0)}+\frac{-n_-^kL_2^{\mu\nu}+(-1-n_-^p)L_4^{\mu\nu}}{q_0+\omega_k+\omega_p+i\eta\epsilon(q_0)}\Big].\end{aligned} \tag{4.9}$$

where we have introduced the Lorentz indices $\mu\nu$. Now to calculate ρ meson self-energy for different meson loops we make the following replacements

$$\begin{aligned}&m_{k,p}\to m_{\pi,h} \qquad\qquad \omega_{k,p}\to\omega_{\pi,h}\\ &n_\pm^{k,p}\to n^{\pi,h}=\frac{1}{\exp(\beta\omega_{\pi,h})-1}\quad\text{(assuming }\mu_{\pi,h}=0).\end{aligned} \tag{4.10}$$

By obtaining the vertices from the interaction Lagrangian, $L^{\mu\nu}$ can be expressed in terms of Lorentz invariant tensors $A^{\mu\nu}$, $B^{\mu\nu}$ and $C^{\mu\nu}$ as

$$\begin{aligned}
L^{(\pi)}_{\mu\nu} &= \left(\frac{2G_\rho}{m_\rho F_\pi^2}\right)^2 C_{\mu\nu}(k,q) \\
L^{(\omega)}_{\mu\nu} &= -4\left(\frac{g_1}{F_\pi}\right)^2 (B_{\mu\nu}(k,q) + q^2k^2A_{\mu\nu}(k,q)) \\
L^{(h_1)}_{\mu\nu} &= -\left(\frac{g_2}{F_\pi}\right)^2 (B_{\mu\nu}(k,q) - \frac{1}{m_{h_1}^2}C_{\mu\nu}(k,q)) \\
L^{(a_1)}_{\mu\nu} &= -2\left(\frac{g_3}{F_\pi}\right)^2 (B_{\mu\nu}(k,q) - \frac{1}{m_{a_1}^2}C_{\mu\nu}(k,q))
\end{aligned} \tag{4.11}$$

where

$$\begin{aligned}
A_{\alpha\beta}(q) &= -g_{\alpha\beta} + q_\alpha q_\beta/q^2, \\
B_{\alpha\beta}(k,q) &= q^2k_\alpha k_\beta - q\cdot k(q_\alpha k_\beta + k_\alpha q_\beta) + (q\cdot k)^2 g_{\alpha\beta}, \\
C_{\alpha\beta}(k,q) &= q^4k_\alpha k_\beta - q^2(q\cdot k)(q_\alpha k_\beta + k_\alpha q_\beta + (q\cdot k)^2 q_\alpha q_\beta.
\end{aligned} \tag{4.12}$$

To get a more realistic estimate we have included vacuum width of a_1 and h_1 internal lines by using the formula [96],

$$\overline{\Pi}^{\mu\nu}_M(q,m_h) = \frac{1}{N_h}\int_{(m_h-2\Gamma_h)^2}^{(m_h+2\Gamma_h)^2} dM^2\frac{1}{\pi}\mathrm{Im}\left[\frac{1}{M^2-m_h^2+iM\Gamma_h(M)}\right]\overline{\Pi}^{\mu\nu}_M(q,M) \tag{4.13}$$

with $N_h = \int_{(m_h-2\Gamma_h)^2}^{(m_h+2\Gamma_h)^2} dM^2\frac{1}{\pi}\mathrm{Im}\left[\frac{1}{M^2-m_h^2+iM\Gamma_h(M)}\right]$ and $\Gamma_h(M) = \Gamma_{h\to\rho\pi}(M)$.

4.1.2 Baryonic loops

In the previous chapter we have seen that in case of two fermion internal lines there are two possible diagrams (denoted previously as $F\overline{F}$ and $\overline{F}F$ loops) for boson self-energy. So for baryon loops consisting of the nucleon N and another baryon B there will be two possible diagrams as shown in Fig. 5.1(b) and (c). Obtaining the imaginary and real part of $N\overline{B}$ and $\overline{N}B$ loops from Eq. (3.36) and (3.38) respectively, we write in a compact form,

$$\begin{aligned}
\overline{\Pi}^{\mu\nu}_{N\overline{B}}(q) &= -\int\frac{d^3k}{(2\pi)^3}\frac{1}{4\omega_k\omega_p}[\frac{(1-n_+^k)L_1^{\mu\nu} - n_-^pL_3^{\mu\nu}}{q_0-\omega_k-\omega_p+i\eta\epsilon(q_0)} + \frac{n_+^kL_1^{\mu\nu} - n_+^pL_4^{\mu\nu}}{q_0-\omega_k+\omega_p+i\eta\epsilon(q_0)} \\
&\quad + \frac{-n_-^kL_2^{\mu\nu} + n_-^pL_3^{\mu\nu}}{q_0+\omega_k-\omega_p+i\eta\epsilon(q_0)} + \frac{n_-^kL_2^{\mu\nu} + (-1+n_+^p)L_4^{\mu\nu}}{q_0+\omega_k+\omega_p+i\eta\epsilon(q_0)}]
\end{aligned} \tag{4.14}$$

and

$$\overline{\Pi}^{\mu\nu}_{NB}(q) = -\int \frac{d^3k}{(2\pi)^3}\frac{1}{4\omega_k\omega_p}[\frac{(1-n^k_-)L_2^{\mu\nu}-n^p_+L_6^{\mu\nu}}{q_0-\omega_k-\omega_p-i\eta\epsilon(q_0)}+\frac{n^k_-L_2^{\mu\nu}-n^p_-L_5^{\mu\nu}}{q_0-\omega_k+\omega_p-i\eta\epsilon(q_0)}$$
$$+\frac{-n^k_+L_1^{\mu\nu}+n^p_+L_6^{\mu\nu}}{q_0+\omega_k-\omega_p-i\eta\epsilon(q_0)}+\frac{n^k_+L_1^{\mu\nu}+(-1+n^p_-)L_5^{\mu\nu}}{q_0+\omega_k+\omega_p-i\eta\epsilon(q_0)}]. \qquad (4.15)$$

The internal lines in these loops contain a nucleon N and a baryon B which represents several spin one-half and three-half 4−star resonances. Here B stands for the $N^*(1520)$, $N^*(1650)$, $N^*(1700)$, $\Delta(1230)$, $\Delta^*(1620)$, $N^*(1720)$ as well as the $N(940)$ itself. The corresponding replacement in Eq. (4.14), (4.15) for the baryon loops are

$$m_{k,p}\to m_{N,B} \qquad \omega_{k,p}\to\omega_{N,B}$$
$$n^{k,p}_\pm \to n^{N,B}_\pm = \frac{1}{\exp\{\beta(\omega_{N,B}\mp\mu)\}+1}. \qquad (4.16)$$

Here μ is the baryonic chemical potential which is taken to be equal for all baryons. Omitting isospin factors (I_F), the ρN couplings with the resonances are described by the gauge invariant interactions [97]

$$\mathcal{L} = \frac{g_{\rho NB}}{m_\rho}[\overline{\psi}_B\sigma^{\mu\nu}\rho_{\mu\nu}\psi_N + h.c.] \qquad J^P_B = \frac{1}{2}^+$$
$$\mathcal{L} = \frac{g_{\rho NB}}{m_\rho}[\overline{\psi}_B\sigma^{\mu\nu}\gamma^5\rho_{\mu\nu}\psi_N + h.c.] \qquad J^P_B = \frac{1}{2}^-$$
$$\mathcal{L} = \frac{g_{\rho NB}}{m_\rho}[\overline{\psi}^\mu_B\gamma^\nu\gamma^5\rho_{\mu\nu}\psi_N + h.c.] \qquad J^P_B = \frac{3}{2}^+$$
$$\mathcal{L} = \frac{g_{\rho NB}}{m_\rho}[\overline{\psi}^\mu_B\gamma^\nu\rho_{\mu\nu}\psi_N + h.c.] \qquad J^P_B = \frac{3}{2}^-. \qquad (4.17)$$

It is essential to point out that for the spin 3/2 resonances this coupling is not quite correct owing to the fact that the free Lagrangian for the Rarita-Schwinger field [98] has a free parameter. A symmetry is associated with a point transformation under which the free Lagrangian remains invariant up to a change in the value of the parameter [99]. The standard practice is to make a choice of the value of this parameter so that the spin-3/2 propagator has a simple form. In order that the interaction also remains invariant under this transformation an additional term is added to it. Thus the Lagrangians involving spin-3/2 fields take the form

$$\mathcal{L} = \frac{g_{\rho NB}}{m_\rho}[\overline{\psi}^\alpha_B\mathcal{O}_{\alpha\beta}\gamma_\nu\gamma^5\rho^{\beta\nu}\psi_N + h.c.] \qquad J^P_B = \frac{3}{2}^+$$
$$\mathcal{L} = \frac{g_{\rho NB}}{m_\rho}[\overline{\psi}^\alpha_B\mathcal{O}_{\alpha\beta}\gamma_\nu\rho^{\beta\nu}\psi_N + h.c.] \qquad J^P_B = \frac{3}{2}^- \qquad (4.18)$$

with $\mathcal{O}_{\mu\alpha} = g_{\mu\alpha} - \frac{1}{4}\gamma_\mu\gamma_\alpha$, the second term contributing only when the spin 3/2 field is off the mass shell. The value of the coupling strength $g_{\rho NB}$ thus remains unaffected by this exercise.

Now we will get four possible structure of $L^{\mu\nu}$ depending upon the spin parity states (J^P) of resonances B but numerically all the seven baryon loops are different because of different coupling strength ($g_{\rho NB}$) as well as the masses of resonances (m_B). The four kinds of tensor structure of $L^{\mu\nu}$ are

$$L^{\mu\nu}(k,q) = -(\frac{g_{\rho NB}}{m_\rho})^2 \begin{cases} tr[\sigma^{\mu\alpha}q_\alpha(\not{k} + Pm_N)\sigma^{\nu\beta}q_\beta(\not{p} + m_B)] & \text{for } J^P = \frac{1}{2}^{\pm} \\ tr[V^{\mu\alpha}(\not{k} + Pm_N)U^{\nu\beta}(\not{p} + m_B)K_{\beta\alpha}] & \text{for } J^P = \frac{3}{2}^{\pm} \end{cases} \tag{4.19}$$

where $K_{\beta\alpha} = -g_{\mu\nu} + \frac{2}{3m^2}k_\mu k_\nu + \frac{1}{3}\gamma_\mu\gamma_\nu + \frac{1}{3m}(\gamma_\mu k_\nu - \gamma_\nu k_\mu)$ and $V^{\mu\alpha} = V_0^{\mu\alpha} + cV_c^{\mu\alpha}$, $U^{\mu\alpha} = U_0^{\mu\alpha} + cU_c^{\mu\alpha}$ with

$$\begin{aligned} V_0^{\mu\alpha} &= \frac{g_{\rho NB}}{m_\rho}(\not{q}g^{\mu\alpha} - \gamma^\mu q^\alpha) & U_0^{\nu\beta} &= \frac{g_{\rho NB}}{m_\rho}(\not{q}g^{\nu\beta} - \gamma^\nu q^\beta) \\ V_c^{\mu\alpha} &= \frac{g_{\rho NB}}{m_\rho}\gamma^\mu(\gamma^\alpha\not{q} - \not{q}\gamma^\alpha) & U_c^{\nu\beta} &= \frac{g_{\rho NB}}{m_\rho}(\gamma^\nu\not{q} - \not{q}\gamma^\nu)\gamma^\beta. \end{aligned} \tag{4.20}$$

The second term $V_c^{\mu\alpha}$ appears due to the off shell projection operator $\mathcal{O}_{\mu\nu} = g_{\mu\nu} + c\gamma_\mu\gamma_\nu$. The constant c (i.e. $c = -\frac{1}{4}$) is introduced to distinguish this contribution separately. Here we will take $p = k + \epsilon_1 q$ where $\epsilon_1 = \mp 1$ for diagrams representing $N\overline{B}$ and $\overline{N}B$ respectively [Fig. 5.1(b) and (c)]. After evaluating the trace we will get

$$L^{\mu\nu}(q,k) = (\frac{g_{\rho NB}}{2m_N})^2 \begin{cases} [(k^2 - \epsilon_1(q\cdot k) + Pm_N m_B)q^2 A^{\mu\nu} + 2B^{\mu\nu}] & \text{for} J^P = \frac{1}{2}^{\pm} \\ [\alpha_{\frac{3}{2}}A^{\mu\nu} + \beta_{\frac{3}{2}}B^{\mu\nu} + \gamma_{\frac{3}{2}}C^{\mu\nu}] & \text{for} J^P = \frac{3}{2}^{\pm} \end{cases} \tag{4.21}$$

where $\alpha_{\frac{3}{2}} = \alpha^{00} + c\alpha^{0c} + c^2\alpha^{cc}$, $\beta_{\frac{3}{2}} = \beta^{00} + c\beta^{0c} + c^2\beta^{cc}$ and $\gamma_{\frac{3}{2}} = \gamma^{00} + c\gamma^{0c} + c^2\gamma^{cc}$. The expressions for the various coefficients are given below

$$\begin{aligned} \alpha^{00} &= \frac{8}{3m_B^2}[(k^2m_B^2 + Pm_N m_B^3 - k^2q^2) - \epsilon_1(q\cdot k)(2k^2 + q^2 - 2(q\cdot k))]q^2 \\ \beta^{00} &= \frac{8}{3m_B^2}[k^2 + m_B^2 + \epsilon_1(q\cdot k)] \\ \alpha^{0c} &= 4\frac{8}{3m_B^2}[Pm_N m_B S_N^2 - \epsilon_1(q\cdot k)(S_N^2 + 3\epsilon_1(q\cdot k) - 2Pm_N m_B)]q^2 \\ \beta^{0c} &= 4\frac{8}{3m_B^2}[k^2 - m_B^2 + 2\epsilon_1(q\cdot k)] \\ \gamma^{0c} &= 4\frac{8}{3m_B^2} \end{aligned}$$

$$
\begin{aligned}
&\alpha^{cc} = 4\frac{8}{3m_B^2}[(m_N^2 + 2Pm_Nm_B)(S_N^2 + 2\epsilon_1(q\cdot k)) - \epsilon_1(q\cdot k)(S_N^2 + 4\epsilon_1(q\cdot k))]q^2 \\
&\beta^{cc} = 4\frac{8}{3m_B^2}[2(k^2 - m_B^2 + 2\epsilon_1(q\cdot k))] \\
&\gamma^{cc} = 4\frac{8}{3m_B^2}[2]
\end{aligned}
$$

$$
\begin{aligned}
\alpha_{3/2} &= \frac{2q^2}{3m_B^2}[p^2(p^2 - 3q^2) + p\cdot q(3p^2 + q^2) \\
&\quad +3m_B^2(p^2 + 2m_Nm_B + p\cdot q) \\
&\quad -2m_Nm_B(p^2 + q^2 - 2p\cdot q)] \\
\beta_{3/2} &= 4(1 + p^2/3m_B^2) \\
\gamma_{3/2} &= -4/3m_B^2 \qquad (4.22)
\end{aligned}
$$

where $S_N^2 = q^2 - m_B^2 + m_N^2$.

R	J^P	$g_{\rho NB}$	$\Gamma_{N\pi}$ (GeV)	$\Gamma_{N\rho}$ (GeV)
$N(940)$	$\frac{1}{2}^+$	7.7	0	0
$N^*(1520)$	$\frac{3}{2}^-$	7.0	0.07	0.023
$N^*(1650)$	$\frac{1}{2}^-$	0.9	0.132	0.013
$N^*(1720)$	$\frac{3}{2}^+$	7.0	0.03	0.155
$\Delta(1232)$	$\frac{3}{2}^+$	10.5	0.118	0
$\Delta(1620)$	$\frac{1}{2}^-$	2.7	0.036	0.023
$\Delta(1700)$	$\frac{3}{2}^-$	5.0	0.045	0.128

Table 4.1: Table showing the coupling constants and partial decay widths of the resonances considered.

Up to now we have been treating the baryon resonances B in the narrow width approximation. It is indeed necessary to consider the width of the unstable baryons in a

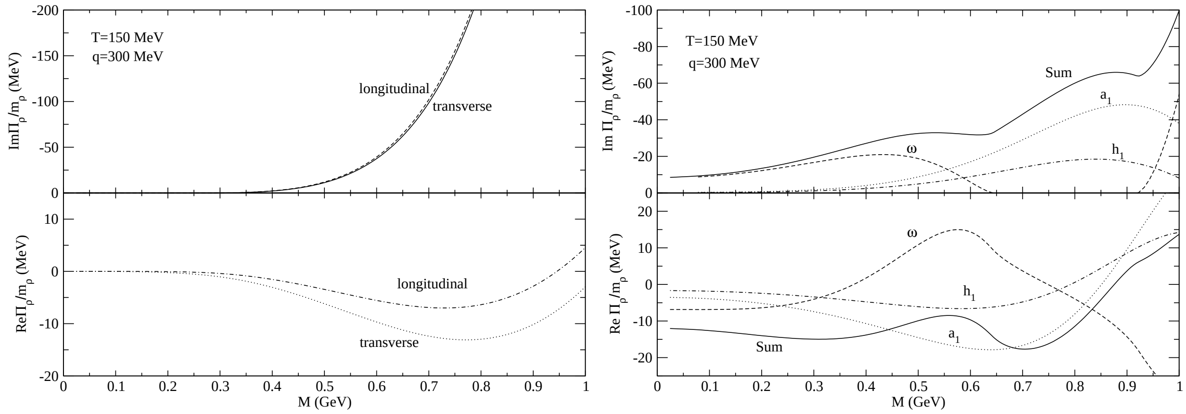

Figure 4.2: In left panel, the imaginary (upper) and the real (lower) parts of self-energy from $\pi\pi$ loop are shown separately in longitudinal and transverse components. In right panel, the spin average of the components for $\pi h (h = \omega, a_1, h_1)$ loops are shown.

realistic evaluation of the spectral function. For this, we follow the procedure [100, 96] of convoluting the self energy calculated in the narrow width approximation with the spectral function of the baryons.

$$\Pi_B(q, m_B) = \frac{1}{N_B}\int_{m_B-2\Gamma_B}^{m_B+2\Gamma_B} dM \frac{1}{\pi}\mathrm{Im}\left[\frac{1}{M - m_B + \frac{i}{2}\Gamma_B(M)}\right]\Pi_B(q, M) \qquad (4.23)$$

with $N_B = \int_{m_B-2\Gamma_B}^{m_B+2\Gamma_B} dM \frac{1}{\pi}\mathrm{Im}\left[\frac{1}{M - m_B + \frac{i}{2}\Gamma_B(M)}\right]$ and $\Gamma_B(M) = \Gamma_{B\to N\pi}(M) + \Gamma_{B\to N\rho}(M)$. The values of these partial decay widths $\Gamma_{B\to N\rho}$, $\Gamma_{B\to N\pi}$ and the coupling constants $g_{\rho NB}$ are organized in Table (4.1). As a consequence of this convolution, the sharp ends of the regions of non-zero imaginary part smoothly goes to zero at a higher value of M depending upon the width of the resonance. It is shown in the dashed lines in the left panels of Fig. (4.3) and (4.4) which correspond to the real and imaginary parts coming from the $NN^*(1520)$ loop computed in the narrow width approximation whereas solid lines give their full width convoluted results

4.2 Results and discussion

We begin with the results of numerical evaluation of Fig. 5.1(A), representing the ρ self-energy for meson loops. As usual, we retain the vacuum contribution in the imaginary parts only, assuming the real (divergent) parts to renormalize the ρ meson mass. We calculate the self-energies as a function of $\sqrt{q^2} \equiv M$ at fixed values of the three-momentum $\vec{q}$ and temperature T. It thus suffices to calculate the self-energies in the time-like region, for positive values of q_0 starting from $q_0 = |\vec{q}|$. So among the six segment of branch cuts (Ch. 3), only two segments will contribute in the time-like region and the corresponding imaginary part of self-energy are given by

$$\begin{aligned}
\mathrm{Im}\,\overline{\Pi}(q_0,\vec{q}) &= -\frac{\epsilon(q_0)}{16\pi\vec{q}}\int_{\widetilde{\omega}_{\pi+}}^{\widetilde{\omega}_{\pi-}} d\widetilde{\omega}_\pi L_2(q\cdot k = \frac{S_\pi^2}{2})\{n(\widetilde{\omega}_\pi) - n(\widetilde{\omega}_h = q_0 - \widetilde{\omega}_\pi)\} \\
&\qquad \text{for Landau cut, } \vec{q} \le q_0 \le \sqrt{\vec{q}^2 + (m_h - m_\pi)^2} \\
&= -\frac{\epsilon(q_0)}{16\pi\vec{q}}\int_{\omega_{\pi-}}^{\omega_{\pi+}} d\omega_\pi L_1(q\cdot k = \frac{S_\pi^2}{2})\{1 + n(\omega_\pi) + n(\omega_h = q_0 - \omega_\pi)\} \\
&\qquad \text{for Landau cut, } q_0 \ge \sqrt{(m_h + m_\pi)^2 + |\vec{q}|^2}
\end{aligned} \tag{4.24}$$

where $S_\pi^2 = q^2 - m_h^2 + m_\pi^2$. The principle value of Eq. (4.9) provide the required real part of self-energy. Excluding the vacuum part (just by excluding the unity in the numerators of (4.9)), we get only thermal real part which may shift the vacuum mass of ρ. The $\pi\pi$ loop is distinguished by a large imaginary part of the self-energy, its vacuum part giving $\Gamma_\rho \equiv \mathrm{Im}\,\overline{\Pi}^{(\pi)}/m_\rho = 153$ MeV at $M = m_\rho$. Clearly it is only the unitary cut in the time-like region that gives the imaginary part. The individual transverse and longitudinal parts for this loop are shown in left panel of Fig. (4.2).

In showing the results for other loops, we average their imaginary and real parts over the transverse and longitudinal components. They are shown in the right panel of Fig. (4.2). Here it is only L_{3b} part of Landau cut ($|\vec{q}| \le q_0 \le \sqrt{(m_h - m_\pi)^2 + |\vec{q}|^2}$), which contributes to the imaginary part. The only exception is the $\pi\omega$ loop, where the unitary cut ($q_0 \ge \sqrt{(m_h + m_\pi)^2 + |\vec{q}|^2}$) also contributes, its threshold for other loops appearing outside the range of M plotted here. The $\pi\omega$ loop dominates up to about $M \sim 500$ MeV, beyond which the πa_1 loop takes over. The rising trend of the imaginary part at the upper end is due to the contribution of the unitary cut. While the imaginary parts add up, there is appreciable cancellation among the real parts of different loops.

As, before, the imaginary part for baryon loops can be evaluated from the discontinuities of the self-energy. However, the threshold for the unitary cut for these loops being far away from the ρ pole we only consider the Landau part (L_{3b}). So by picking up the appropriate terms from Eq. (4.14) and (4.15), contributing in the region of L_{3b}, the expression of the imaginary part for baryon loops is given by

$$\mathrm{Im}\,\overline{\Pi}(q_0,\vec{q}) = \frac{\epsilon(q_0)}{16\pi\vec{q}}\int_{\widetilde{\omega}_{N+}}^{\widetilde{\omega}_{N-}} d\widetilde{\omega}_N [L_2(q\cdot k = \frac{S_N^2}{2})\{-n_-(\widetilde{\omega}_N) + n_-(\widetilde{\omega}_B = q_0 + \widetilde{\omega}_N)\}$$

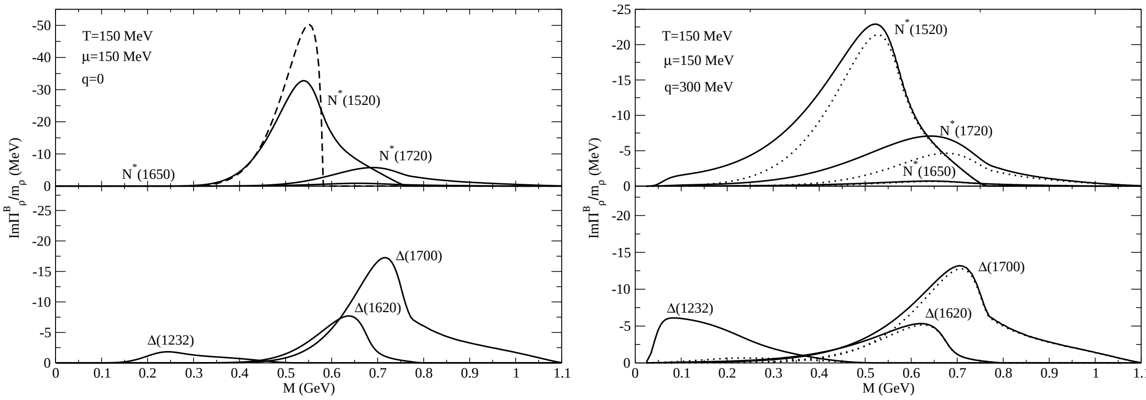

Figure 4.3: Imaginary part of ρ meson self-energy showing the individual contributions for different NB loops. Left panel shows results for $\vec{q} = 0$ and the right panel shows the transverse (solid line) and longitudinal (dotted line) parts for $\vec{q} = 300$ MeV. The dashed line shows the result evaluated in the narrow width approximation for $N^*(1520)$.

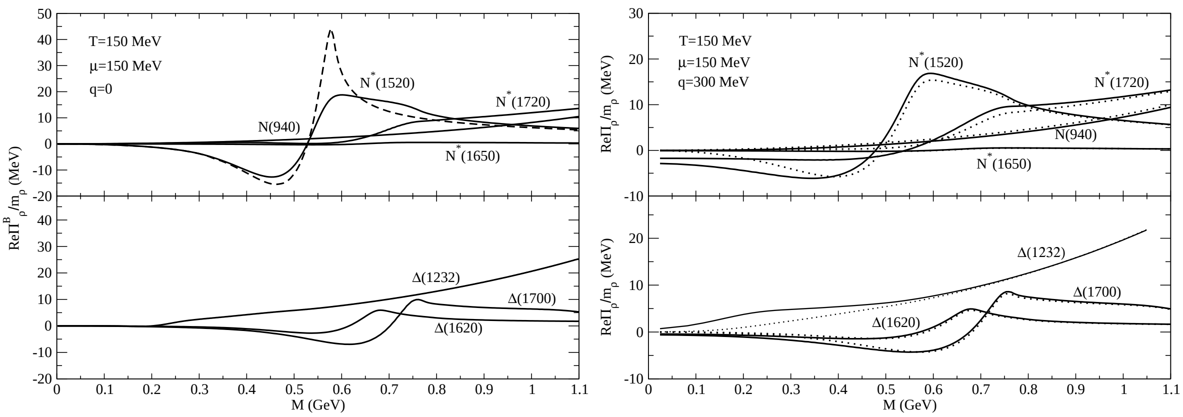

Figure 4.4: Same as Fig. (4.3) for the real part.

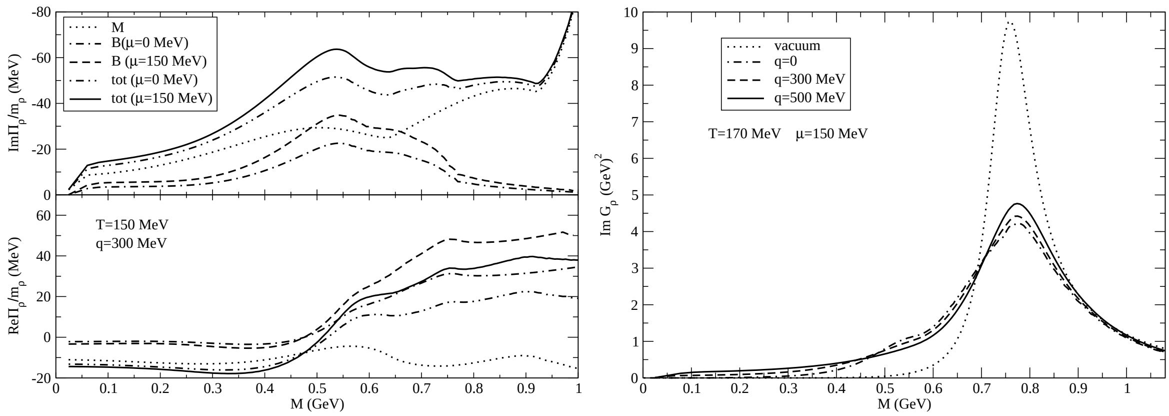

Figure 4.5: Left panel shows The total contribution in self-energy from meson and baryon loops for two different chemical potential. The spectral function for different three momentum of ρ is shown in right panel.

$$+ L_1(q \cdot k = -\frac{S_N^2}{2})\{n_+(\widetilde{\omega}_N) - n_+(\widetilde{\omega}_B = q_0 + \widetilde{\omega}_N)\}]$$
$$\text{for Landau cut, } \vec{q} \leq q_0 \leq \sqrt{\vec{q}^2 + (m_B - m_N)^2}. \qquad (4.25)$$

We evaluate imaginary part of the ρ self-energy as a function of the invariant mass $\sqrt{q^2} \equiv M$ for two values of the three momentum. Shown in Fig. (4.3) left panel are the contributions from the individual NB loops for a ρ meson at rest. The $NN^*(1520)$ loop makes the most significant contribution followed by the $N^*(1720)$ and $\Delta(1700)$. The right panel shows the corresponding results for $\vec{q} = 300$ MeV where the transverse and longitudinal components Π_t and $q^2\Pi_l$ have been plotted separately. (Note that for a ρ meson at rest $\Pi_t = q_0^2\Pi_l$.) The corresponding results for the thermal contribution to the real part are shown in Fig. (4.4).

On the left panel of Fig. (4.5) we plot the individual contribution of imaginary part of spin averaged self-energy from the baryon and meson loops for two values of the baryonic chemical potential. The small positive contribution from the baryon loops to the real part is partly compensated by the negative contributions from the meson loops. The substantial baryon contribution at vanishing baryonic chemical potential reflects the importance of anti-baryons. Finally we come to the spectral function of ρ meson and we have shown the spin average of the transverse and the longitudinal components. In right panel of Fig. (4.5) we see how the vacuum spectral function is modified at temperature, T=170 MeV and chemical potential, μ=150 MeV. In same figure we have also checked the momentum ($\vec{q}$) dependence of thermal spectral function which reflects

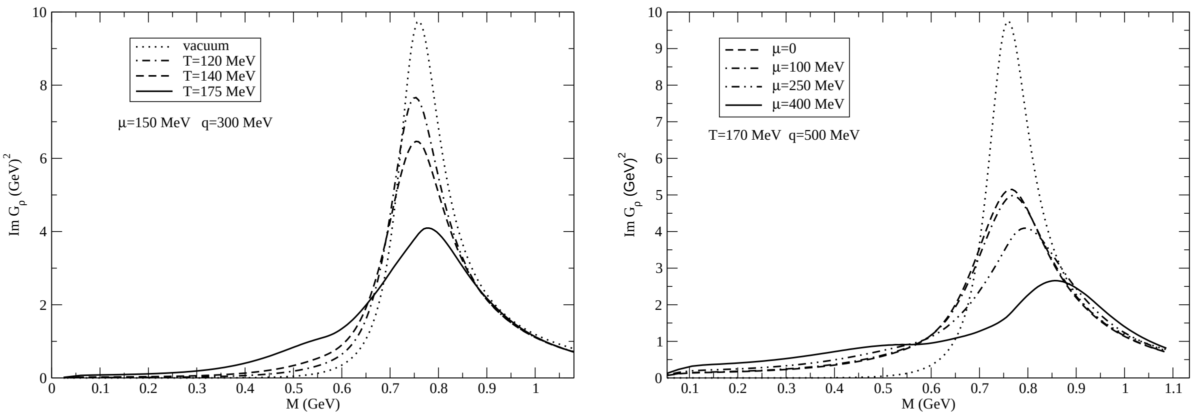

Figure 4.6: The spectral function of the ρ meson for (left) different values of the temperature T and (right) different values of the chemical potential μ.

an important feature at finite temperature. It is the fact that the probability amplitude at finite temperature depends independently on q_0 and $\vec{q}$ because the rest frame of the heat bath chooses a specific Lorentz frame and so unlike in vacuum, Lorentz invariance does not hold at finite temperature. Therefore we see the non-zero differences in thermal spectral function for different values of $\vec{q}$, which can never be seen in vacuum. However, we do not observe much variation with $\vec{q}$ of the ρ as seen in the figure. In left panel of the Fig. (4.6), we plot the spectral function at fixed values of the baryonic chemical potential and three-momentum for various representative values of the temperature. We observe an increase of spectral strength at lower invariant masses resulting in broadening of the spectral function with increase in temperature. This is purely a Landau cut contribution from the baryonic loop arising from the scattering of the ρ from baryons in the medium. Right panel of Fig. (4.6) shows the spectral function for various values of the baryonic chemical potential for a fixed temperature. For high values of μ we observe an almost flattened spectral density of the ρ which indicates an almost entire melting of the resonance structure at the highest temperature and density. Possible consequences for dilepton spectra in heavy-ion collision will be discussed in detail in Chapter (6).

Chapter 5

The ω meson in the medium

A large volume of literature is dedicated to the study of vector mesons in the medium, the bulk of which concerns the ρ meson. Theoretical activities regarding the ω meson have been mostly performed in cold nuclear matter (see e.g. [101] and [17, 102] for a review). Though the lowest order virial expansion has been used in most cases [103, 104, 105] the approaches differ widely in their methods resulting in a large variation in the results concerning the mass and width. Consequently both positive and negative shifts of the peak position have been proposed. On the experimental front the situation is far from settled [17] with different groups reporting a reduction in mass [106] and increase in width [107] in pA and γA collisions respectively. The upcoming experiments at the FAIR facility at GSI thus assumes great significance in resolving some of the issues.

Finite temperature calculations at vanishing baryon density have been done in [108] showing a large increase in width due to $\omega \to 3\pi$ and $\omega\pi \to \pi\pi$ processes. Baryon induced effects on the ω spectral function at finite temperature has been treated within a virial approach in [80] where the self-energy is obtained in terms of empirical scattering amplitudes. In [109], in addition to contributions coming from scattering with mesons, resonance-hole contributions have been included in the self-energy.

Similar to ρ meson scenario (Ch. 4) here also we have evaluated ω self-energy for different meson and baryon loops by using effective Lagrangian and the real time formulation of thermal field theory, which is discussed below.

5.1 Mesonic loops

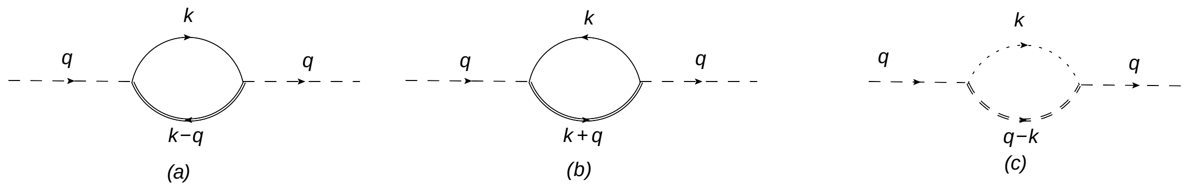

Figure 5.1: One-loop ω self-energy diagrams with baryons (a) & (b) where single and double lines represent nucleon (N) and resonances (B) respectively. Diagram (c) indicates meson loop where dashed, dotted and double dashed lines stand for ω, π and ρ respectively.

Let us start with ω self-energy for $\pi\rho$ loop in where the $\omega\pi\rho$ vertices can be obtained from effective Lagrangian

$$\mathcal{L}_{int} = \frac{g_m}{F_\pi}\epsilon_{\mu\nu\lambda\sigma}(\partial^\nu\omega^\mu\vec{\rho}^\lambda - \omega^\mu\partial^\nu\vec{\rho}^\lambda)\cdot\partial^\sigma\vec{\pi}\ . \tag{5.1}$$

The expression of in-medium self-energy for this case is exactly same as Eq. (4.9), keeping the corresponding replacements

$$\begin{aligned} & m_{k,p} \to m_{\pi,\rho} \qquad\qquad \omega_{k,p} \to \omega_{\pi,\rho} \\ & n_{\pm}^{k,p} \to n^{\pi,\rho} = \frac{1}{\exp(\beta\omega_{\pi,\rho}) - 1} \ \ \text{(assuming } \mu_{\pi,\rho} = 0). \end{aligned} \tag{5.2}$$

Hence to represent ω self-energy for $\pi\rho$ loop, Eq. (4.9) become

$$\begin{aligned} \overline{\Pi}^{\mu\nu}_{(\rho\pi)}(q) &= \int\frac{d^3k}{(2\pi)^3}\frac{1}{4\omega_\pi\omega_\rho}\Big[\frac{(1+n^\pi)L_1^{\mu\nu} + n^\rho L_3^{\mu\nu}}{q_0 - \omega_\pi - \omega_\rho + i\eta\epsilon(q_0)} + \frac{-n^\pi L_1^{\mu\nu} + n^\rho L_4^{\mu\nu}}{q_0 - \omega_\pi + \omega_\rho + i\eta\epsilon(q_0)} \\ &+ \frac{n^\pi L_2^{\mu\nu} - n^\rho L_3^{\mu\nu}}{q_0 + \omega_\pi - \omega_\rho + i\eta\epsilon(q_0)} + \frac{-n^\pi L_2^{\mu\nu} + (-1-n^\rho)L_4^{\mu\nu}}{q_0 + \omega_\pi + \omega_\rho + i\eta\epsilon(q_0)}\Big]. \end{aligned} \tag{5.3}$$

where the expression for $L^{\mu\nu}$ appearing in the ω self-energy for the $\pi\rho$ loop is given by,

$$L^{\mu\nu}_{(\rho\pi)}(q,k) = -4\left(\frac{g_m}{F_\pi}\right)^2(B_{\mu\nu} + q^2k^2A_{\mu\nu}). \tag{5.4}$$

The imaginary part in the relevant Landau and unitary cut regions are respectively given by

$$\mathrm{Im}\overline{\Pi}^{\mu\nu}_{(\rho\pi)} = -\frac{\epsilon(q_0)}{16\pi|\vec{q}|}\int_{\widetilde{\omega}_\pi^+}^{\widetilde{\omega}_\pi^-} d\widetilde{\omega}_\pi L_2^{\mu\nu}\{n(\widetilde{\omega}_\pi) - n(\widetilde{\omega}_\rho = q_0 + \widetilde{\omega}_\pi)\} \tag{5.5}$$

and

$$\mathrm{Im}\overline{\Pi}^{\mu\nu}_{(\rho\pi)} = -\frac{\epsilon(q_0)}{16\pi|\vec{q}|}\int_{\omega_\pi^-}^{\omega_\pi^+} d\omega L_1^{\mu\nu}\{1 + n(\omega_\pi) + n(q_0 - \omega_\pi)\} \tag{5.6}$$

where the integration limits $\omega_\pi^\pm = \frac{S_\pi^2}{2q^2}(q_0 \pm |\vec{q}|W_\pi)$, $\widetilde{\omega}_\pi^\pm = \frac{S_\pi^2}{2q^2}(-q_0 \pm |\vec{q}|W_\pi)$ with $W_\pi = \sqrt{1 - \frac{4q^2m_\pi^2}{S_\pi^4}}$ and $S_\pi^2 = q^2 - m_\rho^2 + m_\pi^2$.

The real part of the self-energy can be easily read off from (5.3) in terms of principal value integrals and we do not write them here separately.

The ω self-energy due to its coupling to 3π states can be estimated by folding the $\rho\pi$ contribution with the ρ spectral function A_ρ as in [105] to find the following expression

$$\overline{\Pi}^{\mu\nu}_M(q) = \frac{1}{N_\rho}\int_{4m_\pi^2}^{(q-m_\pi)^2} dM^2[\overline{\Pi}^{\mu\nu}_{(\rho\pi)}(q,M)]A_\rho(M) \tag{5.7}$$

where $N_\rho = \int_{4m_\pi^2}^{(q-m_\pi)^2} dM^2 A_\rho(M)$ and A_ρ is the ρ spectral function. The value of coupling constant is $g_m = 5.5$ which is fixed by constructing the decay width of ω in 3π channels as $\frac{\mathrm{Im}\Pi_M(q=m_\omega)}{m_\omega} = 7.6$ MeV.

Following [69, 87], the Landau cut contribution from the $\rho\pi$ loop can be interpreted as the probability of occurrence of processes like $\omega\pi \to \rho$ and $\omega\rho \to \pi$ which are responsible for the loss of ω mesons in the medium minus the reverse processes which lead to a gain. Similarly, the unitary cut contribution accounts for processes like $\omega \to \rho\pi$ and its reverse. As a consequence of folding with the ρ spectral function containing its 2π decay width, all possible scatterings like $\omega\pi \to \pi\pi$, $\omega\pi\pi \to \pi$ etc. as well as the decay $\omega \to 3\pi$, proceeding through ρ-exchange are effectively accounted for in the imaginary part.

5.2 Baryonic loops

The internal lines in these loops contain a nucleon N and a baryon B which represents several spin one-half and three-half 4−star resonances. Here B stands for the $N^*(1440)$ $N^*(1520)$, $N^*(1535)$, $N^*(1650)$, $N^*(1720)$ resonances as well as the $N(940)$. For baryon loops, the expression of ω self-energy is exactly same as Eq. (4.14) and (4.15) where we have to keep in mind the resonances B which we are considering here. In the time-like region, the total contribution from the baryon loops is given by

$$\begin{aligned}\mathrm{Im}\,\overline{\Pi}^{\mu\nu}(q_0,\vec{q}) \quad &= \quad \frac{\epsilon(q_0)}{16\pi|\vec{q}|}\int_{\widetilde{\omega}_N^+}^{\widetilde{\omega}_N^-} d\widetilde{\omega}_N[L_1^{\mu\nu}(q\cdot k = -\frac{S_N^2}{2})\{n_+(\widetilde{\omega}_N) - n_+(\widetilde{\omega}_B = q_0 + \widetilde{\omega}_N)\} \\ &\quad + L_2^{\mu\nu}(q\cdot k = \frac{S_N^2}{2})\{-n_-(\widetilde{\omega}_N) + n_-(\widetilde{\omega}_B = q_0 + \widetilde{\omega}_N)\}]\end{aligned} \tag{5.8}$$

where the notations are same as previous chapter *i.e.* $\widetilde{\omega}_N^{\pm} = \frac{S_N^2}{2q^2}(-q^0 \pm |\vec{q}|W_N)$, $W_N = \sqrt{1 - \frac{4q^2m_N^2}{S_N^4}}$ and $S_N^2 = q^2 - m_B^2 + m_N^2$. Here the unitary cut region in time-like domain, being far from the ω pole, can be negligible in the contribution to the ω spectral function.

The real part of the self-energy is obtained by the same technique as done for ρ self-energy.

To include width of the resonances like the previous analysis, we have adopt the same convolution procedure [100] *i.e.*

$$\overline{\Pi}_B(q,m_B) = \frac{1}{N_B}\int_{m_B-2\Gamma_B}^{m_B+2\Gamma_B} dM\frac{1}{\pi}\mathrm{Im}\left[\frac{1}{M-m_B+\frac{i}{2}\Gamma_B(M)}\right]\overline{\Pi}_B(q,M) \tag{5.9}$$

with $N_B = \int_{m_B-2\Gamma_B}^{m_B+2\Gamma_B} dM\frac{1}{\pi}\mathrm{Im}\left[\frac{1}{M-m_B+\frac{i}{2}\Gamma_B(M)}\right]$ and $\Gamma_B(M) = \Gamma_{B\to N\pi}(M)+\Gamma_{B\to N\rho}(M)$; $M=\sqrt{q^2}$.

Now to calculate $L^{\mu\nu}$'s we have to first calculate the ωNB vertices which can be obtained from the interaction Lagrangians [105]

$$\begin{aligned}
\mathcal{L} &= -[\overline{\psi}_B(g_1\gamma_\mu - \frac{g_2}{2m_N}\sigma_{\mu\nu}\partial^\nu_\omega)\psi_N\omega^\mu + h.c.] && J^P_B = \frac{1}{2}^+\\
\mathcal{L} &= i[\overline{\psi}_B\gamma^5(g_1\gamma_\mu - \frac{g_2}{2m_N}\sigma_{\mu\nu}\partial^\nu_\omega)\psi_N\omega^\mu + h.c.] && J^P_B = \frac{1}{2}^-\\
\mathcal{L} &= -i[\overline{\psi}^\mu_B\gamma^5(\frac{g_1}{2m_N}\gamma^\alpha + i\frac{g_2}{4m_N^2}\partial^\alpha_N + i\frac{g_3}{4m_N^2}\partial^\alpha_\omega)(\partial^\omega_\alpha\mathcal{O}_{\mu\nu} - \partial^\omega_\mu\mathcal{O}_{\alpha\nu})\psi_N\omega^\nu + h.c.] && J^P_B = \frac{3}{2}^+\\
\mathcal{L} &= -[\overline{\psi}^\mu_B(\frac{g_1}{2m_N}\gamma^\alpha + i\frac{g_2}{4m_N^2}\partial^\alpha_N + i\frac{g_3}{4m_N^2}\partial^\alpha_\omega)(\partial^\omega_\alpha\mathcal{O}_{\mu\nu} - \partial^\omega_\mu\mathcal{O}_{\alpha\nu})\psi_N\omega^\nu + h.c.] && J^P_B = \frac{3}{2}^-
\end{aligned} \tag{5.10}$$

where $\sigma^{\mu\nu} = \frac{i}{2}[\gamma^\mu\gamma^\nu - \gamma^\nu\gamma^\mu]$ and $\mathcal{O}_{\mu\nu} = g_{\mu\nu} - \frac{1}{4}\gamma_\mu\gamma_\nu$ is the off-shell projector contracted with the vertices containing spin 3/2 fields [99] which contributes only when it is off the mass shell. The values of all the coupling constants in the ωNB Lagrangian are taken from Ref. [105, 110] and are given below in Table (5.1).

For spin $\frac{1}{2}^\pm$ resonances the tensor $L^{\mu\nu}(k,q)$ is given by

$$L^{\mu\nu}(k,q) = -tr[(g_1\gamma^\mu + i\frac{g_2}{2m_N}\sigma^{\mu\alpha}q_\alpha)(\not{k} + Pm_N)(g_1\gamma^\mu - i\frac{g_2}{2m_N}\sigma^{\mu\alpha}q_\alpha)(\not{k} + \epsilon_1\not{q} + m_B)] \tag{5.11}$$

where sign function ϵ_1 has been used to generalize the two possible diagrams for baryon loops as done in previous chapter.

Considering only the four-dimensionally transverse part of the self-energy we have

$$L^{\mu\nu} = 4(\frac{g_2}{2m_N})^2[(k^2 - a(q\cdot k) + bm_Nm_B)q^2A^{\mu\nu} + 2B^{\mu\nu}] \tag{5.12}$$

B	J^P	g_1	g_2	g_3
$N(940)$	$\frac{1}{2}^+$	4.19	-0.79	-
$N^*(1440)$	$\frac{1}{2}^+$	1.53	-4.35	-
$N^*(1520)$	$\frac{3}{2}^-$	3.35	4.80	-9.99
$N^*(1535)$	$\frac{1}{2}^-$	3.79	6.50	-
$N^*(1650)$	$\frac{1}{2}^-$	-1.13	-3.27	-
$N^*(1720)$	$\frac{3}{2}^+$	-6.82	-5.84	-8.63

Table 5.1: Table showing the coupling constants of ωNB vertex where B stands for various resonances considered.

where $A^{\mu\nu}$, $B^{\mu\nu}$ are gauge invariant (transverse) tensors (defined in previous chapter). For spin $\frac{3}{2}^{\pm}$ resonances

$$L^{\mu\nu}(k,q) = -tr[V^{\mu\alpha}(\not{k} + Pm_N)V^{\nu\beta}(\not{k} + \epsilon_1\not{q} + m_B)K_{\beta\alpha}] \tag{5.13}$$

where $V^{\mu\alpha} = V_0^{\mu\alpha} + cV_c^{\mu\alpha}$ for the off shell projection operator $\mathcal{O}_{\mu\nu} = g_{\mu\nu} + c\gamma_\mu\gamma_\nu$ (i.e. $c = -\frac{1}{4}$) with

$$\begin{aligned} V_0^{\mu\alpha} &= \frac{g_1}{2m_N}(\not{q}g^{\mu\alpha} - \gamma^\mu q^\alpha) + \frac{g_2}{4m_N^2}\{(q\cdot k)g^{\mu\alpha} - k^\mu q^\alpha\} - \frac{g_3}{4m_N^2}(q^2 g^{\mu\alpha} - q^\mu q^\alpha) \\ V_c^{\mu\alpha} &= \frac{g_1}{2m_N}\gamma^\mu(\gamma^\alpha\not{q} - \not{q}\gamma^\alpha) + \frac{g_2}{4m_N^2}\gamma^\mu\{\gamma^\alpha(q\cdot k) - \not{q}k^\alpha\} - \frac{g_3}{4m_N^2}\gamma^\mu(q^2\gamma^\alpha - \not{q}q^\alpha)\ . \end{aligned} \tag{5.14}$$

Considering all three coupling constants $L^{\mu\nu}$ is given by

$$L^{\mu\nu} = (\frac{g_1}{2m_N})^2 L_{11}^{\mu\nu} + (\frac{g_2}{4m_N^2})^2 L_{22}^{\mu\nu} + (\frac{g_3}{4m_N^2})^2 L_{33}^{\mu\nu} + \frac{g_1}{2m_N}\frac{g_2}{4m_N^2}L_{12}^{\mu\nu} + \frac{g_1}{2m_N}\frac{g_3}{4m_N^2}L_{13}^{\mu\nu} + \frac{g_2}{4m_N^2}\frac{g_3}{4m_N^2}L_{23}^{\mu\nu} \tag{5.15}$$

where

$$L_{ij}^{\mu\nu} = (\alpha_{ij}^{00} + c\alpha_{ij}^{0c} + c^2\alpha_{ij}^{cc})A^{\mu\nu} + (\beta_{ij}^{00} + c\beta_{ij}^{0c} + c^2\beta_{ij}^{cc})B^{\mu\nu} + (\gamma_{ij}^{00} + c\gamma_{ij}^{0c} + c^2\gamma_{ij}^{cc})C^{\mu\nu} \tag{5.16}$$

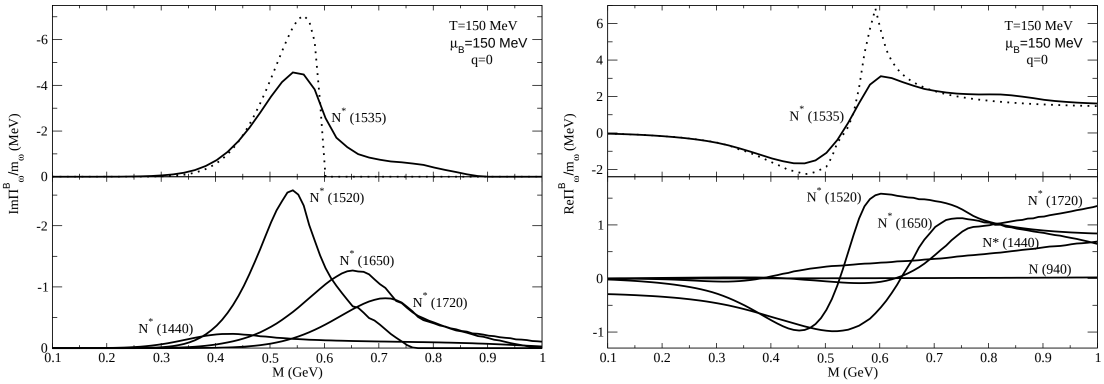

Figure 5.2: Left: The upper panel shows the contribution of the $NN^*(1535)$ loop where the result in the narrow width approximation is indicated by the dotted line. The lower panel shows the contribution of other NB loops. Right: The corresponding results for the real part.

with six possible sets of ij ($ij = 11, 22, 33, 12, 13$ and 23). The expression of all the coefficients are provided in Appendix.

5.3 Results and discussion

We now present the results of numerical evaluation. We start with the spin-averaged self-energy function. In Fig. (5.2) we plot the imaginary and real parts of ω self-energy for vanishing three-momentum in the left and right panels respectively. The contribution of the $NN^*(1535)$ loop is observed to play the most significant role primarily due to the strong coupling of this resonance with the ωN channel and is shown separately in the upper panels. The effect of folding by the spectral function of the resonances denoted by B is also shown where the smoothing of the sharp cut-off in the imaginary part defining the end of the Landau cut is clearly observed in the upper panel on the left. In the lower panels showing the contribution of the other loops the effect of the $N*(1520)$ is seen to be significantly more than the others. In the left and right panels of Fig. (5.3) we have shown the imaginary and real parts of ω self-energy for $\vec{q} = 300$ MeV. Here the transverse component $\overline{\Pi}_t$ is shown along with q^2 times the longitudinal component (note that $\overline{\Pi}_t = q^2\overline{\Pi}_l$ for $\vec{q} = 0$). As before, the $N^*(1535)$ makes the most important contribution and is shown separately in the top panels.

Plotted in the left panel of Fig. (5.4) is the spin averaged ω self-energy from the $\rho\pi$

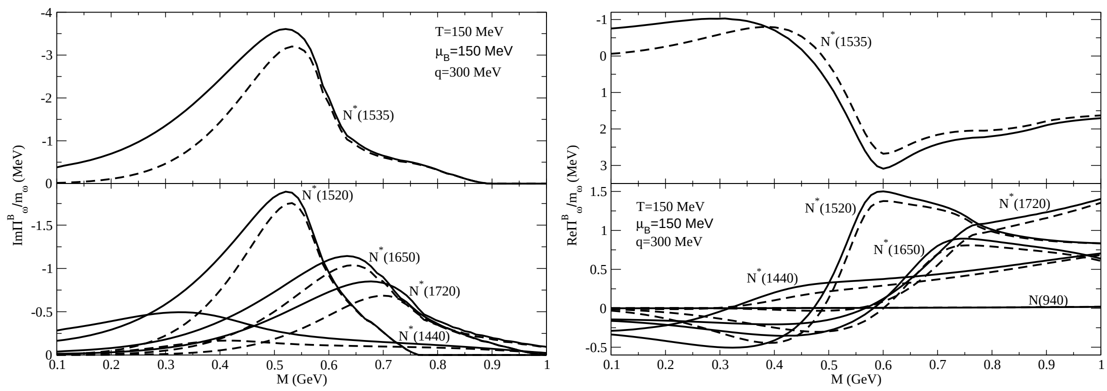

Figure 5.3: Imaginary (left) and real (right) parts of ω self energy for the NB loops with three-momentum $q = 300$ MeV. Solid and dotted lines stand for transverse and longitudinal part of the self energy respectively.

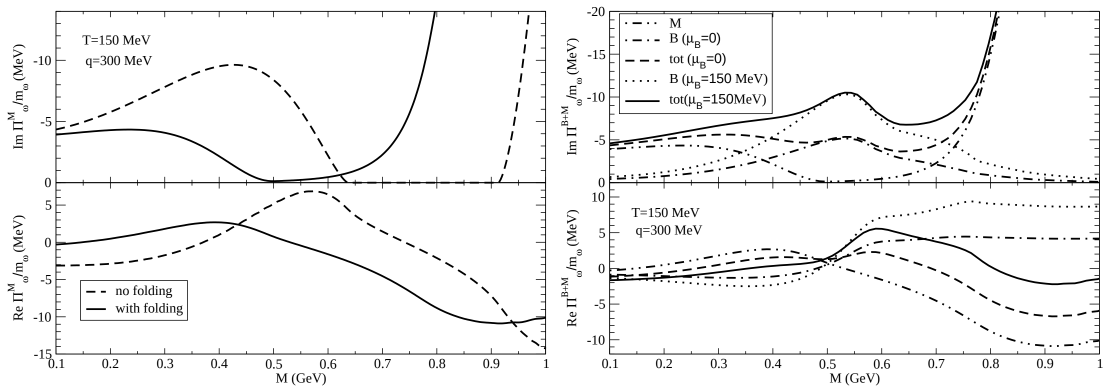

Figure 5.4: Left panel shows imaginary (upper panel) and real (lower panel) part of ω self energy for mesonic loop with and without the convolution with the ρ spectral function. The right panel shows the total imaginary (upper panel) and real (lower panel) parts of ω self energy for meson and baryon loops.

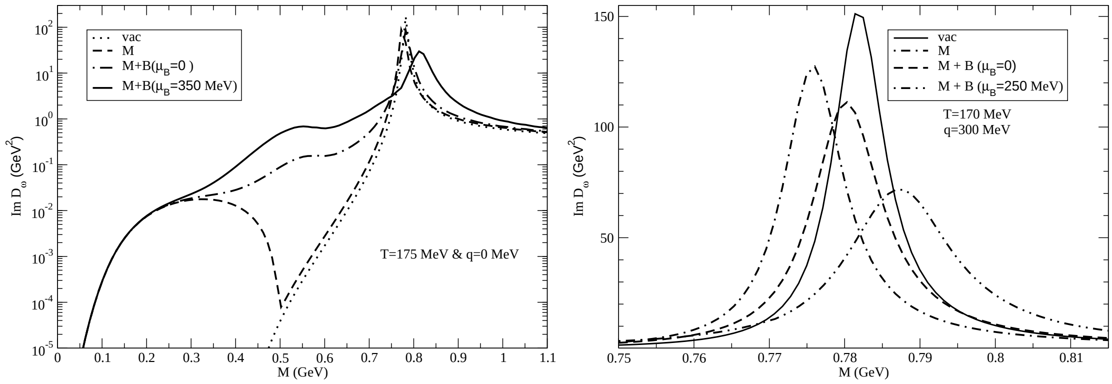

Figure 5.5: Left: The ω spectral function showing individual contributions due to mesonic and baryonic loops. Right: The region close to the ω pole.

loop. The effect of folding the $\rho\pi$ self-energy with the ρ width is clearly visible in the upper panel by the solid line which shows a finite contribution at the ω pole instead of a vanishing contribution in this region when this folding is not done, as shown by the dashed line. This is because the ω pole lies in between the Landau and unitary cut thresholds at $\sim$630 and $\sim$910 MeV respectively. On the right panel is shown the total contribution from the meson and baryon loops for two values of the baryon chemical potential. A noticeable contribution is seen in the imaginary part below the nominal ω mass. In the lower panel is shown the real part where the meson and baryon loops provide a negative and positive contribution respectively at the ω pole which will be manifested in the spectral function.

We now show the results for the spin averaged spectral function of the ω. In Fig. (5.5) we show the contributions of the different loops to the spectral function. To bring out the relative strengths at low invariant masses a logarithmic scale is employed in the left panel. The dashed line represents $\rho\pi$ loop in which the Landau cut contribution falls off in the vicinity of $M = m_\rho - m_\pi$ and then increases as the unitary cut contribution builds up. The Landau cut contributions from the baryonic loops, shown by the solid and dash-dotted lines, however dominate in the region below the ω mass. We now concentrate on a small M range around the ω mass in the right panel of Fig. (5.5). In tune with the real part of the self-energy shown in the lower right panel of Fig. (5.3), the peak shifts a little to the left for the meson loop in contrast to the situation when baryonic contributions are added. The slight increase in mass in this case is also accompanied

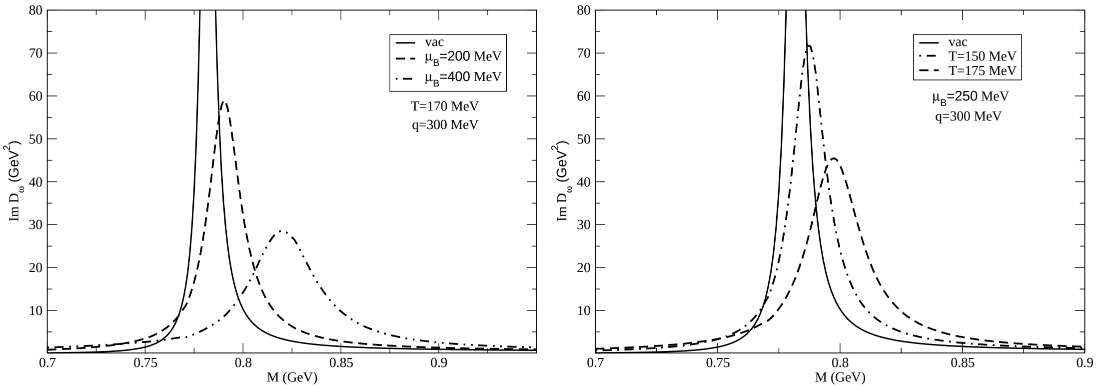

Figure 5.6: The spectral function of ω for different values of μ_B (left) and T (right)

by a larger imaginary part causing more suppression of the spectral strength at the peak. Next we plot the spectral function for different μ_B and T in the left and right panels of Fig. (5.3) respectively for M close to the ω mass. As before, the small positive thermal mass shift of the ω increases with μ_B and T. The corresponding decrease of the ω-spectral function at the peak representing the enhancement of width with increasing μ_B and T is also seen.

In view of the fact that the ρ and ω peaks are close to each other it is worthwhile to compare their relative spectral strengths below their nominal masses. We have plotted the ω spectral function at two values of the chemical potential along with that of the ρ which has been recently calculated in Ref. [88]. The sharp peak of the ω is stands out against the smooth profile of the ρ. The characteristic 2π and 3π thresholds for the ρ and ω in the vacuum case are also visible. Though the spectral strength of the ω is lower than the ρ they do have a sizable contribution in the region below $\sim$700 MeV.

5.4 Appendix

The values of the coefficients for each set are given by

$$\alpha_{11}^{00} = \frac{8}{3m_B^2}[(k^2m_B^2 + bm_Nm_B^3 - k^2q^2) - a(q\cdot k)(2k^2 + q^2 + 2a(q\cdot k))]q^2$$
$$\beta_{11}^{00} = \frac{8}{3m_B^2}[k^2 + m_B^2 + a(q\cdot k)]$$
$$\alpha_{11}^{0c} = 4\frac{8}{3m_B^2}[bm_Nm_BS_N^2 - a(q\cdot k)(S_N^2 + 3a(q\cdot k) - 2bm_Nm_B)]q^2$$

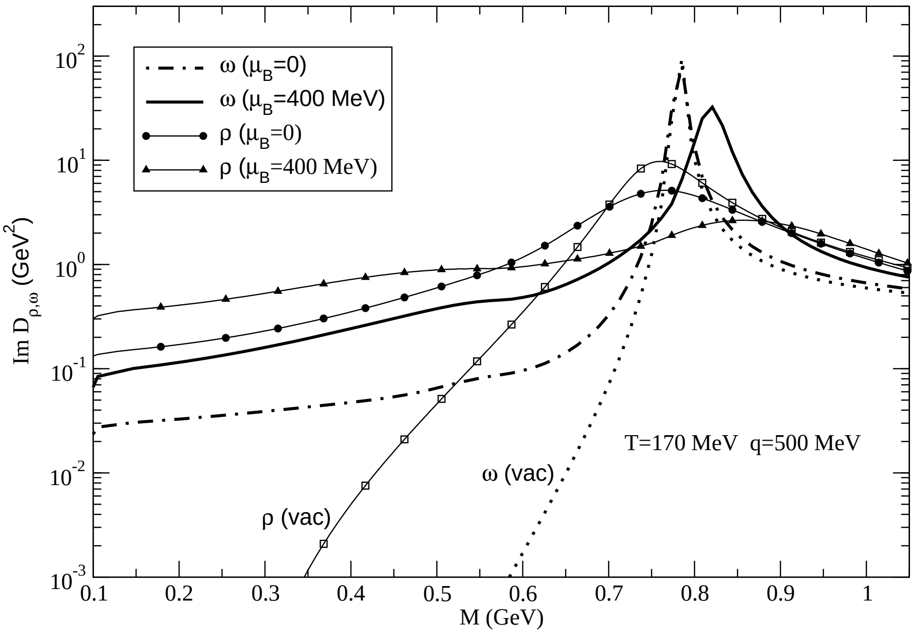

Figure 5.7: The ω spectral function seen in comparison with the ρ.

$$
\begin{aligned}
\beta_{11}^{0c} &= 4\frac{8}{3m_B^2}[k^2 - m_B^2 + 2a(q\cdot k)] \\
\gamma_{11}^{0c} &= 4\frac{8}{3m_B^2} \\
\alpha_{11}^{cc} &= 4\frac{8}{3m_B^2}[(m_N^2 + 2bm_N m_B)\{S_N^2 + 2a(q\cdot k)\} - a(q\cdot k)\{S_N^2 + 4a(q\cdot k)\}]q^2 \\
\beta_{11}^{cc} &= 4\frac{8}{3m_B^2}[2\{k^2 - m_B^2 + 2a(q\cdot k)\}] \\
\gamma_{11}^{cc} &= 4\frac{8}{3m_B^2}[2]
\end{aligned}
\tag{5.17}
$$

$$
\begin{aligned}
\beta_{22}^{00} &= \frac{8}{3m_B^2}[\{k^2 - bm_N m_B + a(q\cdot k)\}m_B^2] \\
\gamma_{22}^{00} &= \frac{8}{3m_B^2}[-k^2 + bm_N m_B - a(q\cdot k)] \\
\beta_{22}^{0c} &= \frac{8}{3m_B^2}[-bm_N m_B\{S_N^2 + 2a(q\cdot k)\}] \\
\beta_{22}^{cc} &= \frac{8}{3m_B^2}[a(q\cdot k)\{S_N^2 + 2a(q\cdot k)\}] \\
\gamma_{22}^{cc} &= \frac{8}{3m_B^2}[(k^2 - bm_N m_B)\{S_N^2 + 2a(q\cdot k)\}]
\end{aligned}
\tag{5.18}
$$

$$\begin{aligned}
\alpha_{33}^{00} &= \frac{8}{3m_B^2}[\{-k^2 + bm_N m_B - a(q\cdot k)\}m_B^2]q^4 \\
\gamma_{33}^{00} &= \frac{8}{3m_B^2}[-k^2 + bm_N m_B - a(q\cdot k)] \\
\alpha_{33}^{0c} &= \frac{8}{3m_B^2}[bm_N m_B\{S_N^2 + 2a(q\cdot k)\}]q^4 \\
\gamma_{33}^{0c} &= \frac{8}{3m_B^2}[-2\{S_N^2 + 2a(q\cdot k)\}] \\
\alpha_{33}^{cc} &= \frac{8}{3m_B^2}[\{k^2 - 2bm_N m_B + a(q\cdot k)\}\{S_N^2 + 2a(q\cdot k)\}]q^4 \\
\gamma_{33}^{cc} &= \frac{8}{3m_B^2}[-2\{S_N^2 + 2a(q\cdot k)\}]
\end{aligned} \tag{5.19}$$

$$\begin{aligned}
\alpha_{12}^{00} &= \frac{8}{3m_B^2}[-k^2 + 2bm_N m_B - a(q\cdot k)]m_B(q\cdot k)q^2 \\
\beta_{12}^{00} &= \frac{8}{3m_B^2}[k^2 - 2bm_N m_B + a(q\cdot k) + m_B^2]m_B \\
\gamma_{12}^{00} &= \frac{8}{3m_B^2}[-m_B] \\
\alpha_{12}^{0c} &= 2\frac{8}{3m_B^2}[abm_N(q\cdot k)\{S_N^2 + 2a(q\cdot k)\}]q^2 \\
\beta_{12}^{0c} &= 2\frac{8}{3m_B^2}[(2m_B - bm_N)\{S_N^2 + 2a(q\cdot k)\}] \\
\alpha_{12}^{cc} &= 4\frac{8}{3m_B^2}[abm_N(q\cdot k)\{S_N^2 + 2a(q\cdot k)\}]q^2 \\
\beta_{12}^{cc} &= 4\frac{8}{3m_B^2}[(2m_B - bm_N)\{S_N^2 + 2a(q\cdot k)\}]
\end{aligned} \tag{5.20}$$

$$\begin{aligned}
\alpha_{13}^{00} &= \frac{8}{3m_B^2}[(k^2 + q^2 + m_B^2 - 2bm_N m_B)(q\cdot k) + aq^2(k^2 - 2bm_N m_B)]m_B q^2 \\
\beta_{13}^{00} &= \frac{8}{3m_B^2}[-am_B q^2] \\
\alpha_{13}^{0c} &= 2\frac{8}{3m_B^2}[\{(2m_B - bm_N)(q\cdot k) - abm_N q^2\}\{S_N^2 + 2a(q\cdot k)\}]q^2 \\
\alpha_{13}^{cc} &= 4\frac{8}{3m_B^2}[\{(2m_B - bm_N)(q\cdot k) - abm_N q^2\}\{S_N^2 + 2a(q\cdot k)\}]q^2
\end{aligned} \tag{5.21}$$

$$\begin{aligned}
\alpha_{23}^{00} &= 2\frac{8}{3m_B^2}[k^2 - 2bm_N m_B + a(q\cdot k)]m_B^2(q\cdot k)q^2 \\
\gamma_{23}^{00} &= 2\frac{8}{3m_B^2}[-a\{k^2 - 2bm_N m_B + a(q\cdot k)\}]
\end{aligned}$$

$$\alpha_{23}^{0c} = 2\frac{8}{3m_B^2}[-bm_N m_B(q\cdot k)\{S_N^2 + 2a(q\cdot k)\}]q^2$$
$$\gamma_{23}^{0c} = 2\frac{8}{3m_B^2}[-a\{S_N^2 + 2a(q\cdot k)\}]$$
$$\alpha_{23}^{cc} = 2\frac{8}{3m_B^2}[(k^2 - 2bm_N m_B)(q\cdot k)\{S_N^2 + 2a(q\cdot k)\}]q^2$$
$$\beta_{23}^{cc} = 2\frac{8}{3m_B^2}[-a\{S_N^2 + 2a(q\cdot k)\}]q^2 \tag{5.22}$$

The rest of the coefficients are zero.

Chapter 6

Probing strongly interacting matter by dileptons

It is well known that dileptons are excellent probes to study the local properties of the transient form of matter produced in nuclear collisions at ultra-relativistic energies as they leave the system almost unscathed after production. In the low invariant mass region, which we study in this chapter, the rate of dilepton production is controlled by the spectral functions of the vector mesons, specially the ρ and hence the modification of the ρ spectral function determines the yield of lepton pairs in this region. The broadening of the vector meson spectral functions leads to an enhancement of lepton pair production in the invariant mass region below the ρ peak. The effect of the evolving matter is handled by relativistic hydrodynamics. The time information in the invariant mass spectra of dileptons is also displayed explicitly in [112] using the invariant mass dependence of the elliptic flow of lepton pairs.

The rate of production of thermal dileptons is proportional to the two-point correlator of vector currents [113] which is intimately related with vector meson spectral function. Consequently, the spectral properties of vector mesons, the ρ meson in particular has been a subject of intense discussion [37, 114, 16, 38].

In previous chapters (Ch.4 and Ch.5) we have extensively discussed about the in-medium spectral properties of ρ and ω. In this chapter we first go through a brief formulation which shows how the neutral vector meson (ρ, ω, ...) spectral function is proportional to the dilepton production rate from hadronic phase. Then using those spectral functions we have calculated dilepton yields as a function of invariant mass as well as transverse mass (or momentum). The static rate of dilepton production is then evolved in space and time from formation to freeze out in order to get the final dilepton yield which can be compared to experimental data. As indicated in introduction, a large no of theoretical attempts [115, 116, 117, 118, 119, 120, 121, 122] have been made to study the low mass dilepton spectra in heavy ion collisions. Their efforts have suggested that medium effects play a very important role and a careful and detailed analysis of low mass vector meson spectral function is necessary. In this chapter we will evaluate the dilepton spectra from heavy ion collisions at SPS, RHIC and LHC energies and show how medium effect of the ρ and ω mesons lead to an excellent agreement with NA60 data.

6.1 Formalism of dilepton emission rate

Let us consider an initial state $|I\rangle$ which goes to a final state $|F\rangle$ producing a lepton pair l^+l^- with momenta p_1 and p_2 respectively. The dilepton multiplicity thermally averaged over initial states is given by [123, 124]

$$N = \sum_I \sum_F |\langle F, l^+l^- | e^{i\int \mathcal{L}_{int} d^4x} | I \rangle|^2 \frac{e^{-\beta E_I}}{Z} \frac{d^3p_1}{(2\pi)^3 2E_1} \frac{d^3p_2}{(2\pi)^3 2E_2} \tag{6.1}$$

where $Z = Tr[e^{-\beta H}]$ and $\mathcal{L}_{int} = e\overline{\psi}_l(x)\gamma_\mu\psi_l(x)A^\mu(x) + eJ^h_\mu(x)A^\mu(x)$ in which $\psi_l(x)$ is the lepton field operator and $J^h_\mu(x)$ is the electromagnetic current of hadrons. Following [113, 123, 114] this expression can be put in the form

$$\frac{dN}{d^4q d^4x} = -\frac{\alpha^2}{6\pi^3 q^2} L\left(M^2\right) f_{BE}(q_0) g^{\mu\nu} W_{\mu\nu}\left(q_0, \vec{q}\right) \tag{6.2}$$

where the factor $L(M^2) = (1 + 2m_l^2/M^2)\ (1 - 4m_l^2/M^2)^{1/2}$ is of the order of unity for electrons, $M(= \sqrt{q^2})$ being the invariant mass of the pair and the electromagnetic (e.m.) current correlator $W_{\mu\nu}$ is defined by

$$W_{\mu\nu}(q_0, \vec{q}) = \int d^4x\, e^{iq\cdot x} \langle [J^{em}_\mu(x), J^{em}_\nu(0)] \rangle \tag{6.3}$$

Here $J^{em}_\mu(x)$ is the electromagnetic current and $\langle\rangle$ indicates ensemble average. The rate given by eq. (6.2) is to leading order in electromagnetic interactions but exact to all orders in the strong coupling encoded in the current correlator $W_{\mu\nu}$. The q^2 in the denominator indicates the exchange of a single virtual photon and the Bose distribution implies the thermal weight of the source.

In the QGP where quarks and gluons are the relevant degrees of freedom, the $W_{\mu\nu}$ can be directly evaluated by writing the hadron current in terms of quarks of flavor f i.e. $J^h_\mu = \sum_f e_f \overline{\psi}_f \gamma_\mu \psi_f$. Confining to the leading order contribution we obtain

$$g^{\mu\nu} W_{\mu\nu} = -\frac{3q^2}{2\pi} \sum_f e_f^2 (1 - \frac{4m_q^2}{q^2}) \ . \tag{6.4}$$

The rate in this case corresponds to dilepton production due to process $q\overline{q} \to \gamma^* \to l^+ l^-$. To obtain the rate of dilepton production from hadronic interactions it is convenient to break up the quark current J^h_μ into parts with definite isospin

$$\begin{aligned} J^h_\mu &= \frac{1}{2}(\bar{u}\gamma_\mu u - \bar{d}\gamma_\mu d) + \frac{1}{6}(\bar{u}\gamma_\mu u + \bar{d}\gamma_\mu d) + \cdots \\ &= J^V_\mu + J^S_\mu + \cdots \\ &= J^\rho_\mu + J^\omega_\mu / 3 + \cdots \end{aligned} \tag{6.5}$$

where V and S denote iso-vector and iso-scalar currents and the dots denote currents comprising of quarks with strangeness and heavier flavors. These currents couple to individual hadrons as well as multi-particle states with the same quantum numbers and are usually labeled by the lightest meson in the corresponding channel [125]. We thus identify the isovector and isoscalar currents with the ρ and ω mesons respectively. Defining the correlator of these currents $W^{\rho,\omega,\phi}_{\mu\nu}$ analogously as in (6.3) we write,

$$W_{\mu\nu} = W^\rho_{\mu\nu} + W^\omega_{\mu\nu}/9 + ... \tag{6.6}$$

The correlator of vector-isovector currents $W^\rho_{\mu\nu}$ have in fact been measured [126] in vacuum along with the axial-vector correlator by studying τ decays into even and odd number of pions. The former is found to be dominated at lower energies by the prominent peak of the ρ meson followed by a continuum at high energies. The axial correlator, on the other hand, is characterized by the broad hump of the a_1. The distinctly different shape in the two spectral densities is an experimental signature of the fact that chiral symmetry of QCD is dynamically broken by the ground state [127]. It is expected that this symmetry may be restored at high temperature and/or density and will be signaled by a complete overlap of the vector and axial-vector correlators [128].

In the medium, both the pole and the continuum structure of the correlation function gets modified [114, 92]. We will first evaluate the modification of the pole part due to the self-energy of vector mesons in the following. Using Vector Meson Dominance the isovector and scalar currents are written in terms of dynamical field operators for the mesons allowing us to express the correlation function in terms of the exact(full) propagators or the interacting spectral functions of the vector mesons in the medium. To reach that goal we have to specify the coupling of the currents to the corresponding vector fields. For this purpose we write, in the narrow width approximation [125],

$$\langle 0|J_\mu^{em}(0)|R\rangle = F_R m_R \epsilon_\mu \tag{6.7}$$

where R denotes the resonance in a particular channel and ϵ_μ is the corresponding polarization vector. The coupling constants F_R are obtained from the partial decay widths into e^+e^- through the relation

$$F_R^2 = \frac{3m_R\Gamma_{R\to e^+e^-}}{4\pi\alpha^2} \tag{6.8}$$

yielding F_R=0.156 GeV, 0.046 GeV and 0.079 GeV for ρ, ω and ϕ respectively. Eq. (6.7) suggests the operator relations

$$J_\mu^\rho(x) = F_\rho m_\rho V_\mu^\rho(x), \quad J_\mu^\omega(x) = 3F_\omega m_\omega V_\mu^\omega(x) \;\; \text{etc.} \tag{6.9}$$

where $V_\mu^{\rho(\omega)}(x)$ denotes the field operator for the $\rho(\omega)$ meson. So using the above relations connecting currents to fields (so-called field-current identity), the current commutator become

$$\begin{aligned} W_{\mu\nu} &= \sum_{R=\rho,\omega,..} F_R^2 m_R^2 \int d^4x\, e^{iq\cdot x}\langle[V_\mu^R(x), V_\nu^R]\rangle \\ &= \sum_{R=\rho,\omega,..} F_R^2 m_R^2 A_{\mu\nu}^R(q_0,\vec{q}) \\ &= 2\epsilon(q_0)\sum_{R=\rho,\omega,..} F_R^2 m_R^2 \mathrm{Im}\overline{D}_{\mu\nu}^R(q_0,\vec{q}) \end{aligned} \tag{6.10}$$

where $A_{\mu\nu}^R$ are the spectral functions of corresponding vector meson resonances (R) and $\overline{D}_{\mu\nu}^R$ is the diagonal element of the thermal propagator matrix. The connection between these two quantities have already been discussed in Chapter 2 (see Eq. 2.97). The form of the diagonal element of the exact thermal propagator matrix for the spin 1 particle has been obtained in section 1.3 by using the Dyson equation. From Eq. (2.120) we get the $\overline{G}_{\mu\nu}^R$ which is the transverse (four dimensional) part of $\overline{D}_{\mu\nu}^R$. So

$$\overline{D}_{\mu\nu}^R(q) = \overline{G}_{\mu\nu}^R - \frac{q_\mu q_\nu}{q^2 m_R^2}$$

$$= \quad -\frac{P_{\mu\nu}}{q^2 - m_R^2 - \overline{\Pi}_t(q)} - \frac{Q_{\mu\nu}/q^2}{q^2 - m_R^2 - q^2\overline{\Pi}_l(q)} - \frac{q_\mu q_\nu}{q^2 m_R^2} \tag{6.11}$$

The imaginary part is then put in eqs. (6.10) and then in eq. (6.2) to arrive at the dilepton emission rate [129, 130]

$$\frac{dN}{d^4q d^4x} = \frac{\alpha^2}{\pi^3 q^2} L(q^2) f_{BE}(q_0) \left[F_\rho^2 m_\rho^2 A_\rho(q_0, \vec{q}) + F_\omega^2 m_\omega^2 A_\omega(q_0, \vec{q}) + \cdots\right] \tag{6.12}$$

where e.g. $A_\rho (= -g^{\mu\nu}\mathrm{Im}\overline{D}^\rho_{\mu\nu}/3)$ is given by

$$A_\rho = -\frac{1}{3}\left[\frac{2\sum \mathrm{Im}\Pi_t^R}{(q^2 - m_\rho^2 - \sum \mathrm{Re}\Pi_\mathrm{t}^\mathrm{R})^2 + (\sum \mathrm{Im}\Pi_\mathrm{t}^\mathrm{R})^2} + \frac{q^2 \sum \mathrm{Im}\Pi_l^R}{(q^2 - m_\rho^2 - q^2\sum \mathrm{Re}\Pi_\mathrm{l}^\mathrm{R})^2 + \mathrm{q}^4(\sum \mathrm{Im}\Pi_\mathrm{l}^\mathrm{R})^2}\right] \tag{6.13}$$

the sum running over all mesonic and baryonic loops.

As indicated earlier, coupling of the hadronic current to multi-particle states gives rise to a continuum structure in the current correlation function $W^{\mu\nu}$. Following Shuryak [125] we take a parameterized form for this contribution and augment the dilepton emission rate with

$$\frac{dN}{d^4q d^4x} = \frac{\alpha^2}{\pi^3} L(q^2) f_{BE}(q_0) \sum_{V=\rho,\omega} A_V^{\mathrm{cont}}. \tag{6.14}$$

where

$$A_\rho^{\mathrm{cont}} = \frac{1}{8\pi}\left(1 + \frac{\alpha_s}{\pi}\right)\frac{1}{1 + \exp(\omega_0 - q_0)/\delta} \tag{6.15}$$

with $\omega_0 = 1.3, 1.1$ GeV for ρ, ω and $\delta = 0.2$ for both ρ and ω. The continuum contribution for the ω contains an additional factor of $\frac{1}{9}$.

Thus, the dilepton emission rate in the present scenario actually boils down to the evaluation of the self energy graphs of ρ and ω, which we have explicitly evaluated in previous chapters as a function of q_0, $\vec{q}$, temperature (T) and net baryon density (ρ_B). Using those functions in the Eq. (6.13) we can get a numerical estimation of dilepton static rates.

6.2 Rate of dilepton production

First we have plotted in Fig. (6.1), upper panel the relative contributions from the cuts in the $\pi - h$ loops keeping only one of them at a time. The unitary and Landau cuts for the π, ω, h_1 and a_1 are seen to contribute with different magnitudes for different values of the energy and three momenta of the off-shell ρ. In the time-like region, in the vicinity of the (bare) rho mass the imaginary part of the self energy from a particular loop receives dominant contribution from only one of the cuts. The $\pi-\pi$ loop for example, has only the unitary cut and this contributes most significantly to dilepton emission near the ρ pole. In contrast, the Landau cut contribution from the $\pi-\omega$ loop is dominant up to about 400 MeV. Since this cut ends at $M=m_\omega-m_\pi$ and the unitary cut starts at $M=m_\omega+m_\pi$ there is no contribution at the ρ pole. The Landau cut for the $\pi-a_1$ self-energy extends up to about 1100 MeV and makes a substantial contribution both at and below the ρ pole. The unitary cut starts at a much higher value of M and hence does not make a significant contribution to the ρ spectral function. We also show the effect of convolution over the width of the a_1 as discussed above. As expected, the contributions from the Landau and unitary cuts are now joined by a continuous line, the boundaries being smeared out due to the substantial width of the a_1. While analyzing the different contributions one must keep in mind that the total contribution from the different loops to the spectral function is not a linear sum of the individual contributions as is clear from the definition given in Eq. (6.13). This is seen in the lower panel where the cumulative contribution to the lepton pair yield is shown for the $\pi-\pi$ and $\pi-h$ loops. Also shown is the enhancement in yield obtained by including baryons at $\mu_B=$ 30 MeV for RHIC energies.

By adding our ω spectral function (from Chapter 5) with the ρ one, a complete in-medium effect in low mass dilepton rate is shown in the right panel of Fig. (6.1). Here the sharp peak of the ω resonance in vacuum has almost been dissolve in the ρ-profile at finite temperature. A significant enhancement is seen in the low mass lepton production rate due to baryonic loops over and above the mesonic ones shown by the dot-dashed line. The substantial contribution from baryonic loops even for vanishing chemical potential points to the important role played by antibaryons in thermal equilibrium in systems created at RHIC and LHC energies. In that panel we have also shown the thermal dileptons contribution from the source of QGP.

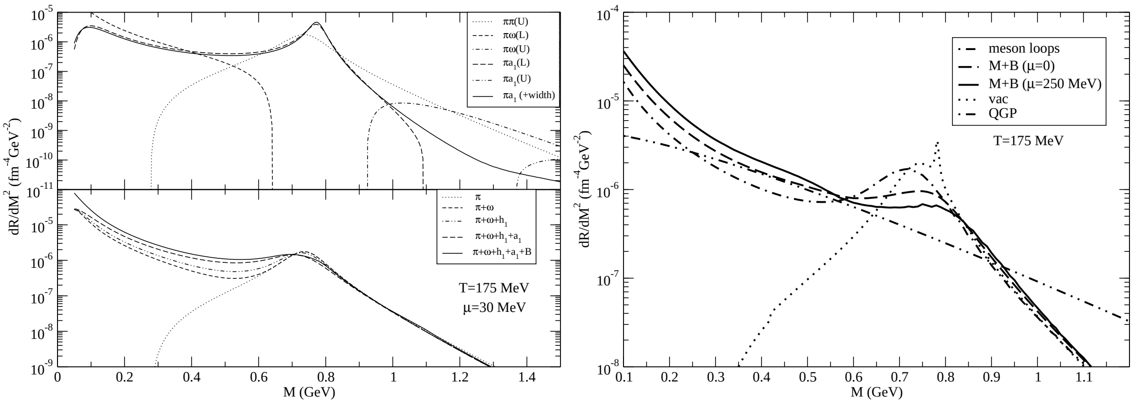

Figure 6.1: Left : Upper panel shows contributions from the discontinuities of the self-energy graphs to the dilepton emission rate at $T = 175$ MeV and $\mu_B = 30$ MeV. L and U denote the Landau and unitary cut contribution. Lower panel shows contributions from the mesons and baryons. Right : The dilepton emission rate from different sources-QGP (dash double dotted line), mesonic interaction (dash dotted line) as well as total (meson + baryon) hadronic interaction (dashed line) at $T = 175$ MeV and $\mu_B = 0$ MeV. Total hadronic interaction at different chemical potential, $\mu_B = 250$ MeV (solid line) and its vacuum contribution (dotted line) are also shown

6.3 Space time evolution

Total yields is obtained by integrating the rate of dilepton emission from a fluid element at $x^\mu \equiv (t, \vec{x})$ at local temperature $T(x^\mu)$ and baryon density $(\mu_B(x))$ over d^4x i.e.

$$\frac{dN}{d^4q} = \int d^4x \frac{dR}{d^4q}[E^*, T(x^\mu), \mu_B(x^\mu)] \tag{6.16}$$

where

$$\begin{aligned} q^\mu u_\mu &= M_T \gamma_T \cosh(\eta - y) - q_T \gamma_T v_r \cos\phi \\ \text{and } d^4q &= dM^2 \pi q_T dq_T dy \end{aligned} \tag{6.17}$$

The space time dependence of the fluid velocity $u^\mu(x)$ and temperature $T(x)$ can be obtained by by solving the the energy momentum conservation equation

$$\partial_\mu T^{\mu\nu} = 0, \qquad T^{\mu\nu} = (\epsilon + P) u^\mu u^\nu \, + \, g^{\mu\nu} P \tag{6.18}$$

where ϵ is the energy density and P is the pressure in the frame co-moving with the fluid. With the assumption that the system undergoes a boost-invariant longitudinal expansion along the z-axis [131] and cylindrically symmetric transverse expansion, the hydrodynamics equations (6.18) reduce to

$$\partial_\tau T^{00} + \frac{1}{r}\partial_r(rT^{01}) + \frac{1}{\tau}(T^{00} + P) \;\; = \;\; 0$$

$$\partial_\tau T^{01} + \frac{1}{r}\partial_r[r(T^{00}+P)v_r^2] + \frac{1}{\tau}T^{01} + \partial_r P \;=\; 0 \tag{6.19}$$

In the set of hydrodynamic equations (6.19), the number of unknown variables exceeds the number of equations by one. This set of equations are closed with the Equation of State (EoS); typically a relation between the pressure P and the energy density ϵ. It is a crucial input which essentially controls the profile of expansion of the fireball. In order to check sensitivity with the equation of state (EoS), we have considered two scenarios: (a) hadronic resonance gas (HRG) with all hadrons up to mass 2.5 GeV for the hadronic phase along with a bag model EoS for the QGP phase and (b) EoS obtained from lattice QCD calculations (LQCD) [132].

One of the most important parameters that go into the space-time evolution are the values of the initial temperature and the thermalisation time. In case of isentropic expansion the experimentally measured hadron multiplicity can be related to the initial temperature and thermalisation time by the following equation [133] :

$$T_i^3(b_m)\tau_i = \frac{2\pi^4}{45\zeta(3)\pi\, R_A^2 4a_k}\langle\frac{dN}{dy}(b_m)\rangle \tag{6.20}$$

where $\langle dN/dy(b_m)\rangle$ is the hadron (predominantly pions) multiplicity for a given centrality class with maximum impact parameter b_m, R_A is the transverse dimension of the system and a_k is the degeneracy of the system created. The initial radial velocity, $v_r(\tau_i, r)$ and energy density, $\epsilon(\tau_i, r)$ profiles are taken as [134], $v_r(\tau_i, r) = 0$ and $\epsilon(\tau_i, r) = \epsilon_0/(e^{\frac{r-R_A}{\delta}} + 1)$ where the surface thickness, $\delta = 0.5$ fm. The hadron multiplicity resulting from nucleus-nucles (A-A) collisions is related to that from proton-proton (pp) collisions at a given impact parameter and collision energy by

$$\langle\frac{dN}{dy}(b_m)\rangle = [(1-x)\langle N_{part}(b_m)\rangle/2 + x\langle N_{coll}(b_m)\rangle]\,\frac{dN_{pp}}{dy} \tag{6.21}$$

where x is the fraction of hard collisions, $\langle N_{part}\rangle$ and $\langle N_{coll}\rangle$ are the average numbers of participants and collisions respectively evaluated by using Glauber model. $dN_{pp}^{ch}/dy = 2.5 - 0.25ln(s) + 0.023ln^2 s$, is the multiplicity of the produced hadrons in pp collisions at center of mass energy, $\sqrt{s}$ [135].

For the space-time picture, we thus work in the following scenario. An equilibrated QGP is formed at initial temperature (time) $T_i(\tau_i)$, the system then cools due to expansion and when the temperature reaches T_c it undergoes a phase transition from QGP to hadrons. After the completion of the phase transition the hadronic matter cools and eventually freezes out first chemically at a temperature T_{ch} and then kinetically at a temperature T_F. The transition temperature is taken as $T_c \sim 175$ MeV. The other inputs which goes into the calculations are chemical ($T_{\rm ch}$) and kinetic freeze-out (T_F) temperatures. The kinetic freeze-out in the system occurs when both the elastic and in-elastic collisions stop i.e. the freeze-out takes place when the collectivity in the system ceases to exist. The value of T_F can be constrained from the hadronic p_T spectra [136]. In the present work we take $T_F = 120$ MeV which reproduces the p_T spectra of pions, kaons reasonably well [137]. The ratios of various hadrons measured experimentally at different $\sqrt{s_{\rm NN}}$ indicate that the system formed in heavy ion collisions chemically decouple at $T_{\rm ch}$ which is higher than T_F [138]. Therefore, the system remains out of chemical equilibrium from $T_{\rm ch}$ to T_F. The deviation of the system from the chemical equilibrium is taken in to account by introducing chemical potential for each hadronic species [139]. The chemical non-equilibration affects the yields through the phase space factors of the hadrons which in turn affects the productions of the EM probes. The chemical potential, μ_j for the hadronic species j as a function of T have been taken from Ref. [140]:

$$\frac{n_j(T,\mu_j)}{s(T,\{\mu_j\})} = \frac{n_j(T_{ch},\mu_j=0)}{s(T_{ch},\{\mu_j\}=0)} \tag{6.22}$$

where n_j is the density of hadron j contains direct as well as contributions from resonance decays. The μ_j is a function of T and it vanishes at $T = T_{ch}$ (= 170 MeV here). Therefore, the space time evolution of μ_j is dictated by the evolution of T. The chemical potentials of pions, ω, h_1, a_1, ϕ and proton enters through their thermal distributions as a fugacity factor. The values of the respective chemical potential at the kinetic freeze-out temperature, $T_F = 120$ MeV are $\mu_\pi = 68$ MeV, $\mu_\omega = 179$ MeV, $\mu_{h_1} = 204$ MeV $\mu_{a_1} = 204$ MeV, $\mu_\phi = 252$ MeV $\mu_{\rm proton} = 258$ MeV. Now we will discuss about numerical results of dileptons for different center of mass energy ($\sqrt{s}$). In space time evolution, only initial conditions will be different which are tabulated in (6.3) for SPS, RHIC and LHC energies.

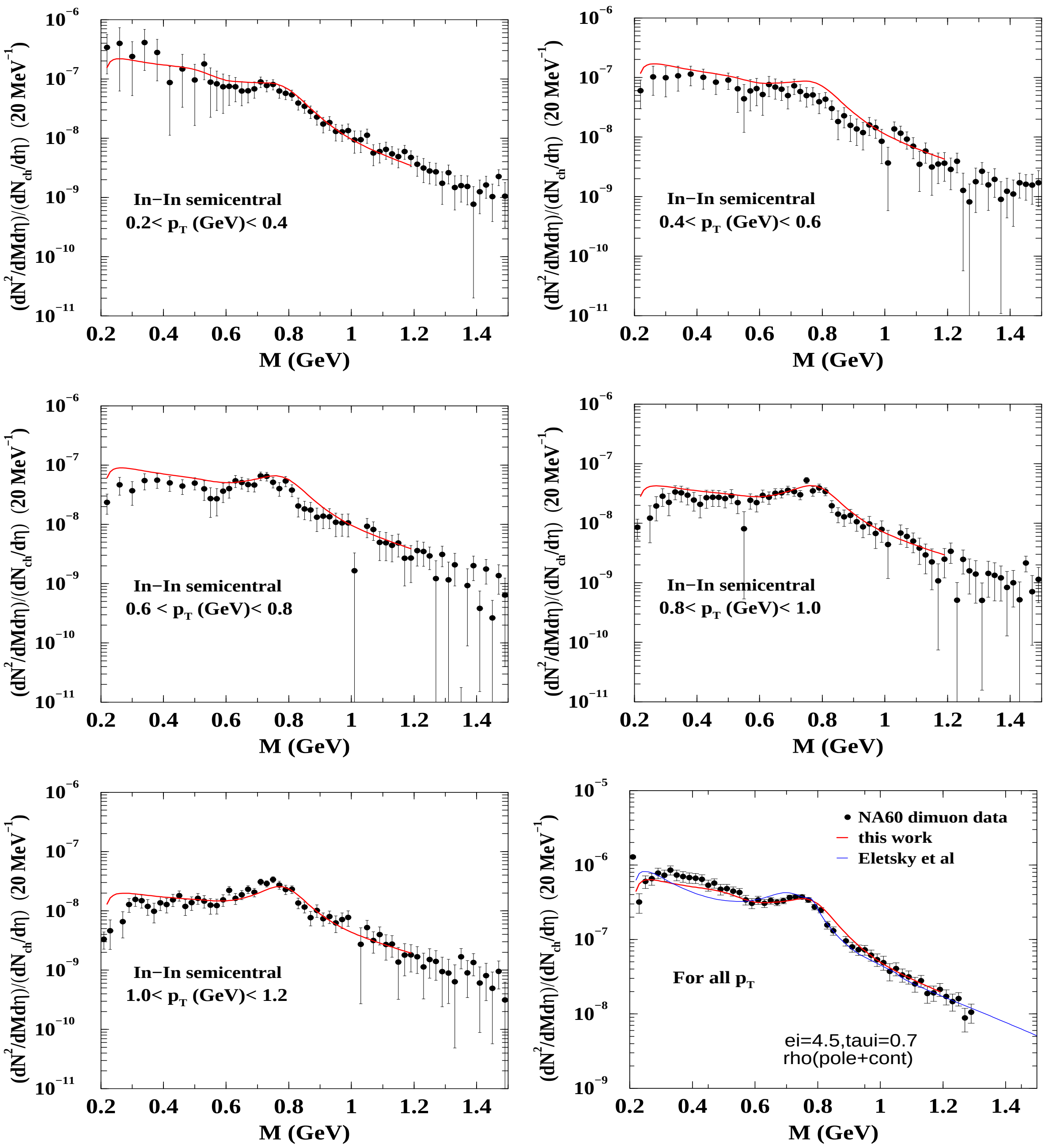

Figure 6.2: Dilepton invariant mass spectra for different p_T-bins compared with the NA60 data.

	$\sqrt{s}$	A-A	τ_i	T_i
SPS	17.3 GeV	Pb-Pb	0.6 fm/c	280 MeV
RHIC	200 GeV	Au-Au	0.2 fm/c	320 MeV
LHC	5.5 TeV	Pb-Pb	0.1 fm/c	756 MeV

Table 6.1: Initial time (τ_i) and temperature (T_i) for different center of mass energy ($\sqrt{s}$) of nucleus-nucleus (A-A) collision.

6.4 Results

6.4.1 At SPS Energy

We have obtained the dimuon yield (dN/dM) in In-In collisions at SPS at a center of mass energy of 17.3 AGeV. The initial energy density is taken as 4.5 GeV/fm^3 corresponding to a thermalisation time $\tau_i = 0.7$ fm. In Fig. (6.2) we have shown the invariant mass spectra for different transverse momentum (p_T) windows. The theoretical curves agree quite well with the experimental data [36] for all the p_T ranges. The strong enhancement in the low M domain is clearly due to the large broadening of the ρ in the thermal medium which comes entirely from the Landau cut in the self-energy diagrams. In the last panel we also plot for comparison the spectra calculated in [141] where the self-energy due to baryons has been evaluated following the approach of [80]. It is seen that this approach depicted by the dashed curve does not produce the required enhancement to explain the data in the range $0.35 \leq M \leq 0.65$ GeV.

6.4.2 At RHIC Energy

Assuming 10% hard (i.e. $x = 0.10$) and 90% soft collisions for initial entropy production the value of dN^{ch}_{pp}/dy turns out to be about 2.43 at $\sqrt{s} = 200$ GeV. For RHIC energy,

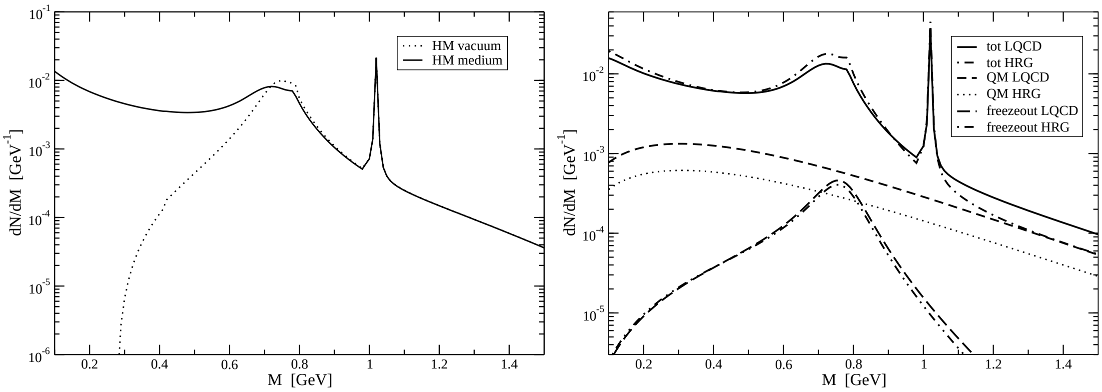

Figure 6.3: Left : invariant mass distribution of dileptons from hadronic matter (HM) for modified and unmodified ρ meson. Right : Freeze out, QGP and total contribution for EoS (a) HRG (dash-double dotted, dotted and dash-dotted lines) and EoS (b) LQCD (long dashed, dashed and solid lines) at RHIC energy.

we take T_i = 320 MeV with initial time τ_i = 0.2 fm/c which acts as inputs to the hydrodynamic evolution.

For studying thermal dileptons at the RHIC energy (as well as the LHC energy) we have included the vacuum spectral function of ϕ meson because its mass appears at a boundary between quark and hadronic sources of dileptons.

We begin by plotting the space-time integrated invariant mass spectra of dileptons. In the left panel of Fig. (6.3) we plot the yield of lepton pairs from the hadronic matter (HM), evaluated with and without the modified ρ spectral function for RHIC energy. The enhancement in the region $0.1 \leq M \leq 0.7$ GeV is purely a medium effect and is a contribution from the Landau cut of the meson and baryon loops. In contrast, the vacuum spectral function naturally starts from the $2m_\pi$ threshold coming from the unity in the unitary cut contribution. The (small) kink at 0.42 GeV in this curve is due to the $3m_\pi$ threshold for ω production. The enhancement in the yield due to medium effects is $\sim$ 20 for M around 400 MeV. In the right panel of Fig. (6.3), we have shown the dependence of the yield from the two phases on the EoS. Dilepton radiation from hadronic phase outshines the emission from quark matter for M up to ϕ mass. Since the internal loops of ρ self energy contains $a_1\pi$ and $\omega\pi$ interactions we ignore the four pion annihilation process [142] to avoid double counting. The contributions from quark matter phase dominates over its hadronic counter part for both the EoS for M beyond ϕ-peak. This fact may be used to extract various properties *i.e. average flow, temperature*

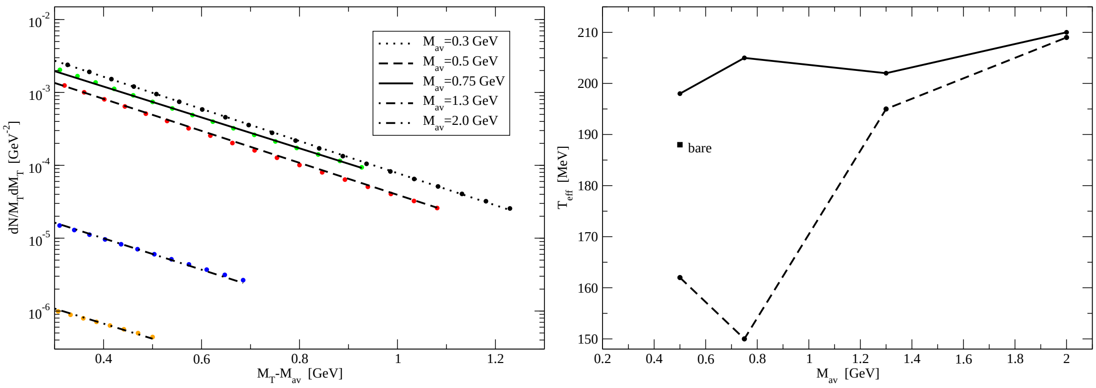

Figure 6.4: Left : the dilepton yield plotted against $M_T - M_{av}$ for different M windows for RHIC initial conditions. Right : corresponding T_{eff} for different values of the M-bins. The dashed line is obtained by setting $v_r = 0$.

etc. of quark matter and hadronic matter by selecting M windows judiciously. The dilepton yield from hadronic matter is observed to be larger when the HRG EoS is employed in comparison to LQCD. This can be understood in terms of the velocity of sound $v_s(= dP/d\epsilon$ evaluated at constant entropy) which controls the rate of expansion. For EoS of the type (a) $v_s \sim 1/3$ in the QGP phase which is larger than the value of the corresponding quantity for EoS of the type (b). Therefore, the rate of expansion in the scenario (b) is comparatively slower, allowing the QGP to emit lepton pairs for a longer time resulting in greater yield for LQCD EoS. In contrast, for the EoS (a), the lower value of v_s for the hadronic phase results in a slower cooling and hence a larger yield. Also shown for comparison is the yield from the decays of ρ mesons at the freeze-out for the two types of EoS used. The yield from this source is much smaller and we will not consider it any further.

Since the invariant mass spectra is invariant under flow we now turn to the $M_T(=\sqrt{p_T^2 + M_{\rm av}^2})$ spectra to study this aspect. The left panel of fig. 6.4 shows the M_T spectra of lepton pairs at RHIC energies. Here the differential yield is integrated over small bins of the pair invariant mass (from M_1 to M_2) and plotted against $M_T - M_{av}$ which is actually a measure of the kinetic energy (KE) of the pair, M_{av} being the average mass $(= [M_1 + M_2]/2)$ of the bin. The average value of M_T for a static system at a temperature T is given by $\langle M_T\rangle \sim M + T$. Therefore, the average KE $\sim T$, is the slope of the M_T distribution. Initially, the entire energy of the system formed in HIC is thermal in nature and with progress of time some part of the thermal energy gets converted to the collective (flow) energy. In other words, during the expansion stage the total energy of the system is shared by the thermal as well as the collective degrees of freedom. As a consequence, unlike the invariant mass spectra the M_T (or p_T) spectra is heavily influenced by the collective flow and the average KE or the inverse slope may be written as $T_{\rm eff} = T + 1/2M_{\rm av}v_r^2$, where v_r is the average radial flow velocity. The M_T spectra of dileptons for various M-bins have an exponential nature, the inverse slope providing an effective temperature $T_{\rm eff}$. It is important to mention at this point that for a radially expanding system the $T_{\rm eff}$ has an explicit (linear) M dependence as mentioned above. However, it has also an implicit M dependence even when $v_r = 0$ (*i.e.* with longitudinal expansion only) because it is expected that the high (low) M pairs predominantly emit from the high (low) temperature or early (late) time zone. For a radially expanding system the M dependence of inverse slope is stronger than for a system which expands longitudinally only.

In the right panel of Fig. (6.4) we have plotted the effective temperature versus M_{av} for various mass windows of the lepton pairs at RHIC energies, evaluated with the in-medium spectral function of the vector mesons. Also shown by a filled square is the value of $T_{\rm eff}$ for the vacuum case in the window $0.4 \leq M \leq 0.6$ where there is substantial difference between the yields in free and medium cases as seen in the left panel of Fig (6.3). The slope of these curves measure the average temperature and the flow of the matter.

Let us try to understand the non-monotonic variation of the inverse slope with $M_{\rm av}$ depicted in the right panel of Fig. (6.4). In the right panel of Fig. (6.3), it is shown that the high M (above ϕ peak) pairs originate predominantly from the partonic source and the low M (below ρ mass) domain, although outshine by the radiation from hadronic source, contains non-negligible contributions from quark matter *i.e.* the low M region contains contributions both from the hadronic as well as QGP phases. Now, the collectivity (or flow) in the system does not develop fully in the QGP because of the small life time of this phase which means that the radial velocity extracted from the high M region is small. Here the temperature decreases mainly due to longitudinal expansion and consequently, the effective slope decreases slowly with decreasing $M_{\rm av}$. In contrast, the lepton pairs with mass around ρ-peak almost totally originate from the hadronic source (which appears in the late stage of the evolving system) and are significantly affected by the flow resulting in higher values of v_r and hence a higher $T_{\rm eff}$. At still lower values of M, v_r cannot be as large despite the substantial medium induced enhancement of the hadronic sources since this domain also contains contribution from the QGP. For a hadronic source with vacuum properties the yield in this region in M will be entirely due to emission from quark matter and the value of v_r will be much lower. Thus the values of v_r for M below and above the ρ-peak are smaller compared to the values around the ρ peak even in the presence of medium effects, resulting in the non-monotonic behavior as displayed in the right panel of Fig. (6.4) for 0.5 $<$ M(GeV) $<$ 1.3.

The slope of the M_T spectra is connected with the average collective flow. It is well known that the average magnitude of radial flow at the freeze-out surface can be extracted from the p_T spectra of the hadrons. However, hadrons being strongly interacting objects can bring the information of the state of the system when it is too dilute to support collectivity *i.e.* the parameters of collectivity extracted from the hadronic spectra are limited to the evolution stage where the collectivity ceases to exist. These collective parameters have hardly any information about the interior of the matter. On the other hand the dileptons are produced and emitted from all space time points. Therefore, the value of v_r estimated from the dilepton spectra will be lower than the value extracted from the hadronic spectra [36]. Indeed, the values of v_r estimated from the slopes of the curve is 0.25 for the M domains $0.5 < M\,(\mathrm{GeV}) < 0.77$. This value is much smaller than the value of v_r extracted from the hadronic spectra [143]. The dashed line in the right panel of Fig. (6.4) is obtained by setting $v_r = 0$. The results indicate that the observed (solid line) rise (for $0.5 < M\,(\mathrm{GeV}) < 0.77$) and fall (for $0.77 < M\,(\mathrm{GeV}) < 1.3$) are due to radial expansion of the system. However, the rise in large M domain is due to cooling of the system due to longitudinal expansion - which is described as the implicit M dependence of $T_{\rm eff}$ above.

6.4.3 At LHC Energy

At LHC the measured values of dN^{ch}_{pp}/dy for $\sqrt{s_{\rm NN}}$ = 900 GeV, 2.36 TeV and 7 TeV are 3.02, 3.77 and 6.01 respectively [144]. The value dN^{ch}_{pp}/dy at $\sqrt{s_{\rm NN}}$ = 5.25 TeV is obtained by interpolating the above experimental data mentioned above. Assuming

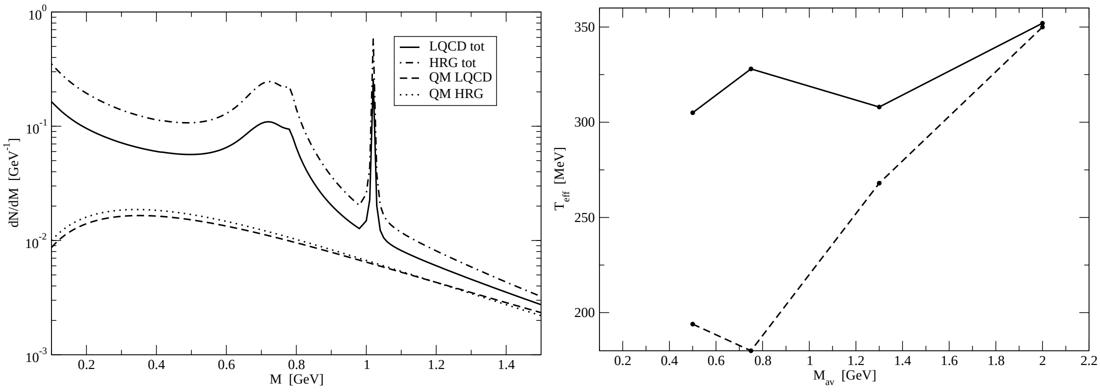

Figure 6.5: Left : QGP and total contribution for EoS (a) HRG (dotted and dash-dotted lines) and EoS (b) LQCD (dashed and solid lines) at LHC energy. Right : T_{eff} for different values of the M-bins for LHC conditions which are extracted from the corresponding M_T spectra. The dashed line is obtained by setting $v_r = 0$.

$x = 0.2$ in Eq. (6.21) we obtain $dN/dy = 2607$ in Pb+Pb collision for 0-10% centrality. For $\tau_i = 0.1$ fm/c we get $T_i = 756$ MeV.

The invariant mass spectra of lepton pairs is displayed for LHC initial conditions in Fig. (6.5). Although, the results are qualitatively similar to RHIC, quantitatively the yield at LHC is larger by an order of magnitude, primarily because of the large initial temperature. This enhancement is also seen in the transverse mass distributions of the lepton pairs at LHC.

Following the same procedure as done for RHIC energy, we have extracted the values of $T_{\rm eff}$ for different mass-bins from the corresponding M_T spectra. The values of $T_{\rm eff}$ for various M-bins are larger than RHIC because of the combined effects of large initial temperature and flow. In fact the value of v_r for $0.5 <$ M(GeV)< 0.77 is ~ 0.52. The radial flow in the system is responsible for the rise and fall of $T_{\rm eff}$ with $M_{\rm av}$ (solid line) in the mass region ($0.5 <$ M(GeV)< 1.3) because for $v_r = 0$ (dashed line) a completely different behavior is obtained. This type of non-monotonic variation of $T_{\rm eff}$ (or v_r) can not be obtained with a single dilepton source [145]. Therefore, such non-monotonic variation of the inverse slope deduced from the transverse mass distribution of lepton pairs with average invariant mass is an indication of the presence of two different phases during the evolution of the system. Thus, such variation may be treated as a signal of QGP formation in heavy ion collisions.

Chapter 7

The spectral function of nucleons

Heavy ion collisions provide an opportunity to investigate particle propagation through strongly interacting media. However, only the vector mesons, particularly the ρ, can at present be studied directly by detecting dileptons, into which they decay in the hot, dense media. The media created by these collisions consist, in general, not only of mesons, but also of nucleons. Thus the effects of both mesons and nucleons on the vector meson spectral functions have been extensively studied in the literature [37]. For a more complete picture, the self-energy of nucleon itself need be investigated [146, 147, 148, 149, 150, 151, 152]. The nucleon self-energy function also determines the equation of state of nuclear matter [153]. Here we have gone through a thermal field theoretical studies in real time formalism to see the in-medium properties of nucleon in hot and dense matter. We have evaluated one loop nucleon self-energy at finite temperature and baryon chemical potential (μ) where πN and $\pi\Delta$ are taken as intermediate states.

7.1 Formalism

7.1.1 Expression of spectral function

We are starting our discussion from the Dyson's equation to get the interaction picture. The Dyson's equation, followed by the diagonal part of Nucleon propagator at finite temperature, is given by

$$\overline{S} = \overline{S}_0 - \overline{S}_0\, \overline{\Sigma}\, \overline{S} \tag{7.1}$$

where $\overline{\Sigma}$, $\overline{S}_0$ are respectively the diagonal elements of the self-energy matrix and and the free propagator at finite temperature.

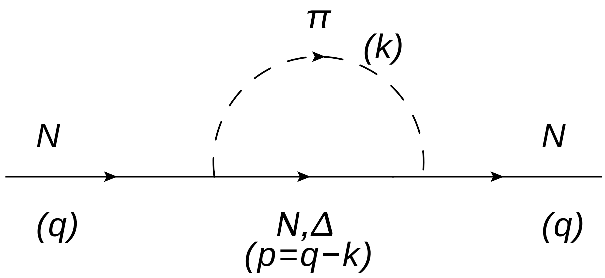

Figure 7.1: One-loop graphs for nucleon self-energy

The free propagator $\overline{S}_0$ turns out to be the same as in vacuum,

$$\overline{S}_0(p) = \frac{-(\not{p} + m_N)}{p^2 - m_N^2 + i\eta}. \tag{7.2}$$

The calculation simplifies if we take $\vec{q} = 0$. Also restricting to the anti-nucleon pole in Eq. (7.1), it becomes

$$\overline{S}_0(p_0) = \frac{(1+\gamma_0)}{2}\frac{-1}{p_0 - m_N + i\eta}. \tag{7.3}$$

Decomposing $\overline{\Sigma}$ and $\overline{S}$ in Dirac space,

$$\overline{\Sigma} \;=\; \Sigma_s + \gamma_0\Sigma_v\,, \qquad \overline{S} \;=\; S_s + \gamma_0 S_v\,, \tag{7.4}$$

it follows from Dyson equation that $S_s = S_v$. Then letting $\Sigma = \Sigma_s + \Sigma_v$, we get the complete propagator as

$$\overline{S}(p_0) = \frac{(1+\gamma_0)}{2}\frac{-1}{p_0 - m_N - \Sigma} \tag{7.5}$$

giving the spectral function

$$A_N(p_0) = \frac{-\mathrm{Im}\Sigma}{(p_0 - m_N - \mathrm{Re}\Sigma)^2 + (\mathrm{Im}\Sigma)^2} \tag{7.6}$$

7.1.2 Vertices of nucleon self-energy

The vertices appearing in Fig. (7.1) may be obtained from chiral perturbation theory [91, 154, 155]. The effective interaction Lagrangians are given by,

$$\begin{aligned}
\mathcal{L}_{\pi NN} &= -\frac{g_A}{2m_N}\overline{\psi}_{Na}\gamma_\mu\gamma_5(\vec{\tau}\cdot\partial^\mu\vec{\pi})^a_b\psi^b_N \\
&= -\frac{g_A}{2m_N}[\{\overline{p}\gamma_\mu\gamma_5 p\partial^\mu\pi_0 - \overline{n}\gamma_\mu\gamma_5 n\partial^\mu\pi_0\} + \sqrt{2}\{\overline{p}\gamma_\mu\gamma_5 n\partial^\mu\pi^+ + \overline{n}\gamma_\mu\gamma_5 p\partial^\mu\pi^-\}]
\end{aligned} \tag{7.7}$$

$$\begin{aligned}\mathcal{L}_{\pi N\Delta} &= \frac{g_\Delta}{\sqrt{2}}\overline{\psi}_{Na}(\vec{\tau}\cdot\partial^\mu\vec{\pi})^c_b\Delta^{abd}_\mu\epsilon_{cd} + h.c. \\ &= g_\Delta[\frac{2}{\sqrt{6}}\{\overline{p}\,\partial^\mu\pi^0\Delta^+_\mu + \overline{n}\,\partial^\mu\pi^0\Delta^0_\mu\} + \frac{1}{\sqrt{3}}\{\overline{p}\,\partial^\mu\pi^+\Delta^0_\mu - \overline{n}\,\partial^\mu\pi^-\Delta^+_\mu\} \\ &\quad - \{\overline{p}\,\partial^\mu\pi^-\Delta^{++}_\mu - \overline{n}\,\partial^\mu\pi^+\Delta^-_\mu\} + h.c.] \qquad (7.8)\end{aligned}$$

where the indices a, b, c, d take values 1 and 2 and $\epsilon_{12} = -\epsilon_{21} = 1$, etc.

A second term is required in $\mathcal{L}_{\pi N\Delta}$ to ensure a *pure* coupling to spin $\frac{3}{2}$ field [99]. In the imaginary part of the self-energy, where Δ is on mass shell, it does not contribute. But in the real part, it does, which, however, we ignore in our calculation. The coupling constants g_A and g_Δ are to be determined phenomenologically. As is well-known [151, 156], such a model requires form factors at the vertices, which we take in the Lorentz invariant form as

$$F(q,k) = \frac{\Lambda^2}{\Lambda^2 + (q\cdot k/m_N)^2 - k^2} \qquad (7.9)$$

where q and k are the four-momenta of nucleon and pion at the vertices and Λ is essentially a cut-off on these momenta. We first check this model with experimental data on πN scattering. The interaction (7.8) allows us to calculate the decay width of $\Delta \to N + \pi$ as a function of its energy as

$$\Gamma(E) = \frac{1}{24\pi}\left(\frac{g_\Delta}{F_\pi}\right)^2 F^2(E)|\vec{q}|^3\frac{(E+m_N)^2 - m_\pi^2}{E^2}. \qquad (7.10)$$

Here $\vec{q}$ is the three-momentum in the centre-of-mass of πN system,

$$\vec{q}^2 = \frac{\{E^2 - (m_N + m_\pi)^2\}\{E^2 - (m_N - m_\pi)^2\}}{4E^2}. \qquad (7.11)$$

In this kinematic configuration, the form factor becomes

$$F(|\vec{q}|) = \frac{\Lambda^2}{\Lambda^2 + (|\vec{q}|E/m_N)^2}. \qquad (7.12)$$

The pion-nucleon partial wave f in the P_{33} channel may now be written in the form

$$f(E) \sim \frac{1}{E^2 - m_\Delta^2 + im_\Delta\Gamma(E)}. \qquad (7.13)$$

We take the resonance parameters at the pole position, $m_\Delta = 1210$ MeV and $\Gamma(m_\Delta) =$ 100 MeV [157]. Taking $g_\Delta = 2.2$ and $\Lambda = 400$ MeV [156], we can satisfy Eq. (7.10) and also achieve reasonable agreement of the phase shift δ_{33} computed from Eq. (7.13) with experiment [158] (left panel of Fig. 7.3). Also we take $g_A = 1.26$ [66] and the same form factor at the πNN vertex.

7.1.3 Expression of self-energy

We now evaluate the self-energy matrices from graphs of Fig (7.1). We don't start from 11-component since a general form of fermion self-energy at finite temperature has been already evaluated in Chapter 3 (see the Section 3.2.2). Now simply adding the imaginary and real parts we get the diagonal element of fermion self-energy at finite temperature and is given by [1]

$$\begin{aligned}\overline{\Sigma}(q) &= \int \frac{d^3k}{(2\pi)^3}\frac{1}{4\omega_k\omega_p}\Big[\frac{(1+n_+^k)L_1 - n_+^p L_3}{q_0-\omega_k-\omega_p+i\eta\epsilon(q_0)} + \frac{-n_+^k L_1 - n_-^p L_4}{q_0-\omega_k+\omega_p+i\eta\epsilon(q_0)} \\ &\quad + \frac{n_-^k L_2 + n_+^p L_3}{q_0+\omega_k-\omega_p+i\eta\epsilon(q_0)} + \frac{-n_-^k L_2 + (-1+n_-^p)L_4}{q_0+\omega_k+\omega_p+i\eta\epsilon(q_0)}\Big]. \qquad (7.14)\end{aligned}$$

In terms of the quantities defined for nucleon self-energy with πB loops, We have to make following replacement

$$\begin{aligned}&\omega_k\ (m_k) \to\ \omega_\pi\ (m_\pi) && \omega_p\ (m_p) \to\ \omega_B\ (m_B) \\ &n_\pm^k \to\ n(\omega_\pi) = \frac{1}{e^{\beta\omega_\pi}-1} && n_\pm^p \to\ n_\pm(\omega_B) = \frac{1}{e^{(\beta\omega_B\mp\mu)}+1}. \qquad (7.15)\end{aligned}$$

In the following we restrict our evaluation to $\vec{q}=0$. In the absence of angular dependence, we get an analytic expression for the imaginary part which gives a physical (or real) value only in the branch cut regions of q_0-axis. With $\vec{q}=0$, the value of $|\vec{k}|$, fixed by the δ-functions contained in the imaginary part (given in Eq. 3.34), is the magnitude of three-momentum in the center-of-mass of the pion-baryon system,

$$|\vec{k}|^2 = \frac{\{p_0^2-(m_B+m_\pi)^2\}\{p_0^2-(m_B-m_\pi)^2\}}{4p_0^2}. \qquad (7.16)$$

In this frame, the form factor (7.12) simplifies to

$$F(|\vec{k}|) = \frac{\Lambda^2}{\Lambda^2+\vec{k}^2}. \qquad (7.17)$$

So in this static assumption, the regions $q_0 \geq (m_B+m_\pi)$ and $q_0 \leq -(m_B+m_\pi)$ define the unitary cuts of nucleon self-energy and the region, $-(m_B+m_\pi) \leq q_0 \leq (m_B+m_\pi)$ defines the Landau cuts. Let us define the variables,

$$\overline{\omega}_\pi = \frac{q_0^2+m_\pi^2-m_B^2}{2q_0}, \qquad \overline{\omega}_B = \frac{q_0^2-m_\pi^2+m_B^2}{2q_0} \qquad (7.18)$$

[1] We have renamed the fermion self-energy as $\overline{\Sigma}$

which actually coincide respectively with ω_π and ω_B on all the cuts. Then the imaginary parts of $\overline{\Sigma}$ for $p_0 \geq 0$ are given by

$$\mathrm{Im}\overline{\Sigma}(p_0) = -\frac{|\vec{k}|}{8\pi q_0}\begin{cases} L(k_0=\overline{\omega}_\pi)\{1+n(\overline{\omega}_\pi)-n_+(\overline{\omega}_B)\}\,, & \text{on unitary cut} \\ L(k_0=\overline{\omega}_\pi)\{n(|\overline{\omega}_\pi|)+n_+(\overline{\omega}_B)\}\,, & \text{on Landau cut.} \end{cases} \tag{7.19}$$

The real part of nucleon self-energy also simplifies for $\vec{q}=0$ to

$$\mathrm{Re}\overline{\Sigma}(p_0) = -\frac{1}{16\pi^2 p_0}P\int_{m_\pi^2}^{\infty}\frac{d\omega_\pi^2\sqrt{\omega_\pi^2-m_\pi^2}\,h(\omega_\pi)}{\omega_\pi\omega_B(\omega_\pi^2-\overline{\omega}_\pi^2)} \tag{7.20}$$

where

$$h(\omega_\pi) = \omega_B\{(\omega_\pi+\overline{\omega}_\pi)L_1-(\omega_\pi-\overline{\omega}_\pi)L_2\}n(\omega_\pi)-\omega_\pi\{(\omega_B+\overline{\omega}_B)L_3n_+(\omega_\pi)-(\omega_B-\overline{\omega}_B)L_4n_-(\omega_\pi)\}. \tag{7.21}$$

Having carried out the evaluation in terms of the (Dirac) matrix-function $L(p,k)$, it remains to write its explicit expressions for the two loops,

$$L(q,k) = \frac{3}{4}\left(\frac{g_A}{F_\pi}\right)^2 F^2(q,k)\{2k\cdot q\not{k}-k^2(\not{q}+\not{k}+m_N)\}\,, \qquad (\pi N\,\text{loop}) \tag{7.22}$$

$$L(q,k) = \frac{4}{3}\left(\frac{g_\Delta}{F_\pi}\right)^2 F^2(q,k)\left\{-k^2+\frac{(q\cdot k-k^2)^2}{m_\Delta^2}\right\}(\not{q}-\not{k}+m_\Delta), \qquad (\pi\Delta\,\text{loop}). \tag{7.23}$$

The fermionic structure of the nucleon self-energy is explicitly reflected in the expression of $L(q,k)$ though we have not explicitly displayed the Dirac indices for notational simplicity. Adding the self-energy coefficients of unity (I) and zeroth component of gamma matrices (γ^0) we get the total self-energy, previously defined as Σ.

A question arises in such calculations, whether a non-relativistic approximation could reproduce the relativistic results in a quantitative way [97]. To define this approximation, we rewrite $E^{11}(q_0,\vec{q})$, the spin-independent factor in the 11-component of baryon propagator as

$$E^{11}(q_0,\vec{q}) = \frac{-1}{2\omega_B}\left\{\frac{1-n_+(\omega_B)}{q_0-\omega_B+i\epsilon}+\frac{n_+(\omega_B)}{q_0-\omega_B-i\epsilon}-\left(\frac{1-n_-(\omega_B)}{q_0+\omega_B-i\epsilon}-\frac{n_-(\omega_B)}{q_0+\omega_B+i\epsilon}\right)\right\}. \tag{7.24}$$

The non-relativistic approximation to this propagator consists in retaining only the first two terms above [159, 160]. Further we set $\omega_B = m_B$ everywhere for baryon [2]. Note that we approximate neither the propagator $D^{11}(k)$ for pion nor its energy-momentum relation.

[2]One also approximates $\omega_B = m_B + (\vec{p}-\vec{k})^2/2m_B$, but it may lead to problems at higher momenta [159].

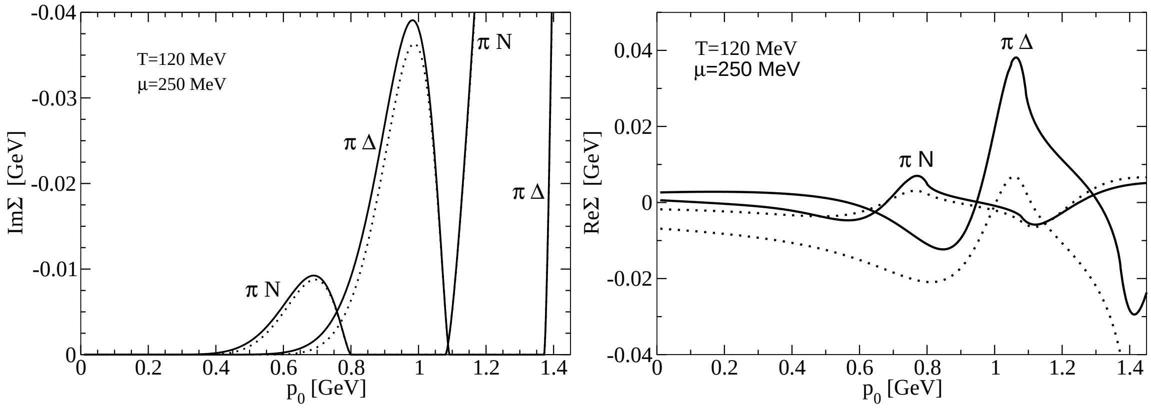

Figure 7.2: Imaginary (left panel) and real (right panel) parts of self-energy from πN and $\pi\Delta$ loops. Solid curves represent the results of our calculation (relativistic, including unitary cuts). Dotted curves result from non-relativistic approximation.

7.2 Results

Fig. (7.2) compares the typical behavior of relativistic results with the non-relativistic ones for the imaginary and real parts of self-energy, separately for the two loops – we see that only the real part for $\pi\Delta$ loop differ significantly between the two. Using the imaginary part of self-energy for relativistic and non-relativistic both cases we have constructed phase shift Δ_{33} for P_{33} partial wave in πN scattering where two parameters, g_Δ and Λ provide us a freedom to fit our calculated values with experimentally observed values [158]. Interestingly we have got a common values of two parameters for both cases as shown in left panel of Fig. (7.3). In the right panel of Fig. (7.3) we compare a typical spectral function of our calculation with its non-relativistic limit.

Having made these comparisons, we come back to our model in Fig. (7.4) to draw the nucleon spectral function at different values of T and μ, which are realized in heavy-ion collisions [161, 162]. As expected, the height of the peak decreases with rise of temperature, while it remains about the same within the interval of chemical potential considered here [77]. We also compare our results with two earlier calculations. Leutwyler and Smilga [146] use virial expansion to leading order to obtain the self-energy for *on-shell* nucleon in pionic medium. In Fig. (7.5) we compare their results for the imaginary and real parts with those from our model, setting anti-particle distribution functions to zero. The good agreement shows that our model is realistic, if we recall that they evaluate the virial formula with *experimental data* on πN scattering. To conclude, we calculate

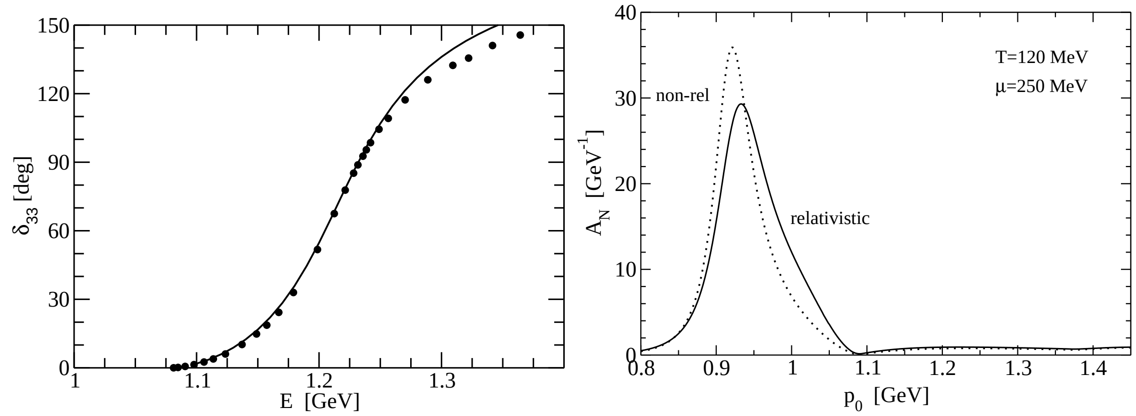

Figure 7.3: Left panel shows the phase shift for P_{33} partial wave in πN scattering from our model compared with experiment [158](solid circles). Comparison of relativistic spectral function (continuous curve) with its non-relativistic limit (dotted curve) is shown in right panel.

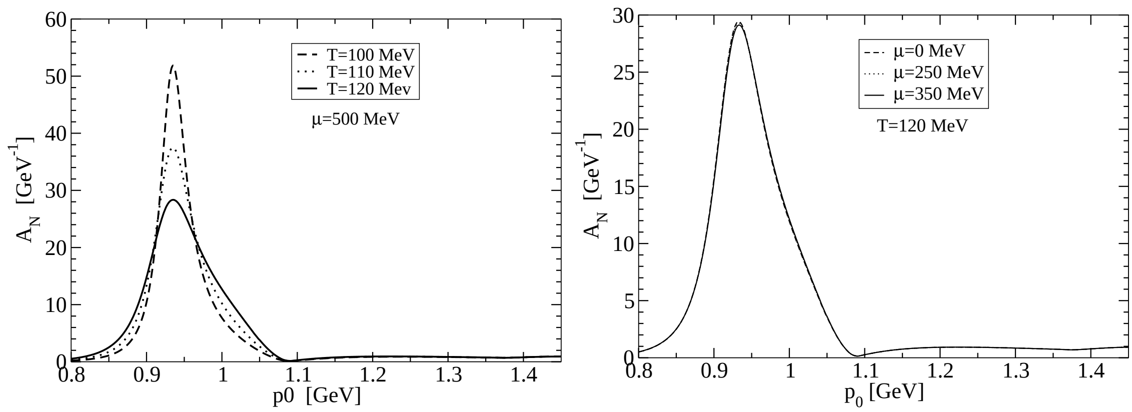

Figure 7.4: Nucleon spectral function at different temperatures for a fixed chemical potential (left panel) and at different chemical potentials for a fixed temperature (right panel)

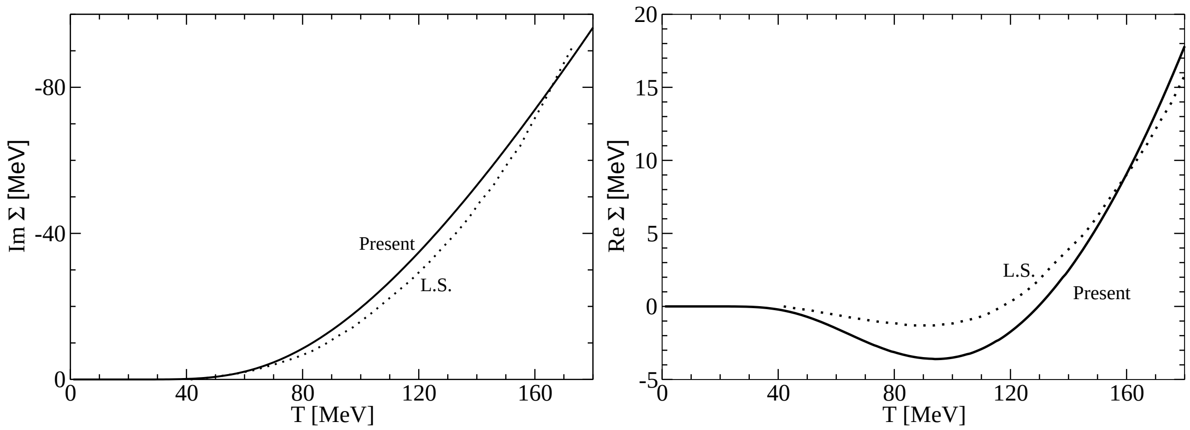

Figure 7.5: The present evaluation of on-shell imaginary (left panel) and the real (right panel) parts of self-energy in pion medium (continuous curve) compared with those of Ref. [146] (dotted curve.)

the self-energy of the nucleon and its spectral function in the real time version of the thermal field theory in the relativistic framework. The imaginary part of the self-energy is built out of contributions from both Landau and unitary cuts from one loop graphs with πN and $\pi\Delta$ intermediate states. In contrast to results in the literature, we find the unitary cut from the $\pi\Delta$ loop to contribute significantly in the upper region of (virtual) mass of nucleon considered. The nucleon spectral function turns out to be sensitive to non-relativistic approximation, establishing the necessity of relativistic treatment for its quantitative determination.

Chapter 8

Heavy-light mesons in hadronic matter

The future CBM experiment of the FAIR project at GSI will provide an opportunity to investigate strongly interacting matter at high baryon density. In particular, the research program will be focused on obtaining the in-medium modifications of hadrons in the charm sector by the annihilation of antiprotons on nuclei as well as heavy ion collisions. The charm hadrons in dense matter will also be investigated in the scattering of electrons off nuclei at Jlab. In-medium modification of open charm mesons (D, $\overline{D}$, D^*, $\overline{D}^*$) are expected to exhibit several interesting features in dense matter like open charm enhancement [163] as well as the possibility of D-mesic nuclei formation. Besides the open charm meson, hidden charm mesons (η_c,J/ψ and higher excited states) also provide the opportunity to investigate the gluon condensate at very high temperature and density [164, 165]. Several theoretical efforts [166, 167, 168, 169, 170] have predicted a larger mass drop of open-charm mesons than that of J/ψ which may help to explain the J/ψ suppression in a hadronic environment although a width enhancement with negligible mass shift of open charm mesons have also been suggested in order to explain the suppression [171]. In view of many interesting and open issues in the charm sector, the modification of the open and hidden charm mesons in a hot and dense environment has become an important issue in recent times. Here also we have used the same thermal field theoretical approaches to investigate the spectral properties of open charm mesons (D and D^*). This in-medium modification of open charm mesons provides a new domain of off-mass shell to open the $D\overline{D}$ type decay channel of charmonium states which is related with J/ψ dissociation in hadronic matter.

8.1 Spectral properties of open charm mesons in hot hadronic matter

Figure 8.1: One-loop graph for two point function contributing to D meson self energy and Φ stands for π, η and K mesons

Let us start with D (D^*) meson self-energy where light pseudoscalar meson Φ and heavy meson D^* (D) are internal lines of the one-loop diagram. Here Φ denote the pseudoscalar octet i.e. π^+, π^0, π^-, K^+, K^-, K^0, $\overline{K}^0$ and η. For any charge state of D (D^*) there are four possible loops. e.g. for D^+ (D^{*+}) meson self-energy, $\pi^+ D^{*0}$, $\pi^0 D^{*+}$, ηD^{*+} and $\overline{K}^0 D_s^{*+}$ ($\pi^+ D^0$, $\pi^0 D^+$, ηD^+ and $K^0 D_s^+$) are the possible loops. Recalling the boson self-energy expression for boson-boson loop (Sec. 3.2.1), we have

$$\overline{\Pi}(q) = \int \frac{d^3k}{(2\pi)^3} \frac{1}{4\omega_k \omega_p} [\frac{(1+n^k)L_1 + n^p L_3}{q_0 - \omega_k - \omega_p + i\eta\epsilon(q_0)} + \frac{-n^k L_1 + n^p L_4}{q_0 - \omega_k + \omega_p + i\eta\epsilon(q_0)} \\ + \frac{n^k L_2 - n^p L_3}{q_0 + \omega_k - \omega_p + i\eta\epsilon(q_0)} + \frac{-n^k L_2 + (-1-n^p) L_4}{q_0 + \omega_k + \omega_p + i\eta\epsilon(q_0)}]. \tag{8.1}$$

The vertices appearing in the calculation of one-loop self-energy may be obtained using chiral perturbation theory. The appropriate field variable for the pseudoscalar octet (Nambu Goldstone fields) representing pions,kaons and η may be described by unitary matrix $u = \exp(\frac{i\lambda_a \Phi_a}{2F_0})$, where,

$$\lambda_a \Phi_a = \sqrt{2} \begin{pmatrix} \frac{\pi^0}{\sqrt{2}} + \frac{\eta}{\sqrt{6}} & \pi^+ & K^+ \\ \pi^- & -\frac{\pi^0}{\sqrt{2}} + \frac{\eta}{\sqrt{6}} & K^0 \\ K^- & \bar{K}^0 & -\frac{2}{\sqrt{6}}\eta \end{pmatrix}, \tag{8.2}$$

and F_0 is Nambu Goldstone Boson decay constant in chiral limit. The lowest order chiral Lagrangian for the heavy-light pseudoscalar and vector meson is,

$$\mathcal{L} = \langle \mathcal{D}_\mu P \mathcal{D}^\mu P^\dagger \rangle + i \frac{g}{F_0} \langle P_\mu^* u^\mu P^\dagger - P u^\mu P_\mu^{*\dagger} \rangle + ... \tag{8.3}$$

where $P = (D^0, D^+, D_s^+)$ and $P_\mu^* = (D^{*0}, D^{*+}, D_s^{*+})_\mu$ are the triplets of D and D^* meson fields and,

$$u_\mu = i(u^\dagger \partial_\mu u - u \partial_\mu u^\dagger) \tag{8.4}$$

.

The covariant derivatives are given by,

$$\mathcal{D}_\mu P_a = \partial_\mu P_a - \Gamma_\mu^{ba} P_b \quad , \quad \mathcal{D}^\mu P_a^\dagger = \partial^\mu P_a^\dagger + \Gamma_{ab}^\mu P_b^\dagger$$
$$\text{with } \Gamma_\mu = \frac{1}{2}(u^\dagger \partial_\mu u + u \partial_\mu u^\dagger) \tag{8.5}$$

where a,b denote SU(3) flavor index. The numerical value of the coupling constant g is fixed by reproducing the $D^{*+} \to D^0\pi^+$ decay width [172]. To lowest order in Φ the vector and axial-vector currents are

$$\Gamma_\mu = \frac{1}{8F_\pi^2}[\Phi, \partial_\mu \Phi], \qquad u_\mu = -\frac{1}{F_\pi}\partial_\mu \Phi \ . \tag{8.6}$$

Using these lowest order part we get the interaction Lagrangian for $P^*P\Phi$ and $P\Phi P\Phi$ vertices as given below

$\mathcal{L}_{int}^{LO} = \mathcal{L}_{P^*P\Phi} + \mathcal{L}_{P\Phi P\Phi}$,where

$$\mathcal{L}_{P^*P\Phi} = -i\frac{g}{F_0}\langle P_\mu^* \partial^\mu \Phi P^\dagger - P \partial^\mu \Phi P_\mu^{*\dagger} \rangle \tag{8.7}$$

$$\mathcal{L}_{P\Phi P\Phi} = \frac{1}{8F_\pi^2}\langle \partial_\mu P[\Phi, \partial^\mu \Phi] P^\dagger - P[\Phi, \partial^\mu \Phi] \partial_\mu P^\dagger \rangle \tag{8.8}$$

This $\mathcal{L}_{P\Phi P\Phi}$ part which gives seagull graph shown in right side of Fig. (8.1), arises from the Lagrangian (8.8). The other one-loop self energy graph shown in left side of Fig. (8.1) is coming from the $\mathcal{L}_{P^*P\Phi}$ (8.7). The required part of Lagrangian from Eq. (8.7) and Eq. (8.8) to calculate the self-energy of D^+ are given by

$$\begin{aligned}
\mathcal{L}_{D^+P^*\Phi} = -i\frac{g}{F_0}[&\sqrt{2}(D^+\partial^\mu \pi^- \overline{D}_\mu^{*0} - D^-\partial^\mu \pi^+ D_\mu^{*0}) \\
&+ (D^-\partial^\mu \pi^0 D_\mu^{*+} - D^+\partial^\mu \pi^0 D_\mu^{*-}) \\
&+ \frac{1}{\sqrt{3}}(D^+\partial^\mu \eta D_\mu^{*-} - D^-\partial^\mu \eta D_\mu^{*+}) \\
&+ \sqrt{2}(D^+\partial^\mu K^0 D_{s\mu}^{*-} - D^+\partial^\mu \overline{K}^0 D_{s\mu}^{*+})]
\end{aligned} \tag{8.9}$$

$$\begin{aligned}
&\mathcal{L}_{D^+\Phi D^+\Phi} = \frac{-1}{F_0^2}[(D^+\partial_\mu \pi^+ \partial^\mu D^- \pi^- \\
&-\partial^\mu D^+ \partial_\mu \pi^+ D^- \pi^- + \partial^\mu D^+ \pi^+ D^- \partial_\mu \pi^- \\
&-D^+\pi^+\partial^\mu D^- \partial_\mu \pi^-) + (D^+\partial_\mu \overline{K}^0 \partial^\mu D^- K^0 \\
&-\partial^\mu D^+ \partial_\mu \overline{K}^0 D^- K^0 + \partial^\mu D^+ \overline{K}^0 D^- \partial_\mu K^0 \\
&-D^+\overline{K}^0 \partial^\mu D^- \partial_\mu K^0)]
\end{aligned} \tag{8.10}$$

However, the contribution of the seagull graph vanishes because the integrand is an odd function of momentum (k). So we have to concentrate on the other graph, whose vertices can be obtained from (8.9). The $L(q,k)$'s for all loops have same form only differing by their different normalization factor α attached with the coupling g in Eq. (8.9). So the form of $L(q,k)$ ($L^{\mu\nu}(q,k)$) in the expression of D (D^*) meson self energy is given by

$$\begin{aligned} L(k,q) &= -\alpha^2(\frac{g}{F_0})^2[k^2 - \frac{(k\cdot q - k^2)^2}{m_p^2}] \\ (L^{\mu\nu}(k,q) &= -\alpha^2(\frac{g}{F_0})^2[k^\mu k^\nu]) \end{aligned} \tag{8.11}$$

where $\alpha = \sqrt{2}, 1, \sqrt{2}, \frac{1}{\sqrt{3}}$ for $\pi^+ D^{*0}(D^0)$, $\pi^0 D^{*+}(D^+)$, $K^0 D_s^{*+}(D_s^+)$ and $\eta D^{*+}(D^+)$ loops respectively and m_p in Eq. (8.11) is the mass of D^* meson.

We have evaluated the self energies as a function of $\sqrt{q^2} = M$ at fixed values of the three-momentum $\vec{q}$ and temperature T. It thus suffices to calculate the self-energies in the time-like region, for positive values of q_0 starting from $q_0 = |\vec{q}|$.

The left (right) panel of Fig (8.2) show the imaginary and real parts of D (D^*) mesons. The thermal contribution to the imaginary part leads to an enhancement in the width and that of the real part produces a shift in the pole position. From the upper panel of both curves, we can see a clear distinction between the two branches of $\Pi(q^0,\vec{q})$. One observes a region in between the Landau and unitary cuts, where the imaginary part of the self-energy is exactly zero. We also see a negligible in-medium mass shift from the lower panels of these figures.

The spectral modification of the D and D^* mesons which comes from the Landau cut is basically a result of collisional broadening, which can lead to a substantial contribution to J/ψ suppression through its dissociation in hadronic matter. The J/ψ can in fact decay sub-threshold into the $D\overline{D}$ and $D^*\overline{D}$ channels, resulting in a finite dissociation width in these otherwise closed modes. By folding the spectral function of the D and D^* mesons, J/ψ decay rate in medium can be obtained from the equation [173]

$$\begin{aligned} \Gamma_{med}(J/\psi \to D\overline{D}) = \int \frac{g^2_{\psi D\overline{D}}}{3\pi m^2_{J\psi}} |\vec{P}^{cm}(m^2_{J\psi}, p^2_D, p^2_{\overline{D}})|^3 \\ \times \mathrm{Im}G_D(p^0_D,\ \vec{p}_D)\ \ \mathrm{Im}G_{\overline{D}}(p^0_{\overline{D}},\ \vec{p}_{\overline{D}})\ \ dp^2_D\ \ dp^2_{\overline{D}} \end{aligned} \tag{8.12}$$

where the $\vec{P}^{cm}$ is center of mass momentum for decay of J/ψ meson to D and $\overline{D}$ mesons with masses $p_D = \sqrt{(p^0_D)^2 - (\vec{p}_D)^2}$ and $p_{\overline{D}} = \sqrt{(p^0_{\overline{D}})^2 - (\vec{p}_{\overline{D}})^2}$. For the other channels

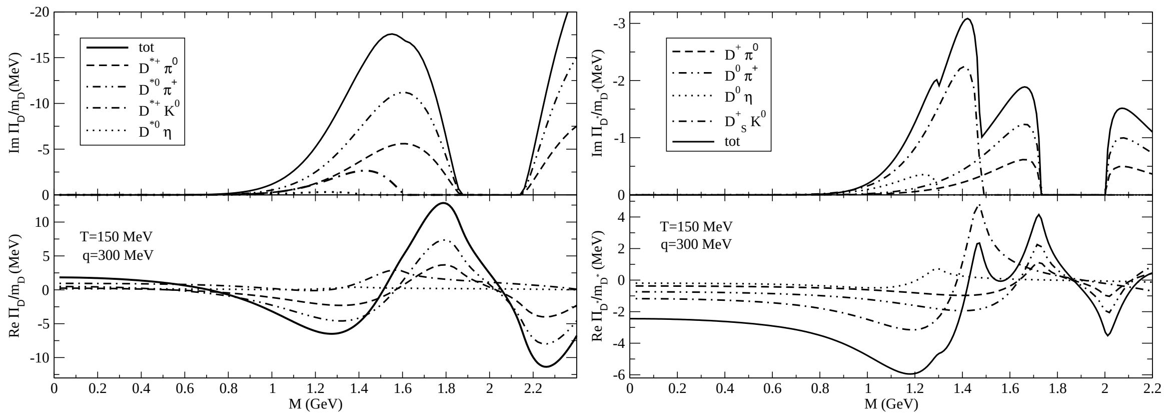

Figure 8.2: Left : Imaginary and real part of self-energy of D for different $D^*\Phi$ loops in the upper and lower panel respectively. Right : Corresponding quantities of D^* for different $D\Phi$ loops

$D^*\overline{D}$, $D\overline{D}^*$ and $D^*\overline{D}^*$ we have to replace corresponding in-medium spectral functions. We have taken the value of $g_{\psi D\overline{D}} = 7.8$ for all channels [173].

The variation of J/ψ rate in $D\overline{D}$ and $D^*\overline{D}$ channels with temperature is shown in Fig. (8.3). This estimate compares well with existing results in the literature [173] .

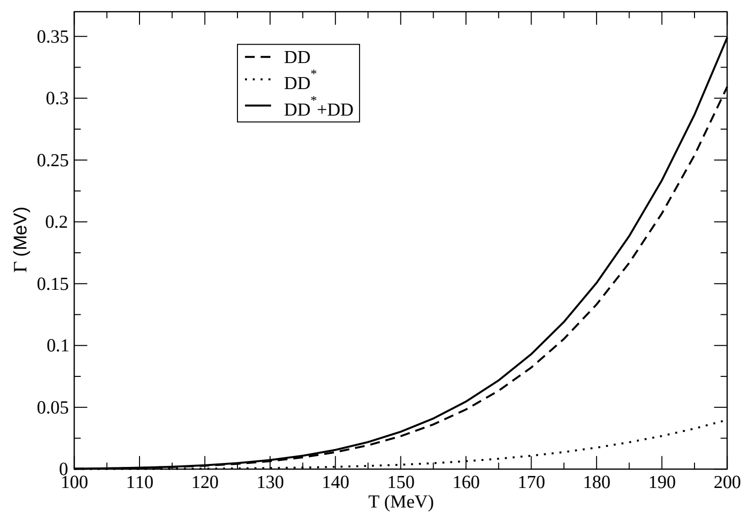

Figure 8.3: In medium collision rate vs temperature for J/ψ for $D\overline{D}$ (dashed line), $D^*\overline{D}$ (dotted line) channels and their summation (solid line).In dotted line $D^*\overline{D}$ and $D\overline{D}$ both channels are taken.

8.2 Transport properties of Heavy-light mesons in hot hadronic matter

Besides thermal spectral properties, transport properties of heavy-light mesons play an important role to characterize the medium formed in heavy ion collisions.

Let us imagine the scenario of pollen grains in water. The water molecules provide an equilibrated background in which the pollen grains execute Brownian motion. We consider a non-equilibrated heavy meson (D) executing Brownian motion in the hadronic medium of thermalized light mesons (π, K, η). The Fokker-Planck (FP) equation provides an appropriate framework for such processes. To arrive at the FP equation, let us starts from the Boltzmann transport equation

$$\left[\frac{\partial}{\partial t} + \frac{\vec{p}}{E}.\vec{\nabla}_x + \vec{F}.\vec{\nabla}_p\right] f(\vec{x}, \vec{p}, t) = \left[\frac{\partial f}{\partial t}\right]_{col} \tag{8.13}$$

where $\vec{p}$ and E denote momentum and energy, $\vec{\nabla}_x$ ($\vec{\nabla}_p$) are spatial (momentum space) gradient and $f(\vec{x}, \vec{p}, t)$ is the phase space distribution (in the present case f stands for heavy meson distribution). $\vec{F}$ represents external forces acting on the heavy mesons and here we ignore its effect *i.e.* $\vec{F} = 0$. Further assuming that the matter is uniform, that is, that the distribution functions of light particles appearing in the right-hand side of Eq. (8.13) are x independent, we can average (8.13) over x. Defining

$$f(\vec{p}, t) = \frac{1}{V}\int d^3\vec{x} f(\vec{x}, \vec{p}, t) \tag{8.14}$$

which is the normalized probability distribution in momentum space, we have

$$\frac{\partial f}{\partial t} = \left[\frac{\partial f}{\partial t}\right]_{\text{col}} \tag{8.15}$$

If we define $\omega(\vec{p}, \vec{k})$, the rate of collisions which change the momentum of the heavy meson from $\vec{p}$ to $\vec{p} - \vec{k}$, then we have [174]

$$\left[\frac{\partial f}{\partial t}\right]_{col} = \int d^3\vec{k}\left[\omega(\vec{p} + \vec{k}, \vec{k}) f(\vec{p} + \vec{k}) - \omega(\vec{p}, \vec{k}) f(\vec{p})\right] \tag{8.16}$$

The first term in the integrand represents gain of probability through collisions which knock the heavy meson into the volume element of momentum space at $\vec{p}$, and the second term represents loss out of that element. If we expand $\omega(\vec{p} + \vec{k}, \vec{k}) f(\vec{p} + \vec{k})$ around $\vec{k}$,

$$\omega(\vec{p} + \vec{k}, \vec{k}) f(\vec{p} + \vec{k}) \approx \omega(\vec{p}, \vec{k}) f(\vec{p}) + k_i \frac{\partial}{\partial p_i}(\omega f) + \frac{1}{2} k_i k_j \frac{\partial^2}{\partial p_i \partial p_j}(\omega f) \tag{8.17}$$

and substitute in Eq. (8.16), we get:

$$\left[\frac{\partial f}{\partial t}\right]_{col} = \frac{\partial}{\partial p_i}\left[A_i(\vec{p})f + \frac{\partial}{\partial p_j}[B_{ij}(\vec{p})f]\right] \tag{8.18}$$

where we have defined the kernels

$$\begin{aligned} A_i &= \int d^3\vec{k}\omega(\vec{p},\vec{k})k_i \\ B_{ij} &= \int d^3\vec{k}\omega(\vec{p},\vec{k})k_ik_j. \end{aligned} \tag{8.19}$$

for $\mid \vec{p} \mid \to 0$, $A_i \to \gamma p_i$ and $B_{ij} \to D\delta_{ij}$ where γ and D stand for drag and diffusion coefficients respectively. The function $\omega(\vec{p},\vec{k})$ is given by

$$\omega(\vec{p},\vec{k}) = g_\Phi \int \frac{d^3\vec{q}}{(2\pi)^3}\hat{f}(q)v\sigma_{p,q\to p',q'} \tag{8.20}$$

where $\hat{f}$ is the equilibrium distribution function of light particles, v is the relative velocity between the two collision partners, and g_Φ is the degeneracy of thermalized light particles. The cross section of $D\Phi$ scattering (where Φ denotes the light particles of the medium) can be expressed in terms of matrix element $M_{D\Phi}$ as

$$\sigma_{p,q\to p',q'} = \frac{1}{(2\pi)^6\ v\ 2E_q 2E_p g_D g_\Phi}\sum |M_{D\Phi}|^2 \frac{1}{2E_{q'}2E_{p'}}(2\pi)^4\delta(E_p+E_q-E_{q'}-E_{p'}) \tag{8.21}$$

So using Eq. (8.21) and (8.20) in (8.19), the drag may be defined as the thermal average of the momentum transfer weighted by the square of the invariant transition amplitude ,

$$\begin{aligned} A_i = \frac{1}{2E_p}\int \frac{d^3\vec{q}}{(2\pi)^3E_q}\int \frac{d^3\vec{p}\,'}{(2\pi)^3E_{p'}}\int \frac{d^3\vec{q}\,'}{(2\pi)^3E_{q'}} \\ \frac{1}{g_D}\sum |M|^2\,(2\pi)^4\delta^4(p+q-p'-q')\hat{f}(q)[(p-p')] \\ \equiv \langle\langle (p-p')\rangle\rangle \end{aligned} \tag{8.22}$$

where g_D is the degeneracy factor of the heavy meson. The temperature dependence of the drag coefficient enter through the phase space distribution.

Similarly the diffusion coefficients is a measure of the thermal average of the square momentum transfer, weighted by the interaction through the square of the invariant amplitude, $\overline{\mid M \mid^2}$,

$$B_{ij} = \langle\langle (p-p')_i(p-p')_j\rangle\rangle \tag{8.23}$$

with the scalar function

$$B_{ij} = \frac{1}{4}\left[\langle\langle p'^2\rangle\rangle - \frac{\langle\langle(p.p')^2\rangle\rangle}{p^2}\right] \tag{8.24}$$

Using the effective Lagrangian (8.3), we have evaluated the transport coefficients, namely the drag and diffusion co-efficients of a hot hadronic medium consist of pions, kaons and eta where heavy-light mesons are treated as a probe. Let us first discuss the drag and diffusion coefficients of D^+ meson. The relevant diagrams to calculate the Born amplitude are shown in Fig. (8.4). Here the first part of Lagrangian (8.3) *i.e.* Lagrangian (8.10) become important for giving the non-zero matrix element of contact diagrams (right most diagram of Fig. 8.4). In terms of Mandelstam variables (s, t, u)

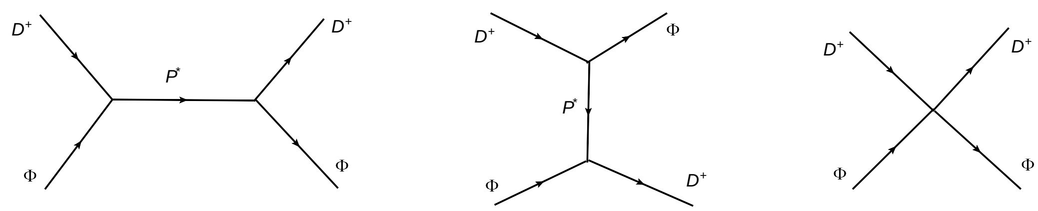

Figure 8.4: Feynman diagrams for the scattering of D mesons with pseudoscalar mesons Φ (pion, kaon and eta) in the medium. Here P^* denotes charmed vector meson resonances.

these matrix elements in the charge state basis are given below

$$\begin{aligned}
M_{D^+\pi^+} &= -M_{D^+\pi^-} = -\frac{1}{4F_0^2}(s-u)\\
M_{D^+\pi^0} &= M_{D^+\eta} = M_{D^+K^+} = M_{D^+K^-} = 0\\
M_{D^+\overline{K}^0} &= -M_{D^+K^0} = -\frac{1}{4F_0^2}(s-u)
\end{aligned} \tag{8.25}$$

From the interaction Lagrangian $\mathcal{L}_{D^+P^*\Phi}$ (8.9), we get the exchange diagrams of s and t channels exhibiting D^+ elastic scattering from the pseudoscalar mesons, Φ $(D^+(p_1) + \Phi(p_2) \rightarrow D^+(p_3) + \Phi(p_4))$. These invariant amplitudes in charge basis are as follows

$$\begin{aligned}
M_{D^+\pi^+} &= \frac{2g^2}{F_0^2}\frac{\{p_1\cdot p_4 - (p_1\cdot p_3 - m_\pi^2)^2/m_{D^*}^2\}}{t - m_{D^*}^2}\\
M_{D^+\pi^-} &= \frac{2g^2}{F_0^2}\frac{\{p_1\cdot p_3 - (p_1\cdot p_2 + m_\pi^2)^2/m_{D^*}^2\}}{s - m_{D^*}^2}\\
M_{D^+\pi^0} &= \left(\frac{g^2}{F_0^2}\right)^2 [\frac{\{p_1\cdot p_3 - (p_1\cdot p_2 + m_\pi^2)^2/m_{D^*}^2\}}{s - m_{D^*}^2}
\end{aligned}$$

$$
\begin{aligned}
&\quad + \frac{\{p_1 \cdot p_4 - (p_1 \cdot p_3 - m_\pi^2)^2/m_{D^*}^2\}}{t - m_{D^*}^2}] \\
M_{D^+\eta} &= \left(\frac{g^2}{3F_0^2}\right)^2 [\frac{\{p_1 \cdot p_3 - (p_1 \cdot p_2 + m_\eta^2)^2/m_{D^*}^2\}}{s - m_{D^*}^2} \\
&\quad + \frac{\{p_1 \cdot p_4 - (p_1 \cdot p_3 - m_\eta^2)^2/m_{D^*}^2\}}{t - m_{D^*}^2}] \\
M_{D^+K^0} &= \frac{2g^2}{F_0^2} \frac{\{p_1 \cdot p_3 - (p_1 \cdot p_2 + m_{K^0}^2)^2/m_{D_s^*}^2\}}{s - m_{D_s^*}^2} \\
M_{D^+\overline{K}^0} &= \frac{2g^2}{F_0^2} \frac{\{p_1 \cdot p_4 - (p_1 \cdot p_3 - m_{\overline{K}^0}^2)^2/m_{D_s^*}^2\}}{t - m_{D_s^*}^2}
\end{aligned} \tag{8.26}
$$

The various invariant amplitudes can be expressed in terms of the Mandelstam variables using the relations: $p_1 \cdot p_2 = \frac{s - m_D^2 - m_\Phi^2}{2}$ $p_1 \cdot p_3 = \frac{m_D^2 + m_\Phi^2 - t}{2}$ and $p_1 \cdot p_4 = \frac{m_D^2 + m_\Phi^2 - u}{2}$ where m_D is the mass of D meson and m_Φ is mass of thermalized hadrons. The drag coefficient (γ) can be expressed as a thermal average of the square of the momentum exchanged between the heavy mesons and the bath particle, weighted by the interaction strength through the above mentioned Born amplitudes. In Fig. 8.5 the variation of drag and diffusion coefficients with T have been depicted for D-mesons. We observe [175] that the values of both the transport coefficients increases with temperature and the dominant contributions come from the pions in the medium. However, at higher temperature the contributions from heavier hadrons become significant. The value of the spatial diffusion coefficients, D_x may be expressed in terms of drag coefficients as $D_x = T/(M_D\gamma)$. The value of D_x at $T = 180$ MeV is $\sim 2.5/(2\pi T)$ *i.e.* 2.5 times larger than the thermal wave length.

Recently the diffusion coefficient of D meson has been calculated using heavy meson chiral perturbation theory [176] and also by using the empirical elastic scattering amplitudes [177] of D mesons with thermal hadrons. The authors of Ref. [178] used unitarized chiral effective $D\pi$ interactions to evaluate the drag. Our results are not very far from their predicted values.

Now we can apply the formalism described above to calculate the drag and diffusion coefficients for the B meson. Here we replace our heavy-light meson triplet as :

$$
\begin{aligned}
P &= (D^0, D^+, D_s^+) \rightarrow (B^0, B^+, B_s^+) \\
P_\mu^* &= (D^{*0}, D^{*+}, D_s^{*+})_\mu \rightarrow (B^{*0}, B^{*+}, B_s^{*+})_\mu
\end{aligned} \tag{8.27}
$$

But due to lack of empirical information in B sector we can not get any effective value

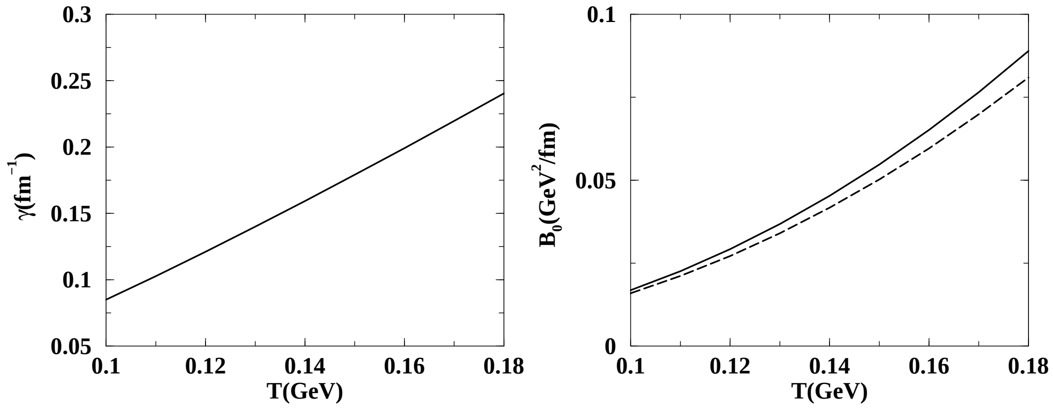

Figure 8.5: The variation of drag (left panel) and diffusion (right panel) coefficients with temperature due to the interaction of the D with thermal pions, nucleons, kaons and eta.

of coupling strength. So we have depend on T-matrices from LQCD [172, 179, 180], predicting the scattering length in hadronic sector.

For contact diagrams of B meson scattering we get similar forms of matrix elements in charge basis as given in (8.25). For $B\Phi$ scattering, these can be represented in the isospin basis as

$$\begin{aligned} M_{B\pi}^{(3/2)} &= -\frac{1}{4F_\pi^2}(s-u), \quad M_{B\pi}^{(1/2)} = \frac{1}{2F_\pi^2}(s-u), \\ M_{B\eta} &= 0, \quad M_{BK}^{(1)} = 0, \quad M_{BK}^{(0)} = -\frac{1}{2F_K^2}(s-u), \\ M_{B\overline{K}}^{(1)} &= -M_{B\overline{K}}^{(0)} = -\frac{1}{4F_K^2}(s-u) \end{aligned} \tag{8.28}$$

where the isospin of the $B\Phi$ system appears in the superscript. Denoting the threshold matrix elements by T, these are obtained from (8.28) and are given by

$$\begin{aligned} T_{B\pi}^{(3/2)} &= -\frac{m_B m_\pi}{F_\pi^2}, \quad T_{B\pi}^{(1/2)} = \frac{2m_B m_\pi}{F_\pi^2}, \\ T_{B\eta} &= 0, \quad T_{BK}^{(1)} = 0, \quad T_{BK}^{(0)} = -\frac{2m_B m_K}{F_K^2}, \\ T_{B\overline{K}}^{(1)} &= -T_{B\overline{K}}^{(0)} = -\frac{m_B m_K}{F_K^2} \end{aligned} \tag{8.29}$$

One can reproduce these T-matrix elements in the isospin basis using the lowest order $HM\chi PT$ Lagrangian for heavy mesons containing a heavy quark Q and a light antiquark of flavor a as given below [181]

$$\mathcal{L}_{HM\chi PT} = -i\, tr_D(\bar{H}_a^Q v^\mu \partial_\mu H_a^Q)$$

$$-i\ tr_D(\bar{H}_a^Q v^\mu \Gamma_\mu^{ab} H_b^Q)$$
$$+\frac{g}{2}\ tr_D(\bar{H}_a^Q \gamma^\mu \gamma^5 u_\mu^{ab} H_b^Q) + ... \tag{8.30}$$

where $H_a^Q = \frac{1+\not{v}}{2}(P_{a\mu}^* \gamma^\mu + iP_a\gamma^5)$ and $\bar{H}_a^Q = (P_{a\mu}^{*\dagger}\gamma^\mu + iP_a^\dagger\gamma^5)\frac{1+\not{v}}{2}$ and tr_D denotes trace in Dirac space. In this formalism, since the factor $\sqrt{m_P}$ and $\sqrt{m_{P^*}}$ have been absorbed into the P_a and $P_{a\mu}^*$ fields, the threshold T-matrix element ($\tilde{T}_{th}^{P\Phi}$) now has the dimension of scattering length a_P whereas in $C\chi PT$, we get a dimensionless T-matrix element ($T_{th}^{P\Phi}$). The relation between these two T-matrix elements and the scattering length a_P is given by

$$T_{th}^{P\Phi} = m_P \tilde{T}_{th}^{P\Phi} = 8\pi(m_\Phi + m_P)a_P \tag{8.31}$$

The square of the isospin averaged T-matrix element is given by

$$\sum \overline{|T_{B\Phi}|^2} = \overline{|T_{B\pi}|^2} + \overline{|T_{BK}|^2} + \overline{|T_{B\overline{K}}|^2} \tag{8.32}$$

where $\overline{|T_{B\pi}|^2} = \frac{1}{(2+4)}(2|T_{B\pi}^{(1/2)}|^2 + 4|T_{B\pi}^{(3/2)}|^2)$

and $\overline{|T_{BK/\overline{K}}|^2} = \frac{1}{(1+3)}(|T_{BK/\overline{K}}^{(0)}|^2 + 3|T_{BK/\overline{K}}^{(1)}|^2)$. We evaluate the drag coefficients of the B-meson by using the momentum dependent and momentum independent matrix elements given by Eqs.(8.28) and (8.29) respectively. Inspired by the fact that the results for the two scenarios are not drastically different in the LO we proceed to evaluate the drag coefficient of heavy mesons by replacing $\sum\overline{|M|^2}$ by $\sum\overline{|T|^2}$ in NLO and NNLO also where the T-matrix elements will be obtained from the scattering lengths. Liu *et al* [180] have obtained the $B\Phi$ scattering lengths up to NNLO in $HM\chi PT$ by using the coupling constant from recent unquenched lattice results [182]. Using these NLO and NNLO results we estimate the isospin averaged drag coefficients of B mesons [183]. The magnitude of B meson drag coefficient reveals that the B mesons dissipate significant amount of energy in the medium.

These non-negligible values of D and B meson drag coefficients might have crucial consequences on quantities such as the nuclear suppression factor of single electrons originating from the decays of heavy mesons. Though the charm and beauty quark diffusion play a major role to explain this nuclear suppression factor but to make the characterization of QGP reliable, the role of the hadronic phase should be taken into consideration and its contribution must be subtracted out from the observables.

Chapter 9

Summary

The fundamental properties of low energy QCD, namely chiral symmetry and confinement at finite temperature and baryon density are intimately related with the rich structure of the nuclear many-body problem. We have devoted chapter 1 to describe possible connections between the two. The change in the vacuum structure of QCD under extreme conditions of T and μ possibly reached in heavy ion collision experiments is reflected in the modified properties of hadrons which are manifested in their spectral function. In this thesis we have evaluated the spectral function of various hadrons using effective interaction in the framework of the real-time formalism of thermal field theory.

In chapter 2 we have derived the in-medium propagators for scalar, vector and spin 1/2 fermions in the real-time formulation. The 2×2 matrix structure of the propagator resulting from the real-time contour is elaborately discussed.

In chapter 3 the matrix structure of the self-energy in this formalism is introduced. It is explicitly shown that the diagonalisation of this matrix leads to the simplification that the required self-energy function can be obtained by evaluating any one component of the matrix. The general forms of one-loop digram involving bosons and fermions have been obtained and their analytic structure in the complex energy plane have been discussed.

Among the hadrons, neutral vector mesons are very special as their in-medium properties are reflected in the invariant mass spectra of the lepton pairs. In Chapter 4 and 5 we have investigated the in-medium spectral properties of ρ and ω respectively in which the interaction of the vector mesons with other mesons and baryons have been obtained from effective Lagrangians.

We have derived the discontinuities across all the cuts of a self-energy loop of these light vector mesons. The novelty in this approach is the evaluation of the imaginary part from the discontinuities of the self-energy function which provides an unified treatment of various scattering and decay processes occurring in the thermal medium. Since the excited nuclear matter consists of different mesons and baryons, we have to take into account them as internal lines of one-loop diagrams. We have taken four different meson loops for ρ self-energy. Near the ρ pole, the major contribution comes from the $\pi\pi$ loop, which provides Bose enhancement in the unitary cut region. Due to unequal masses, the other loops have some non-zero spectral strength in Landau cut region along with the unitary cut. Only the Landau cut contribution is numerically important near the ρ pole for the πh_1 and πa_1 loops whereas for $\pi\omega$ loop both cuts become important.

Baryon loop graphs in the ρ self-energy involving the nucleon and 4-star N^* and Δ resonances up to spin 3/2 were evaluated using gauge invariant interactions and full relativistic propagator to obtain the correct relativistic expressions. The singularities in the complex energy plane were analyzed and the imaginary part obtained from the Landau cut contribution. Results for the real and imaginary parts at non-zero three-momenta for values of the temperature and baryonic chemical potential were shown for the individual loop graphs. Adding meson and baryon loops we obtained the spectral function of ρ meson as a function of temperature and density. In addition, deviations from the neglect of the anti-baryon poles in the Lindhard function approach have been numerically established.

For ω meson, one-loop self-energy graphs have been evaluated for an extensive set of spin one-half and three-half N^* resonances in addition to the $\rho\pi$ loop using fully relativistic propagators and off-shell corrections for spin three-half fields. Similar to ρ, for ω we have also presented results of the real and imaginary parts for all the loops considered and the full spectral function for several combinations of temperatures and baryon chemical potentials relevant in heavy ion collisions.

We have made a comparison of the ρ and ω spectral functions finding the ω contribution to be lower but of comparable magnitude. However, the fact that the latter is suppressed by a factor ~ 10 compared to the ρ in the dilepton emission rate makes a quantitative study of the ω difficult. Additional hindrances could arise due to matter induced $\rho-\omega$ mixing [111]. Nevertheless, the contribution of the ω spectral strength is essential for a quantitative description of the dilepton data from heavy ion collisions [130]. In view of high quality data expected in future from heavy ion collisions at the FAIR facility at GSI we can conclude that an exhaustive evaluation of the spectral strength at finite temperature and baryon density is necessary for a quantitative analysis.

The vector meson spectral function at finite temperature and baryon density have been used to evaluate low invariant mass spectra of lepton pairs in chapter 6. Here we have attempted to bring out distinguishing features stemming from many body effects in the lepton pair yield from relativistic heavy ion collisions. We observe a significant enhancement in the dilepton yield in the mass region below the ρ pole compared to vacuum. The Landau cut contribution for various meson and baryon loops play the main role in this enhancement. Since dileptons are produced at all stages of the collision it is necessary to integrate the emission rates over the space-time volume from creation to freeze-out. Relativistic hydrodynamics with cylindrical symmetry and boost invariance along longitudinal directions has been used for space-time description. Equation of states from lattice QCD and hadronic resonance gas have been used as input. After a space-time evolution, the invariant mass spectra for various p_T windows was found to be in very good agreement with the experimental data obtained in In-In collisions at 17.3 AGeV. Comparing with the empirical approach of Ref. [80] using resonance dominance in the forward scattering amplitude, our baryon loop calculation is more successful to fit the low mass dilepton data. For RHIC and LHC energies we have seen similar low mass enhancement in invariant mass spectra. It is argued that the non-monotonic variation of the inverse slope deduced from the transverse mass distribution of lepton pairs for various values of the average invariant mass is an indication of the presence of two different phases during the evolution of the system. Thus, such a variation may be treated as a signal of QGP formation in heavy ion collisions.

In Chapter 7 we have calculated the self-energy of the nucleon and its spectral function in the same thermal field theoretic formalism. The imaginary part of the self-energy is built out of contributions from both Landau and unitary cuts from one loop graphs with πN and $\pi\Delta$ intermediate states. In contrast to results in the literature, we find the unitary cut from the $\pi\Delta$ loop to contribute significantly in the upper region of (virtual) mass of nucleon considered. The nucleon spectral function turns out to be sensitive to non-relativistic approximation, establishing the necessity of relativistic treatment for its quantitative determination.

In Chapter 8 we have investigated in-medium change of hadrons of heavy quark sector. The same formalism of thermal field theory is applied to study D and D^* mesons propagation in a hot matter composed of pions, kaons and eta. Here we have adopted the effective Lagrangian coming from Heavy meson chiral perturbation theory. After obtaining the full modified spectral function of open charm mesons, we have used it to fold the J/ψ decay width in $D\overline{D}$ channels. Here we take into account the fact that in the medium the open charm mesons are not stable particles but resonances with finite collisional widths. The D (or D^*) spectral function, owing to the Landau cut contribution, will have some strength in the invariant mass region below their bare poles and that may help the J/ψ to decay into $D\overline{D}$ (or $D\overline{D}^*$, $D^*\overline{D}$, $D^*\overline{D}^*$) channels. A non-negligible value of imaginary part of the self-energy for D-$\overline{D}$ loop at J/ψ mass give an estimation of J/ψ width at finite temperature, indicating the J/ψ suppression in hadronic environment.

It is also interesting to study in-medium properties of heavy mesons by investigating its transport properties in the medium. The drag and diffusion coefficients of hadronic matter have been evaluated using open charm and beauty mesons as probes where the interactions of the probes with the hadronic matter have been treated in the framework of effective field theory. It is observed that the magnitude of both the transport coefficients are significant, indicating substantial amount of interaction of the heavy mesons with the thermal hadronic system. It is expected that this should non-trivially affect the results on the nuclear suppression factor of single electron spectra measured in high energy heavy ion collision experiments.

Bibliography

[1] D. Gross and F. Wilczek, Phys. Rev. Lett. **30**, 1343 (1973); Phys. Rev **D 8**,3633 (1973).

[2] H. D. Politzer, Phys. Rev. Lett. **30**, 1346 (1973).

[3] G. t' Hooft, *Under the Spell of Gauge Theory*, (Advanced Series in Mathematical Physics, Vol. 19, World Scientific, 1984).

[4] G. t' Hooft, Nucl. Phys. **B 138**, 1 (1978); Nucl. Phys. **B 190**, 455 (1981).

[5] K. G. Wilson, Phys. Rev. **D 10**,2445 (1974).

[6] Thesis by Robert Craig Group (http://www-cdf.fnal.gov/ group/WORK/DISS_PAGE/thesis_final.pdf)

[7] S. Bethke, J. Phys G 26, R27 (2000).

[8] E.V. Shuryak, *The QCD Vacuum, Hadrons and Superdense Matter*, (World Scientific Lecture Notes in Physics, Vol. 71 2004).

[9] Ta-Pei Cheng, Ling-Fong Li, *Gauge theory of elementary particle physics*, (New York : Oxford University Press, 1984).

[10] C. Vafa and E. Witten, Nucl. Phys. **B 234**, 173 (1984).

[11] B. R. Holstein, Progress in Particle and Nuclear Physics 61 (2008) 3.

[12] J. Goldstone, Nuovo Cim. 19 (1961) 154; J. Goldstone, A. Salam, S. Weinberg, Phys. Rev. 127 (1962) 965.

[13] C.P. Burgess, Goldstone and Pseudo-Goldstone Bosons in Nuclear, Particle, and Condensed Matter Physics, hep-ph/9808176.

[14] M. Gell-Mann, R. J. Oakes and B. Renner, Phys. Rev. 175, 2195 (1968).

[15] T. D. Cohen, R. J. Furnstahl and D. K. Griegel, Phys. Rev. C 45 (1992) 1881.

[16] "The CBM Physics Book," eds. B. Friman et al, Lect. Notes Phys. **814**, 1 (2011).

[17] R. S. Hayano and T. Hatsuda, Rev. Mod. Phys. **82** (2010) 2949.

[18] lecture by Prof. Chaden Djalali at the Ecole Joliot Curie international school, 2009, (web link : http://www.cenbg.in2p3.fr/heberge/EcoleJoliotCurie/coursannee/cours/C-Djalali.pdf)

[19] M. Cheng, N. H. Christ, S. Datta, J. van der Heide, C. Jung et al., Phys. Rev. **D 77**, 014511 (2008).

[20] T. Hatsuda et al, Phys. Rev. Lett. 55 (1985)158

[21] W. Weise et al, Nuc. PHys. A 553 (1993)59.

[22] P. Gerber and H. Leutwyler, Nucl. Phys. B 321, 387 (1989).

[23] A. Bazavov et al., Phys. Rev. D 80 (2009) 014504.

[24] D. H. Perkins, *Introduction to high energy physics* (Cambridge Univ. Press, 2000)

[25] J. D. Bjorken, FERMILAB-PUB-82-059-THY (1982)

[26] M. Gyulassy, I. Vitev, X. N. Wang, and B.W. Zhang, in QuarkGluon Plasma 3, edited by R. C. Hwa and X. N.Wang (World Scientific, Singapore, 2004) [arXiv:nucl-th/ 0302077]; X. N. Wang and M. Gyulassy, Phys. Rev. Lett. 68, 1480 (1992).

[27] J. Adams et al. (STAR Collaboration) Nucl. Phys. A 757, 102 (2005).

[28] K. Adcox et al. (PHENIX Collaboration), Nucl. Phys. A 757, 184 (2005).

[29] T. Matsui and H. Satz, Phy. Lett. **B 178** (1986) 416.

[30] J. Y. Ollitrault, Phys. Rev. D 46, 229 (1992).

[31] G. Roche et al. [DLS collaboration], Phys. Rev. Lett. **61** (1988) 1069

[32] C. Naudat et al., Phys. Rev. Lett. **62** (1989) 2652

[33] R.J.Porter et al. [DLS collaboration], Phys. Rev. Lett. **79** (1997) 1229

[34] G. Agakishiev et al. [CERES collaboration], Phys. Rev. Lett. **75** (1995) 1272

[35] M. Masera et al. [DLS collaboration], Nucl. Phys. **A 590** (1995) 93C

[36] R. Arnaldi et al for the NA60 collaboration, Phys. Rev. Lett. **100** 022302 (2008); Eur. Phys. J. C **61**, 711 (2009); S. Damjanovic et al for the NA60 Collaboration, J. Phys. G: Nucl. Part. Phys. **35**, 104036 (2008).

[37] R. Rapp and J. Wambach, Adv. Nucl. Phys. **25**, 1 (2000); R. Rapp, J. Wambach and H. van Hees, arXiv:0901.3289 [hep-ph]

[38] S. Leupold, V. Metag, U. Mosel, Int.J.Mod.Phys. E 19 (2010) 147-224

[39] G. Agakichiev et al., CERES collaboration, Phys. Rev. Lett. 75 (1995) 1272; P. Wurm for the CERES collaboration, Nucl. Phys. A590 (1995) 103c;

[40] S. Sarkar, J. Alam and T. Hatsuda, J. Phys. G **30**, 607(2004).

[41] H. V. Hees, R. Rapp, Nucl. Phys. **A 806**, 339 (2008)

[42] J. Ruppert, C. Gale, T. Renk, P. Lichard and J. I. Kapusta, Phys. Rev. Lett. **100**, 162301 (2008).

[43] A. Adare *et al.* [PHENIX Collaboration], Phys. Rev. C **81** (2010) 034911

[44] K. Dusling and I. Zahed, Nucl. Phys. **A825**, 212 (2009).

[45] E. L. Bratkovskaya, W. Cassing and O. Linnyk, Phys. Lett. B **670** (2009) 428.

[46] S. Pal, Phys. Rev. C **85** (2012) 011901(R).

[47] A. Drees, Nucl. Phys. A **830**, 435c (2009).

[48] A. Zee, *Quantum field theory in a nutshell* (Princeton University Press, 2010)

[49] M. E. Peskin and D. V. Schroeder, *Introduction to quantum field theory* (Westview Press, cop. 1995).

[50] A. Lahiri and P.B. Pal, *A first book of quantum field theory* (Narosa Publishing House, 2005)

[51] K F Riley, M P Hobson, S J Bence, *Mathematical methods for physics and engineering* (Cambridge University Press, Cambridge, 2007).

[52] A. Das, *Finite Temperature Field Theory* (World Scientific, Singapore, 1998)

[53] M. Le Bellac, *Thermal field theory* (Cambridge University Press, Cambridge, 1996).

[54] J.I. Kapusta, C. Gale *Finite-temperature field theory : principles and applications* (Cambridge Univ. Press, Cambridge, 2006).

[55] Hiroomi Umezawa, *Advanced field theory : micro, macro, and thermal physics* (American Institute of Physics, New York, 1995).

[56] F.C. Khanna, A.P.C. Malbouisson, J.M.C. Malbouisson, A.E. Santana *Thermal quantum field theory : algebraic aspects and applications* (World Scientific, Singapore, 2009).

[57] R. Kubo, J. Phys. Soc., Japan **12**, 570 (1957).

[58] P.C. Martin and J. Schwinger, Phys. Rev. **115** 1342 (1959).

[59] H. Matsumoto, Y. Nakano and H. Umezawa, J. Math. Phys. **25**, 3076 (1984)

[60] L.V. Keldysh, Sov. Phys. JETP **20**, 1018 (1964)

[61] A. J. Niemi and G. W. Semenoff, Annals of Physics **152**, 105 (1984)

[62] R.L. Mills, *Propagators for many-particle systems* (Gordan and Breach, New York, 1969).

[63] G.N. Semenoff and H. Umezawa Nucl. Phys.**B 220** 196 (1983)

[64] R.L. Kobes and G.W. Semenoff, Nucl. Phys. **B260**, 714 (1985)

[65] C. Itzykson, J-B Zuber, *Quantum field theory* (New York, NY : McGraw-Hill, 1980)

[66] S. Weinberg, *The Quantum Theory of Fields*, vol I, Cambridge University Press, 1995

[67] L. H. Ryder *Quantum field theory* (Cambridge Univ. Press, Cambridge, 1998)

[68] F. Mandl, G. Shaw *Quantum field theory* (Wiley, 2008)

[69] H.A. Weldon, Phys. Rev. **D 28**, 2007 (1983)

[70] J. Alam, S. Sarkar, P. Roy, T. Hatsuda and B. Sinha, Ann. Phys. 286, 159 (2000).

[71] P.C.Raje Bhageerathi and Amruta Mishra, Int. J. Mod. Phys. **E 21** (2012) 1250063.

[72] R. Arnaldi, et al (NA60 Collaboration), Eur. Phys. J. **C61**, 711 (2009).

[73] http://www.gsi.de/forschung/fair_experiments/CBM/1intro_e.html

[74] C. Gale and J. I. Kapusta Nucl. Phys. **B357**, 65 (1991)

[75] K. Haglin, Nucl. Phys. **A 584**, 719 (1995)

[76] S. Gao, C. Gale, C. Ernst, H. stocker and W. Greiner, Nucl. Phys. **A 661**, 518 (1999) nucl-th/9812059

[77] R. Rapp and C. Gale, Phys. Rev. **C 60**, 024903 (1999)

[78] S. Jeon and P.J. Ellis, Phys. Rev. **D 58**, 045013 (1998)

[79] S. Mallik, Eur. Phys. J. **C 24**, 143 (2002).

[80] V. L. Eletsky, M. Belkacem, P. J. Ellis and J. I. Kapusta, Phys. Rev. C **64** (2001) 035202

[81] M. Herrmann, B. Friman and W. Norenberg, Nucl. Phys. **A 560**, 411 (1993)

[82] B. Friman and H.J. Pirner, Nucl. Phys. A617 (1997) 496.

[83] W. Peters, M. Post, H. Lenske, S. Leupold and U. Mosel, Nucl.Phys. **A 632**, 109 (1998) ; M. Post, S. Leupold and U. Mosel, Nucl.Phys. **A 689**, 753 (2001) ;

[84] G. Chanfray and P. Schuck, Nucl. Phys. A555 (1993) 329.

[85] D. Cabrera, E. Oset, M.J. Vicente Vacas, Nucl. Phys. **A 705** (2002) 90.

[86] R. Rapp, G. Chanfray and J. Wambach, Nucl. Phys. A **617**, 472 (1997)

[87] S. Ghosh, S. Sarkar and S. Mallik, Eur. Phys. J. C **70**, 251 (2010)

[88] S. Ghosh, S. Sarkar, Nucl. Phys. **A 870**, 94 (2011)

[89] S. Ghosh, S. Sarkar, and S. Mallik, Phys. Rev. **C 83**, 018201 (2011)

[90] S. Mallik and S. Sarkar, Eur. Phys. J. C **61**, 489 (2009).

[91] H. Leutwyler, arXiv:hep-ph/9406283.

[92] S. Mallik and S. Sarkar, Eur. Phys. J. C **25**, 445 (2002)

[93] G. Ecker, J. Gasser, A. Pich, E. de Rafael, Nucl. Phys. B 321,311 (1989)

[94] G. Ecker, J. Gasser, H. Leutwyler, A. Pich, E. de Rafael, Phys. Lett. B 223 425 (1989).

[95] C. Amsler et.al. (Particle Data Group) Phys. Lett. **B667**,1 (2008).

[96] P. Gonzalez, E. Oset and J. Vijande, Phys. Rev. C **79**, 025209 (2009)

[97] M. Post, S. Leupold and U. Mosel, Nucl. Phys. A **741** (2004) 81

[98] W. Rarita and J. Schwinger, Phys. Rev. **60**, 61 (1941)

[99] R. D. Peccei, Phys. Rev. **176**, 1812 (1968).

[100] S. Sarkar, E. Oset and M. J. Vicente Vacas, Nucl. Phys. A **750**, 294 (2005).

[101] M. Kaskulov, E. Hernandez and E. Oset, Eur. Phys. J. A **31**, 245 (2007)

[102] S. Leupold, V. Metag and U. Mosel, Int. J. Mod. Phys. **E 19**, 147 (2010)

[103] F. Klingl, N. Kaiser and W. Weise Nucl. Phys. **A 624**, 527 (1997)

[104] M. F. M. Lutz, G. Wolf and B. Friman, Nucl. Phys. A **706** (2002) 431 [Erratum-ibid. A **765** (2006) 431]

[105] P. Muehlich, V. Shklyar, S. Leupold, U. Mosel, M. Post, Nucl. Phys. A **780**, 187 (2006).

[106] E325 Collaboration, K. Ozawa *et al.*, Phys. Rev. Lett. **86** (2001) 5019

[107] M. Kotulla *et al.* [CBELSA/TAPS Collaboration], Phys. Rev. Lett. **100**, 192302 (2008) [arXiv:0802.0989 [nucl-ex]].

[108] R. A. Schneider, W. Weise, Phys. Lett. **B 515**, 89 (2001).

[109] R. Rapp, Phys. Rev. C **63**, 054907 (2001)

[110] V. Shklyar, H. Lenske, U. Mosel, and G. Penner Phys. Rev. C **71**, 055206 (2005).

[111] P. Roy, A.K. Dutt-Mazumder, S. Sarkar, J. Alam, J. Phys. **G 35**, 065106 (2008)

[112] P. Mohanty, V. Roy, S. Ghosh, S. K. Das, B. Mohanty, S. Sarkar, J. Alam and A. Chaudhuri, Phys. Rev. C 85, 031903(R) (2012) arXiv:1111.2159 [nucl-th].

[113] L. D. McLerran and T. Toimela, Phys. Rev. D **31**, 545 (1985).

[114] J. Alam, S. Sarkar, P. Roy, T. Hatsuda, B. Sinha, Ann. Phys. 286, 159 (2000).

[115] D.K. Srivastava, B. Sinha and C. Gale, Phys. Rev. C53 (1996) R567.

[116] V. Koch and C. Song, Phys. Rev. C54 (1996) 1903.

[117] G.Q. Li, C.M. Ko and G.E. Brown, Phys. Rev. Lett. 75 (1995) 4007; Nucl. Phys. A606 (1996) 568.

[118] W. Cassing, W. Ehehalt and C.M. Ko, Phys. Lett. B363 (1995) 35; W. Cassing, W. Ehehalt and I. Kralik, Phys. Lett. B377 (1996) 5.

[119] R. Baier, M. Dirks and K. Redlich, Phys. Rev. D55 (1997) 4344; Proc. of the 28th Int. Conf. on High Energy Physics, Warszawa, Poland (July 1996), hep-ph/9612448.

[120] C.M. Hung and E.V. Shuryak, Phys. Rev. C56 (1997) 453.

[121] J. Murray, W. Bauer and K. Haglin, Phys. Rev. C57 (1998) 882.

[122] T. Renk, A. Mishra, Phys. Rev. **C 69** (2004) 054905.

[123] H. A. Weldon, Phys. Rev. D **42**, 2384 (1990).

[124] S. Sarkar, arXiv:nucl-th/0007011v2

[125] E. V. Shuryak, Rev. Mod. Phys. **65** (1993) 1.

[126] R. Barate *et al.* [ALEPH Collaboration], Eur. Phys. J. C **4**, 409 (1998), K. Ackerstaff *et al.* [OPAL Collaboration], Eur. Phys. J. C **7**, 571 (1999)

[127] S. Sarkar, Nucl. Phys. A **862-863** (2011) 13.

[128] J. I. Kapusta and E. V. Shuryak, Phys. Rev. D **49**, 4694 (1994).

[129] S. Ghosh, S. Sarkar, J. Alam Eur. Phys. J. C **71**, 9 (2011).

[130] S. Sarkar, S. Ghosh, J. Phys. (Conference Series) 374 (2012) 012010.

[131] J. D. Bjorken, Phys. Rev. D **27**, 140 (1983).

[132] C. Bernard *et al.*, Phys. Rev. D **75** (2007) 094505.

[133] R. C. Hwa R C and K. Kajantie, Phys. Rev.**D32**, 1109 (1985).

[134] H. von Gersdorff, M. Kataja, L. McLerran and P. V. Ruuskanen, Phys. Rev.**D34** 794; *ibid.* **D34** (1986).

[135] D. Khazreev and M. Nardi, Phys. Lett. **B507**, 121 (2001).

[136] I. Arsene *et al.* (BRAHMS Collaboration), Nucl. Phys. A **757**, 1 (2005); B. B. Back *et al.* (PHOBOS Collaboration), Nucl. Phys. A **757**, 28 (2005); J. Adams *et al.* (STAR Collaboration), Nucl. Phys. A **757**, 102 (2005); K. Adcox *et al.* (PHENIX Collaboration), Nucl. Phys. A **757**, 184,(2005).

[137] J. Alam, J. K. Nayak, P. Roy, A. K. Dutt-Mazumder and B. Sinha, J. Phys. G **34**, 871 (2007); B. K. Patra, J. Alam, P. Roy, S. Sarkar and B. Sinha, Nucl. Phys. A **709**, 440 (2002).

[138] P. Braun-Munzinger, K. Redlich and J. Stachel in Quark Gluon Plasma 3, R. C. Hwa and X. N. Wang (Eds.), World Scientific Publishing, Singapore, 2003.

[139] H. Bebie, P. gerber, J. L. Goity and H. Leutwyler, Nucl. Phys. B **378**, 95 (1992).

[140] T. Hirano and K. Tsuda, Phys. Rev. C **66** (2002) 054905.

[141] J. K. Nayak, J. e. Alam, T. Hirano, S. Sarkar and B. Sinha, arXiv:0902.0446 [nucl-th].

[142] P. Lichard and J. Juran, Phys. Rev. D **76**, 094030 (2007)

[143] X. Nu and M. Kaneta, Nucl. Phys. A **698**, 306c (2002).

[144] K. Aamodt *et al.* (for ALICE collaboration), Eur. Phys. J. C **68**, 89 (2010).

[145] T. Renk and J. Ruppert, Phys. Rev. C **77**, 024907 (2008).

[146] H. Leutwyler and A. Smilga, Nucl. Phys. **B342**, 302 (1990)

[147] T. Ericson and W. Weise, *Pions and Nuclei* (Clarendon Press, Oxford, 1988).

[148] C.L. Korpa, M.F.M. Lutz, Nucl.Phys. **A 742**, 305 (2004)

[149] W.M. Alberico, G. Gervino, and A. Lavagno, Phys. Lett. **B 321**, 177 (1994)

[150] H. van Hees and R. Rapp, Phys. Lett. **B 606**, 59 (2005)

[151] C.L. Korpa, R. Malfliet, Phys. Rev. **C 52**, 2756 (1995)

[152] S. Mallik, H. Mishra, Eur. Phys. J. **C 50** (2007) 889.

[153] B. tar Haar and R. Malfliet, Phys. Rep. **149**, 207 (1987)

[154] G. Ecker, J. Gasser, H. Leutwyler, A. Pich and E. de Rafael, Phys. Lett. **B 223**, 425 (1989)

[155] T. Becher and H. Leutwyler, JHEP **0106**, 017 (2001).

[156] W. Weinhold, B. Friman and W. Noerenberg, Phys. Lett. **B 433**, 236 (1998).

[157] Particle Data Group, Phys. Lett. B **667**, 1 (2008).

[158] R. Koch and E. Pietarinen, Nucl. Phys. A **336**, 331 (1980).

[159] A.L. Fetter and J.D. Walecka, *Quantum Theory of Many-Particle Systems*, 2003, Dover publications, New York.

[160] B. D. Serot and J. D. Walecka, Adv. Nucl. Phys. **16** (1986) 1.

[161] A. Andronic, P. Braun-Munzinger and J. Stachel, Nucl. Phys. A **772** (2006) 167

[162] J. Cleymans and K. Redlich, Phys. Rev. C **60** (1999) 054908

[163] W. Cassing, E. L. Bratkovskaya, and A. Sibirtsev, Nucl. Phys. A691, 753 (2001).

[164] G. Krein, A.W. Thomas, K. Tsushima, Phys. Lett. **B 697**, 136 (2011)

[165] A. Mishra, E. L. Bratkovskaya, J. Schaffer-Bielich, S. Schramm, and H. Stocker, Phys. Rev. **C 69**, 015202 (2004)

[166] Bengt Friman, Su Houng Lee, Taesoo Song, Physics Letters B 548 (2002) 153-160

[167] A. Hayashigaki, Phys. Lett. B 487, 96 (2000).

[168] L. Tolos, J. Schaffner-Bielich, A. Mishra Eur. Phys. J. **C 43** (2005) 127; J. Phys. **G 31** (2005) S1213

[169] L. Tolos, A. Ramos, and T. Mizutani, Phys. Rev. **C 77**, 015207 (2008); L. Tolos, J. Schaffner-Bielich, H. Stocker, Phys. Lett. **B 635** (2006) 85 ; L. Tolos, C. Garcia-Recio, and J. Nieves, Phys. Rev. **C 80**, 065202 (2009) ; L. Tolos, J. Schaffner-Bielich, and A. Mishra, Phys. Rev. **C 70**, 025203 (2004).

[170] K. Tsushima, D. H. Lu, A. W. Thomas, K. Saito, and R. H. Landau, Phys. Rev. C 59, 2824 (1999); A. Sibirtsev, K.Tsushima, and A. W. Thomas, Eur. Phys. J. A 6, 351 (1999).

[171] D. Blaschke, P. Costa, Yu.L. Kalinovsky, Phys.Rev. **D 85**, 034005 (2012)

[172] L.S. Geng, N. Kaiser, J.Martin-Camalich and W.Weise, Phys. Rev. **D82**, 054022 (2010)

[173] C. Fuchs, B.V. Martemyanov, A. Faessler and M. I. Krivoruchenko, Phys. Rev.**C73**, 035204 (2006)

[174] B. Svetitsky, Phys. Rev. D **37**, 2484(1988)

[175] S. Ghosh, S. K. Das, S. Sarkar and J. Alam, Phys. Rev. D(R) **84**,011503(R) (2011)

[176] M. Laine, JHEP **04** 124, 2011, arXiv:1103.0372 [hep-ph].

[177] M. He, R. J. Fries and R. Rapp, Phys. Let. **B701**, 445 (2002)

[178] L. Abreu, D. Cabrera, F. J. Llanes-Estrada and J. M. Torres-Rincon, Ann. Phys. **326**, 2737 (2011).

[179] F.K. Guo, C. Hanhart, U. G. Meissner, Eur. Phys. J. A **40** 171 (2009)

[180] Y.R. Liu, X. Liu, and S.L.Zhu Phys. Rev. D **79**, 094026 (2009)

[181] A. V. Manohar and M. B. Wise, Heavy quark physics, Camb. Monogr. Part. Phys. Nucl. Phys. Cosmol. 10, 1 (2000).

[182] H. Ohiki, H. Matsufuru, and T. Onogi, Phys. Rev. D 77, 094509 (2008).

[183] S. K. Das, S. Ghosh, S. Sarkar, and J. Alam, Phys. Rev. **D 85**, 074017 (2012).